Universidad
del País Vasco

eman ta zabal zazu

Euskal Herriko
Unibertsitatea

IBeA
Ikerkuntza eta
Berrikuntza Analitikoa

Analytical and Chemometrical approaches for Bioimaging, Sensing and Metabolomics

Mireia Irazola Duñabeitia

2016

A thesis submitted for the international degree of
Philosophiae Doctor in Environmental Contamination and
Toxicology

supervised by
Dr. Kepa Castro Ortiz de Pinedo
Dr. Nestor Etxebarria Loizate

Bekak eta Finantziazioa

Esker onak

Badira sei urte IBeA ikerkuntza taldean sartzeko aukera izan nebala. Nestorri eskerrak Maitane ezagutu eta berarekin batera ikerkuntzaz gozatzen ikasi neban. Urte hauetan amestu ezin nebazan ikerketa proiektu zirraragarri pila batean parte hartzeko aukera izan dot: Silexetik hasita pintura muralen mundura eta hipertermia proiektutik ingurumen analisira.

Ilusioz eta borondate onez ahalegindu naz ikerkuntzaren bide berri hau jorratzen eta askori eskertu behar deutsuet horrenbeste amets errealitate bihurtu izana. Emandako aukerengatik, bidean zehar erakutsitako gauza guztiengatik eta nigan jarritako konfiantzagatik nabarmendu nahi zaituet.

IBeA ikerkuntza taldeari eta staff-ari (Nestor, Kepa, Juanma, Luis Angel, Olatz, Are, Gorka, Alberto, Ailette, Silvia, Marian, Maite, Iran, Maitane, Asier, Dani, Mirari) eskerrik asko zuekin lan egiteko aukera emotearren eta horrenbeste gauza erakustearren, segi zuen horretan, etorkizun oparoa opa deutsuet!

Nire zuzendariei ere mila esker, Kepa eta Nestorri, azken hilabeteetan bereziki jo eta su aritu zarielako nirekin batera lanean.

Unibertsitateko zerbitzu orokorretako taldeari (SGIker) eskerrik asko erakutsitako guztiarengatik eta prestatutako laguntzarengatik, batez ere, Alfredo, Pati, Juancar, Txesko, Bea eta Maribeleri.

Mintegian eta Zamudion izandakoei eta zaudenoi: Maitane, Unai, Ekhine, Laura, Naiara, Arantza, Haizea, Leire K., Leire M., Olaia, Itsaso, Oier, Iratxe, Nerea, Maite, Ibo, Joana, Jone, Julen, Azibar, Pati, Alfredo, Aini, Asier, Josu, Sandra, Ainhoa, Oscar, Josean, Oihana, Julene, Leti, Niko, Ane, Olivia, Nagore, Iratxe, Cristina, Hector, Maite, Marco, Marta, Arri e.a. Zuek gabe ez neban ezta horren ondo pasatuko ezta horrenbeste ikasiko. Eskerrik asko zuen laguntza guztiagatik!! Eta eskerrik asko batez be azkenaldian horrenbeste animo eta laguntza emon dostezuenoi!! Zuekin bizi izandako hamaika oroitzapen edar daroadaz nirekin; mendiko ibilaldiak, parrandak, Suediako bidaia, Dinamarkako bidaia, Manchesterreko bidaia, Eskoziako bisita, Dimako asteburu pasa, txokolatilua, bariku arratsalde *berdeak*, e.a. Etorkizunian be bizipen edar batzuk bizi daiguzan elkarrekin eiten dot gaur topa! Oraindik abentura asko daukoguz aurretik... Maitanekin kutxura tortila patata jatera, Laurarekin Errioxako laginketa... Eta gogoratu ondinon Leunganeko bueltia daukula eiteko Ekhine!!

Bizitza lana baino askoz gehiago dalako...

Eskerrik asko Eider, Leire eta Arantza!! Zuek izan zarie nire LEMA eta unian baita gure bidaia berezietan hain ondo pasatu izanaren arrazoia. Bizitza osorako lagunak izan gaitezan egiten dot gaur topa!

Bizitzari saltsa berezia emoten deutsazuen nire kuadrilakuei eta lagunei: Alaitz, Ylenia, Itziar, Itxaso, Elene, Izarne, Nahikari, Jago, Beñat, Adri, Gaizka eta Iturri. Eskerrik asko zuon animuengatik. Laster eingu aindutako bazkaixa, nire kontu!

Etxekuei eta Kepai eskerrik berezienak, hor baitzaudete beti niretako. Gaur zauzienoi eta nire ondoan izan zinatenoi eskerrik asko, eskerrik asko

amama Flora arratsaldero eiten zostazun arrera beruangatik, ez zatut inoiz ahaztuko.

Aita eta amari nola ez, beti aurrerantz eiten laguntzen dostazuelako. Tia Begoña be ezin ahaztu, bera barik ez nintzakeen ikastolara garaiz behin bez ailegauko!

Kepa, zuk badakizu, bidai honen errekonpentsa onena zu izan zarela. Eskerrik asko bizitza horren interesgarri eitiearren eta nirekin batera mendietan horrenbeste abentura konpartitziarren. Prestatu motxila! Abentura gosez nau ta!

Eskerrik asko danoi familia!! Ama, aita, Kepa, tia Begoña, Iontxu, tia Rosa, Irati, tio Patxi, Maddi, Beñat, Leire, Alberto, tio Juan Mari, tia Mila, Naiara, Xane, Oskar, Iñaki, Eneritz, Imanol,e.a. Etapa honen amaiera eta berriaren hasiera zuekin ospatzeko desiatzen nago!!

Ziur nago eskertu nahiko neban beste norbait ahaztuko nebala lerro hauetan, eta parkatu esker on hauek idaztian zutaz oroitu ez banaz (prisen kontuak badakizu...), baina bihotzez zuri ere eskerrik asko. Nire bizitzan zehar topo egin dodan pertsona guztiei eskerrak, zuek gabe ziur nago ez nintzakela gaur egun naizena izango.

Laburpena

Lan honetan zehar, hiru arazo analitikori irtenbidea eman zaie. Lehena, NMR-aren bidezko azterketa metabolikoa izan zen, muskuiluen esposizio kontrolatuaren ondorioak neurtzeko. Bigarrena nanopartikulen bidezko hipertermia tratamendua ardatz hartuta bi eginkizun bete ziren, alde batetik gibelaren ehunen erresonantzia magnetiko nuklearraren bidezko analisi metabolomikoa eta, bestetik, infragorri (FTIR) eta Raman irudi hiperespektralen aplikazioa ehunak aztertzeko. Azkena, gainazaleko handipeneko Raman espektroskopiaren (SERS) irudi hiperespektrala hazkuntza zelularretan bideratu nahian zenbait nanopartikula eta hauek funtzionalizatzeko organokonplexu aztertu ziren.

Tesiaren lehen atalean, ingurumen analisirako metodologia planteamendu berri bat proposatu da. Horretarako, kimikariok eta biologoak baldintza kontrolatutako esposizioa egiteko elkarlanean jardun genuen. Esperimentu honetan, muskuiluak eta baita lagin biltze pasiboko tresnak hainbat mikrokutsatzaile hidrofoboren eraginpean jarri ziren. Batetik, kutsatzaileen kontzentrazioak neurtu ziren, lagin biltze puntualen bitartez baita lagin biltze pasiboz. Bestetik, muskuiluetan kutsatzaileen kontzentrazioak neurtu ziren. Biologoek euren aldetik, muskuiluen azterketa histopatologikoa egin zuten. Azkenik, NMR-n oinarritutako metabolomika erabili zen muskuiluek kutsatzaileen aurrean zuten

erantzuna aztertzeko. Lau estrategien konbinazioarekin, kausa (kokteleko mikrokutsatzaileen kontzentrazioak eta muskuiluek metatutakoa) eta eragindako efektuen (histologia azterketetan behatutakoa) ulermen handiagoa eskura dezakegu, kutsatzaileek eragiten dituzten aldaketak ulertzeko eta ondorioak azaltzeko metabolomika baliabide erabilgarria dela ondorioztatu genuen. Kutsatzaileen koktelak errute goiztiarra eragin zien muskuiluei eta izan ere, NMR metabolomika erabiliz aldaketa metaboliko nabarienak errute egunean aurkitu ziren.

Tesiaren bigarren atal nagusian, Euskal Herriko Unibertsitateko (UPV/EHU) jakintza-alor anitzeko kideak (medikuak, fisikoak, kimika ez-organikokoak, organikokoak eta analitikariak) elkartu ginen proiektu baten inguruan, kolon eta ondoesteko minbiziaren gibeleko metastasiari aurre egiteko hipertermia magnetikoaren terapia garatzeko helburuarekin. Proiektu honetan, arginina, glizina eta azido aspartikodun tripeptido (RGD) estekatzaileekin inguratutako nanopartikula magnetikoak animalien odol-zirkulazioan txertatzen dira hipertermia saiakera baino 24 ordu lehenago. RGD estekatzaile ziklikoei esker nanopartikulak gibeleko minbizi zeluletara itsasten dira eta eremu magnetiko alternoen ondorioz arratoien gibeleko tumoreko tenperaturak gora egin eta zonalde hauetan nekrosia lortzen da. Tratamendua zela eta, jakin nahi genuen ia terapia magnetikoak ondorio kronikorik ote zekarkiokeen gaixoari, arratoiari gure kasuan. Horretarako NMR metabolomikan oinarritutako estrategia eta Raman eta FTIR irudi hiperespektralen analisia garatu eta aurrera eraman genuen diagnosiaren eta terapiaren baliabide berritzaile gisa. Batetik, Raman, FTIR eta NMR bidez kolon eta ondesteko minbiziaren eta ehun osasuntsuen profilak determinatu eta bereizi ziren. Gainera, Raman eta FTIR bidez ehunen irudi analisia egiteko metodologia garatu zen. Bestetik, emaitza

metabolikoek, arratoiek tratamendua jaso eta 10 egunera gibeleko mintzak sortutako kalteetatik errekuperatzen direla frogatu genuen.

Tesiaren azken kapituluan, Glasgow-n (Eskozian) egin nuen egonaldian ikasitakoa aurkezten dut. Bertan, Ru eta Os zeukaten organokonplexu bi aztertu ziren. Aldi berean, konposatu hauekin SERS analisian oinarritutako bio-irudiak egitea posible ote zen aztertu zen. Horretarako, urrezko eta zilarrezko SERS egiteko nanopartikulak sintetizatu genituen baita karakterizatu ere. Konposatuen egonkortasuna frogatu zen nanopartikula ezberdinekin eta ur eta zelulen hazkuntza-baldintzetan. Behin baldintza egokienak finkatuta, hamster txinatarren obuluak (CHO) hazi eta gure konposatuekin funtzionalizatutako nanopartikulei esposatu ondoren SERS irudiak eskuratu genituen. Aztertutako konbinaziorik egonkorrena urrezko nanopartikulak Os organokonplexuarekin funtzionalizatuta izan zen. Funtzionalizatutako nanopartikula hauek CHO zelulak bizirik daudela SERS bidezko irudiak egitea baimendu zigun.

Abstract

In this doctoral thesis, three analytical issues were resolved. The first one was the application of nuclear magnetic resonance (NMR) measurements of mussels tissues and biofluids to accomplish an environmental metabolic study. The second was carried out in the framework of the magnetic hyperthermia treatment based on the use of nanoparticles. In this case, we tackled two objectives, the application of Raman and infrared (FTIR) hyperspectral imaging to distinguish healthy and tumour tissues, and the application of NMR based metabolomic analysis of liver and tumour tissues to understand the mechanisms of the treatment. The last one was the study of surface enhanced Raman spectroscopy (SERS) tags to develop hyperspectral imaging in live cell cultures.

In the first chapter, the effects of hydrophobic microcontaminants such as alkylphenols, organophosphorus compounds, organochloride pesticides, phthalates and musk fragances were studied in mussels . The proposed analytical strategy is based on the combination of passive sampling studies, bioconcentration measurements of micropollutants in mussels, environmental NMR metabolomics of two tissues (gonad, muscle) and hemolymph of mussels and histological analysis. By means of this work, it was verified the feasibility of this strategy in controlled conditions with intent to use it in future environmental studies. The micropollutants

mixture was responsible of early spawning in mussels. In fact, the most significant metabolic changes were observed in the same day that spawning took place.

In the second chapter, magnetic nanoparticles induced therapy against colorectal liver metastasis (CLM) project is explained. This project was carried out in collaboration with the Hospital of Galdakao-Usansolo (Basque Country), physicians, physicists, inorganic and organic chemists and doctors from the University of the Basque Country. In this manuscript, we show the methodologies developed to diagnose the presence of CLM by Raman and FTIR imaging, and by using NMR metabolomics. In addition, NMR metabolomics together with chemometrics were used to find out the metabolomic changes and effects produced by the proposed magnetic hyperthermia therapy in rat liver tissue, in both tumour tissues and healthy tissues. We were able to determine the profile of hepatic and tumour tissue with CLM using Raman, FTIR and NMR based methodologies. Moreover, we developed a methodology to do hyperspectral image analysis with Raman and FTIR. Finally, we demostrated that the liver was recovered from the hyperthermia therapy in ten days.

Finally, in the third main chapter, we show the work developed at Strathclyde University (Glasgow, Scotland), in the laboratory of Prof. Duncan Graham. During this stay, osmium and ruthenium organocomplexes synthesized by the group of Prof. Tia Keyes, were used for *in vivo* SERS imaging. In this manuscript we show the steps followed to fulfil this purpose. Different silver and gold nanoparticles functionalised with osmium and ruthenium organocomplexes were prepared and their stability in culture media was studied. The best combination was the gold nanoparticles functionalised with the Os organicomplex. Once the best

combination was chosen, chinese hamster ovary (CHO) cells were exposed to the functionalised nanoparticles to do in vivo SERS imaging to observe the uptake.

Aurkibidea

Irudien zerrenda

Taulen zerrenda

Laburdurak

4-MBA 4-mercaptobenzoic acid

4nOP 4-nonylphenol

4tOP 4-tert-octylphenol

AC Alternating current

acetyl CoA Acetyl coenzyme A

ADP Adenosine diphosphate

AgNPs Silver nanoparticles

AHTN Tonalide

ALS Alternating least squares

ALT Alanine aminotransferase

APEO Alkylphenols ethoxilate

AST Aspartate aminotransferase

ATP Adenosine triphosphate

ATR-FTIR Attenuated total reflectance-Fourier Transform infrared spectroscopy

AuNPs Gold nanoparticles

BBP Benzyl butyl phthalate

BC Before Christ

C Control sample

CARS Coherent anti-stokes Raman scattering

CAS Chemical Abstracts Service

CEB Ethical Committee of Animal Welfare

CHO Chinese Hamster Ovary

CK Creatine kinase

CLM Colorectal liver metastasis

Clor Chlorpyrifos

Clorp Chlorfenvinphos

CluPA Cluster-based Peak Alignment

COW Correlation Optimized Warping

CRC Colorectal cancer

CSI Crime Scene Investigation

CT Computed tomography

CV Cross-validation

DBP Dibutyl phthalate

DCHP Dicyclohexyl phthalate

DDD Dichlorodiphenyldichloroethane

DDE Dichlorodiphenyldichloroethylene

DDT Dichlorodiphenyltrichloroethane

DEHP Bis(2-ethylhexyl)-phthalate

DEP Diethyl phthalate

DESIMS Desorption electrospray ionization mass spectrometry

DIOP Di-isooctyl phthalate

DLS Dynamic Light Scattering

DMP Dimethyl phthalate

DNA Deoxyribonucleic acid

DNOP Di-n-octyl phthalate

DOP Di-octyl phthalate

EB Europar Batasuna, European Union

EM Electromagnetic

EOC Emerging Organic Compound

ESA European Space Agency

FA Fatty acid

FECS Federation of European Chemical Societies

FTIR Fourier transform infrared

FUSLE Focused ultrasound solid-liquid extraction

FWHM Full width at half-maximum

G6P Glucose 6-phosphate

GOT Serum glutamic oxaloacetic transaminase

GPT Glutamate-pyruvate transaminase

H Hepatocellular tissue

H & **E** Hematoxylin and eosin stain

HCH Hexachlorocyclohexane

HHCB Galaxolide

HHT10d Hepatic healthy tissue from a healthy rat 10 days after the hyperthermia protocol without NPs

HHT12h Hepatic healthy tissue from a healthy rat 12 h after the hyperthermia protocol without NPs

HRMS High resolurtion mass spectrometry

HRTC Hepatic healthy tissue from a rat that developed a tumour

HRTHT10d Hepatic healthy tissue from a rat that developed a tumour and 10 days after the hyperthermia protocol without NPs

HRTHT12h Hepatic healthy tissue from a rat that developed a tumour and 12 h after the hyperthermia protocol without NPs

HRTHTSI12h Hepatic healthy tissue from a rat that developed a tumour and 12 h after the saline infusion that emulates the surgical protocol for the NP infusion and the hyperthermia protocol

HSI12h Hepatic healthy tissue from a healthy rat 12 h after the saline infusion that emulates the surgical protocol for NP infusion

HT Hyperthermia therapy

IBeA Ikerketa eta Berrikuntza Analitikoa, Analytical Research and Innovation

icoshift Interval correlated shifting

ICP-MS Inductively coupled plasma mass spectrometry

LC-MS Liquid chromatography coupled to mass spectrometry

LDH Lactate dehydrogenase

LIBS Laser-induced breakdown spectroscopy

LOC Lab on a chip

LSPR Localized surface plasmon resonance

LV Latent variables

lysoPCs Lysophosphatidylcholines

MAE Microwave assisted extraction

MALDI matrix assisted laser desorption-ionization

Matlab MATrix LABoratory

MCR Multivariate curve resolution

MCR-ALS Multivariate curve resolution alternating least squares

MIA Multivariate Image Analysis

MIMASPEC Microstructural, magnetic and spectroscopic characterization of materials with high-tech and biomedical application

MIP Molecularly-imprinted polymers

MLR Multiple Linear Regression

MNPs Magnetic nanoparticles

MRI Magnetic resonance imaging

MRS Magnetic resonance spectroscopy

MS Mass spectrometer

MSC Multiplicative Signal Correction

MSD Marine Strategy Directive

MSPD Matrix solid-phase dispersion

NA Number of aperture

NADH Nicotinamide adenine dinucleotide

NADPH Nicotinamide adenine dinucleotide phosphate

NASA National Aeronautics and Space Administration

NIBS Non-Invasive Back Scatter

NIR Near-infrared spectroscopy

NMR Nuclear magnetic resonance

NP Nanoparticle

OGK Ongarria den gehienezko kontzentrazioak, Environmental Quality Standard (EQS)

OPLS-DA Orthogonal signal correction-partial least squares discriminant analysis

OSC Seinaleen zuzenketa ortogonala, *orthogonal signal correction*

PAH Polycyclic aromatic hydrocarbons

PALS Phase analysis Light Scattering

PBS Phosphate-bufered saline

PC Phosphatidylcholine

PCA Principal Component Analysis

PCB Polychlorinated biphenyl

PCDD Polychlorinated dibenzodioxin

PCP Personal Care Products

PCR Principal Component Regresion

PDCF Polychlorinated dibenzofuran

PDI Polidispersity index

PDMS Polydimethylsiloxane

PEG polyethylene glycol

PES Polysulfones

PET Positron emission tomography

PLE Pressurised liquid extraction

PLS Partial Least Squares

PLS-DA Partial Least Squares discriminant analysis

PLS-R Partial Least Squares Regression

PMAO Poly(maleic anhydride-alt-1-octadecene)

POP Persistent organic pollutant

qRT-PCR Real-time reverse transcription-Polymerase Chain Reaction

RGD Arginine – glycine – aspartic acid

RMSEC Root Mean Square of Calibration

RMSECV Root Mean Square Error of Cross-validation

RNA Ribonucleic acid

RNV Robust Normal Variate

RRS Resonance Raman spectroscopy

SAR Specific absorption rate

SB Stir-bar

SEM Scanning electron microscopy

SERS Surface enhanced Raman scattering

SFE Supercritical fluid

SI Sham surgery using saline infusion

ssDNA single stranded DNA

SIMCA Soft Independent Modeling of Class Analogy

SIMS Secondary ion mass spectrometry

SNV Standard Normal Variate

SOP Standard Operating Procedure

SORS Spatially offset Raman spectroscopy

SPR Surface plasmon resonance

SRS Stimulated Raman spectroscopy

SVD Singular value descomposition

TC Tumour control

TCA Tricarboxylic acid cycle

TEM Transmission electron microscopy

TERS Tip-enhanced Raman spectroscopy

THT10d Tumour tissue 10 days after the hyperthermia protocol without nanoparticles.

THT12h Tumour tissue 12 hours after the hyperthermia protocol without nanoparticles.

TMA Trimethylamine

TMAO Trimethylamine-N-oxide

TMS Tetramethylsilane

TMSPA (trimethylsilyl)propinoic-2,2,3,3,-d4 acid

TSIHT12h Tumour tissue 12 hours after the saline infusion and the hyperthermia protocol without nanoparticles.

UPV/EHU University of the Basque Country

UV Ultraviolet

UV-Vis Ultramore ikuskorrak, *ultraviolet visible*

VAST Variable Stability Scaling

VIP Variables Importance on Partial Least Squares (PLS) projections

WFD Water Framework Directive

XRF X-izpien fluoreszentzia, *X-ray fluorescence*

Sarrera

Chapter 1

Sarrera

1.1 Kimika analitikoa: iragana, oraina eta etorkizuna

Kimika analitikoaren jatorria apala da. Analisi zerbitzu bezala jaio zen, baina zientziako adar garrantzitsu bihurtu da.

1991.urtean, Europako kimikako elkarteen federazioak (FECS) antolatutako *Working Party on Analytical Chemistry* batzarrean lehiaketa bat proposatu zuten. Bertan, kimika analitikoari zegokion definizio onena saritu zen. Lehiaketaren helburua ideien elkartrukea zen, hain zuzen ere, kimika analitikoa jakintzak momentu hartan zientzialariendako zuen esangura ezagutu nahi zen [1]. Asko izan ziren aurkeztutako definizioak, hala ere, guk horien artean bost aukeratu ditugu:

"Hainbat substantzia zein osagai ezagutzeko artea... zeinek helburu tekniko baita zientifikoak dituen prozesu kimikoak abian jartzerakoan sortzen diren galderak erantzutea baimentzen duena... eta kimikako arlo guztietan erabiltzen diren neurketarako metodoak erabiltzen dituena" [2].

3

"Lagin natural edota sintetikoen konposizio kimikoaren determinazioari dagozkion printzipio, lege eta teknikak aztertzen dituen zientzia da" [3].

"Kimika analitikoaren helburua arazo baten ebazpena da, ez lagin batena. Izan ere, azken honi mugatuz gero helburua, kimika analitikoaren funtzioa mugatzen da" [4].

"Analisi kimikoa egitea ez da kimika analitikoaren helburua bere horretan, gizarteko arazoei erantzuna emateko medio bezala ulertu beharra dago" [5].

"Kimika analitikoa neurketetan oinarritutako zientzia da. Arlo askotariko arazoei, zientzia arlokoei baita gizartekoei, erantzuna emateko bitartekoak jartzen ditu. Bere horretan, estrategia eta natura askotariko lanabesak (kimika, fisika, matematika, biokimika, biologia, e.a.) garatuz, optimizatuz eta aplikatuz, hainbat sistemetako informazio (bio)kimikoa eskuratzeko gai da, espazio eta denbora bezalako aldagaiak ere kontutan hartuz" [6].

Instrumentazioa eta neurketak kimika analitikoaren oinarriak dira eta aspaldi aitortu da haien garrantzia [7]. Kimika analitikoa, kimika klasikoaren eta modernoaren garapenerako funtsezkoa izan eta izango da [8]. Spiechiger-Keller andereinoaren esanetan kimika analitikoa existituko ez balitz, berehala asmatu beharko litzateke [9].

Zoritxarrez, askok eta askok kimika analitikoa sasi-zientzia bezala ulertzen dute, kimika analitikoa analisietara bakarrik mugatzen dute. Besteek gutxiesten gaituzten bitartean, guk, kimika analitikariok, aukerak besterik ez ditugu ikusten, beste jakintza arlo batzuetan lan egiten duten kideen arazoak entzun, aztertu eta konponbidea bilatzen diegu, gure balioa agerian jarriz.

Zeresan handia dugu arlo askotan eta gaur egun, aipagarrienak iruditzen zaizkigun arloak bioteknologia, klinika, jakiak, industria, sukaldaritza, ingurumena, auzitegiko medikuntza, arkeologia, kirola eta nekazaritza dira. Guzti hauen artean, bio-medikuntzak puri-purian dagoen gaia da. Jariakin biologikoetan (odol, plasma, gazura edota gernua) izan ditzakegun sustantzia toxikoak detektatzeko edota berezkoak ditugun organismo zein metabolitoen neurketa dira gai entzutetsuenak. Kasu batzuetan klinikako laborategi batean egin beharreko analisiak dira baina beste kasu batzuetan, farmakoen diseinurako eta gaixoen jarraipenerako analisi bereziak izaten dira. Sendagaiak gaixoarengan izango duen eragina aurresatea oso garrantzitsua da eta gero eta ahalegin handiagoak bideratzen ari dira ildo honetan, hasieran *in vitro*-ko azterketak eginez, ondoren *in vivo* egiteko eta azkenik gizakietan aplikatzeko. Argi dago, hiru kasuak konparatzea ezinezkoa dela, ondo baitakigu zelula batek bere horretan estres jakin bateri erantzuna emateko dituen baliabideak organismo batenak baino hamaika aldiz txikiago direla. Baina, beti bezala, nonbaitetik hasi beharra dago, eta pixkanaka arlo honetan ere, gero eta eraginkorragoak gara.

Industrian gure zerbitzuak ezinbestekoak dira, hainbat eta hainbat enpresetan kalitate kontrolerako baliabide analitikoak erabiltzen dira eta horietariko askotan automatizatutakoak izaten dira, aldez aurretik eraikitako modeloetan oinarrituta erantzuna emateko gai diren ekipoak izaten dira.

Urte askotan gizakiok ekonomikoki aberasteko asmo hutsarekin ingurumenean eragindako inpaktua neurrigabekoa izan da. Europar Batasuna (EB) bezalako erakundeak sortutako arazoari erantzuna ematen saiatzen ari dira. Orain arazoa ebatzi beharra dago eta konponbideak bilatu behar dira. Horretan zientzialariok eta kimika analitikariok badugu zertan

lagundu. Ingurumen kimikak erronkak aurkitu ditu arlo honetan, esate baterako, hondakin arriskutsuen kudeaketa.

Nekazaritza arloan, kimika analitikoak garrantzi berezia du zoruko elikagaien kontrolerako eta nola ez, intsektu zein gaixotasun izurriteen aurkako pestiziden kontrolerako. Abeltzaintzan ere, gizakiengan eragin kaltegarria izan ditzaketen eta aski ezagunak diren hormonen eta antibiotikoen arazoen aurrean zurruntasunez jokatu ahal izateko kontrolerako metodologiak garatzeko ardura du.

Gaur egun, nork ez ditu entzun hedabideetan goi mailako kiroletan dopin kontrolen joan etorriak. Aski entzuna da dopinaren aurkako kontrolak dopin sustantzia berrien ostetik doazela, etengabeko lasterketa bailitzan. Hala ere, gero eta sentikorragoak diren teknikak eta metodoak garatzen ari dira eta gidatu gabeko analisiak (*non target*) eta ekortze analisietan oinarritutako (*screening*) metodologien garapenek ere zeresan handia emango dute etorkizunean.

Hedabideek azkenaldian sona handia eman diete auzitegiko analistei *CSI* bezalako saioekin. Errealitatera bueltatuz, egia da gaur egun munduko polizia guztiek laborategiak dituztela auzitegiko analisiak egiteko. Ile, azazkal, odol, pintura, aurkitutako edozein zantzu analisatzeko metodoak etengabe garatu eta balidatu behar dira auzitegietan froga fidagarri bezala aurkezteko.

Arkeologia edo arte ederretan ere badugu zertan lagundu, nahiz eta gure jakintza eremutik urruti daudela iruditu. Hain zuzen ere, azken hamarkadan jauzi garrantzitsua eman dugu arlo hauetan. Mota hauetako laginak bakarrak eta errepikaezinak izaten dira. Beraz, euren balioa eskerga da. Mota hauetako laginak neurtzeko asmoz, gure ikerkuntza taldean adibidez, ohikoak zituzten metodologietatik aldendu

eta metologia ez-suntsikorretara egin zuten salto. Ildo honetan, Raman, infragorri, X-izpien fluoreszentzia (*X-ray fluorescence*, XRF) eta laser bidez sorturiko plasman oinarritutako espektroskopiak (*Laser-induced breakdown spectroscopy*, LIBS) dira nagusi.

Are gehiago, mugiezinak diren ondare kulturalak neurtzeko asmoz, teknika eramangarrien alde postura egin eta arrakasta lortu zuten. Arrakasta hedatuz joan da, ondare historiko eta kulturaleko azterketetatik eguzki sitemako planeten esplorazioan jasotako laginen neurketara. Hori nahikoa ez bazen, azken urte honetan Aeronautika eta Espazioaren Agentzia Nazionala (NASA) eta Europako Espazio Agentziarekin (ESA) elkarlanean gaude Martera bidaliko den erabilera anitzetako ibilgailurako beharrezkoak diren kalibratu sistemetariko bat diseinatzen. Ibilgailu berezi hauek automatikoki baita urrutiko kontrolaz kudea daitezke eta *in situ* analisi mota asko egiteko gai izaten dira, hala nola, Raman, XRF eta LIBS-eko neurketak.

Esan bezala, kimika analitikoak aldaketa handiak jasan ditu historian zehar, gizarteak jasan dituen bezain beste. Aldaketa, eboluzioa da, guztiz positiboa. Gaur egun, gizarteak aho batez metodo analitiko azkar, eraginkor, merke eta *kimika berdean* (*Green Chemistry*) oinarritutakoak eskatzen ditu. Egoera honi ere erantzuna ematen saiatzen gabiltza.

Azkenaldian, gizarteak bioteknologia eta biokimikan duen interesa aipagarria da; prozesu biologikoak eta sendagaien eragina ulertzeko eta jarraitzeko beharrezina handituz doa. Horretarako, analitikariok begiz jota dugu *in situ* eta *in vivo* neurketak ahalbideratzen dituzten sentsoreen garapena. Ildo honetan, aurrerapenen artean, azken hamarkadan, joera berri bat indarrez garatzen ari da, *lab on a chip* (LOC) ideia (ikusi 1.1 Irudia). LOC gailuen bidez, milimetro edo zentimetro eskaz batzuetan

1.1. Irudia: Laborategia txip batean.

laborategi batean egiten ohi diren prozedurak batu nahi dira. LOC gailuen garapena mikrofluidikaren eskutik doa eta azkenaldian jasandako garapena eta aplikazioak asko hazi dira.

Eraginkortasuna analitikariok bi modutan ulertzen dugu. Bata, argi dago arazoa ebaztea dela, baina bestetik, tekniken bereizmena eta detekzio mugen hobekuntza da. Analitikariok muga horiek gainditzeko gau eta egun lan egiten dugu: detekzio-mugen hobekuntza, elementu eta konposatuen banaketaren bereizmen espaziala eta kimikoa. Hau guztia hainbat tekniken akoplamenduari eta aurrerapen teknikoei zor diegu.

Etorkizunean izango ditugun erronkak gizartearen beharrizanekin bat datoz. Adibidez, gizarteak naturari eta lurrari eragindako kalteen hedadura neurtzea eta irtenbideak bilatzea izango da gai nagusietariko bat. Garapenak aberastasun ekonomikoa ekarri digu lehen munduko biztanleoi baina planetarengan izan duen eragina oraindik ez dugu ondo ezagutzen. Biztanleria hazkuntza handia (10 aldiz handitu da planetako biztanleria azken mendeetan), urbanizazio neurrigabea, ingurumen kutsadura larria, berotze globala, klima aldaketa, basamortutze, e.a., azken finean planetako gainazalaren erdia gure gogoaren arabera moldatu dugu ondorioetan pentsatu gabe. Pixkana-pixkanaka badirudi egoera honen erantzukizun politikoa dutenek, dagokien ardura hartzen dabiltzala, eta zientzialarion laguntzaren eske dabiltzala. Gaur egungo gizartea eta industria garapen jasangarrira moldatzea da Europar Batasunaren helburu nagusietariko bat, eta neurri berean, sortutako kalteen eragina neurtu nahi da. Ildo honetan, zeresan handia dute proteomikak, metabolomikak eta genomikak besteak beste. Lanabes hauek, gizarteak sorturiko eta ingurumenera isuritako hondakinek bizidunengan duten eragina aztertzea dute helburu, bakoitza bere neurrian eta esparruan baina elkarren eraginpean.

Esan bezala, kutsatzaileen zerrenda gero eta luzeagoa da eta sailkapena nahitaezkoa bihurtu da (ikusi 1.1, 1.2, 1.3 eta 1.4 Taulak). Alde batetik kutsatzaile organikoak ditugu, eta bestetik metalen kutsadura. Azken talde honetan, ezin ditugu nanopartikulak ahaztu. Nanopartikulek industrian harrera oso ona izan dute aurkezten dituzten propietate bereziengatik, baita medikuntzan ere, farmakoen garraiatzaile bezala adibidez. Baina euren detekzioan eta beste teknika batzuen garapenerako ere funtsezkoak izan dira, adibidez, Raman seinalearen haundipenean (SERS, *Surface Enhanced Spectroscopy)* biosentsore nanometriko bezalaxe.

1.1. Taula: Europar Batasuneko lehentasuneko kutsatzaileen zerrenda I eta ingurumen kalitatearen arabera onargarriak diren gehienezko kontzentrazioak (OGK, μg/L).

CAS zenbakia	Lehentasuneko kutsatzailea	Arriskutsuenak	OGK
15972-60-8	Alaklor		0.3
120-12-7	Antrazenoa	X	0.1
1912-24-9	Atrazina		0.6
71-43-2	Bentzenoa		10
	Brominatutako difeniloeterrak	X	0.5 ng/L ($\sum$)
32534-81-9	Pentabromodifeniloeterra (28, 48, 99, 100, 153 eta 154)		0.5 ng/L ($\sum$)
7440-43-9	Kadmioa eta eratorriak	X	0.08-0.25
85535-84-8	Kloroalkanoak, C10-13		0.4
470-90-6	Klorfenbinfos		0.1
2921-88-2	Klorpirifos (Klorpirifos etiloa)		0.03
107-06-2	1,2-Dikloroetanoa		10
75-09-2	Diklorometanoa		20
117-81-7	Di(2-etilhexil)ftalatoa (DEHP)		1.3
330-54-1	Diuron		0.2
115-29-7	Endosulfan	X	0.005
206-44-0	Fluorantenoa		0.0063
118-74-1	Hexaklorobentzenoa	X	0.05
87-68-3	Hexaklorobutadienoa	X	0.6
608-73-1	Hexakloroziklohexanoa	X	0.03
34123-59-6	Isoproturon		0.2
7439-92-1	Beruna eta eratorriak		1.2
7439-97-6	Merkurioa eta eratorriak	X	0.07
91-20-3	Naftalenoa		2
7440-02-0	Nikela eta eratorriak		4

1.2. Taula: Europar Batasuneko lehentasuneko kutsatzaileen zerrenda II eta ingurumen kalitatearen arabera onargarriak diren gehienezko kontzentrazioak (OGK, μg/L, ingurumen kalitate estandarrak gainazaleko ur kontinentalendako)

CAS zenbakia	Lehentasuneko kutsatzailea	Arriskutsuenak	OGK
25154-52-3	Nonilfenolak	X	0.3
104-40-5	4-nonilfenola	X	0.3
1806-26-4	Oktilfenolak		0.1
140-66-9	4-(1,1',3,3'-tetrametilbutil)-fenola		0.1
608-93-5	Pentaklobentzenoa	X	0.007
87-86-5	Pentaklorofenola		0.04
	Hidrokarburo poliaromatikoak	X	$1.7 \ 10^{-4} \ (\sum)$
50-32-8	Benzo(a)pirenoa	X	$1.7 \ 10^{-4} \ (\sum)$
205-99-2	Benzo(b)fluorantenoa	X	$1.7 \ 10^{-4} \ (\sum)$
191-24-2	Benzo(g,h,i)perilenoa	X	$1.7 \ 10^{-4} \ (\sum)$
207-08-9	Benzo(k)fluorantenoa	X	$1.7 \ 10^{-4} \ (\sum)$
193-39-5	Indeno(1,2,3-cd)pirenoa	X	$1.7 \ 10^{-4} \ (\sum)$
122-34-9	Simazine		1
	Tributil-eztainuzko konposatuak	X	0.0002
36643-28-4	Tributil-eztainu katioia	X	0.0002
12002-48-1	Triklorobentzenoa		0.4
67-66-3	Triklorometanoa (kloroformoa)		2.5
1582-09-8	Trifluralin		0.03

1.3. Taula: 2013.urtean Europar Batasuneko lehentasuneko kutsatzaileen zerrendan gehitzeko konposatuak eta ingurumen kalitatearen arabera onargarriak diren gehienezko kontzentrazioak (OGK, μg/L, ingurumen kalitate estandarrak gainazaleko ur kontinentalendako).

CAS zenbakia	Lehentasuneko kutsatzailea	Arriskutsuenak	OGK
115-32-2	Dikofola	X	$1.3\ 10^{-3}$
1763-23-1	Azido perfluorooktanosulfonikoa eta deribatuak (PFOS)	X	$6.5\ 10^{-4}$
124495-18-7	Kinoxifenoa	X	0.15
	Dioxinak eta antzerakoak	X	$0.008\ \mu$g/Kg totala
74070-46-5	Alkonifenoa		0.12
42576-02-3	Bifenox		0.012
28159-98-0	Zibutrina		0.0025
52315-07-8	Zipermetrina		$8.0\ 10^{-5}$
62-73-7	Diklorbosa		$6.0\ 10^{-4}$
	Hexabromoziklododekanoa (HBCDD)	X	0.0016
76-44-8 / 1024-57-3	Heptakloro/heptakloro Epoxide	X	$2.0\ 10^{-7}\ (\sum)$
886-50-0	Terbutrinoa		0.065
57-63-6	17α-etinilestradiola		$3.5\ 10^{-5}$
50-28-2	17β-etinilestradiola		$4.0\ 10^{-4}$
15307-79-6	Diklofenakoa		0.1

1.4. Taula: Kutsatzaile emergenteen EB-ko zerrendako adibideak.

Familia eta erabilera	kutsatzailea (adibidea)
Farmakoak	
Antibiotikoak	Trimetoprima,eritromizina, linkomizina, sulfametaxozola
Analgesikoak, hanturaren aurkako farmakoa	Kodeina, ibuprofenoa, azetaminofenoa, az. azetilsalizilikoa, diklofenakoa, fenoprofenoa
Psikiatriako farmakoak	Diazepam
Lipidoen erregulatzaileak	Bezafibrate, azidoa klofibrikoa , azido fenofibrikoa
β-blokeatzaileak	Metoprolola, propanolola, timolola
X-izpien kontrastea	Iopromida, iopamidola, diatrizoatoa
Esteroideak eta hormonak	Estradiola, estrona, estriola, dietilstilbestrola
Zaintza pertsonalerako produktuak	
Fragrantziak	Nitro, poliziklikoak eta makroziklikoak diren musketak
Eguzki krematako agenteak	Bentzofenona, metilbentzilidenoa kanforra
Eltxoak uxatzeko produktuak	N,N-dietiltoluamida
Antiseptikoak	Triklosan, Klorofenoa
Sugar-atzeratzailea	Polibrominatuak diren difenil eterrak (PBDEs) Tetrabromo bisfenol A, C10-C13 kloroalkanoak Tris (2-kloroetil)fosfatoa
Industriarako gehigarriak	keladun agenteak (EDTA), sulfonato aromatikoak
Gasolinaren gehiagarriak	Dialkil eterrak, metil-t-butil eterra (MTBE)

Ikerkuntza esparru berriek lanabes berrien beharrizana plazaratzen dute. Emandako garapen metdologiko eta instrumentalek sortu zuten lehen beharrizana, datu eta emaitzen kudeaketa aurreratuago bat izan zen. Tekniken bereizmenean emandako hobekuntzak datu kopuruaren hazkuntza dakar eta ez edonolakoa. Beharrizan honi esker osagai askotariko analisia edo kimiometria jaio zen (1.2 Irudian ikus dezakegu baliabide batzuen sailkapena). Hiru gauza nagusi eskatzen dira datu-analisi eta ereduen eraikuntzan: datuen fidagarritasuna bermatzea, metodo azkarrak izatea eta metodoa sendoa izatea.
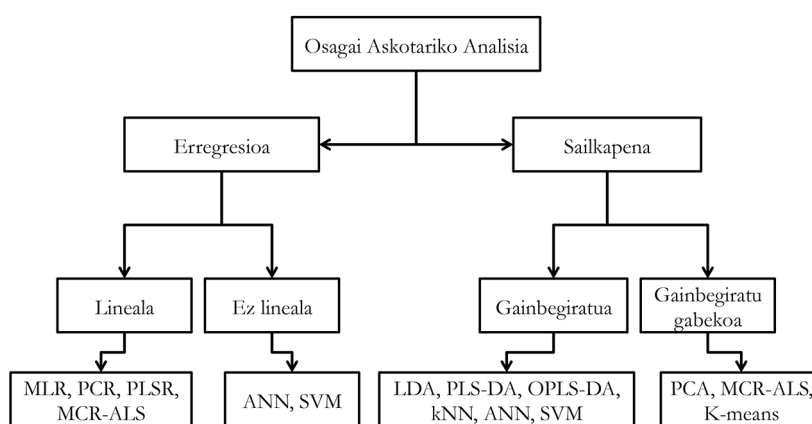
1.2. Irudia: Zenbait kimiometria baliabideren sailkapena.

1.2 Tesiaren planteamendua

Erronkak gainditzea da kimika analitikarion eguneroko zeregina. Tesi hau, hain zuzen ere, modu berean planteatu genuen, aurrean genituen erronkak gainditzeko helburuarekin. Bizitzan bezala, tesi honetan garatutako ikerkuntza lana patuaren nahia izan da. Izan ere, gure lankideei lau urte

hauetan sortu zaizkien arazoetariko batzuei irtenbidea bilatzen ahalegindu gara. Onartu behar da edozein putzutan botatzeko aukerak begi onez ikusten ditugula, batzuk behinik behin.

Biologiak, fisikak, medikuntzak, kimika ezorganikoak, kimika organikoak, jakintza arlo guzti hauek, niretzat, pertsonalki, kimika analitikoa dute amankomunean. Hain zuzen ere, lan honetan isladatuta sentitzen dugu kimika analitikarion lanaren funtsa, ilusioa eta abenturarako gogoa, gure lanabes eta sormen analitikoak lanean jarriz arazoei irtenbidea emateko. Esan beharrik ez dago, arazo askori konponbidea biltzeko, neurketarik egin ezean ezin dela erabakirik hartu.

Orain arte lagin biologikoen irudi analisian eta neurketa metabolikoetan eskarmentua izan ez bagenuen ere, gure ikerkuntzako esperientziari eta hainbat teknika analitikoekin genuen eskarmentuari esker, erronka berri bati ekin genion.

Lan honetan zehar, lau urte hauetan egindako lanetatik hiru proiektu nagusi azaltzen ditugu.

Lehen atalean, ingurugiro analisirako metodologia planteamendu berri bat dakargu. Bertan, kimikariok eta biologoek elkarlanean jardun genuen baldintza kontrolatuetan egindako esperimentu bat egiteko. Esperimentu honetan muskuiluak baita laginketa pasiboko tresneria hainbat mikrokutsatzaile hidrofoboen eraginpean jarri ziren. Lehen pausoan, uren kontzentrazioak neurtu ziren, laginketa puntualen bitartez baita laginketa pasiboz. Lan hau, Oscar Posadak, nire lankide batek, egin zuen [10].

Bigarren pausoan, biokontzentrazioak neurtu ziren, Haizea Ziarrusta lankideak garatutako metodo bat aplikatuz [11]. Honekin batera, biologoek muskuiluen azterketa histologikoa egin zuten. Azkenik, erresonantzia

magnetiko-nuklearrean (NMR) oinarritutako metabolomika erabili zen muskuiluek kutsatzaileen aurrean zuten erantzuna aztertzeko.

Gure ustetan, planteamendu honek, itsasertzetan sarri gertatzen diren kutsadura arazoen aurrean azterketa sakonago bat egitea bidea eman zigun. Beraz, itsasertzetan frogatu orduko, baldintza kontrolatuetan aztertzea logikoena zen eta hola egin genuen tesi honetan. Aipatutako lau estrategien konbinazioarekin, kausa (kokteleko mikrokutsatzaileen kontzentrazioak eta muskuiluak metatutakoa) eta eragindako efektuen (histologia azterketetan behatutakoa) ulermen handiago bat eskura dezakegu. Kutsatzaileek eragiten dituzten aldaketak ulertzeko eta ondorioak azaltzeko metabolomika dugu.

Lan honen bigarren atalean, Euskal Herriko Unibertsitateko (UPV/EHU) jakintza-arlo askotariko kideak (medikuak, fisikoak, kimika ezorganiakoak, organiakoak eta analitikariok) elkartu ginen proiektu interesgarri baten inguruan: kolon eta ondoesteko minbiziaren gibeleko metastasiari aurre egiteko hipertermia magnetikoaren terapia. Proiektu honetan, arginina-glizeril-azido aspartiko tripeptidoa (RGD) estekatzaileekin inguratutako nanopartikula magnetikoak animalien odol-zirkulazioan txertatzen dira hipertermia saiakera baino 24 ordu lehenago. RGD estekatzaile ziklikoei esker, nanopartikulak gibeleko minbizi zeluletara itsasten dira eta eremu magnetiko alternoen ondorioz arratoien gibeleko tumoreko tenperaturak gora egin eta zonalde hauetan nekrosia lortzen da. Tratamendua zela eta, zenbait bidezko galdera zetozkigun burura behin eta berriz:

(i) Lehenengo, ia nanopartikulak bideratzeko estrategiak ondo funtzionatzen ote zuen, eta zonalde bakoitzean metatzen zen nanopartikulen kontzentrazioa zein zen jakiteko, induktiboki

akoplatutako plasma bidezko masa espektrometria (ICP-MS) bidezko neurketak proposatu ziren.

(ii) Hortik sortu zen ehun osasuntsu eta minbiziaren arteko bereizketa antzemateko aukera espektrofotometrikoa. Raman eta FTIR irudi hiperespektralen analisia garatu zen mintzen karakterizazioa burutzeko.

(iii) Azkenik, ia gure terapia magnetikoak ondorio kronikorik ote zekarkion gaixoari jakin nahi zen, arratoiari gure kasuan. Horretarako analitikariok NMR metabolomikan oinarritutako estrategia aurkeztu genuen.

Lan honen azken atalean, Glasgow-n (Eskozian) egin nuen egonaldian ikasitakoa aurkezten dut. Bertan, Ru eta Os zeukaten organokonplexu bi aztertu ziren. Aldi berean, konposatu hauekin SERS analisian oinarritutako bio-irudiak egitea posible ote zen aztertu zen. Horretarako, urrezko eta zilarrezko gainazaleko hobekuntzako Raman espektroskopia (SERS, *Surface enhancement Raman spectroscopy*) egiteko nanopartikulak sintetizatu nituen baita karakterizatu ere. Konposatuen egonkortasuna hainbat nanopartikulekin, ur eta zelulen hazkuntza-baldintzetan frogatu zen. Behin baldintza egokienak finkatuta, hamster txinatarren obuloak hazi eta gure konposatuekin funtzionalizatutako nanopartikulekin aplikatu ondoren SERS irudi hiperespektralak sortu genituen.

Ikusi dezakezuen moduan, gai ezberdinen inguruan hitz egingo dizuet tesi honetan zehar baina gaur egun bor-borrean dauden gaietara hurbiltzeko informazio baliagarria ematen dudala uste dut.

Jakintza-arlo arteko eremuak oso estuak badiruten arren, bide berriak zabaltzen ahalegintzean oztopoak aurkitu ditugu behin eta berriz. Norbere jakintza-arloko adituei ez ezik gainerako taldekideei ere gure ideiak helarazteko komunikazioa landu behar izan dugu, metodologia eta lanabes berriak aurkezteko eta adosteko.

Imagina dezekezuen moduan, tesi honetan zehar datu multzo erraldoiak lortu ditugu gure neurketetan eta ezinbesteko lanabes bihurtu da kimiometria edo osagai askotariko analisia.

1.3 Osagai askotariko analisia lanabes moduan

Naturaren osagaiak anitzak dira eta instrumentu analitikoen erantzunak aldagai askotarikoak dira. Mundu honetan ez duzu ezer aurkituko aldagai bakar batez azal daitekeenik. Pentsa dezagun eguneroko bizitzako adibide batean: eguraldian. Eguraldia azaldu beharko bagenu tenperaturan, airearen presioan, haizearen abiaduran, hodeien presentzian, etab. luze batean pentsa beharko genuke. Era berean laborategian egiten dugun neurketa bakoitzean. Hain zuzen ere, osagai anitzeko analisiak, eragina izan dezaketen aldagai guztiak batera aztertzea baimentzen du eta benetan garrantzitsuak diren aldagaiak agerian jartzen ditu [12]. Hitz bakarrean, lana *errazten* digu.

Gaur egungo instrumentuek zerbait eskaitzen badute, aspaldian ez bezalaxe, zera da, datu eta neurketa asko eman ditzaketela aldi berean edota datuak arin eskaintzeko aukera dutela. Hori dela eta, neurketa instrumental askok oso emaitz oparoak dituzte eta bidean informaziorik ez galtzeko osagai askotariko analisia giltzarri bihurtu da.

Osagai askotariko analisiaren helburuak hiru dira [12]:

(i) *Datuak aztertzea.* Karakterizazio prozesu honetan datuen arteko korrelazioa, desbiderazioak eta ereduan eragin handiena duten aldagaien identifikaziorako baliagarria da. Osagai nagusien analisia dugu (*Principal Component Analysis*, PCA) metodorik ezagunena helburu hau betetzeko.

(ii) *Datuen bereizketa eta sailkapena.* Mota honetariko analisia egitean, datuen taldekatzea aztertzen da eta aldagaien kontzentrazioekiko bereizketa egiteko aukera azaltzen dute.

Bi sailkapen mota erabiltzen dira: gainbegiratua edo gainbegiratu gabekoa. Kasu honetarako ere PCA erabil dezakegu, antzeko klaseen eredugintza independente leuna (SIMCA, *Soft Independent Modeling of Class Analogy*) analisiaren abantailarekin. Kasu honetan klase bakoitza PCA modelu batekin ezaugarrituta dago eta modeluan erabili ez diren laginei dagokien klasea aurreikusteko erabiltzen da.

(iii) *Erregesioa eta iragarpena.* Erregresioaren bitartez bi aldagai multzo erlazionatzen dira: Y aldagaiak eta X aldagaiak, non Y aldagaia, neurtutako X aldagaien menpekoan den. Beraz, mota honetako analisiaren helburua, X aldagai berriei dagokien Y balioak aurresatea da, aldez aurretik eraikitako eredu batean oinarrituta. Osagai nagusien erregresioa (*Principal Component Regresion*, PCR), linea anitzeko erregresioa (*Multiple Linear Regression*, MLR) eta minimo karratu partzialen erregresioa (*Partial Least Squares Regression*, PLS-R) bezalako metodoak erabil ditzakegu helburu hauek lortzeko.

Osagai askotariko analisiak egiteko software egoki bat aukeratu beharra dugu. Programatzeko trebezia izanez gero, sarean badaude oso interesgarriak diren erabilera askeko softwareak, phyton

(https://www.python.org), R (https://www.rstudio.com) edota GNU
Octave (https://www.gnu.org/software/octave/), besteak beste. Era
berean, Matlab (http://es.mathworks.com) ere oso erabilgarria da
programazioa jakinda eta hainbat *toolbox* erabiliz, baina ordainpeko
softwarea dugu hau.

Guk Matlab erabiltzeko aukera izan dugu. Matlab, MATrix
LABoratory-ren akronimoa da eta MathWorks Inc. (Natick,
Massachusetts, USA) korporazioaren softwarea da. Matlab-ek datu
matrizeak kudeatzeko, datuen eta funtzioak irudikatzeko, algoritmoak
erabiltzeko, funtzio eta algoritmo berriak sortzeko, erabiltzaileendako
interfazeak sortzeko (Simulink eta GUIDE lanabesak erabiliz) eta beste
programa eta instrumentu batzuekin elkarrekin lan egiteko baliabideak
sortzeko aukera ematen duen ingurune konputazional berezi bat eskaitzen
du. Esan bezala, Matlab-en aurrez sortutako interfaze eta hainbat
toolbox-etaz (lanabes-kutxa) baliatuz lana erraztu eta arindu egiten da.

Gure kasuan, tesi honetan sortu ditugun datuekin lan egiteko, bi
toolbox erabili ditugu: PLS eta MIA. PLS-Toolbox-ean oinarrizko eta
goi mailako kimiometria analisirako lanabesak aurki ditzakegu. Bertan,
zientzialari eta ingeniariok beharrezkoak ditugun lanabesak aurkitzen
ditugu datuak aztertzeko eta iragarpen ereduak eraikitzeko. MIA-Toolbox-
a PLS-Toolbox-aren luzapen bezala erabili dugu irudi hiperespektralen
kasuan. Irudi hiperespektralak hiru dimentsiotako matrizeak dira, gainazal
batean neurtutako informazio espektrala (Raman, infragorri eta abar
luze batekin eskura daitekeen informazio) batzen dutenak. Beraz, irudi
hiperespketralen datu matrizearen egitura $\mathbf{X}$ (M x N x λ) da, non M
eta N-k informazio espaziala ematen duten bitartean λ-k espektroaren
dimentsioak azaltzen dituen (1.3 Irudia ikusi). PLS-Toolbox-aren bitartez,

irudi hiperespektralen osagai askotariko analisia egin eta behin eredua eraikita dugula, MIA-Toolbox-ari esker, analisiaren irudikapen kimikoa sor dezakegu.
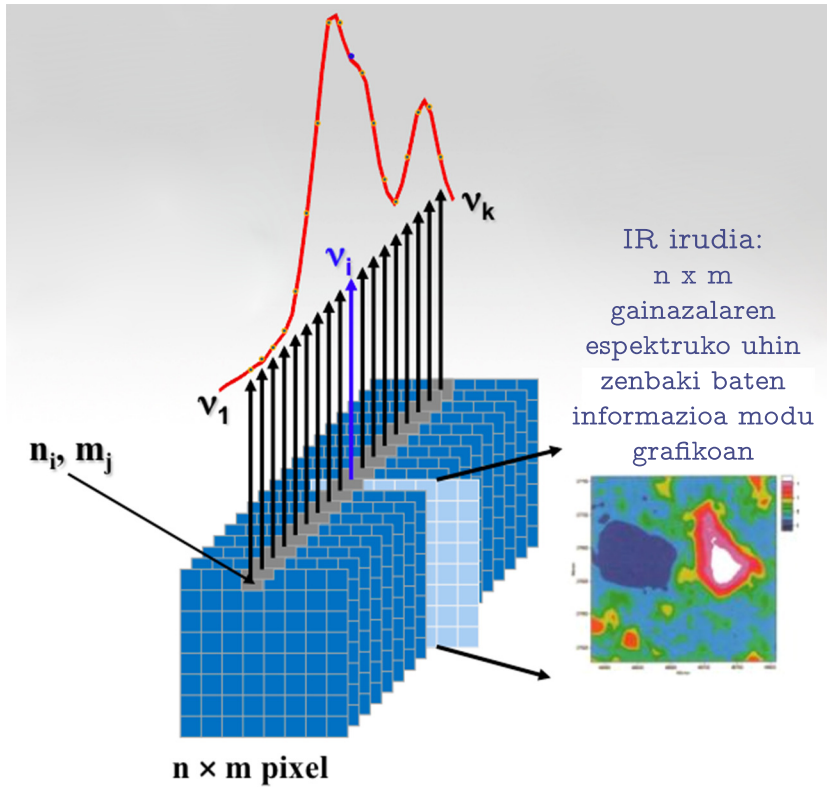
1.3. Irudia: Infragorri irudi hiperespektrak baten egitura.

Datuen aurretratamendua

Datuen aurretratamenduaren helburu nagusiak, datu matrizeko laginak konparagarri bihurtzea eta datuen analisia hobetzea dira. Datuen aurretratamendua erabakigarria da baina kontu handiz egin beharrekoa ere bai [13]. Datuen aurretramenduan pausorik ohikoenak hauek dira: datuen inportazioa, aldagaien aukeraketa, oin-lerroaren zuzenketa,

seinale-zarata erlazioaren hobekuntza, datuen lerrokatzea, aldagaien multzokatzea (*binning*), normalizazioa, eskalatzea, batazbesteko erdiratzea, transformazioak eta gainbegiratutako aurretratamenduak, besteak beste.

(i) Datuen inportazioa Matlabera

Laginen neurketa burutu ondoren, lehenbizi datuak inportatu behar ditugu Matlab-era. Erabilitako instrumentuaren arabera datuen fitxategi-luzapen (mota) jakin batean eskuratzen dira datuak. Matlab-ek baditu inportazeko zenbait funtzio eraikita eta inplementatuta, baina beste kasu batzutan, guk programatu edo idatzi beharko ditugu inportazioa burutzeko gidoiak Matlab-en (*script*). Tesi honetan zehar, Raman eta infragorri irudiak baita erresonantzia magnetiko nuklear (NMR, *nuclear magnetic resonance*) espektroak inportatzeko beharrezkoak ziren gidoiak idatzi behar izan genituen.

(ii) Aldagaien aukeraketa

Tesi honetan jasotako espektroak asko dira, era berean, aldagai kopurua oso handia da. Zorionez badaude seinalerik gabeko guneak edota kanporatu behar diren tarteak espektroetan. Honek aukera ematen digu gune horiek baztertzeko, ereduak errazteko eta datu kopurua gutxitzeko. NMRko espektroetan, adibidez, ur seinalea kendu ahal da 4.7 ppm eta 5.0 ppm tartean. Aurretratamenduaren hasierako pausuetan gomendatzen da tarte hauen ezabapena egitea ondorengo pausuak errazteko eta azkartzeko.

(iii) Oin-lerroaren zuzenketa

Oin-lerroaren aldaketek analisi estatistikoan eta kuantifikazioan eragin oso handia dute eta honen eragina saiheztea oso gomendagarria

da. Oin-lerroaren zuzenketan erabiltzen diren estimazio metodo ohikoenak *detrending* eta minimo karratu asimetrikoen leunketa (*Assymmetric Least Squares Smoothing*, ALS) bidezko estimazioak dira.

Detrending egiterakoan, polinomio bidezko doiketa egin eta laginaren seinaleari polinomio horren kenketa egiten zaio [14]. *Assymmetric Least Squares Smoothing* egiterako orduan, datuen leunketa (*smoothing*) egiten da lehenbizi eta zarata kendutako seinaleen desbiderazio asimetrikoen ponderazioarekin konbinatuz oin-lerroa estimatzen da [15].

Oin-lerroa seinalearen deribatua eginez ere zuzen dezakegu. Izan ere, lehen deribatua egiterakoan oin-lerroaren ordenatu-jatorria ezabatzen da eta bigarren deribatua egiterakoan malda ere ezabatzen da.

(iv) Datuen leunketa edo seinale-zarata erlazioaren hobekuntza

Lagin biologikoen Raman espektroetan adibidez, oso adierazgarria da espektroetan dugun zarata. Hau konposatu biologikoek duten dispertsio (*scattering*) baxuaren ondorioz sortzen da. Seinale-zarata erlazioaren hobekuntza, *smoothing* edo leunketa delako prozedurak aplikatuz lortzen da.

Datuen leunketarako deribatuetan oinarritutako Savitzky-Golay algoritmoa da erabiliena. Deribatuak eginez seinale-zarata erlazioa hobe dezakegu eta doitutako polinomioaren deribatuak kalkulatuz, hau da, Savitzky-Golay algoritmoa aplikatuz, zarata murrizten da. Horretarako leihoaren tamaina eta polinomioaren maila aukeratu beharra dago. Zenbat eta leihoaren tamaina handiagoa izan eta

polinomioaren maila txikiagoa izan, orduan eta datuen leunketa handiagoa lortuko da.

(v) Argiaren dispertsioaren zuzenketa

Argiaren erabilera oinarritzat duten teknika analitiko orok, dispertsioaren edo *scattering*-aren efektuak ditu. Askotan erreferentzia seinale batekiko zuzentzen dira baina badaude zenbait aurretratamendu mota eragin hau zuzentzen dutenak, adibidez, ohiko aldagarritasun normala (*Standard Normal Variate*, SNV), sendoa den aldagarritasun normala (*Robust Normal Variate*, RNV) edo seinale biderkatzailearen zuzenketa (*Multiplicative Signal Correction*, MSC). SNV-ren kasuan adibidez, aldagai bakoitzeko batazbesteko espektroa kalkulatzen da eta berorren desbideratze estandarrarekin zatitzen da (ikusi 1.4 Irudia).
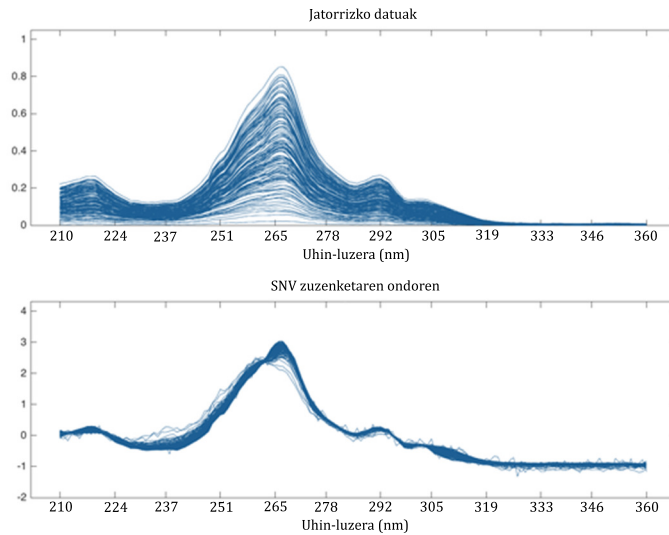
1.4. Irudia: Goian jatorrizko datuak eta behean SNVaren bidez zuzendutakoak.

(vi) Datuen lerrokatzea

Datuen lerrokatzea (*alignment*), NMR espektroen arazo handienetariko bat da, seinaleen posizioan desplazamenduak gertatzen direlako (ikusi 1.5 Irudia). Desplazamentu hauek espektroen artean estandarrak edo jokabide berdineko espektroak aurkitzea zailtzen dute. Bost dira desplazamendu hauen arrazoi nagusiak:

(1) Instrumentazioari dagokienak. Izan ere, gure kasuan, espektro bakoitzaren x ardatza aldatu egiten da espektroz-espektro. Hau da, x ardatzaren desplazamendu kimikoaren lehen balioa espektro bakoitzean aldatu egiten da, balioak parekoak diren arren. Beraz, ardatz bera jarri ahal izateko espektro denei,

espektro baten ardatza kontutan izanda lerrokatuko behar izan genituen gure NMR espektroak.

(2) pH-ren aldaketak.

(3) Gatzen kontzentrazioen aldaketak.

(4) Laginaren kontzentrazio aldaketak (diluzioa).

(5) Ioi jakin batzuen kontzentrazio erlatiboaren aldaketak.

Hala ere, kontuz ibili beharra dugu aldagaien lerrokatzearekin. Kasu batzuetan, seinaleen desplazamenduek konposatu horrengan gertatu den aldaketa bat adierazi ahal dutelako.

NMR-ko espektroen lerrokatzerako 0 ppm adierazten duten estandarrak erabili genituen. Erabili zen disolbatzailearen arabera patroi mota bat aukeratu zen. Kloroformo deuteratuaren kasuan tetrametilsilanoa (TMS) erabili genuen eta ur deuteratuaren kasuan, ostera, azido (trimetilsilil)propinoikoa-2,2,3,3,-d4 (TMSPA) erabili genuen. Beraz, zeroarekiko zuzenduz, desplazamendu globalak zuzen ditzakegu baina ez da nahikoa desplazamendu lokalizatuak zuzentzeko.

Seinale bakoitzak jasan ditzakeen desplazamenduak zuzentzeko erabilienak diren lerrokatze metodoak hurrengoak dira: tarteka korrelazionatutako desplazamenduan (icoshift, *interval correlated shifting*) oinarritutako zuzenketa [16], korrelazioaren optimizazio moldaketa (COW, *Correlation Optimized Warping*) [17] eta taldeetan oinarritutako seinaleen lerrokatzea (CluPA, *Cluster-based Peak Alignment*) [18].

Datuen lerrokatze metodoek bi muga nagusi dituzte. Lehena, arazo teknikoekin guztiz erlazionatuta dago, erabiltzen diren algoritmoak

geldoak direlako eta beharrezkoa den optimizazioa egitea zaila delako. Bigarren muga, datuetan ditugun artefaktuak dira, hau da, oinlerroaren eraginak edota zarata maila altuek lerrokatze metodo gehienen errendimendua okertzen dute.
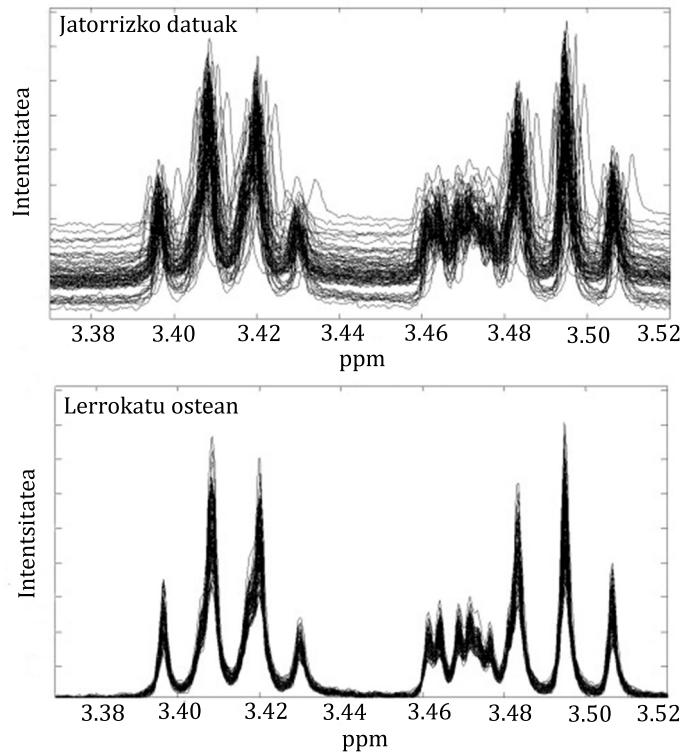
1.5. Irudia: Goian jatorrizko datuak eta behean lerrokatutako datuak adierazi dira.

(vii) Aldagaien multzokatzea

Aldagaien multzokatzearen (*binning*) bitartez datu matrizearen dimentsioen murrizketa lortu nahi da (ikusi 1.6 Irudia). Matrize datua segmentutan (*bin* edo *buckets* deitzen dira ingelesez) zatitzen

da eta segmentu bakoitzari dagokion azalera kalkulatzen da. Behin multzo bakoitzeko integrazioa egin den, dimentsionaltasun txikiagoa izango duen espektro berria eraikitzen da.

Bi estrategia aurki ditzakegu aldagaien multzokatze honetan. Batetik, segmentu finkoen estrategia dugu. Adibidez, 0.04 ppm tartea ezarri eta tarte horietan integratutako balioekin espektro berria eratuko da. Estrategia honen bitartez ordea, seinaleen gailurrak tartetik ebakiz gero, seinalean aldaketak sor ditzakegu [19]. Horrelako arazoak ekiditzeko, tarte finkoetan oinarritzen ez diren metodoak daude. Aurki ditzakegun hainbat metodoren artean moldaera-adimendun multzokatzea (adaptative-intelligent binning, AI-binning) [20], multzokatze Gaussiarra (*Gaussian binning*) [21], uhin-eraldaketan oinarritutako moldatutako multzokatzea (*adaptive binning using wavelet transform*) [22] eta multzokatze dinamikoa (*Dynamic adaptive binning*) [23] ditugu.

Jatorrizko datuak

Aldagaiak multzokatu ostean
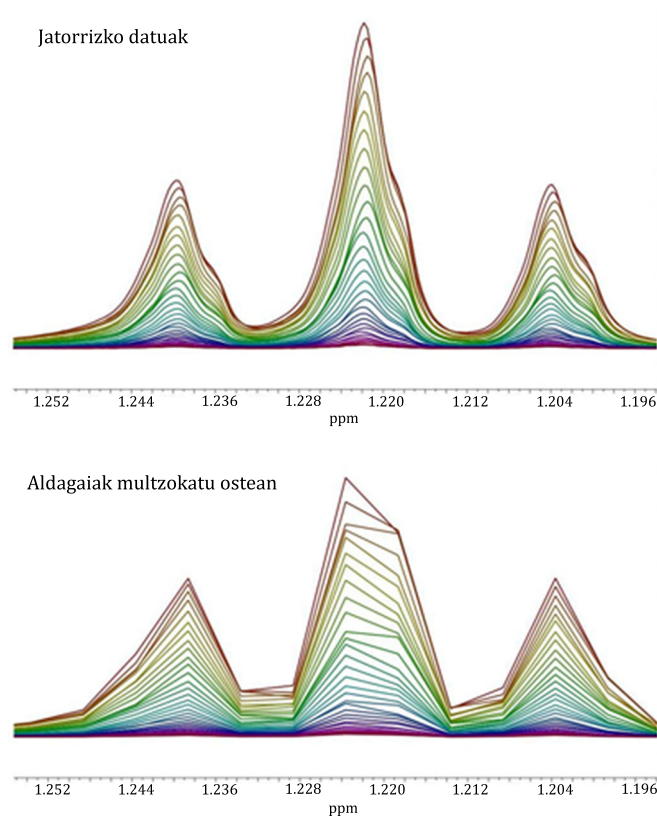
1.6. Irudia: Goian jatorrizko datuak eta behean aldagaiak multzokatu (*binning*) ondorengo datuak adierazi dira.

(viii) **Normalizazioa, eskalatzea, batezbesteko erdiratzea eta gainerako transformazioak**

Datuen aurretratamenduko pausu honen helburua, laginen arteko kontzentrazio orokorren aldaketak kontutan hartzea eta laginak elkarren artean konparagarri bihurtzea da (ikusi 1.7 Irudia). Analisiaren helburuaren araberakoa izango da kontzentrazio globalaren aldakortasunaren eragina kontutan hartu nahi izatea edo ez. Diluzio faktorearen zuzenketa balitz bezala erabil daiteke.

Normalizazioa egiterakoan, orokorrean balio konstante batekin biderkatzen da lerro bakoitza (lagin espektro bakoitza gure kasuan). Konstante hau era askotan kalkula daiteke. Ohiko metodoa integrazioaren bidezko normalizazioa da. Nahi izanez gero, espektro osoaren integrazioaren balioarekin normaliza daiteke edota konposatu jakin baten kontzentrazioa konstantea izaten dela jakinez gero, horrekiko normaliza daiteke.

Datuak eskalatzerakoan, NMR bidezko metabolomikako neurketetan adibidez, metabolito batzuen kontzentrazioa beste batzuena baino askoz handiagoa izaten da eta PCA edo PLS bezalako analisietan metabolito hauek eragin handiagoa izango dute. Metabolito guztiek pisu bera izan dezaten nahi bada, datuak eskalatu behar dira.

Datuak eskalatzerako orduan, batazbesteko erdiratzea, auto-eskalatzea, Paretoren printzipioan oinarritutako eskalatzea, tarte jakin bateko eskalatzea (*range scaling*), aldakortasunaren egonkortasunean oinarritutako eskalatzea (*VAST scaling*) eta eskalatze mailakatua (*level scaling*) bezalako baliabideak ditugu [24].

Batazbesteko erdiratzea (*mean centering*) egiterakoan, kontzentrazio altuan eta baxuan agertzen diren seinaleen aldakortasunak zeroren inguruko balioetara doitzen dira, erdian seinale bakoitzaren batazbestekoa geratzen delarik. Batazbesteko erdiratzea beste normalizazio, eskalatze eta transformazioekin batera erabiltzen da [25].

Eskalatzearen aukeraketan kontuz ibili beharra dago. Adibidez, NMRko espektroak auto-eskalatuko bagenitu, zarataren eragina ereduan oso handia izango litzateke eta ez zaigu hori interesatzen.

Hain zuzen ere, datuak auto-eskalatzerako orduan aldagai guztiei ematen zaie garrantzi bera, aldagai guztien desbideratze estandarra bat bihurtzen delako. Badaude tarteko eskalatze metodoak, Paretoren printzipioan oinarritutako eskalatzea adibidez. Kasu honetan, desbideratze estandarraren ordez desbideratze estandarraren erro karratua erabiltzen da [25].

Eskalatzeaz gain beste transformazio mota batzuk aplika ditzakegu, logaritmoa, Box-Cox eraldaketa edo erro karratua adibidez. Mota honetako eraldaketak sasi-eskalatze bezala ezagutzen dira, balio handiko seinaleen garrantzia murrizteko oso erabilgarriak baitira. Horretaz gain, logaritmoaren erabilpenak desbideratze estandar erlatiboa konstante deneko kasuetan zoriozko zararaten dispertsioa (bariantza gabezia) ere zuzentzen laguntzen du [25].
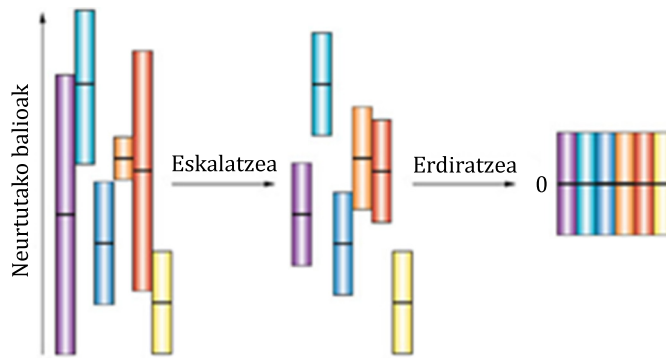
1.7. Irudia: Datuen eskalatzea eta batazbesteko erdiratzea.

(ix) Gainbegiratutako aurretratamendua

Gainbegiratutako aurretratamendu ezagunena seinaleen zuzenketa ortogonala (*orthogonal signal correction*, OSC) da [26] eta PLS-DA bezalako analisi motan oso erabilia da. PLS bezalako metodoetan X

matrizeak (espektroek) eta bere aldakortasun sistematikoek eragin zuzena dute, ez ordea Y matrizearen erantzunek (kontzentrazioak adibidez). OSC-ren bitartez, X matrizearen aldakortasuna saihestu nahi da eta Y erantzunarekin erlazionatuta ez dauden aldagaiak ezabatzen dira. OSC-k behin eta berriz erakutsi du PLS modeluen iragartzeko ahalmenean hobekuntzak ekartzen dituela, eta ereduetako aldagaiak murriztu egiten dituela, interpretazioa erraztuz.

OSC algoritmoak, lehenbizi, X matrizearen osagai askotariko analisiko lehen osagaia identifikatzen du. Ondoren, *loading*-a biratu egiten du *score*-ak Y blokearekiko ortogonalak izateko. Orduan, PLS eredua eraikitzen du eta bertan X matrizetik *score* ortogonal hauek aurresaten ditu. Era honetan, zenbait artefakturen eragina ere, oinlerroa adibidez, ezabatzeko gai gara.

Osagai nagusien analisia (PCA)

PCA gainbegiratu gabeko analisi mota bat da eta kimiometriako lanabes erabiliena dela esan genezake. PCAk datu multidimentsionalak aztertu eta bariantza maximoa azaltzen duten faktoreak adierazten ditu. Faktore horiek osagai nagusiak deitzen dira (*Principal Components*, PC's). PC bakoitza aldagai originalen konbinazio lineal bat da, eta PC guztien baturak bariantza maximoa azaltzen du (bigarrenak lehenengoak azaltzen ez duena azaltzen baitu). Beraz, PCA analisitik lortutako *score* eta *loadings* direlakoak (ikusi 1.8 Irudia) matrize originalaren interpretazioa errazten dute.

Score-en irudikapen grafikoan, lagin bakoitzaren koordenatu berriak eskuratzen ditugu, eta puntu bakoitzak espektro bat adierazten du gure kasuan. Beraz, espektro guztien laburpena da.

Loading-en irudikapen grafikoan, ereduan eragin handiena duten aldagaiak identifika ditzakegu. *Score*-ak identifikatzeko *loading*-ak erabiliko dira, *loading*-ek zehazten baitute *score*-en kokapena, eta ondorioz, laginen taldekatzea.
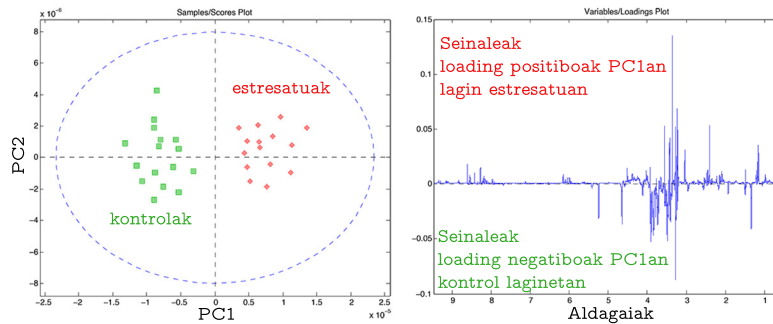
1.8. Irudia: PCA analisi baten *score*-ak, non estresatutako eta kontroleko laginak multzokatzen diren eta *loading*-a, non taldekatzea ezaugarritzen dituzten seinaleak identifikatzen diren.

Karratu txiki partzialen erregresioan oinarritutako diskriminazio analisia (PLS-DA)

PLS-DA gainbegiratutako teknika kimiometrikoa da. PLSa X datu matrizea Y erantzun matrizearekin erlazionatzen duen erregresio teknika da. PLS-DA ordea, PLS erregresio teknikaren alternatiba bat da. PLS-DAn PCAren kasuan gertatzen den modu beretsuan, datu matrize originala, jatorrizko aldagaien konbinazio linealak diren aldagai latenteekin azaltzen da (PCak edo LVak).

PLS-DA, PLS erregresio bat da baina erantzuna aldagai kategorikoa da, lagin bakotzaren klasea, guk aurrez adierazi dioguna. Ondorioz, neurtutako aldagaietatik lortuko diren PLSko osagaiek bi konpromiso bete behar

dituzte: erantzunak (klaseak) iragartzeko gai izan behar dira eta klase bakoitzeko laginen neurtutako aldagai guztiak azaltzeko gai izan behar dira.

Eredu sinplifikatuago bat lortzeko asmoz, OPLS-DA erabiltzen da, hau da, OSC zuzenketa aplikatutako PLS-DA da. Azken finean, OSC zuzenketan erantzunak edo klaseak azaltzeko balio ez dituzten aldagaiak baztertzen ditu eredua eraikitzean. Orduan, erantzunekin erlaziorik ez dituzten aldagaiak zarata edo laginen arteko diferentziak eragindako ezberdintasunak izan daitezke. OPLS-DA asko erabiltzen da NMR metabolomikan, adibidez, adina, sexua, dieta, etab. bezalako faktoreen eragina murrizteko.

PLS-DA eta OPLS-DA analisietatik VIPak (*Variables Importance on Partial Least Squares (PLS) projections*) eskuratzen dira. Izan ere, analisi hauetako aldagai garrantzitsuenen proiekzioak dira. VIP balioak, PLSko ereduan aldagaiek duten pisuaren eta azaltzen duten bariantzaren adierazpena dira. VIPak aztertzerako orduan, 1 baino balio altuagoa duten balioak hartzen dira kontutan [27].

Aldagai askotariko kurben bereizmena - txandakako karratu txikiak (MCR-ALS)

MCR-ALS analisia oso erabilgarria da datu hiperespektralen analisian, hau da, gainazal bat ezaugarritzen duten espektroen azterketan eta zenbait konposaturen distribuzioa adierazteko. MCR-ALS analisiak ere, PCAk bezala, modelo matematiko bi-linearra erabiltzen du baina MCRko emaitzek interpretazio errezagoa eskaitzen digute. MCR-ALS analisiaren bitartez aztertutako gainazalean dauden osagai puruak lortuko ditugu, irudiko espektroetatik lortutako konbinazio linealak izango direnak

eta horrekin batera, neurtutako puntu edo pixel bakoitzean duten ugaritasunaren informazioa (kontzentrazioa) lortuko da [28].

MCR-ALS analisirako matrize hiru dimentsionalak, bi dimentsioko matrize bihurtu beharko ditugu eta behin analsiaren emaitzak izanda, puntu bakoitzean osagai bakoitzaren kontzentrazioa irudikatu ahal izango dugu konposizioaren berri izateko. Analisiaren lehen pausua, hasierako osagai nagusi kopurua zehaztea da, balio singularren deskoposizioa (SVD, *singular value decomposition*) eginez. Behin hasierako osagai puru kopurua estimatuta izan den, MCR-ALS analisia egiten da eta analisian zehar iteratiboki lantzen ditu aukeratutako ALS edo arauak espektroendako baita kontzentrazioendako: zenbaki ez-negatiboak, modalitate bakarra (*unimodality*), mugak (*closure*), e.a. Behin prozesua bukatuta, optimizatutako osagai puruak eta kontzentrazioak eskuratuko dira.
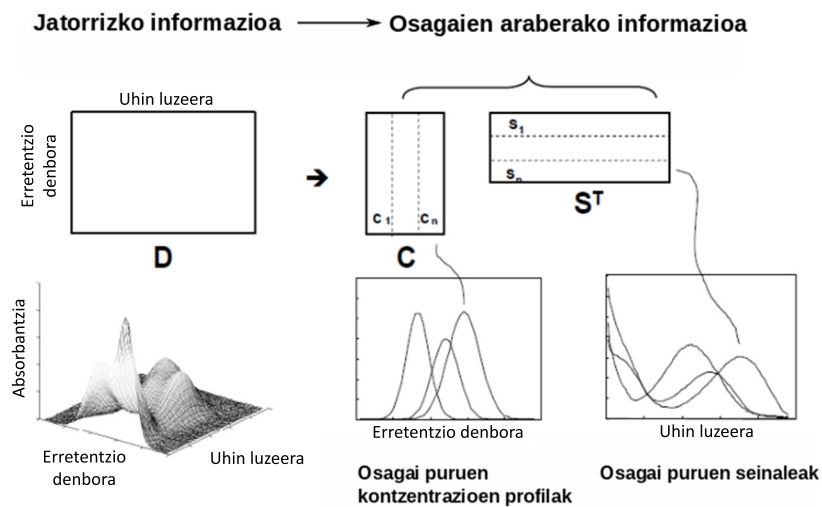
1.9. Irudia: MCR analisia.

Aldagai askotariko irudi analisia (MIA)

Irudi analisia gaur egun, gero eta garrantzitsuago bilakatzen ari da. Gainazal bateko hainbat konposaturen distribuzioa jakiteak arlo askotan kritiko bihurtu da, biologian, geologian, kimikan, e.a. [29]. Gure kasuan, lagin biologikoen karakterizazioa egiteko beharrezkoa izango dugu irudi analisia egitea, era askotariko ezaugarri biokimikoak dituzten azalerak identifikatu ahal izateko. Horretarako Matlab-ek baliabide oso interesgarria dauka, MIA-Toolbox-a hain zuzuen ere. Komando sinple bati esker, gure hiru dimentsiotako matrizearen analisi kimiometrikoaren ondorengo *score*-en irudikapena ikus baitezakegu gainazal eran. Horretarako Matlab-en, gure matrizea komando honekin moldatu besterik ez dugu egin behar: myimage = buildimage(data ,[1 2], 1, 'myNewImage'). Ondoren PCA eta PLS-DA bezalako metodoen emaitzak era adierazgarri eta erabilgarri batean irudikatzeko gai izango gara.

Ereduen berrezpena

Eredu estadistikoen berrezpenak, ereduetatik ondorioztatutako emaitzei beharrezkoa duten fidagarritasuna eskeitzen die. Modu honetan, zoriz lortutako ereduak baztertuko dira. Beraz, beharrezkoa da ereduak duen iragarpen ahalmena aztertzea eta balioztatzea.

Eredu bat berrezteko hainbat modu ditugu. Berrezpen gurutzatua (*Cross-validation*, CV) eta berrezpen gurutzatu bikoitza (*double cross-validation*) dira erabilienak. Permutazioa ere berrezteko beste hurbilketa bat dugu. Hala ere, eredutik kanpo utzitako lagin multzoa erabiltzea da iragarpen ahalmena frogatzeko erarik fidagarriena [30].

Eredua eraikitzeko eta berrezteko erabiliko diren datuak, multzo bitan banatzeko, algoritmo bikoitza (*Duplex algorithm*), Kennard-eta-Stone edo

zorizko aukeraketa (*random selection*) erabiltzen dira. Hala ere, berrezpena datu matrize berri batekin egin daiteke, esperimentu independente bat erabiliz adibidez. Era honetako berrezpena egokiena litzateke, baina esperimentazioaren kostua asko igotzen denez ez da asko erabiltzen [30].

Gure kasuan, berrezpen gurutzatua erabiliko genuen ereduen balidazioa egiteko. Berrezpen gurutzatuak bi funtzio erabakigarri betetzen ditu kimiometrian:

(i) Ereduaren konplexutasun optimoa ebaluatzen du.

(ii) Ereduaren iragarpen errendimendua estimatzen du.

Berrezpen gurutzatuaren emaitzen artean, berrezpen gurutzatuaren errore karratuaren batazbestearen errore (RMSECV, *Root Mean Square Error of Cross-validation*) balioa dugu. Balio honek, ereduaren iragarpen ahalmenaren eta egokitasunaren berri emango digu.

Matlab-eko PLS-Toolbox erabiliz berrezpen gurutzatua egiteko bost prozedura ditugu aukeran: veneziar leiho-sareta (*venetian blinds*), aldameneko blokeak (*contiguous blocks*), zorizko azpimultzoak (*random subsets*), bat-kanpora-atera (*leave-one-out*) eta pertsonalizatua (*custom*).

Guk veneziar leiho sareta berrezpen gurutzatua erabili genuen, erabilterreza eta sinplea baita. Gainera, taldeen arteko iragarpenerako gomendagarria da Eigenvetor-en arabera.

Erreferentziak

[1] M. Grasserbauer. Competition "analytical chemistry — today's definition and interpretation". *Fresenius J. Anal. Chem.*, 341(9):A9, 1991.

[2] W. Ostwald. *Wissenchafichen grundlagen der analytischen chemie.* Leipzig, 1894.

[3] S. Arribas F. Burriel and F. Lucena. *Química analítica cualitativa.* Madrid, 1964.

[4] H. A. Laitinen. Analytical chemistry in a changing world. *Anal. Chem.*, 52(6):605A–609A, 1980.

[5] B.G.M. Vandeginste. Optimization of analytical information. *TrAC*, 1(9):210–215, 1982.

[6] Miguel Valcárcel. A modern definition of analytical chemistry. *TrAC*, 16(3):124–131, 1997.

[7] E. Heftmann. *Chromatography-A laboratory handbook of chromatographic and electrophoreric methods, tercera edición.* Van Nostrand, Reinhold, Nueva York, 1975.

39

[8] D.T. Burns and H. Deelstra. Analytical chemistry in belgium: an historical overview. *Microchim. Acta*, 161(1):41–66, 2008.

[9] U.E. Spiechiger-Keller. What is that analytical chemists do? *Fresenius J. Anal. Chem.*, p 283–284, 2001.

[10] O.Posada-Ureta, M. Olivares, L. Zaton, A. Delgado, A. Prieto, A. Vallejo, A. Paschke and N. Etxebarria. Uptake calibration of polymer-based passive samplers for monitoring priority and emerging organic non-polar pollutants in WWTP effluents. *Anal. Bioanal. Chem.*, 408(12):3165–3175, 2016.

[11] H. Ziarrusta, M. Olivares, A. Delgado, O. Posada-Ureta, O. Zuloaga and N. Etxebarria. Multiscreening determination of organic pollutants in molluscs using matrix solid phase dispersion. *J. Chromatogr. A*, 1391:18–30, 2015.

[12] K. H. Esbensen. *An introduction to multivariate data analysis and experimental design, 5th edition.* CAMO ASA, 2001.

[13] T.M.D. Ebbels, J.C. Lindon and M. Coen. Processing and modeling of nuclear magnetic resonance (NMR) metabolic profiles. *Methods Mol. Biol.*, 708:365–388, 2011.

[14] R.J. Barnes, M.S. Dhanoa and S.J. Lister. Standard normal variate transformation and de-trending of near-infrared diffuse reflectance spectra. *Appl. Spectrosc.*, 43(5):772–777, 1989.

[15] P.H.C. Eilers. Parametric time warping. *Anal. Chem.*, 76(2):404–411, 2004.

[16] F. Savorani, G. Tomasi and S.B. Engelsen. icoshift: A versatile tool for the rapid alignment of 1D NMR spectra. *J. Magn. Reson.*, 202(2):190–202, 2010.

[17] T.Skov, F. van den Berg, G.Tomasi and R. Bro. Automated alignment of chromatographic data. *Journal of Chemometrics*, 20(11-12):484–497, 2006.

[18] T.N. Vu, D. Valkenborg, K. Smets, K.A. Verwaest, R. Dommisse, F. Lemière, A.Verschoren, B. Goethals and K. Laukens. An integrated workflow for robust alignment and simplified quantitative analysis of NMR spectrometry data. *BMC Bioinform.*, 12(1):1–14, 2011.

[19] J.L. Izquierdo-Garcia, P. Villa, A. Kyriazis, L. del Puerto-Nevado, S. Perez-Rial, I. Rodriguez, N. Hernandez and J. Ruiz-Cabello. Descriptive review of current NMR-based metabolomic data analysis packages. *Prog. Nucl. Magn. Reson. Spectrosc.*, 59(3):263–270, 2011.

[20] T. De Meyer, D. Sinnaeve, B. Van Gasse, E. Tsiporkova, E.R Rietzschel, M.L De Buyzere, T. C Gillebert, S. Bekaert, J.C Martins and W. Van Criekinge. NMR-based characterization of metabolic alterations in hypertension using an adaptive, intelligent binning algorithm. *Anal. Chem.*, 80(10):3783–3790, 2008.

[21] P.E. Anderson, N.V. Reo, N.J. DelRaso, T.E. Doom and M.L. Raymer. Gaussian binning: a new kernel-based method for processing NMR spectroscopic data for metabolomics. *Metabolomics*, 4(3):261–272, 2008.

[22] R.A. Davis, A.J. Charlton, J. Godward, S.A. Jones, M. Harrison and J.C. Wilson. Adaptive binning: An improved binning method

for metabolomics data using the undecimated wavelet transform. *Chemometr. Intell. Lab.*, 85(1):144–154, 2007.

[23] P.E. Anderson, D.A. Mahle, T.E. Doom, N.V. Reo, N.J. DelRaso and M.L. Raymer. Dynamic adaptive binning: an improved quantification technique for NMR spectroscopic data. *Metabolomics*, 7(2):179–190, 2011.

[24] A. Craig, O. Cloarec, E. Holmes, J.K. Nicholson and J.C. Lindon. Scaling and normalization effects in NMR spectroscopic metabonomic data sets. *Anal. Chem.*, 78(7):2262–2267, 2006.

[25] R.A van den Berg, H.C.J. Hoefsloot, J.A. Westerhuis, A.K. Smilde and M.J. van der Werf. Centering, scaling, and transformations: improving the biological information content of metabolomics data. *BMC Genomics*, 7:142, 2006.

[26] S. Wold, H. Antti, F. Lindgren and J. Öhman. Orthogonal signal correction of near-infrared spectra. *Chemometr. Intell. Lab.*, 44(1–2):175–185, 1998.

[27] U.G. Indahl, K. Hovde Liland, and T. Næs. Canonical partial least squares—a unified PLS approach to classification and regression problems. *J. Chemometrics*, 23(9):495–504, 2009.

[28] J. Felten, H. Hall, J. Jaumot, R. Tauler, A. de Juan and A. Gorzsás. Vibrational spectroscopic image analysis of biological material using multivariate curve resolution–alternating least squares (MCR-ALS). *Nat. Protocols*, 10(2):217–240, 2015.

[29] J.M. Prats-Montalbán, A. de Juan, and A. Ferrer. Multivariate image analysis: A review with applications. *Chemometr. Intell. Lab.*, 107(1):1–23, 2011.

[30] A. Smolinska, L. Blanchet, L.M.C. Buydens and S.S. Wijmenga. NMR and pattern recognition methods in metabolomics: From data acquisition to biomarker discovery: A review. *Anal. Chim. Acta*, 750:82–97, 2012.

Ingurumen metabolomika

Chapter 2

Ingurumen metabolomika

2.1 Sarrera

2.1.1 Ingurumena eta mikrokutsatzaile organiko hidrofobikoak

Airea, ura, lurra eta biota bezalako ingurumen-konpartimentuetan, mota askotariko kutsatzaile organikoak akumulatzen dira. Kutsatzaile hauek jatorri antropogenikoa dute orokorrean: industriako prozesuak, jakien industria, farmakoak, kosmetikoak, e.a. Hain zuzen ere, gizartearen neurri gabeko kontsumoak eta hondakinen kudeaketa desegokiak ingurumen arazo larri bat sortu du. Kutsatzaile hauek ingurumen-konpartimentuetan aztarna mailan aurkitu arren, ingurumen, animali eta gizakiengan eragin ditzaketen ondorioen inguruko ardura asko handitu da azken urteotan [1,2].

Kutsatzaile organiko iraunkorren (*Persistent Organic Pollutants*, POPs) Estokolmoko hitzarmena, giza eta ingurumen osasuna; ingurumenean iraunkorrak, munduan zehar hedatu, gantz-ehunetan metatu eta izakiendako baita ingurumenerako kaltegarriak diren kutsatzaileez

babesteko itun globala da. POP esposizioak osasun arazo larriak eragin ditzake: minbizia, jaiotza-akatsak, ugalketa eta disfuntzio immunologikoa, gaixotasunen aurrean suszeptibilitatea eta nerbio-sistemako kalteak. Arazo global honen aurrean 2001.urtean onartu zen Estokolmoko hitzarmena, eta 2004.urtean jarri zen indarrean (http://chm.pops.int).

Hasiera batean Estokolmoko hitzarmenak hiru motatako 12 POP aintzatetsi zituzten:

1. Pestizidak: aldrin, klordanoa, DDT, dieldrin, endrin, heptakloroa, hexaklorobentzenoa, mirex, toxafeneoa.

2. Industriako kimikoak: hexaklorobentzenoa, bifenilo poliklorinatuak (PCB).

3. Eratorriak: hexaklorobentzenoa, poliklorinatutako dibentzo-p-dioxinak eta poliklorinatutako dibentzofuranoak (PCDD/PCDF) eta PCBak.

Denbora aurrera joan den einean, gero eta konposatu gehiago aintzakotzat hartu dira eta beste zenbait gainbegiratzeko zerrendan daude.

Arazoaren larritasunaren eta kezkaren erantzun gisa kutsatzaileen erregulaziorako araudiak sortu ziren Europar Batasunean batez ere kutsatzaileen kontrolerako eta prenbentziorako. Ur-zuzentaraua (*European Water Framework Directive* , WFD, 2013/39/EU) eta itsas-estrategiaren zuzentaraua (*Marine Strategy Directive*, MSD, 2008/56/ECC) araudi berrienek ingurumenerako kalitate estandarrak ezartzen dituzte.

Azken bi hamarkadetan, kutsatzaile kimikoen azterketak kutsatzaile organiko iraunkorren (POPs) analisira mugatu dira [2–4]. POPen artean, pestizida organokloratuak, hidrokarburo polizikliko aromatikoak (PAH) eta bifenil polikloratuak (PCB) aurki ditzakegu. WFDan ingurumenerako

2.1. Irudia: Uraren kutsadura iturrien irudikapena.

kalitate estandarrak betetzeko kutsatzaileen kontzentrazio mailen mugak hainbat konpartimentutan adierazten dira. Gure gizartean gero eta material eta konposatu berri gehiago sintetizatzen ditugu, industrian, kosmetikoetan, farmako berriak, hormonak, detergenteak, e.a. eta ingurumenera isurtzen dira kutsatzaileak (ikus 2.1 Irudia). Horren eraginez, analisirako eta erauzketarako teknikak berriak garatu behar izan ditugu, gorabideko kutsatzaile organiko (*Emerging Organic Compounds*, EOCs) eta potentzialki arriskutsuak izan daitezkeenak aztertzeko [5, 6]. EOC konposatu hauen kontzentrazioak $ng\,L^{-1}$ edo $\mu g\,L^{-1}$ mailan aurkitzen dira.

Gure lan taldean zenbait konposatu organiko hidrofobikoren eraginak aztertu dira: alkilfenolak, konposatu organofosforatuak, konposatu organokloratuak, musketa polizilklikoak eta ftalatoak (ikusi 2.1 Taula, [19]).

(i) Alkilfenolak

Alkilfenol etoxilatoak (*Alkylphenol ethoxylates*, APEOs) surfaktante ez-ionikoak dira eta detergente edota agente dispertsatzaile bezala oso erabiliak dira [7]. Araztegietan gertatzen den kutsatzaile hauen degradazioaren produktuak are kutsatzaileagoak dira, horien artean noninfenolak (*nonylphenols*, NP) eta oktilfenolak (*octylphenols*, OPs). Hala ere, hauek ere plastifikatzaileen eta detergenteen ekoizpenean erabiltzen dira [8]. Konposatu hauek endokrino disruptiboak dira, hau da, gizakien baita animalien ugalketan eragin negatiboak sortzen dituzte (intersex) [9]. Alkilfenolak WFD-ko POP zerrenden barruan daude eta hauen kontzentrazio mugak hauek dira [10]:

(i) 4-nonilfenola (*4-nonylphenol*,4nOP), itsas-uretan eta gainazaleko uretan, $0.3\,\mu g\,L^{-1}$ eta $2\,\mu g\,L^{-1}$ hurrenez-hurren (urteko batezbestekoa).

(ii) 4-tert-oktilfenola (*4-tert-octylphenol*, 4tOP), itsas-uretan eta gainazaleko uretan, $0.01\,\mu g\,L^{-1}$ eta $0.1\,\mu g\,L^{-1}$ hurrenez-hurren (urteko batezbestekoa).

(ii) Konposatu organofosforatuak

Nekazaritza munduan konposatu organofosforatuak pestizida eta intsektizida moduan oso erabiliak izan dira, erabilterrazak eta eraginkorrak zirelako. Talde honetan klorpirifos (*chlorpyrifos*, Clor), klorfenbinfos (*chlorfenvinphos*, Clorf), atrazina (*atrazine*), malation (*malathion*), paration (*parathion*) eta diazinon moduko konposatuak sailkatzen dira. Uretan aurkezten duten disolbagarritasun altuak, ingurumen konpartimentuetan aurkitzeko aukerak handitzen ditu. Izan ere, ingurumenean egonkorrak dira eta efektu neurotoxikoak

eragiten dituztela uste da [11]. Zenbait ikerketa taldek jadanik konposatu hauen determinazioan eta monitorizazioan lan egiten dute, ikerketa lan batean, adibidez, lur-azpiko uretan neurtu dituzte eta Clorf-en kasuan $0.1 \, \mu\text{g} \, \text{L}^{-1}$-ko balioetatik gora agertzen dira, hau da, ingurmeneko kalitate estandarrak gainditzen ditu [12].

(iii) Konposatu organokloratuak

Hauek ere nekazaritza munduan erabiltzen diren pestizidak dira eta aspalditik ezagunak dira ingurumenean baita giza-osasunean eragin ditzakeen kalteak [13]: kartzinogenesia, immunotoxikotasuna, neurotoxikotasuna, ugal-zikloan eraginak, arnasketa arazoak, e.a. [14].

Konposatu organokloratuak; lindano, hexakloroziklohexanoa (HCH), dikloro difenil trikloroetanoa (DDT) eta eratorriak adibidez, POPen zerrendan azaltzen dira, ingurumeneko konpartimenduetan duen eraginarengatik, akumulatzeko gaitasunarengatik eta kate trofikoan duen biomagnifikazioarengatik [15]. Euren erabilera asko murriztu bada ere, oraindik aurkitzen dira gure lur eta uretan, hain zuzen ere, azaltzen duten iraukortasun eta bioakumulazioarengatik.

(iv) Musketa poliziklikoak

Zaintza pertsonalerako produktuen (*personal care products*, PCPs) ekoizpenak gorakada amaigabe bat bizitzen ari da eta musk poliziklikoak PCP hauen ohiko osagaia izaten dira. PCP-en taldea, kosmetikoak, detergenteak, perfumeak, txanpuak, garbiketarako produktuak eta abar amaigabe batek osatzen dute.

Zenbait ikerkuntza lanetan musketak ingurumenean iraukorrak, bioakumulazio handikoak eta disruptore endokrino bezala jokatzen

dutela uste da [16]. Adibide ezagunenak, galaxolide (HHCB), tonalide (AHTN), zelestolide (*celestolide*, ADBI) eta kasmeran (*cashmeran*, DPMI) dira. HHCB eta AHTN dira merkatutako musketa fragantzien %95a [17].

(v) Ftalatoak

Ftalatoen aplikazioak nonahi agertzen dira: industrian, plastifikatzaile moduan, kosmetikan, e.a. Ftalatoen %87a PVCa ekoizteko erabiltzen da mundu mailan eta eskala handian. Beraz, ez da arraroa ftalatoen kontzentrazio altuak aurkitzea naturan.

Zenbait ftalatoren disolbagarritasuna uretan baxua da, oktanol-ur partizio koefiziente altua dute eta hauek esekiduretan dauden materia partikulatuan edota sedimentutan kontzentratzen dira.

Kate laburreko ftalatoak, dimetil ftalatoa (*dimethyl phthalate*, DMP), dietil ftalato (*diethyl phthalate*, DEP) edota dibutil ftalatoak (*dibutyl phthalate*, DBP), biodegradazio prozesuak jasaten dituzte gainazaleko ur oxigenatuetan. Kate luzekoak ordean, dioktil ftalatoak (*di-octyl phthalate*, DOP) bezalakoak, iraukorragoak dira sendimentuetan.

DMP eta DEPak ez dute bioakumulatzeko joera handirik, BBP (*benzyl butyl phthalate*, BBP) eta DBPk joera handiago aurkezten dute. Hala ere, 2-etilhexil ftalatoak (*bis(2-ethylhexyl)-phthalate*, DEHP), biziklohexil ftalatoak (*dicyclohexyl phthalate*, DCHP), Bi-n-oktil ftalatoak (*Di-n-octyl phthalate*, DNOP) eta biisooktil ftalatoek (*di-isooctyl phthalate*, DIOP) adibidez sedimentu eta biotarekiko afinitate handiagoa dute.

Ftalatoek sedimentuetan bizi diren organismoengan eragin kaltegarria izateaz gain disruptore endokrino moduan ere jokatzen dute [18].

2.1.2   Lagin biltze pasiboa

Lagin biltze pasiboa bi helburu nagusi dituen monitorizazio lanabes berritzailea da:

(i) Denboran zeharreko kutsatzaileen kontzentrazio aldaketak neurtzea.

(ii) Zentinela lana egitea, hau da, bieskuragarri dagoen kontzentrazioaren erakusle izatea. Adibidez, muskuilua bezalako zentinela batek akumulatuko lukeena akumulatuz.

Lagin biltze pasiboaren bitartez monitorizazio baliabide sendo, fidagarri eta merkea lortzea espero da. Baina egia da, oraindik, metodo honen heldutasun puntura heltzeko lanean jarraitu beharra dagoela emaitzak konparagarriak izateko herrialde ezberdinetako laborategi eta laginketetan.

Lagin biltze pasiboan, lagin biltze pasiboko gailuak uretan dauden analitoak fluxu aske baten baitan jasotzen ditu. Prozesu honetan, bi medioen, uretan eta lagin biltze pasiboko materialaren arteko ezaugarriek berebiziko funtzioa jokatuko dute. Akumulazio zinetika hau ekuazio honen bitartez azal daiteke:

$$Cs(t) = Cw\frac{k1}{k2}(1 - e^{-k_2 t}) \qquad (2.1)$$

non Cs, denbora jakin batean (t) lagin biltze pasiborako materialak jaso duen analitoaren kontzentrazioa den. Cw, uraren kontzentrazioa momentu horretan eta k_1 eta k_2 akumulazio eta askapen abiadura konstanteak dira hurrenez-hurren.

2.1. Taula: Esperimentuetako kutsatzaileen zerrenda eta dagokien log K_{ow} eta uretan duten disolbagarritasun balioa.

Kutsatzailea	CAS zenb.	log K_{ow}	disolbag. (mg/L)
Alkilfenolak			
4tOP	140-66-9	5.28	4.82
4nOP	104-40-5	5.28	4.82
Organofosforatuak			
Klorpirifos	2921-88-2	4.96	0.357
Klorfenbinfos	470-90-6	3.81	3.022
Organokloratuak			
α-HCH	319-84-6	3.72	4.044
β –HCH	319-85-7	3.72	4.044
γ-HCH	58-89-9	3.72	4.044
δ-HCH	319-86-8	3.72	4.044
2,4'-DDD	53-19-0	5.87	0.0902
4,4'-DDD	72-54-8	6.02	0.0676
2,4'-DDE	3424-82-6	6.00	0.0729
4,4'-DDE	72-55-9	6.51	0.0265
2,4'-DDT	789-02-6	6.79	0.00917
4,4'-DDT	50-29-3	6.91	0.00731
Triklosan	3380-34-5	4.76	4.621
Musketa poliziklikoak			
HHCB	1222-05-5	5.43	0.490
AHTN	1506-02-1	5.80	0.239
Ftalatoak			
BBP	85-68-7	4.73	0.949
DOP	117-84-0	8.54	0.0004
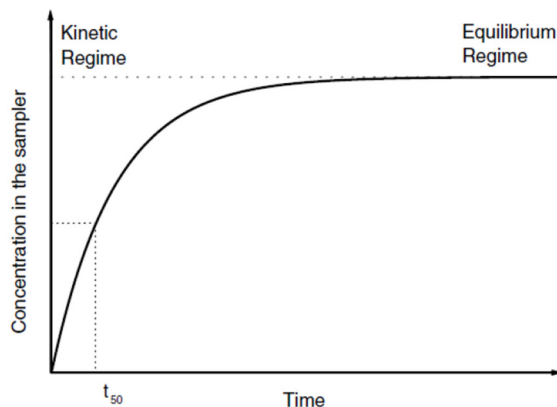
2.2. Irudia: Lagin biltze pasiboko tresneriak egoera zinetikoan edo oreka egoeran lan egin dezake.

Lagin biltze pasiboaren prozesuan bi egoeratan lan egin daiteke, lehenbizi, egoera zinetikoa dugu eta amaieran, oreka egoera, laginketa pasiboko materiala edo fasea asetu deneko puntua (ikusi 2.2). Orekan dagoeneko puntuan abiadura konstanteak bat egiten dira, eta haien zatiketa K_D partizio konstante bezala ezagutzen da.

$$Cs(t) = CwK_D \qquad (2.2)$$

Jokabide zinetikoan, laginketa pasiboko faseak jasotzen duena denborarekiko zuzenki proportzioana da

$$Cs(t) = CwK_1 t \qquad (2.3)$$

Eta jasotako masa bezala adierazi nahi baldin bada:

$$Ms(t) = CwRst \qquad (2.4)$$

Ms-k, denbora jakin baten ondoren lagin biltze pasiborako fasean aurkitzen den analitoaren masa adierazten du eta Rs (L day^{-1}) lagin biltze abiadura

da.   Azaldutakoarekin honela idatz dezakegu analitoaren xurgapena deskribatzen duen eredua:

$$Ms(t) = CwV_sK_D(1 - exp(\frac{Rst}{K_DV_s})) \tag{2.5}$$

V_s, laginketa pasiboko fasearen bolumena da.

Lagin biltze pasiboa burutzeko hainbat medio ezberdinak edo hainbat fase mota erabiltzen dira gaur egun. Lan honetan, polidimetilsiloxanozko (PDMS) stir-bar (SB), MESCO/Stir-bar (M-SB) eta polietersulfonazko (PES) tuboak erabili ziren. MESCOk, dentsitate baxuko polietilenozko mintza erabiltzen du fase polimerikoa babesteko.

2.1.3   Muskuiluak eta biokontzentrazioa

Organismo urtarrak uraren kalitatearen berri emateko lekuko aproposak dira. Muskuiluak mundu osoan zehar dauden organismoak dira eta euren zentinela erabilera oso zalbalduta dago munduan. Biotak berak duen gantz ehunei esker eta kutsatzaile hidrofobikoek gantzei dieten afinitateari esker, kutsatzaileak akumulatu eta gu neurtzeko gai gara. Horretarako erauzketa teknika eta neurketa teknika egokiak erabili behar dira. Gure kasuan, muskuiluen erauzketa matrize solidoko fase dispertsioaren bidez egin genuen eta neurketarako, masa espektrometro bateri akoplatutako gas kromatografia erabili genuen.

Gaur egun, Soxhlet-a eta ultrasoinu bidezko erauzketak alderatuta geratu dira eta erabilienak diren tekniken artean fluido superkritikoko erauzketa (*supercritical fluid extraction*, SFE), mikrouhin bidezko erauzketa (*microwave assisted extraction*, MAE), presiopeko likido erauzketa (*pressurised liquid extraction*, PLE), ultrasoinu fokatu bidezko solido-likido erauzketa (*Focused ultrasound solid-liquid extraction*, FUSLE) edota

matrize solidoko fase dispertsioa (*matrix solid-phase dispersion*, MSPD) aurki ditzakegu [20], erauzketa denbora laburragoak eta disolbatzaile organikoen kantitate txikiagoak erabiltzen dituztelako.

MSPD teknika, 2000.urtetik erabiltzen den teknika da eta bere prozedura erraza eta fidagarria da. Izan ere, muskuiluetan hainbat kutsatzaileren erauzketan oso erabilia da [21–25].

Azken urteotan, MSPD teknikan ere aurrerapenak eman dira, hala nola, selektiboagoak diren faseak erabiliz: molekularki inprimitutako polimeroak (*molecularly-imprinted polymers*, MIPs) eta karbonozko nanotuboak (MWCNTs). Hala ere, C18 eta Florisil dira oraindik faserik erabilienak.

2.1.4 Metabolomika

Metabolomikak, mintz, zelula eta jariakin biologikoetako metabolitoen konposizioa neurtzeko prozedura analitiko osoa hartzen ditu beregain. Analisi metabolomikoa teknologia omikoen parte da. Teknologia omikoek sistema biologikoen azterketan ezinbesteko baliabide bihurtu dira. Adibidez, genomikak geneak aztertzen dituen bitartean, transkriptomikak RNA mezulariak aztertzen ditu, proteomikak proteinak eta metabolomikak metabolitoak (lipidomika metabolomikaren azpitalde bezala lipidoak aztertzen ditu, ikusi 2.3 Irudia [26]).
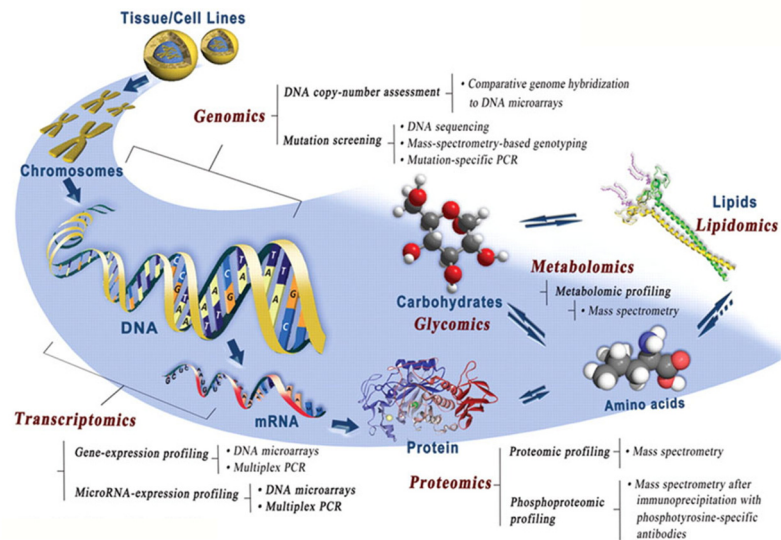
2.3. Irudia: Teknologia omikoen eskema, dagokien analisi-helburu eta metodoekin.

Metabolitoak sistema biologikoetan aurkitzen diren pisu molekular baxuko ($<1500\,\text{Da}$) konposatu organikoak dira. Metabolitoak, sistema biologikoetako bide metabolikoetako entzimen erreakzioetako sustratu, tarteko-produktu edota produktuak izan daitezke. Bi metabolito mota bereizi daitezke, endogenoak eta exogenoak. Endogenoak, sistema biologiko naturalaren parte dira, geneek adierazitako entzimen sustratu edota produktuak. Exogenoak ordea, konposatu xenobiotikoen eraldaketa produktuak dira.

Metabolomikaren bidez hiru helburu bete daitezke gaur egun. Alde batetik profil metabolikoa bildu, bestetik hatz marka metabolikoa zehaztu eta azkenik bide metabolikoa argitu.

Metabolomikako analisietan lau teknika dira nagusi, NMR espektroskopia, HRMS (erresoluzio altuko masa espektrometria), LC-MS eta GC-MS.

NMR eta masa espektroskopian (MS) izandako azken aurrerabideei esker sistema biologikoetatik eskura dezakegun informazio kopuruak gora egin du. Profil metabolikoaren determinazioak aplikazio asko ditu gaur egun, horien artean, osasun egoeraren diagnosia, elikadura arloko ikerketak, landareen mekanismoen azterketa, farmakoen garapenean edota ingurugiroko analisietan.

NMR neurketa, nukleo atomikoaren momentu magnetikoaren eta kanpo eremu magnetiko baten arteko erresonantzian oinarritzen da. Nukleo atomikoak eta bere desplazamendu kimikoak, inguruan dituen atomoen eragin zuzena jasatzen du, analitoaren egituraren berri emanez. Fenomeno hau Felix Bloch eta Edward Mills Purcellek deskribatu zuten 1946an eta lan honengatik 1952an Nobel Saria jaso zuten.

Lagin biologikoen analisian erabiliak diren teknika ^{1}H-NMR (protoien ugaritasunarengatik lagin biologikoetan hau da erabiliena), ^{13}C-NMR eta ^{31}P-NMR dira. Dimentsio bakarreko baita biko informazioa eskura daiteke NMRko neurketetan.

NMRko datuen interpretazioak metabolitoen kontzentrazioaz gain egitura kimikoaren informazioa ematen du. Espektroko gailurren azalerak eta garaierak metabolitoen kuantifikazioan erabiltzen dira.

NMR-n oinarritutako metabolomikako analisi bat egiterakoan ehundaka metabolito neur genitzake aldi berean eta modu ez-zuzendu batean (*non-target*). Datuak eskuratutakoan beharrezkoa izango da osagai askotariko analisia egitea hiru helburu nagusi betetzeko:

(i) Klaseen arteko bereizketa eragiten duten aldagaiak bereiztea.

2.2. Taula: NMR, GC-MS eta LC-MS tekniken konparazioa.

Teknika	Abantailak	Desabantailak
NMR	Kuantitatiboa	Ez da sentikorra (LOD=5 µM)
	Ez-suntsikorra	Ekipoaren kostu altua
	Arina (2-5 min lagineko)	Ioiak eta gatzak ezin ditu identifikatu
	Deribatizazio gabe	Protoi gabeko konposatuak ezin detektatu
	Banaketarako teknika gabe	Bolumen handiak neurketarako (0.5 mL
	Konposatu organiko gehientsuenak detektatu	Data baseen eskuragarritasun baxua
	Konposatu berrien identifikazioa	Seinaleen aldagarritasun altua
	Egonkorra, sendoa, teknologia garatua	
	Irudi analsia	
	Automatizatua	
	Likidoak eta solidoak	
	Bizitza luzeko instrumentua	
GC-MS	teknologia garatua, sendoa	Suntsikorra
	Instrumentuaren kostu ertaina	Deribatizazioa beharrezkoa kasu askotan
	Kalibratuarekin kuantitatiboa	Lagin prestaketa luzea
	Lagin tamaina/bolumen ertaina (0.1-0.2 mL	Geldoa (20-40 min lagineko)
	Sentikortasun ona (LOD=1 µg L^{-1})	Irudi analisia ezinezkoa
	Database handia identifikaziorako	Solidoekin ez-bateragarria
	Konposatu organiko gehienak neurtu eta ezorganiko batzuk	Konposatu berrien identifikazioa zaila (ionizazioaren araberakoa)
	Banaketa errepikakorra	
	Ia automatizatu daiteke	
	Gas eta likido laginak	
LC-MS	Sentikortasun ona (LOD=0.5 nM	Suntsikorra
	Konposatu organiko gehienak detektatu eta zenbait ezorganiko	Ekipoaren kostu oso handia
	Lagin bolumen txikiak (10-100 µl)	Geldoa kasu batzutan (5-40 min lagineko)
	Irudi analisia (MALDI edo DESI)	Banaketa
	Injekzio zuzena	Ez da egonkorra
	Metabolomako metabolito gehienak detektatu	Gas lagina ezin
	Ia automatizatua	Konposatu berrien identifikazioa zaila
		Instrumentuaren bizitza laburra (<9 urte)
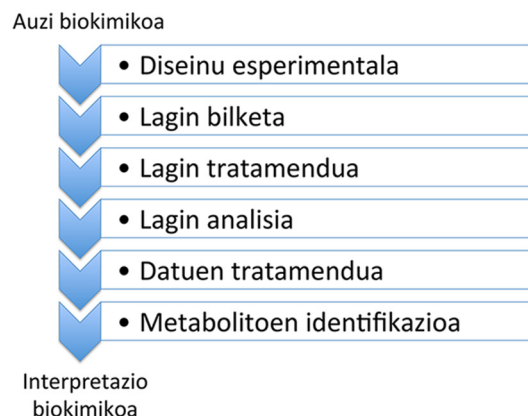
2.4. Irudia: Metabolomikako prozedura analitikoa.

(ii) Klase bakoitzaren profila lortzea.

(iii) Klaseen sailkapena eta taldekatzeak behatzea.

Behin informazio hori jasota, web gune eta artikuluetako seinaleen desplazamenduetan oinarrituz gure aldagaien identifikazioa burutuko dugu. Behin metabolitoak identifikatu direla, zeintzuk bide metaboliko alteratuta dauden aztertuko dira. Jasotako informazioarekin gaixotasunen diagnosia, toxikologia azterketa, nutrizio-egoera eta estresen efektuen eraginak ulertzeko gai izan gaitezke. Laburbilduz, metabolomikako prozedura analitikoa 2.4 Irudian adierazi dugu.

2.1.5 Histologia

Esan bezala, muskuiluak zentinela organismo moduan erabiltzen dira itsasoko kutsadura monitorizatzeko [27]. Baina batzutan, monitorizazio hauetatik lortutako datu biologikoak eta kimikoak interpretatzea zaila izaten da, batez ere, kontrolpean ez dauden aldagai kopurua oso handia delako. Tenperaturak, gazitasunak, janariaren eskuragarritasunak,

urtaroak, gonaden garapenak, e.a., faktore guzti hauek neurtutako parametroen erantzunean eragin zuzena dute [28]. Nahasgarriak izan daitezkeen faktoreak ezagutzea eta emaitzen interpretaziorako kriterio sendoak izatea erabakigarria da kutsaduraren eraginak identifikatu ahal izateko.

Ahalik eta faktore gehien kontrolpean izateko, laborategiko baldintza kontrolatuetan egindako esperimentua egin genuen, kutsatzaileen koktelaren eraginak ulertu ahal izateko.

Ingurumeneko hainbat kutsatzailek, hala nola, metalek, hidrokarburo aromatikoek, konposatu kloratuek, alkilfenolek, olioak, petrolioak, eta gure itsaso eta itsasbazterretan aurki ditzakegun eta abar luze honen eraginez muskuiluetan gaixotasunak eragiten dituzte [29]. Eraginaren garrantzia ehunen kalteberatasunaren menpekoa izango da baina baita kutsatzailearen natura eta kontzentrazioaren araberakoa. Alterazio biokimikoak zelulen prozesuetan eta funtzioetan eragiten du eta denborarekin aldaketa fisiologiko eta morfologikoak azaltzen dituzte. Aldaketa fisiologiko eta morforlogikoek gaixotasun jakin batzuk identifikatzeko balio dute. Beraz, aldaketa histopatologikoen kausak aldaketa metabolikoetan oinarritzen dira. Hanturako kalteak eta erantzun hiperplastikoak adibidez, organismoaren osasun eskasaren adierazgarri dira.

2.2 Helburuak

Oraindik ez dago ingurumen monitorizaziorako estrategia bateraturik eta jakintza arlo bakoitzean, bakoitzak beren ohiko analisiak egiten jarraitzen ditu. Guk lan honetan, baldintza kontrolatuetan eraikitako esperimentuan, biologoen eta kimikoen elkarlana proposatzen dugu monitorizazio estrategia

bezala. Estrategia honen erabilera frogatu nahi izan dugu lan honetan. Lau zatitan banatzen da gure estrategia:

(i) Lagin biltze pasiboa eta uraren analisi puntualak.

(ii) Muskuiluak zentinela organismo moduan biokontzentrazioaren neurketarako.

(iii) Erresonantzia magnetiko nuklearrean oinarritutako metabolomikako analisiak muskuiluaren hemolinfa, oin eta gonadetan. Lantaldean NMR analisietan oinarritutako ingurumen metabolomika lehen aldiz erabili dugu eta duen erabilgarritasuna frogatu nahi zen lan honetan.

(iv) Histologiako analisiak.

2.3 Materialak eta metodoak

2.3.1 Kontrolatutako baldintzetan burututako esperimentuak

Esperimentuak Euskal Herriko Unibertsitateko Plentziako itsas estazioan (PiE, UPV/EHU) egin ziren baldintza kontrolatuetan. PiEren abantaila nagusienetako bat zera da, itsasoko ur naturalaren emari jarraia dugula da, eta ura hartzeko orduan harearen bidez iragazita lortzen denez, garbi dela onar daiteke.

Bi esperimentu mota planteatu ziren. Lehen esperimentuan, bi egunik behin ur dopatuaren berritzea egin zen (10, 100 eta $1000\,\mathrm{ng\,L^{-1}}$-ko kutsatzaile hidrofoboen koktela erabiliz) eta bigarren motako esperimentuan, kutsatzaile hidrofoboen koktelaren fluxu emari konstantean lan egin genuen. Fluxu emari konstatean bi esperimentu egin genituen, batetik, kutsatzaileen kontzentrazio altua ($100\,\mathrm{ng\,L^{-1}}$) eta nahaste zabala

erabili genuen, eta bestetik, kutsatzaileen maila baxua $(20\,\mathrm{ng}\,\mathrm{L}^{-1})$ eta nahaste sinplea erabili genuen.

(i) Muskuiluen bilketa eta aklimatazioa

Muskuiluak (*Mytilus galloprovincialis*) Mundakako itsasertzean batu ziren. Laginketa puntu hau, Bizkaiko kostaldeko erreferentziako puntu "garbia" da [30]. Laginak 2014ko otsailan eskuz jaso ziren. Batutako muskuiluen tamaina 3.5-4.5 cm tarteko luzeerakoak eta adin tarte antzekoa zutenak batu ziren [31].

Aklimatazioa eta purga $1\,\mathrm{m}^3$-ko tanke batean egin zen eta lehenengo $48\,\mathrm{h}$-tan ez zitzaien janik eman. Esperimentuetan, aurrez iragazitako itsasoko ur naturala erabili zen. Denbora tarte hori pasatu ostean, jan komertziala (Coraliquid, SERA) eman zitzaien aste beteko aklimatazioan.

(ii) 1. esperimentua: bi egunik behin aldatutako ur dopatua

Esperimentu honetan lau talde izan genituen: kontrola, kontzentrazio baxuko taldea $(10\,\mathrm{ng}\,\mathrm{L}^{-1},\,\mathrm{L})$, tarteko kontzentraziokoa $(100\,\mathrm{ng}\,\mathrm{L}^{-1},\,\mathrm{ME})$ eta kontzentrazio altukoa $(1000\,\mathrm{ng}\,\mathrm{L}^{-1},\,\mathrm{H})$. Tanke bakoitzean $30\,\mathrm{L}$ ur, 36 muskuilu eta airea etengabe pasarazten zen (ikusi 2.5 Irudia).

Ura, bi egunik behin aldatzen zen eta zegokion kutsatzaile nahastea gehitzen zen. 14.egunean jaso ziren metabolomikarako laginak (hemolinfa bakarrik). Metabolomikako analisietarako talde bakoitzeko 5-10 muskuilu erabili genituen esperimentu guztietan.

Esperimentuan erabili zen kutsatzaile koktela:

- Alkilfenolak: 4-tert-oktilfenola (4tOP), 4-nonilfenola (4nOP)

- Konposatu organofosforatua: klorpirifos (Clorp), Klorfenbinfos (Clor)

- Konposatu organokloratuak:α-HCH, β –HCH, γ-HCH, δ-HCH, 2,4'-DDD, 4,4'-DDD, 4,4'-DDE, 2,4'-DDT, 4,4'-DDT, Triklosan

- Musketa poliziklikoak: galaxolide (HHCB), tonalide (AHTN)

- Ftalatoak: BBP, DOP

  Esperimentuko behaketa garrantzitsuena: 13.egunean, $1000\,\mathrm{ng}\,\mathrm{L}^{-1}$-ko kutsatzaileen nahasteko tankeko muskuilu denen errutea gertatu zen (kontrolean ez).
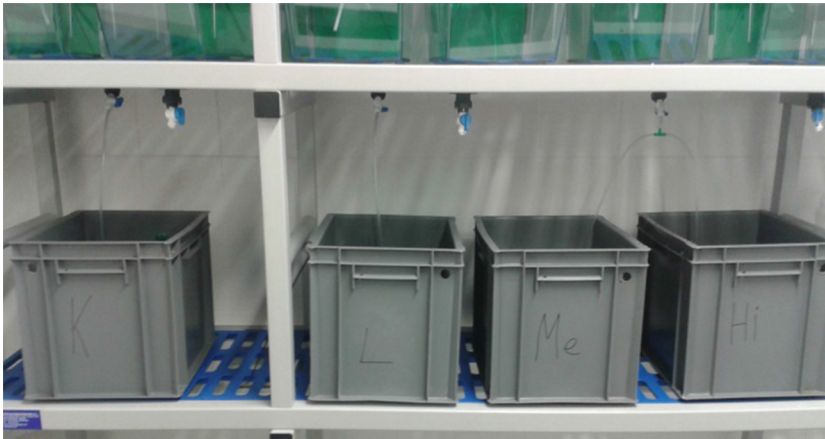
2.5. Irudia: 1. esperimentuaren diseinua.

(iii) **2. esperimentua:** $100\,\mathrm{ng}\,\mathrm{L}^{-1}$ **kutsatzaile hidrofoboen koktelaren fluxu emari konstantean**

2.6 eta 2.7 Irudietan ikus dezakegun moduan, hiru tanke erabili ziren esperimentuan: (1) laginketa pasiborako, $50\,\mathrm{L}$; (2) ur kutsatutan muskuiluak jartzeko, (1) tankeari konektatuta zegoena, $65\,\mathrm{L}$ eta (3) kontrolerako muskuiluena, ur emari garbi independenteduna, $65\,\mathrm{L}$.

Muskuiluak 160ko talde bitan banatu ziren, kontrolak eta kutsatutakoak, eta dentsitate altuko polietilenozko 65 L-ko tanketan sartu ziren.

Kutsatzaile nahastea altzairu herdolgaitzez eginiko tankera gehitzen zen lehenbizi. Bertan, laginketa pasiborako karrusela jarri zen. $5\,\mathrm{L\,h^{-1}}$-ko ur emari kontrolatua erabili zen (ponpekin kontrolatua), ura berritzeko eta kutsatzaileen kontzentrazioa $100\,\mathrm{ng\,L^{-1}}$-takoa mantentzeko (1) eta (2) tankeetan.

2.6. Irudia: 2. esperimentuaren eskema.

Esperimentuan erabili zen kutsatzaile koktela:

- Alkilfenolak: 4tOP, 4nOP

- Konposatu organofosforatua: Clorp, Clor

- Konposatu organokloratuak:α-HCH, β –HCH, γ-HCH, δ-HCH, 2,4'-DDD, 4,4'-DDD, 4,4'-DDE, 2,4'-DDT, 4,4'-DDT, Triklosan

- Musketa poliziklikoak: HHCB, AHTN

- Ftalatoak: BBP, DOP

Esperimentuko behaketa garrantzitsuena: Esperimentu honetan 0, 3, 5, 8, 10, 12 eta 14 egunetan laginak jasotzeko asmoa genuen baina esperimentua hasi zen egun berean muskuiluen errute orokorra gertatu zen eta 5 egunetara muskuilu denak hil ziren (kontrolean ez).

2.7. Irudia: 2. esperimentuaren diseinua, laginketa pasiboko karrusela eta erabilitako muskuiluak.

(iv) 3. esperimentua: $20\,\mathrm{ng\,L^{-1}}$ **kutsatzaile hidrofoen koktelaren fluxu emari konstantean**

2. esperimentuko diseinu bera erabili zen 3.esperimentu honetan. Kasu honetan ordea, kutsatzaile nahastearen kontzentrazioa bost aldiz txikioagoa izan zen, $20\,\mathrm{ng\,L^{-1}}$. Gainera, kutsatzaile nahaste sinpleagoa eraibili zen koktelean.

Esperimentuan erabili zen kutsatzaile koktela:

- Alkilfenolak: 4tOP

- Konposatu organofosforatua: Clorp

- Konposatu organokloratuak:α-HCH, 2,4-DDD, 4,4'-DDD, 4,4'-DDE, Triklosan

- Musketa poliziklikoak: HHCB, AHTN

- Ftalatoak: BBP, DOP

Esperimentuko behaketa garrantzitsuena: 3.egunean errutea hasi zen (kontrolean ez).

2.3.2 Lagin biltze pasiboa eta laginketa puntualak

Esan bezela, proiektu hau lan taldean egin genuen eta lagin biltze pasiboari eta lagin biltze puntualari zegokion atala Oscar Posada lankideak egin zuen. Esperimentu honetarako erabilitako metodologia, argitaratuta dagoen artikuluan aurki daiteke [32]. Guk, 2.8 Irudian, laburbildu ditugu pausurik garrantzitsuenak. Lagin biltze pasiboko hiru hurbilketa erabili ziren: PDMS hagatxo birakaria (SB, *stir-bars*), MESCO/hagatxo birakaria (M-SB, MESCO/stir bars) eta PES tuboak (PES). Hagatxo birakarien kasuan, zuzenean neurtu ziren Gerstelean desortzio termikoan oinarritutako

erauzketari esker. PESak, ordea, kimikoki desorbatu eta bolumen handiko GC-MS kromatografiaren bitartez neurtu ziren.

Lagin biltze puntualean (*spot sampling*) SB hagatxo birakariekin egin zen erauzketa laborategian eta hau ere TD-GC-MS bitartez neurtu zen zuzenean.
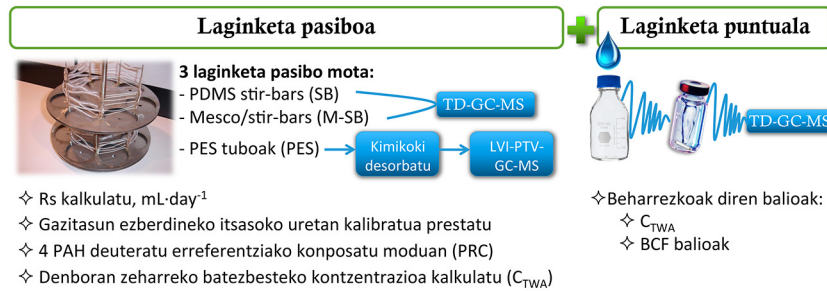
2.8. Irudia: Lagin biltze pasiboko eta lagin biltze puntualeko prozeduraren eskema.

2.3.3 Muskuiluak eta biokontzentrazioak

Muskuiluek minuturo $30\,\mathrm{mL}$ ur iragazteko gai dira [33] jakiak eskuratzeko eta ura kutsatuta dagoenean kutsatzaileak metatzen dituzte. Hau horrela izanik, muskuiluen biokontzentrazioa kalkulatzeko Haizea Ziarrusta lankideak optimizatutako metodoa erabili genuen [22]. Kasu honetan MSPD erauzketa erabili genuen (ikusi 2.9 Irudia).

Metodoaren optimizatutako baldintzak erabili ziren analisian. $0.3\,\mathrm{g}$ liofilizatutako lagin (15 muskuilutako *pool*-ak egin ziren baldintza bakoitzerako) eta $0.3\,\mathrm{g}$ Florisil dispertsante erabili ziren [22]. Beirazko mortero batean oso ondo nahastu ziren 2 minutuz, guztiz homogenizatuta egon arte. $10\,\mathrm{mL}$-ko beirazko xiringetan polietilenozko frita sartu zen lehenbizi eta ondoren, $0.6\,\mathrm{g}$ silika desaktibatua (labean izan ez duguna),

4 g silika aktibatua eta amaieran, dispersatutako matrizea gehitu ziren. Jarraian, isotopikoki markatuta zeuden trazagarriak gehitu ziren $50 \, \text{ng g}^{-1}$-ko kontzentrazioan dispersatutako matrizera eta azkenik, bigarren frita jarri zen (2.9 Irudian agertzen den era berean). Behin, MSPDrako xiringa prest genuela, 25 mL diklorometanorekin (DCM) eluitu zen, eta eluitutakoa Turbovap LV Evaporator eta nitrogeno gasa erabiliz lurrundu ostean 140 µL n-hexanotan berreratu zen. Erauziak GC-MS bidez neurtu ziren.

Kasu honetan, Agilent HP6890N gas kromatografoa erabili zen Agilent 5973N masa espketrometroari akoplatutakoa eta Agilent 7683 injekzio portu automatikoa erabili zen. 2 µL injektatu ziren banaketa gabeko (*splitless*) bidez, 1.5 min 300 °C-tan Agilent HP−5ms kapilare zutabea (30 m x 0.25 mm, 0.25 µm) erabiliz eta gas eramangarri moduan hidrogenoa erabiliz, 1.3 mL/ min. Labeko tenperatura programa: 60 °C (1 min), 140 °C-ra 30 °C/ min-ko abiaduran, 200 °C 3 °C/ min-ko abiaduraz, 240 °C-ra 5 °C/ min-ko abiaduraz eta azkenik, 30 °C/ min-ko abiaduraz 300 °C lortu arte, eta 10 minutuz mantendu zen tenperatura.

Masa espektrometroa elektroi talka (*electron impact*, EI) bidez neurtu zen, 70 eV-ko potentzial diferetzia aplikatuz. Interfaseko tenperatura 310 °C-tan mantendu zen eta ionizazio iturriaren eta koadrupoloaren tenperatura, 230 °C eta 150 °C-an mantendu ziren hurrenez-hurren.

Neurketa ioi jakin batzuen monitorizazioa eginez burutu zen (SIM, *selected ion monitoring*). Bi ioi erabili ziren konposatu bakoitzaren kasuan monitorizaziorako, kuantifikatzeko erabiliko zena eta konposatua identifikatzeko erabiliko zena.

Datuak tratatzeko eta integrazioa burutzeko Chemstation softwarea (Agilent Technologies) erabili zen.
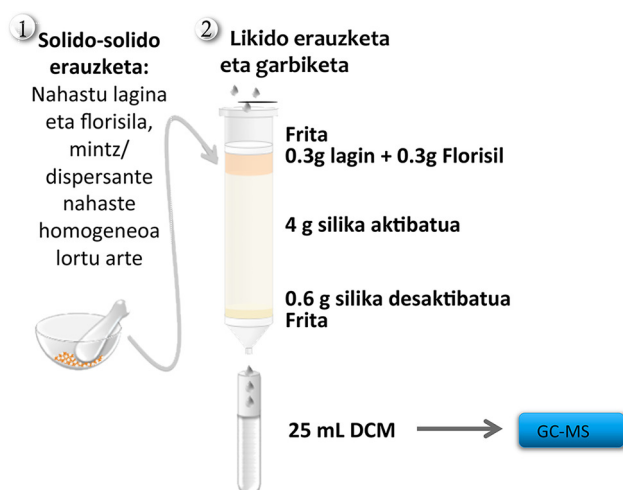
2.9. Irudia: Muskuiluen biokontzentrazioa neurtzeko prozeduraren eskema, MSPD bidezko erauzketa.

2.3.4 NMR metabolomika

Metabolomikako analisietan laginaren tratamendua pausu kritikoa da. Batez ere, laginaren integritatea mantentzeko kate-hotza ez apurtzea berebizikoa da.

NMR metabolomikarako erabili zen lagin tratamendua aurrez optimizatutako bi lanetan oinarritzen da. Hain zuzen ere, mundu mailan, NMRko ingurumen metabolomikan erreferente den taldekoek eginiko lanetan. Mark Viant ikerlariaren taldekoek, Birmingham-eko unibertsitatekoek, garatutako lan bitan oinarritu genuen gure prozedura [34, 35].

Laginaren aurretratamenduak pausu hauek ditu:

(i) *Muskuiluen ehunak bildu eta gorde*

- Lan honetan muskuiluen jariakina eta 2 ehun aztertu ziren: hemolinfa, oina eta gonada.

- Hemolinfa, muskuilua bizi zegoelarik, muskulutik xiringa batekin jaso zen, (150 μL-450 μL inguru jasotzeko gai izan ginen.

- 25-100 mg masa tarteko oin eta gonadak batu genituen eskalpelo eta artazien laguntzaz. Ahal bezain lasterren nitrogeno likidotan bat-batean izozten genuen.

- −80 °C-tan gorde ziren laginak.

(ii) *Hemolinfaren prestatze lana*

- Hemolinfa liofilizatu egin genuen behin izoztuta zegoela.

(iii) *Ehunen metabolito hidrofiliko eta hidrofoboen erauzketa konbinatua*

- Homogeneizazio hodiak izotzetan mantendu.

- 4 mL metanol hotz eta 0.85 mL Milli Q ur hotz gehitu genuen lagin gramoko, biak 4 °C-tan.

- Aldez-aurretik pisatutako lagina (25-100 mg) gehitu.

- Lagina Precellys-cryolys ekipoa erabiliz homegeneizatu zen. Laginaren arabera egokitu zen denbora esperimentalki, hau da, lagin denaren homogeneizazioa lortu arte: gonada (2x30 s eta 5 s-ko atsedenarekin) eta oina (2x60 s eta 5 s-ko atsedenarekin), kasu bietan SI5000rpm-ko abiaduran.

- Homogeneizatutako lagina Pasteur pipeta erabiliz kromatografiako bial batera pasatu.

- Homogeneizazio hodiei garbiketa pausu bat aplikatu: $1\,\mathrm{mL\,g^{-1}}$ metanol hotz eta $0.9\,\mathrm{mL\,g^{-1}}$ Milli Q ur hotz gehitu.

- $15\,\mathrm{s}$-z nahastu vortex-ean.

- Garbiketa pausukoa ere bial kromatografikora gehitu Pasteur pipeta erabiliz.

- Fase bakarreko puntuko igaropena erauzketaren eraginkortasuna hobetzeko egin zen eta horretarako $2\,\mathrm{mL\,g^{-1}}$ kloroformo ($CHCl_3$) hotz gehitu ziren eta $60\,\mathrm{s}$-z vortex-ean nahasten dira bialak.

- $3\,\mathrm{mL\,g^{-1}}$ $CHCl_3$ eta $2\,\mathrm{mL\,g^{-1}}$ Milli Q ur hotz gehitu eta $60\,\mathrm{s}$-z vortex-ean nahastu ziren bialak. Bitartean, izotzetan manetendu genituen beti laginak.

- Bialak zentrifugatu egin ziren baldintza hauetan: $2000\,\mathrm{g}$, $5\,\mathrm{min}$ eta $4\,°\mathrm{C}$-tan.

- Behin zentrifugatuta $2\,\mathrm{min}$ inguru utzi ziren laginak izotzetan eta hiru fase bereizi ziren: goiko fasea (metanol ur nahastea metabolito polarrekin), tarteko fasea (hondar solidoak biltzen ziren non proteinak eta zenbait gantz edo ehun bil zitezkeen) eta beheko fasea (metabolito hidrofobikoak).

- Pasteur pipeta erabiliz eta kontu handiz bi faseak jaso ziren. Batetik, fase polarra plastikozko saiodietan jaso zen eta bakoitzari $3\,\mathrm{mL}$ MilliQ ur hotz gehitu zitzaizkion eta nitrogeno likidotan bat-batean izoztu ziren. Bestetik, fase hidrofobikoa

kromatografia bial batean bildu zen eta hau ere nitrogeno likidotan bat-batean izoztu zen.

- Fase polarra liofilizatu egin zen eta apolarra Turbovap-ean lurrundu zen. Erauzi biak neurketa egunerarte $-80\,°C$-tan gorde ziren.

(iv) *Hemolinfaren prestaketa NMR neurketarako*

- $550\,μL$ NMR tanpoian berreratu zen, $60\,s$-z vortex-ean nahastuz.

- NMR tanpoia: $100\,mM$ sodio fosfatozko tanpoian, pH 7.4an eta ur deuteratuarekin prestatuta. Erabilitako ur deuteratua Sigma Aldrich etxekoa zen eta $0.5\,mM$ TMSP zeukan, zero seinalea ezartzeko erabili zena.

- Lagina zentrifugatu egin zen $10\,000\,rpm$-tan eta NMRko tubora isuri zen.

(v) *Erauzi polarraren prestaketa NMR neurketarako*

- $550\,μL$ NMR tanpoain berreratu zen, $60\,s$-z vortex-ean nahastuz.

- NMR tanpoia: $100\,mM$ sodio fosfatozko tanpoian, pH 7.4an eta ur deuteratuarekin prentatuta. Erabilitako ur deuteratua Sigma Aldrich etxekoa zen eta $0.5\,mM$ TMSP zeukan desplazamenduaren jatorria ezartzeko. Ondoren, nahastea NMR hodira eraman zen.

(vi) *Erauzi apolarraren prestaketa NMR neurketarako*

- $550\,μL$ kloroformo deuteratutan berreratu zen, $60\,s$-z vortex-ean nahastuz. Kloroformo deuteratua Carlo Erba etxekoa zen eta $0.5\,mM$ TMS zuekan.

NMRko neurketak SGIkerreko (UPV/EHU)ko 500 MHz Bruker AVANCE 5OO espektrometroan egin ziren eta neurketako baldintzak hauek izan ziren:

(i) ^{1}H NMR espektroak neurtzeko parametroak: pultso sekuentzia zgpr (Bruker programa estadarra) erabiliz egin zen, 6 kHz espektro zabalera, ur asetzea 2 s erlaxazio tartean, 64 akumulazio eta 32K datu puntu.

(ii) ^{1}H NMR espektroak tratatzeko parametroak: Fourier Transformatua (FT), biderketa esponentziala (EM, *exponential multiplication*, TMS edo TMSP-rekiko erreferentziatu ziren desplazamendu kimikoak (0 ppm balioa ezarriz), polinomioen bidezko oin-lerroaren zuzenketa eta faseak (zero eta lehen mailakoa) zuzenduz.

Behin NMRko datuak eskuratu ziren, espektroak Matlabera inportatu ziren *RBNMR* funtzioa erabiliz. Sarean Bruker ekipoetarako NMR-ko espektroak inportatzeko gidoia aurki daiteke, Nils Nyberg-ek idatzitako RBNMR funtzioa (http://www.mathworks.com/matlabcentral/fileexchange/40332-rbnmr). Datuen tratamendua PLS-Toolbox-aren bitartez egin zen. Espektroen aurretratamenduan jarraitutako pausuak esperimentalki optimizatu ziren: COW lerrokatzea, aldagaien aukeraketa (ur eta TMS edota TMSParen seinaleak ezabatuz baita daturik gabeko zatiak), logaritmoan (log10) oinarritutako eraldaketa, normalizazioa (espektro osoaren azalera kontutan hartuz), batezbesteko erdiratzea eta seinale ortogonalaren zuzenketa (OSC, OPLS-DA) egiteko.

Bi analisi mota egin ziren, PCA eta OPLS-DA. PCAren bitartez datuen distribuzio eta ezabatu beharreko lagin susmagarriak topatzeko

erabiltzen da. OPLS-DA gainbegiratutako teknika erabiliz ordea, taldeen edo klaseen arteko bereizmena handitu eta VIPak eskuratzea du helburu. Modu honetan lortutako informazioarekin, aldagai garrantzitsuenen seinaleen identifikazioa egin zen. Behin seinale (desplazamendu kimikoak) bereizgarriak zeintzuk diren ezagututa, metabolitoen seinaleen esleipena egiteko sarean aurkitutako data baseetan [36–38] eta artikulu zientifikoetan oinarritu ginen [39–43, 43].
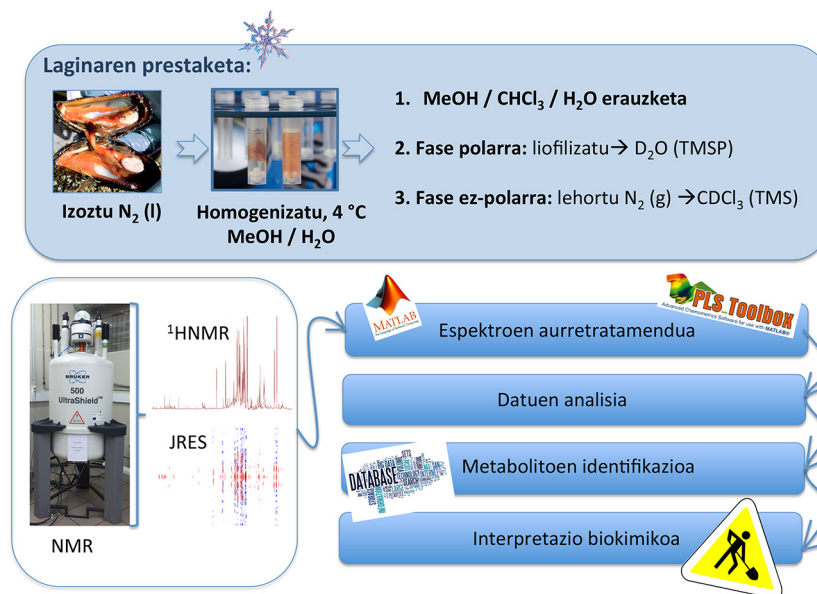
2.10. Irudia: NMR metabolomikako prozeduraren eskema.

2.3.5 Muskuiluen analisi histopatologikoa

Biologoek egindako analisi histopatologikoaren bidez lortutako emaitzik adierazgarrienak jaso ziren. Horretarako laginak fixatu eta parafinatan prestatu ziren. Ondoren, $5\,\mu$m-ko ebakiak egin ziren mikrotomoan, eta albumina erabiliz beirazko portetan jarri ziren. 24 orduz lehortzen izan eta

gero, 37 °C hematoxilina eta eosina tindaketa egin zen. Mikroskopioaren bidez digestio glandulako zelula motak, epitelioa eta egituran aldaketak behatu ziren. Era berean, zelula basofilikoen bolumena, gonaden garapen puntua, etab. behatu ziren.

2.4   Emaitzak eta eztabaida

Atal hau bi zati nagusitan banatu da. Alde batetik muskuiluetako eta biltze pasiboko akumulazioari dagokion emaitzak, eta, bestetik, azterketa metabolikoari dagozkionak.

2.4.1   Muskuiluen akumulazioa eta lagin biltze pasiboaren bidezko jarraipena

Lan esperimental honetan, aldi berean, bi eginkizun bete ziren: SBaren (hagatxo birakaria, *stir-bar*) kalibrazio lagin biltze gisara eta baldintza bereko muskuiluen esposizioa. Horrez gain, beste saiaketa batean muskuiluen esposizioa modu ez-jarraituan egin zen eta han neurtutako akumulazioren berri emango da. Lagin biltze pasiboari dagokionez, SBei dagozkien biltze edo xurgatze abaidurak (Rs, sampling rate, L·egun^{-1}) determinatu ziren bi gazitasun mailetan (%15 eta %30), Posada-Ureta et al. (2016) [44] adierazi zuten bezala eta lortutako Rs-en emaitzak 2.11 Irudian erakutsi dira.
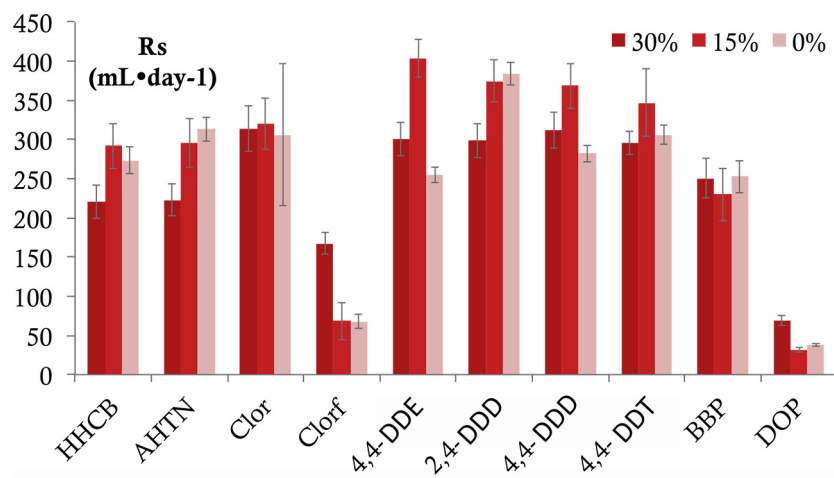
2.11. Irudia: Gazitasun ezberdinetan SB-k duen erantzuna.

2.3. Taula: 1. eta 3. esperimentuetako muskuiluetan neurtutako kutsatzaileen kontzentrazioen laburpena (ng/g), dagokien desbideratze estandarrarekin (esperimentala).

				kontzentrazioa (ng/g)			
Saiaketa	HHCB	AHTN	Clorp	4,4-DDE	2,4-DDD	4,4-DDD	4,4-DDT
$C_{w,1000ngL^{-1}}$	49±7	42±8	31±44	499±44	539±49	713±6	7556±2546
$C_{w,100ngL^{-1}}$	11.2±0.5	6±3	28±5	64±5	71±10	99±11	603±66
$C_{w,10ngL^{-1}}$	9.2±0.4	2.29±0.07	15±6	8.4±0.2	5.91±0.08	7.6±0.3	47.9±0.6
$C_{w,20ngL^{-1},3e}$	6±1	2.1±0.2	11.0±0.4	12.0±0.7	29±1	15±1	22±1
$C_{w,20ngL^{-1},7e}$	8.8±0.4	2.7±0.2	23±2	15.5±0.8	41±1	17.4±0.9	30±2
$C_{w,20ngL^{-1},14e}$	10±1	4±0.2	32±1	17.4±0.6	46±2	20±2	45±5

Lehen eta hirugarren saiaketetan, esposizio ez-jarraitua (1. esperimentua) eta $20\,\mathrm{ng\,L^{-1}}$-ko esposizio jarraituan (3.esperimentuan) hain zuzen, kutsatzaile organikoen kontzentrazioak muskuiluetan determinatu ziren. Emaitza horiek 2.3 Taulan laburbildu dira. Taulan ikus daitekeen bezala, muskuilutan bildutako analitoen kontzentrazioak oso bestelakoak dira. Kontzentrazio maila altuenak DDD, DDE eta DDT kasuetan neurtu ziren.

Lehen saiaketari dagokionez, emaitza guztiak 14 egun esposatuta izan ondorengoak dira eta lortutako kontzentrazioakk ikusita, haien arteko erlazioak aztertu ziren. Izan ere, akumulazioa egoera iraunkorrean gertatuko balitz, hau da denborarekiko jiterik gabe, eta uretako kontzentrazioa 10 aldiz handitu ostean muskuiluetako kontzentrazioak ere modu berean gora egin beharko luke. Hori horrela balitz, kontzentrazio nominalak 10-tik 100-ra edo 100-tik 1000-ra igaro ondoren hamar aldiko jauziak nabarmendu beharko genituzke muskuiluetan eta 10-tik 1000ra, aldiz, 100 aldiko jauzia. Erlazio esperimental guztiak 2.12 Irudian irudikatu dira eta ikus daitekeen bezala, espero ziren jauziak soilik betetzen dira DDT eta haren eratorriekin. Musketak eta klorpirifosekin, ordea, jauziak espero zirenak baino askoz apalagoak izan dira.
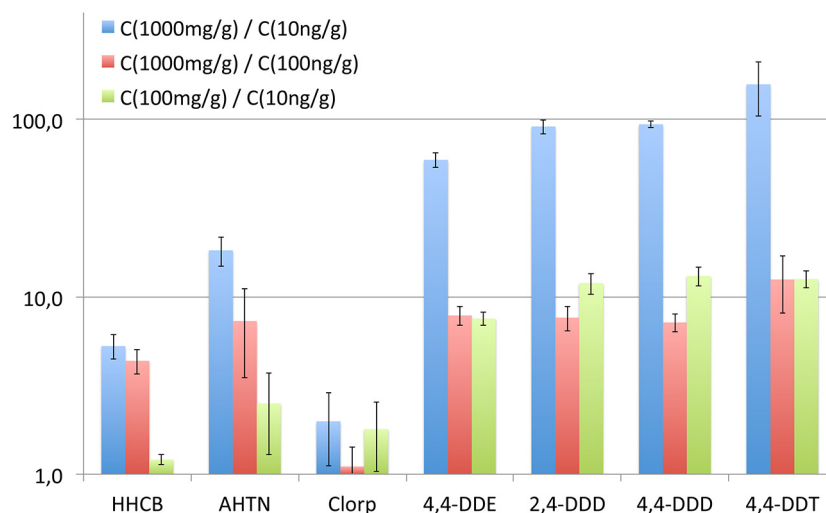
2.12. Irudia: 1. esperimentuko kontzentrazioen proportzioak, kontzentrazioa 10 aldiz eta 100 aldiz handitzean, dagokien desbideratze estandarrarekin.

Gertakizun horren arrazoiak ematearren, bi aipa daitezke: alde batetik, muskuiluen akumulazioa egoera iraunkorretik urrun izatea, eta beraz, oraindik nolabait asetu gabe izatea, eta bestetik uretako kontzentrazioa nominala baino baxuagoa izatea hormetan eta hodietan eta abarretan atxikitu ondoren.

Nolanahi ere, 2.4 Taulan bildu dira DDT eta eratorrien log BCF balio esperimentalak, erreferentzietan muskuiluen kasurako aurkitutako balio esperimentalak [45] eta EPA Suite delakoaren bidez estimatutako balio teorikoak (https://www.epa.gov/tsca-screening-tools/epi-suitetm-estimation-program-interface) ChemSpider-tik eskuragarriak. Ikusten denez, balio esperimentalak doiak izan arren erreferentzietatik behera daudela ikus daiteke. Ziurrenik, kasu horietan ere, kontzentrazio nominala

2.4. Taula: 1. esperimentuko kutsatzaileen kontzentrazioaren eta uretako kontzentrazioaren arteko erlazio logaritmikoa (log BCF), dagokien desbideratze estandarrarekin.

	4,4-DDE	2,4-DDD	4,4-DDD	4,4-DDT
$\log \text{BCF}_{1000ng/L}$	2.71 ± 0.04	2.74 ± 0.04	2.86 ± 0.01	3.9 ± 0.1
$\log \text{BCF}_{100ng/L}$	2.81 ± 0.04	2.86 ± 0.06	3.01 ± 0.05	3.79 ± 0.05
$\log \text{BCF}_{10ng/L}$	2.94 ± 0.01	2.78 ± 0.01	2.89 ± 0.02	3.69 ± 0.01
$\log \text{BCF}_{esp}$		3.96-4.42	3.96-4.42	4.37
$\log \text{BCF}_{teor}$	4.31	3.82	3.93	4.62

ez da izan benetakoa eta saiaketa berak ere ura aldizka aldatu beharra zuenez, espero ziren baliotatik urrun aurkitu ziren.

Hala ere, BCF balioen esperimentalen erkaketa egitea ez da horren zuzena, analitoaren ezaugarriak kontuan izateaz gain matrize biologikoaren ezaugarriak kontuan hartu behar baitira. Espeziaren, tamainaren, adinaren, jatorrizko tokiaren, ugalketa mailaren baita urtaro edo garaiaren arabera asko aldatzen da proteina eta lipidoen proportzioa, iragazte ratioa baita izandako elikadura eta faktore guzti hauek zuzenki erlazionatuta daude muskuiluek aurkezten dituzten BCF balioekin.

Hirugarren saiaketatako emaitzek denboraren araberako neurriak zituen eta hortik biokontzentrazio faktoreen (BCF) balio esperimentalak eta denborarekiko mendetasuna aztertzeko aukera eman zuen. Kasu honetan nabarmendu zen 3. egunetik 14 egunerako bitartean balioak gero eta handiagoak egiten zirela modu lineal batean (ikus 2.3Taula), beraz argi zegoen BCF balioak ez zirela egoera iraunkor bati egokitu zitzaizkionak. Hori dela eta, SB-ekin bezalako tratamendua egitea egokitu zen, hau

da, azterketa zinetiko bat bezalakoa non, alde batean SB-ek akumulatzen zituzten erabilitako kutsatzaileak eta geroago muskuiluek ere.

Akumulazioari dagokion eredurik sinpleena atal bakarrekoa da eta haren akumulazioaren adierazpena hauxe da:

$$C_{musk}(t) = C_w.k_1/k_2(1 - e^{(-k_2t)}) \tag{2.6}$$

non C_{musk} eta C_w muskuiluetan eta uretan dauden kontzentrazioak diren, k_1 eta k_2 akumulazioa eta eliminazioaren abiadura konstanteak diren hurrenez hurren eta t igarotako denbora. Egoera iraunkorretik urrun bada eliminazioa arbuiagarria da akumulazioarekiko beraz adierazpen hori honelaxe laburtu ahal da:

$$C_{musk} = C_w.k_1.t \tag{2.7}$$

Azken ekuazio hori aplikatu zen SB-en emaitzetan, non SB bakoitzak akumulatutako masa (ng-tan) determinatu zen esperimentalki eta SB bakoitzak zuen PDMS-ko bolumenetik eta haren dentsitatetik (47 µL eta 965 kgm^3) SB-tako kontzentrazioak ziren. Modu beretsuan muskuiluetako kontzentrazioak kalkulatu zirenez, bien erlazioa (C_{musk} eta C_{SB}) denborarekiko irudikatu zen 2.13 Irudian 2,4-DDD-ren kasuan. Kasu bietan uretako kontzentrazioa (CW) bera eta ezaguna izan zenez, Irudi horietatik kalkulatu genituen akumulazio konstatearen balioak (k1, malda) eta haien balioak 2.5 Taulan bildu dira, doiketaren erregresio koefizienteekin batera.
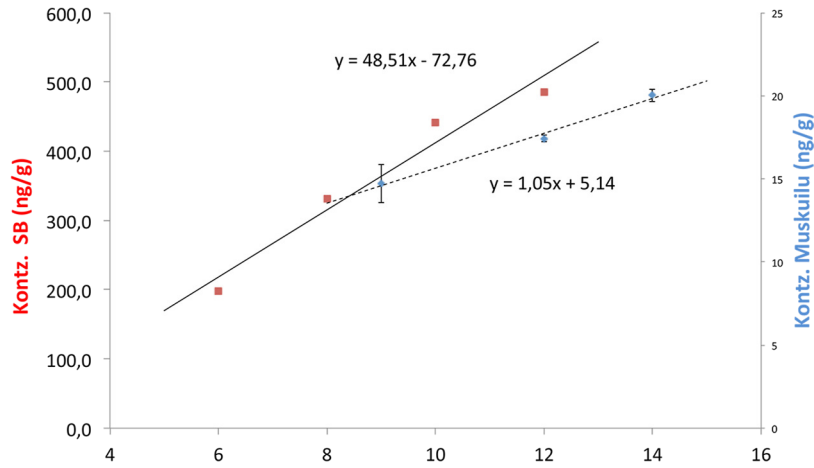
2.13. Irudia: Zinetikoki SBak eta muskuiluek zuten jokamoldearen erakusgarri 2,4-DDDren adibidea.

Emaitza horietatik bi ondorio atera ditzakegu: alde batetik, muskuiluen akumulazioa askoz mantsoagoa dela SB-renak baino, nahiz eta muskuiluak ura etengabe ponpatzen edo xurrupatzen duen, batezbestez, $1.8\,\mathrm{L}\,\mathrm{ordu}^{-1}$-ko eta SB-batek "ikusten duen" ur bolumena hori baino gutxiago den. Edonola ere, ondo doitzen dira eredu sinple berera, eta beraz, batean antzematen diren ondorioak besteari egokitu ahal zaizkio.

2.5. Taula: Zinetikaren azterketa: muskuiluen eta SBren konparaketa.

	HHCB	AHTN	Clorp	4,4-DDE	2,4-DDD	4,4-DDD
malda muskuilu(k1, egun^{-1})	0.75	0.29	4.28	1.08	3.37	1.05
R^2 muskuilu	1.00	0.95	1.00	1.00	0.98	0.99
malda SB (k1, egun^{-1})	58.43	62.84	62.84	22.05	48.51	
R^2 SB	0.97	0.98	0.99	0.98	0.98	

2.4.2 NMR metabolomika

NMR-ko analisiak hemolinfan, oinetan eta gonadetan egin ziren. Behin metabolito hidrofilikoei dagozkien NMR espektroak jasota kimiometria erabili zen emaitzak aztertzeko. Aldakortasun biologikoa oso handia aurkezten dute muskuilu basatiek. Ingurumenak, genetikak, sexuak, adinak edota elikadurak, faktore natural guzti hauek, ezkutatu egiten dituzte kutsaduraren ondorioak. Hori dela eta, OPLS-DA bezalako analisi baliabideak beharrezkoak izan ziren faktore naturalen eragina murrizteko eta guk eragindako estres faktorearen eragina azaleratzeko. Aipatu beharra dugu, ahal izan den neurrian, metabolitoak desplazamendu kimiko bat baino gehiagorekin esleitzen saiatu garela.

(i) 1. eta 2.esperimentuko hemolinfaren analisia

2.14 Irudian aurkeztutako *score*ak 1. esperimentuko (goikoa) eta 2.esperimentuko (behekoa) hemolinfa laginekin eskuratuko OPLS-DA ereduetatik lortu dira.

1.esperimentuan 2 osagai nagusi (LV) behar izan genituen x matrizearen (aldagaien matrizea) %29.50ko bariantza azaltzeko eta y matrizearen (klaseak) %51.57ko bariantza azaltzeko. 2.6 Taulan adierazi ditugu ereduari dagozkion erroreak, RMSEC eta RMSEV balioak.

1.esperimentuko score-tan (2.14 Irudia, goikoa) bi talde nagusi antzematen dira: kontrola EX2-L klasearekin ($10\,\mathrm{ng\,L^{-1}}$) batera agertzen da eta EX2-ME ($100\,\mathrm{ng\,L^{-1}}$) eta EX2-H ($1000\,\mathrm{ng\,L^{-1}}$) klaseek bigarren taldea osotzen dute.

2.esperimentuko eredua hiru osagai nagusi erabiliz eraiki zen eta x matrizearen %76.36ko bariantza eta y matrizearen %91.57ko

2.6. Taula: 1. esperimentuko muskuiluen hemolinfen ereduaren informazioa, RMSEC eta RMSECV balioak.

	EX2-K (kontrola)	EX2-L ($10\,\mathrm{ng\,L^{-1}}$)	EX2-ME ($100\,\mathrm{ng\,L^{-1}}$)	EX2-H ($1000\,\mathrm{ng\,L^{-1}}$)
RMSEC	0.33	0.38	0.26	0.22
RMSECV	0.49	0.48	0.48	0.38

2.7. Taula: 2.esperimentuko ($100\,\mathrm{ng\,L^{-1}}$ko koktela erabilitako saiaketa) muskuiluen hemolinfen ereduaren informazioa, RMSEC eta RMSECV balioak.

	K1-H (3 egun)	K2-H (5 egun)	K3-H (kontrola)
RMSEC	0.15	0.16	0.01
RMSECV	0.31	0.28	0.15

bariantza azaltzeko gai da. 2.7 Taulan adierazi dira ereduari dagozkion erroreak.

2.esperimentuan lehen osagaiak argi eta garbi desberdintzen ditu kontroleko laginak kutsatutako laginetatik. Bigarren osagaiak, 3.eguneko klasekoak 5.egunekoetatik (denak hil ziren eguna) bereizten ditu.
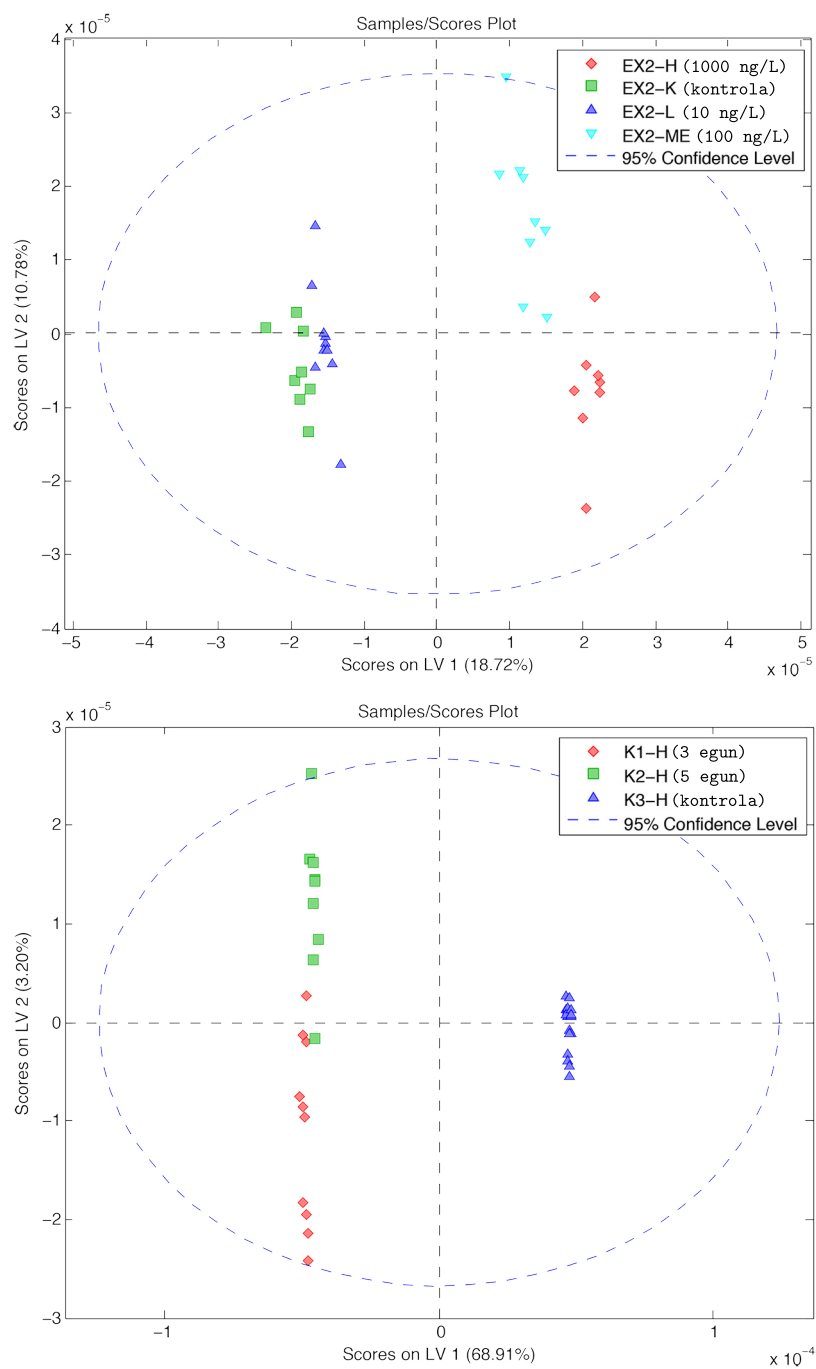
2.14. Irudia: 1. (goikoa) eta 2.esperimentuetako (behekoa) OPLS-DA ereduetatik eskuratutako *score*ak.

(ii) 3. esperimentua

3. esperimentu honetan hemolinfa, gonada eta oina aztertu ziren. Jariakinaren eta ehunen analisi kimiometrikoa egin ostean, emaitzak bateratu eta interpretazio bateratua ematen saiatu ginen.

Behin metabolitoen seinaleen esleipena egiaztatuta, VIPen tauletan batu genituen zenbait metabolito interesgarri.

Interpretazioa errazteko asmoz, kontrolarekiko erreferentziatu genituen seinaleak eta metabolitoen joerak koloreen bitartez adierazi ditugu beromapetan (*heatmap*).

Hemolinfa

3. esperimentuko hemolinfa laginekin eraikitako OPLS-DA ereduan 3 osagai nagusi erabili ditugu x matrizearen %45.55ko bariantza eta y matrizearen %82.19ko bariantza azaltzeko. 2.8 Taulan adierazi ditugu klase bakoitzari dagozkien RMSEC eta RMSECV balioak.

2.15 Irudiko *score*etan lehen osagaiak 7.eguneko klasea kontrol eta 3.eguneko klasearekiko bereizten ditu. Bigarren osagaiak, kontrola 3.eguneko datuetatik bereizten laguntzen du.

2.9 Taulan adierazitako VIPek agerian uzten dituzte 7. eguneko klasean homarina eta betaina bezalako osmolitoen igoerak. Aipagarria da 3. egunean VIPetan aditzera ematen den aldaketa nabarmena metabolito gehienetan.
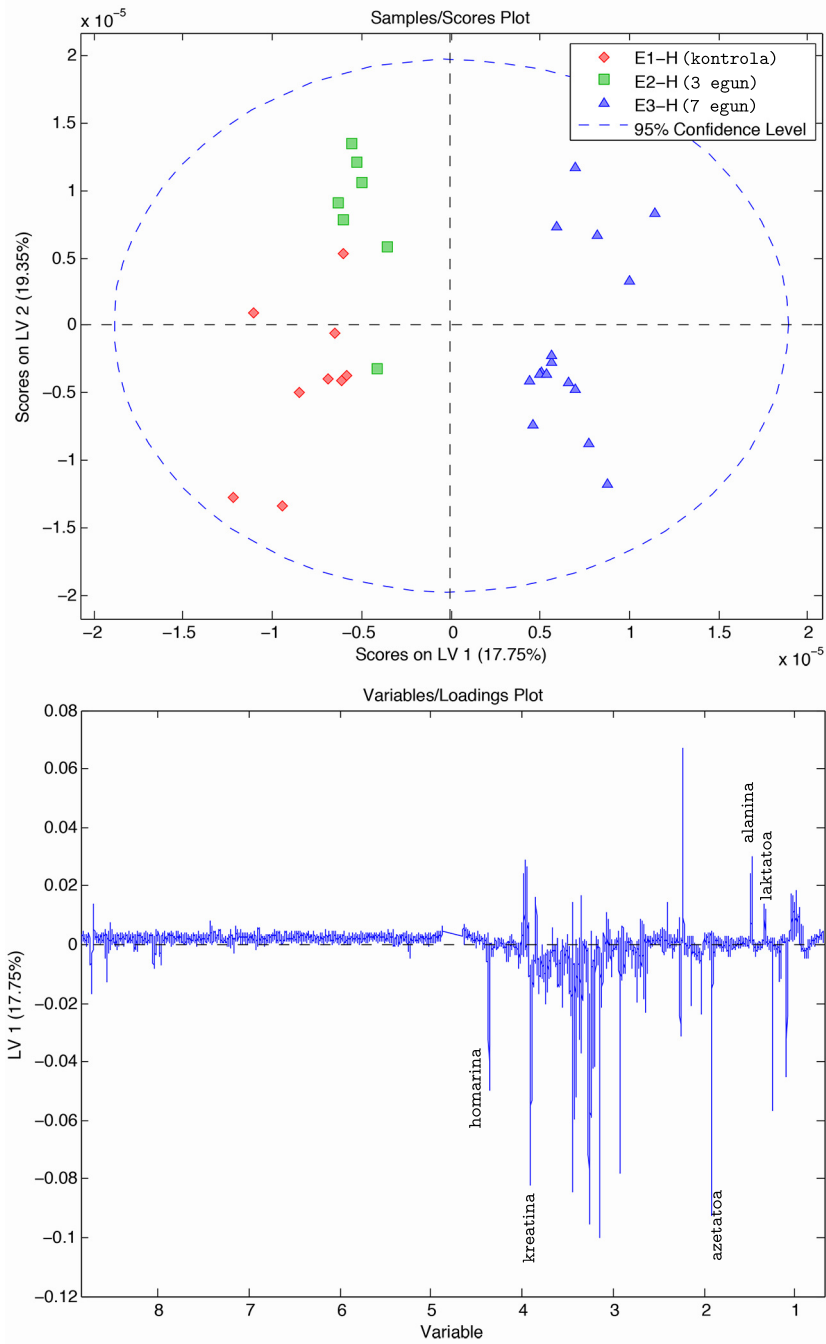
2.15. Irudia: 3.esperimentuko hemolinfa datuekin eraikitako OPLS-DA ereduaren *score*ak (goikoa) eta *loading*ak (behekoa).

2.8. Taula: 3.esperimentuko muskuiluen hemolinfen ereduaren informazioa, RMSEC eta RMSECV balioak.

	E1-H	E2-H	E3-H
RMSEC	0.18	0.23	0.13
RMSECV	0.35	0.42	0.39

2.9. Taula: 20ng/L-ko esperimentuan jasotako hemolinfen klaseak ezaugarritzen dituzten VIPetako metabolito garrantzitsuenen aldaketak laburbiltzen dituen taula. Datuak kontrolarekiko erreferentziatuak daude eta euren joerak errezago interpretatzeko koloreztatuak daude (berdez balio txikiagoak eta gorriz altuagoak).

Metabolitoa	ppm	E1_H_kontrola	E2_H_3egun	E3_H_7egun
leuzina/isoleuzina	0,953	1,00	1,34	0,06
metilmalonatoa	1,248	1,00	0,49	1,48
lactate	1,335	1,00	1,42	0,23
alanina	1,485	1,00	1,65	0,12
azetatoa/azetoazetatoa	1,923	1,00	1,91	0,71
ornitina	1,935	1,00	2,73	0,25
pirubatoa	2,402	1,00	0,43	1,55
sukzinatoa	2,424	1,00	1,80	0,10
aspartatoa	2,849	1,00	1,70	0,06
kolina	3,204	1,00	0,82	1,11
glizerofosfokolina	3,222	1,00	1,35	0,92
fosfokolina	3,227	1,00	0,91	1,19
betaina	3,276	1,00	0,44	1,55
glukosa	3,424	1,00	0,42	1,54
glizina	3,557	1,00	2,03	0,23
homarine	4,364	1,00	0,44	1,56
ATP/ADP	8,542	1,00	2,18	0,11

Gonada

Gonadaren kasuan 3.eguneko zenbait lagin baztertu egin behar izan genituen arazo teknikoak medio eta 2 lagin bakarrik ditugu klase hau azaltzeko. 2.16 Irudian ikusten den bezalaxe, OPLS-DA eredua kontrol taldeak distortsionatu egiten du, kontrol taldea gainerako taldeekin konparatuz oso ezberdina delako. OPLS-DA eredu hau eraikitzeko (ikusi 2.16 eta 2.17 Irudiak) PC erabili ditugu, x matrizearen %54.32ko bariantza eta y matrizearen %36.70ko bariantza azaltzeko. 2.10 Taulan erakutsi ditugu eredu honi dagozkien erroreak.

2.17 Irudian eta 2.11 Taulan adierazi dira ereduaren *loading*ak eta VIPak. 3.egunean dugu aldaketarik nabariena, hots, kreatina, α-zetoglutarato, metilmalonato, fosfokreatina, serina eta hidroxibutirato metabolitoen igoera handienak. Guztiak estres egoera honen erantzun gisa azaldu ahal dira.

2.10. Taula: 3.esperimentuko muskuiluen gonaden ereduaren informazioa, RMSEC eta RMSECV balioak.

	E1-G	E2-G	E3-G	E4-G
RMSEC	0.13	0.21	0.44	0.37
RMSECV	0.27	0.23	0.55	0.45
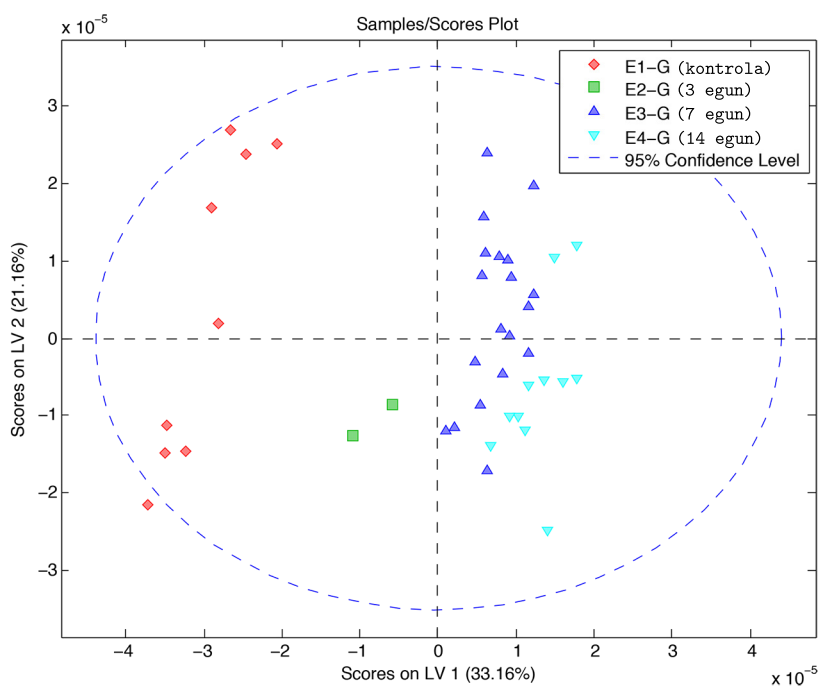
2.16. Irudia: 3.esperimentuko oinen datuekin eraikitako OPLS-DA ereduaren *score*ak.
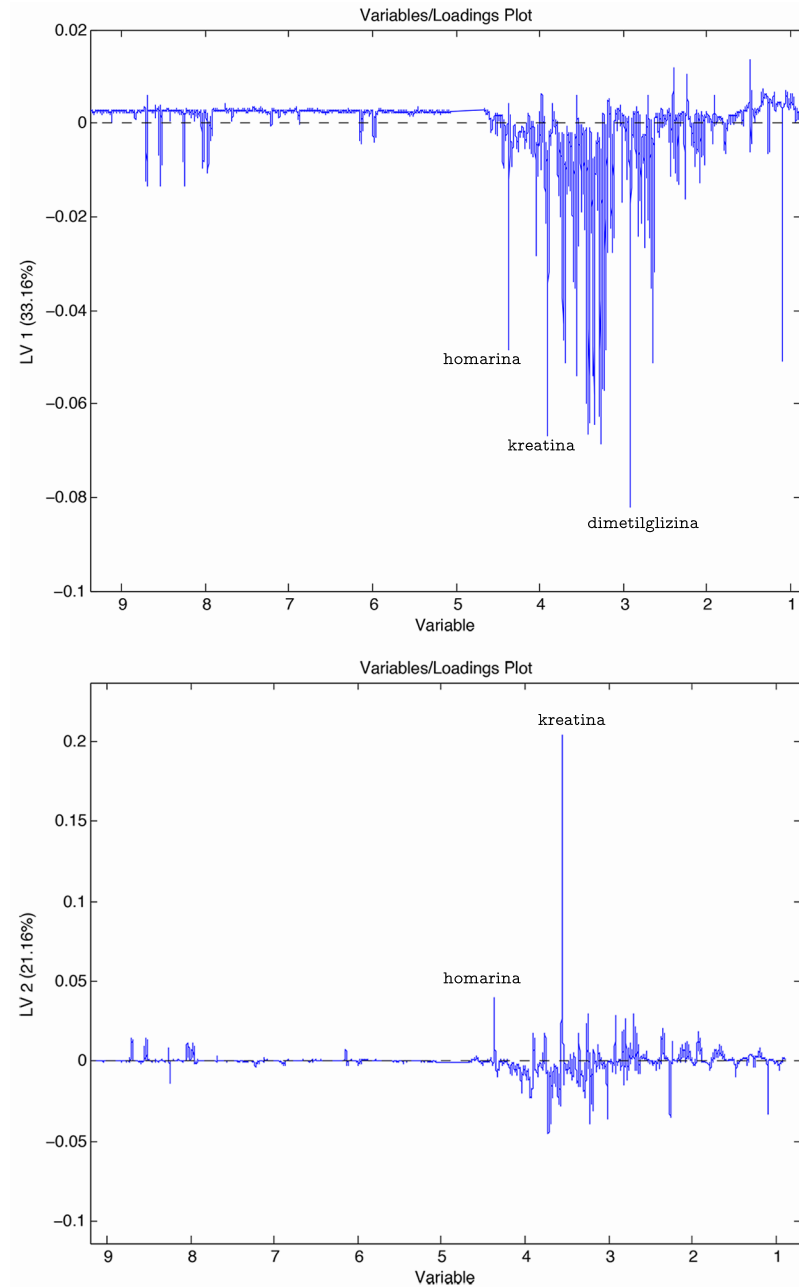
2.17. Irudia: 3.esperimentuko gonaden datuekin eraikitako OPLS-DA ereduaren *loading*ak (goikoa lehen osagaikoa eta behekoa bigarren osagaikoa).

2.11. Taula: 20 ng/L-ko esperimentuan jasotako gonaden klaseak ezaugarritzen dituzten VIPetako metabolito garrantzitsuenen aldaketak laburbiltzen dituen taula. Datuak kontrolarekiko erreferentziatuak daude eta euren joerak errezago interpretatzeko koloreztatuta daude (berdez balio txikiagoak eta gorriz altuagoak).

Metabolitoa	ppm	E1_G_kontrola	E2_G_3egun	E3_G_7egun	E4_G_14egun
leuzina/isoleuzina	0,961	1,00	3,87	1,82	2,07
balina	0,980	1,00	1,79	1,23	1,30
D-3-Hidroxibutiratoa	1,180	1,00	18,14	5,88	7,41
laktatoa	1,333	1,00	0,61	0,89	0,85
alanina	1,471	1,00	1,76	0,87	0,82
azetatoa/azetoazetatoa	1,915	1,00	13,88	4,66	5,82
glutamate	2,060	1,00	0,68	0,91	0,88
pirubate	2,400	1,00	5,58	2,30	2,71
hipotaurina	2,659	1,00	0,45	0,84	0,80
aspartatoa	2,824	1,00	2,63	1,46	1,61
α-zetoglutaratoa	3,010	1,00	31,55	9,69	12,43
kreatinina	3,023	1,00	30,90	9,51	12,18
zisteina	3,112	1,00	0,47	0,85	0,80
metilmalonatoa	3,177	1,00	6,41	2,54	3,02
kolina	3,203	1,00	0,58	0,88	0,84
glizerofosfokolina	3,226	1,00	0,79	0,94	0,92
fosfokolina	3,226	1,00	0,93	0,98	0,98
betaina	3,277	1,00	1,14	1,04	1,05
taurina	3,284	1,00	5,88	2,39	2,83
glukosa	3,423	1,00	0,38	0,82	0,77
glizina	3,567	1,00	3,97	1,84	2,11
serina	3,845	1,00	15,29	5,07	6,35
fosfokreatina	3,951	1,00	29,64	9,15	11,71
ATP/ADP	8,543	1,00	0,33	0,81	0,75
ezezaguna	8,700	1,00	28,29	8,76	11,21

Oina

Azkenik, oinaren eredua aipatuko dugu. OPLS-DA eredua eraikitzeko 2 PC erabili dira x matrizearen %51.11-ko bariantza eta y matrizearen %49.83ko bariantza azaltzeko. 2.12 Taulan erakutsi ditugu eredu honen erroreak.

2.18 Irudian lehen osagaiak bi talde nagusi banatzen dituela ikus dezakegu, kontrola eta 3.eguneko laginal 7. eta 14.egunekoetatik banatzen ditu. Bigarren osagaiak ordea, kontrola 3.egunekotik eta 7.eguna 14.egunekotik banatzen ditu.

2.20 Irudian OPLS-DA eredutik eskuratutako VIPen tartean eta 2.19 Taulan ikus daitekeen bezala, oinean aurkitutako aldaketa handienak, hots, homarina, kreatina, betainak, kolina, taurina eta azetato metabolitoetan aurkitzen dira.

2.12. Taula: 3.esperimentuko muskuiluen oinen ereduaren informazioa, RMSEC eta RMSECV balioak.

	E1-O	E2-O	E3-O	E4-O
RMSEC	0.21	0.29	0.29	0.37
RMSECV	0.36	0.33	0.40	0.41
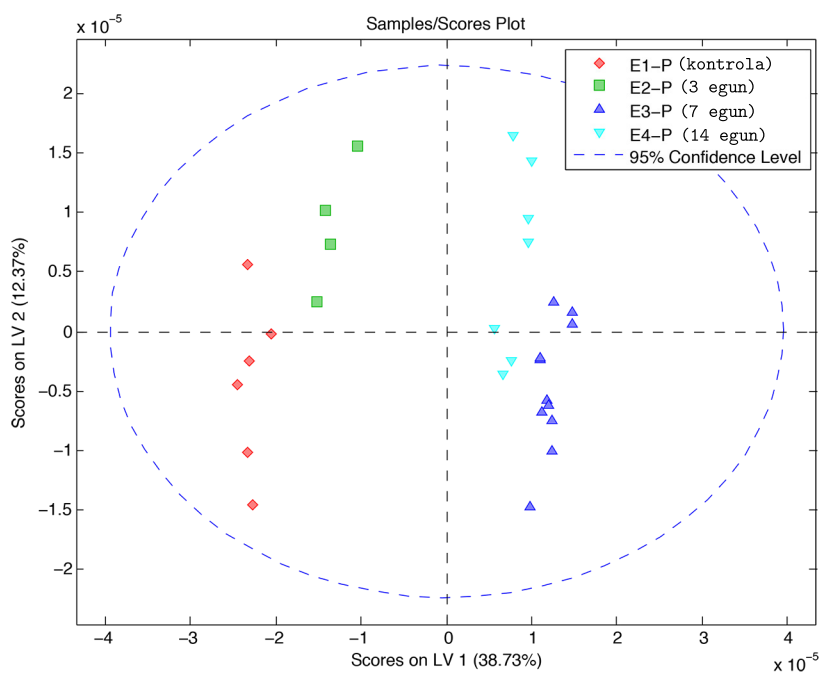
2.18. Irudia: 3.esperimentuko oinen datuekin eraikitako OPLS-DA ereduaren *score*ak.
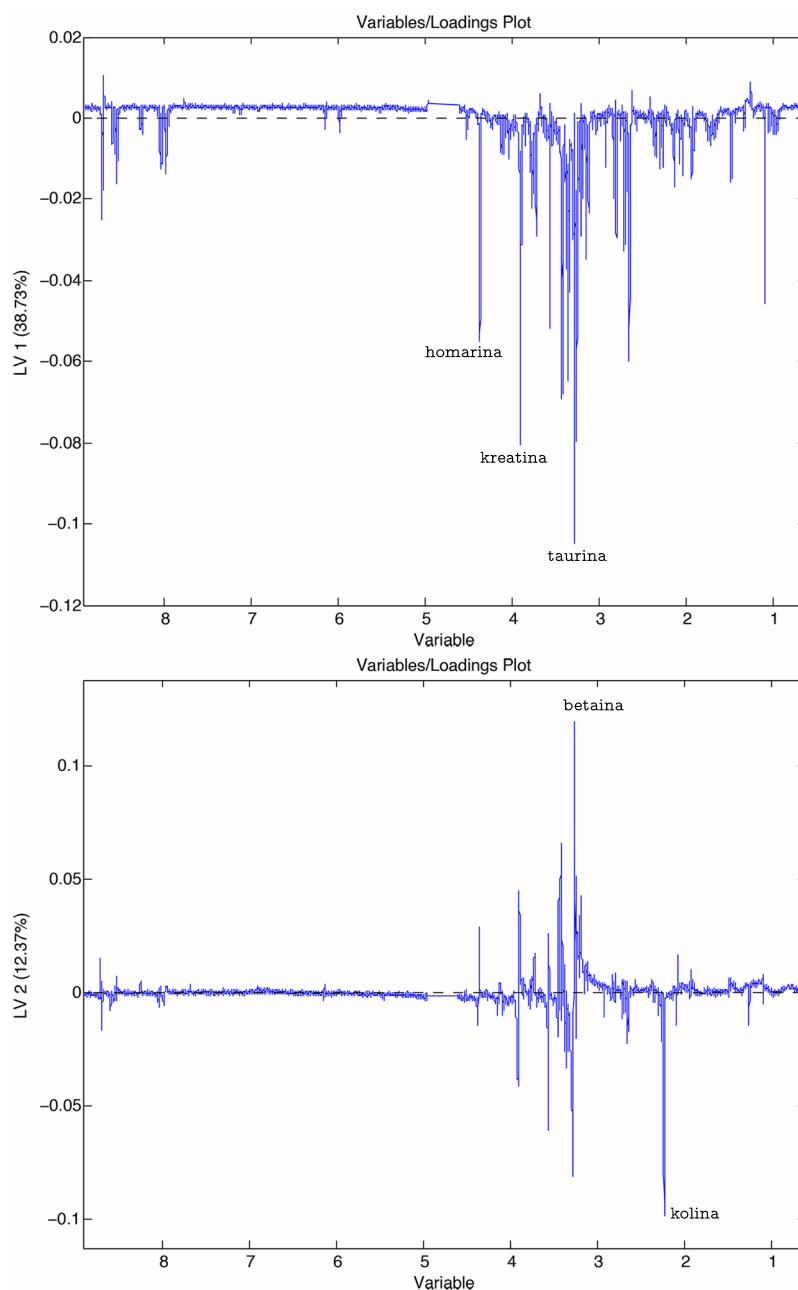
2.19. Irudia: 3.esperimentuko oinen datuekin eraikitako OPLS-DA ereduaren *loading*ak (goikoa lehen osagaikoa eta behekoa bigarren osagaikoa).
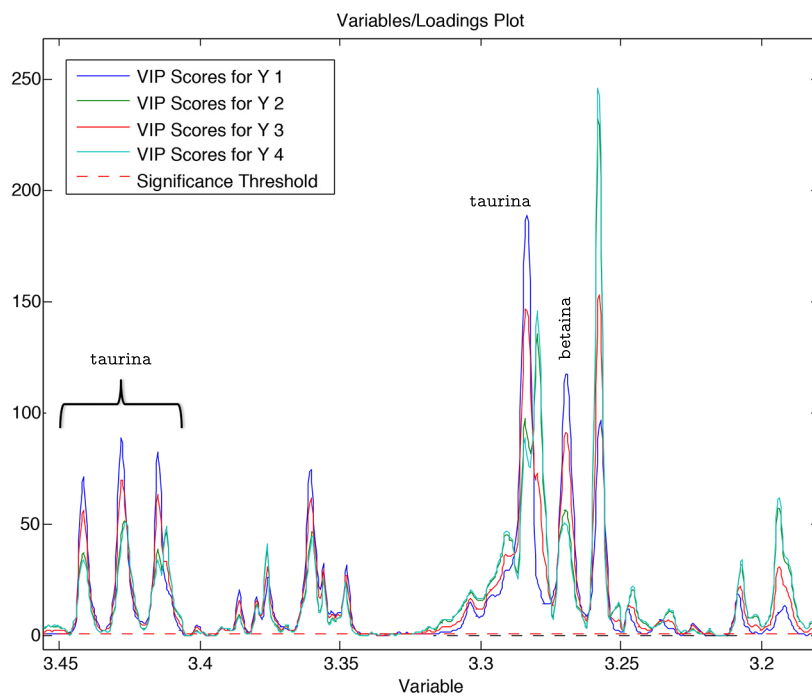
2.20. Irudia: 3.esperimentuko oinen datuekin eraikitako OPLS-DA ereduaren VIPen erakusgarri den tartea.

2.13. Taula: 20ng/L-ko esperimentuan jasotako oinen klaseak ezaugarritzen dituzten VIPetako metabolito garrantzitsuenen aldaketak laburbiltzen dituen taula. Datuak kontrolarekiko erreferentziatuak daude eta euren joerak errezago interpretatzeko koloreztatuta daude (berdez balio txikiagoak eta gorriz altuagoak).

Metabolitoa	ppm	E1_P_kontrola	E2_P_3egun	E3_P_7egun	E4_P_14egun
alanina	1,478	1,00	0,63	0,84	0,60
azetatoa/azetoazetatoa	1,921	1,00	5,60	2,99	6,04
ornitina	1,935	1,00	0,48	0,77	0,43
pirubatoa	2,409	1,00	1,54	1,23	1,59
zitratoa	2,639	1,00	1,17	1,07	1,19
hipotaurina	2,667	1,00	0,50	0,78	0,45
aspartatoa	2,809	1,00	2,47	1,64	2,61
asparagina	2,928	1,00	0,97	0,99	0,97
zisteina	3,114	1,00	0,48	0,77	0,43
histidina	3,146	1,00	0,60	0,83	0,56
metilmalonatoa	3,192	1,00	2,72	1,75	2,89
kolina	3,208	1,00	1,07	1,03	1,08
glizerofosfokolina	3,224	1,00	0,58	0,82	0,53
fosfokolina	3,227	1,00	3,00	1,87	3,20
betaina	3,270	1,00	0,53	0,79	0,48
taurina	3,280	1,00	5,43	2,92	5,86
glukosa	3,415	1,00	0,47	0,77	0,42
glizina	3,564	1,00	1,29	1,13	1,32
homarina	4,371	1,00	0,53	0,80	0,49
ATP/ADP	8,548	1,00	0,51	0,79	0,46

Ondorioak ateratzeko orduan lehentasuna eman diegu gonadekin eta oinekin lortutako emaitzei. Izan ere, hemolinfa hartzeko eskarmentu berezia izan behar zen, zeren eta arrisku handia baitzegoen ehunetako zelula asko (obozitoak, muskuluko zelulak, e.a.) jaso izana eta horiek zorizko artefakto asko sar zitzakeela uste dugu. Gainera jasotako hemolinfa bolumenean zaila da errepikakorra izatea. Honetaz gain, 14.eguneko hemolinfa laginekin arazoren bat izan genuen. VIPak aztertzerakoan 14.eguneko eta kontroleko VIPak oso antzekoak zirela ohartu ginen, nahiz eta laginen kudeaketa eta tratamenduan arazorik antzeman ez genuen, beraz, 14.eguneko taldea eredutik kentzea erabaki genuen.

Aldaketa handiena, 3.egunean ikusten dugu, oinean, gonadan zein hemolinfan. Aldaketa nabarmenena hala ere, gonadan antzeman zen, ondoren oinean eta azkenik hemolinfan. Aipatu beharra dugu, 3.egunean errutea gertatu zela eta gertaera honek azal ditzake egun honetan bereziki antzemandako aldaketa metabolikoak.

Kontrolarekin konparatuz kutsatzaileen eraginpean izandako laginek, hidroxibutirato, azetato, taurina, kreatina eta α-zetoglutaratoaren mailetan igoera handiak aurkeztu zituzten. Hidroxibutirato, azetato eta kreatina mailen igoera, hantura orokorraren adierazle metabolikoak izaten dira, ugaztunetan behinik behin hipertermiaren kapituluan azalduko dugun bezalaxe. Aminoazidoen kontzentrazioek ere gora egin zuten baina glutamatoa, zisteina, glizina eta histidinaren mailak jaitsi egin ziren oinean eta baita gonadan. Alanina eta aspartatoaren kasuan ordea, oinean bakarrik antzematen da metabolito hauen jaitsiera.

3.egunean ATP/ADPren mailan jaitsiera nabarmenena aurkitu genuen, gonadan bereziki. Ziur aski, energia kontsumo hau errutearekin

erlazionatuta dago. Energia beharrizan hau agerian dago glukosaren mailan jaitsiera ere antzeman baitugu.

Oro har, esposizioak aldaera nabariak ekarri ditu muskuiluetan. Alde batetik, kutsatzaileen metaketa garbia eta bestetik aldaketa metabolitko eta fisiologikoak.

2.4.3   Analisi histopatologikoa

Muskuiluetan antzeman zen ondoriorik larriena, errute goiztiarra izan zen. Argi ikus daiteke 2.21 Irudian, nola muskuiluak obozitoak askatu zituen. Muskuiluak estres egoera handian daudenean, errutea dute erantzun ohiko bat, egoera aktibo batetik pasiboago batera joateko bizirauteko asmo bakarrarekin.
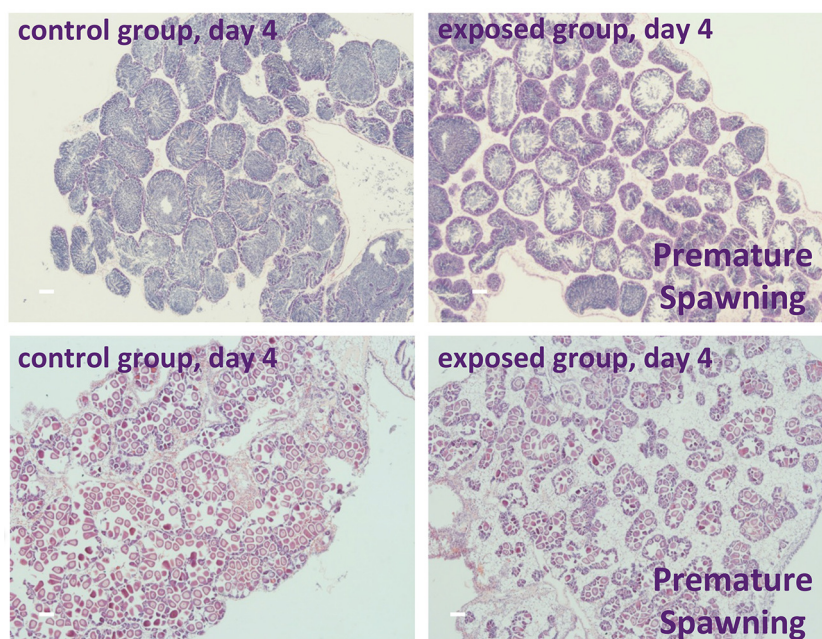
2.21. Irudia: Gonaden hematoxilina eta eosina tindaketaren ondoren lortutako irudiak, gonaden garapenean aldaketa nabarmena dugu, errutea.

2.5   Ondorioak

Laginketa pasiboaren bitartez itsasadarretako kutsatzaileen kontzentrazioak kalkulatzeko gai izan gaitezkela frogatu dugu, ur gezatan baita gazitan duten eragikortasuna frogatu delako. Horretarako laginketa pasiboa oso egokia da baina muskuiluak akumulatutakoarekin alderatuz gero, laginketa pasiboaren bitartez neurtutako kontzentrazioak ez datoz bat. Erreza da azaltzea azken gertaera hau. Laginketa aktiboan milaka mekanismo eta bide metabolikoren menpe daude organismoan sartutako kutsatzaileak eta eraldaketa eta kanporatzeak jasan ditzake. Muskuiluak aktibo daudenean 30 mLur/minko iragazten dute, bitartean, laginketa pasiboko tresneria inguruko urarekin izango du kontaktua (kontaktu hau handitzeko karrusel birakarian kokatu dira). Bi neurketa mota hauetatik, informazio osagarria eskuratzen dugu, laginketa pasiboak argi erakutsi baitu, oso aproposa dela denboran zehar gertatutako kutsatzaileen aldaketak neurtzeko. Gainera, ur oso kutsatua analisatu beharko bagenu, muskuiluek ez lukete ezertarako balio izango, hil egingo zirelako eta kasu horietan laginketa pasiboa oso interesgarria litzateke.

Muskuiluen analisiari dagokionez, 2,4-DDD konpasatuan aurkitu dira kontzentrazio altuenak. Uretako kutsatzaile honen kontzentrazioa igoterakoan, proportzionalki igoten da muskuiluko kontzentrazioa. Badirudi, analitoek biokontzentrazioa eta log K_{ow} balioen artean korrelazioa dagoela, zenbat eta logK_{ow} balio altuagoa izan, gehiago akumulatzen da muskuiluan.

Metabolomika oso lanabes erabilgarri eta interesgarria da eta gure sistemaren "osasun" egoeraren berri ematen digu. Gainera histopatologiako emaitzekin alderatuz informazio gehiago lortzeko gai izan gara. Erantzun biologiko garrantzitsuena errute goiztiarra izan da eta metabolomikako

emaitzak ikusiz, esan dezakegu, eragindako aldaketa metabolomikoek ugalketa zikloan eragin dutela zuzenean.

Amaitzeko, gure ustetan, planteatutako estrategia oso erabilgarria da eta etorkizunean gure estuario eta itsasertzetan aplikatu nahi dugu.

Erreferentziak

[1] R.P. Schwarzenbach, T. Egli, T.B. Hofstetter, U. von Gunten and B. Wehrli. Global water pollution and human health. *Annu. Rev. Environ. Resour.*, 35(1):109–136, 2010.

[2] S.D. Richardson and S.Y. Kimura. Water analysis: Emerging contaminants and current issues. *Anal. Chem.*, 88(1):546–582, 2016.

[3] B. Vrana, A. Paschke and P. Popp. Calibration and field performance of membrane-enclosed sorptive coating for integrative passive sampling of persistent organic pollutants in water. *Environ. Pollut.*, 144(1):296–307, 2006.

[4] F. Rigét, K. Vorkamp, R. Bossi, C. Sonne, R. J. Letcher and R. Dietz. Twenty years of monitoring of persistent organic pollutants in greenland biota. a review. *Environ. Pollut.*, 2015: 1–10.

[5] B. Petrie, R. Barden and B. Kasprzyk-Hordern. A review on emerging contaminants in wastewaters and the environment: Current knowledge, understudied areas and recommendations for future monitoring. *Water Res.*, 72:3–27, 2015.

[6] V. Geissen, H. Mol, E. Klumpp, G. Umlauf, M. Nadal, M. van der Ploeg, S.E.A.T.M. van de Zee and C.J. Ritsema. Emerging pollutants

in the environment: A challenge for water resource management. *Int. Soil and Water Cons. Res.*, 3(1):57–65, 2015.

[7] A. Soares, B. Guieysse, B. Jefferson, E. Cartmell and J.N. Lester. Nonylphenol in the environment: a critical review on occurrence, fate, toxicity and treatment in wastewaters. *Environ. Int.*, 34(7):1033–1049, 2008.

[8] M.H. Devier, K. Le Menach, L. Viglino, L. Di Gioia, P. Lachassagne and H.Budzinski. Ultra-trace analysis of hormones, pharmaceutical substances, alkylphenols and phthalates in two french natural mineral waters. *Sci. Total Environ.*, 443:621–632, 2013.

[9] M. Ortiz-Zarragoitia, C. Bizarro, I. Rojo-Bartolome, O. Diaz de Cerio, M. P Cajaraville, and I. Cancio. Mugilid fish are sentinels of exposure to endocrine disrupting compounds in coastal and estuarine environments. *Mar. Drugs*, 12(9):4756–4782, 2014.

[10] N. Salgueiro-Gonzalez, I. Turnes-Carou, S. Muniategui-Lorenzo, P. Lopez-Mahia and D. Prada-Rodriguez. Membrane assisted solvent extraction coupled with liquid chromatography tandem mass spectrometry applied to the analysis of alkylphenols in water samples. *J. Chromatogr. A*, 1281:46–53, 2013.

[11] P.R. Rivadeneira, M. Agrelo, S. Otero and G. Kristoff. Different effects of subchronic exposure to low concentrations of the organophosphate insecticide chlorpyrifos in a freshwater gastropod. *Ecotoxicol. Environ. Saf.*, 90:82–88, 2013.

[12] A. Jurado, E. Vàzquez-Suñé, J. Carrera, M. López de Alda, E. Pujades and D. Barceló. Emerging organic contaminants in groundwater in

Spain: A review of sources, recent occurrence and fate in a european context. *Sci. Total Environ.*, 440:82–94, 2012.

[13] C. Turgut. The contamination with organochlorine pesticides and heavy metals in surface water in Kucuk Menderes river in Turkey, 2000-2002. *Environ. Int.*, 29(1):29–32, 2003.

[14] G.O. Guler, Y.S. Cakmak, Z. Dagli, A. Aktumsek and H. Ozparlak. Organochlorine pesticide residues in wheat from Konya region, Turkey. *Food. Chem. Toxicol.*, 48(5):1218–1221, 2010.

[15] H. Kuranchie-Mensah, S. Manukure Atiemo, L. Maud N. Palm, S. Blankson-Arthur, A. Osei Tutu, and P. Fosu. Determination of organochlorine pesticide residue in sediment and water from the Densu river basin, Ghana. *Chemosphere*, 86(3):286–292, 2012.

[16] M.S. Díaz-Cruz and D. Barceló. *Personal care products in the aquatic environment.* Springer, 2015.

[17] O. Posada-Ureta, M. Olivares, P. Navarro, A. Vallejo, O. Zuloaga, and N. Etxebarria. Membrane assisted solvent extraction coupled to large volume injection-gas chromatography-mass spectrometry for trace analysis of synthetic musks in environmental water samples. *J. Chromatogr. A*, 1227:38–47, 2012.

[18] P. Ventrice, D. Ventrice, E. Russo, and G. De Sarro. Phthalates: European regulation, chemistry, pharmacokinetic and related toxicity. *Environ. Toxicol. Pharmacol.*, 36(1):88–96, 2013.

[19] ChemSpider Chemspider. http://www.chemspider.com (last visit: may 2016).

[20] N. Fidalgo-Used, E. Blanco-Gonzalez and A. Sanz-Medel. Sample handling strategies for the determination of persistent trace organic contaminants from biota samples. *Anal. Chim. Acta*, 590(1):1–16, 2007.

[21] A. Iparraguirre, R. Rodil, J.B. Quintana, E. Bizkarguenaga, A. Prieto, O. Zuloaga, R. Cela and L.A. Fernandez. Matrix solid-phase dispersion of polybrominated diphenyl ethers and their hydroxylated and methoxylated analogues in lettuce, carrot and soil. *J. Chromatogr. A*, 1360:57–65, 2014.

[22] H. Ziarrusta, M. Olivares, A. Delgado, O. Posada-Ureta, O. Zuloaga and N Etxebarria. Multiscreening determination of organic pollutants in molluscs using matrix solid phase dispersion. *J. Chromatogr. A*, 1391:18–30, 2015.

[23] S.A. Barker. Matrix solid phase dispersion (MSPD). *J. Biochem. Biophys. Methods*, 70(2):151–162, 2007.

[24] E. Villaverde-de Saa, J. Benito Quintana, R. Rodil, R. Ferrero-Refojos, E. Rubi and R. Cela. Determination of perfluorinated compounds in mollusks by matrix solid-phase dispersion and liquid chromatography-tandem mass spectrometry. *Anal. Bioanal. Chem.*, 402(1):509–518, 2012.

[25] M. Munoz-Ortuno, Y. Moliner-Martinez, S. Cogollos-Costa, R. Herraez-Hernandez and P. Campins-Falco. A miniaturized method for estimating di(2-ethylhexyl) phthalate in bivalves as bioindicators. *J. Chromatogr. A*, 1260:169–173, 2012.

[26] R.Q. Wu, X.F. Zhao, Z.Y. Wang, M. Zhou and Q.M. Chen. Novel molecular events in oral carcinogenesis via integrative approaches. *J. Dent. Res.*, 90(5):561–572, 2011.

[27] L. Garmendia, M. Soto, U. Vicario, Y. Kim, M.P. Cajaraville and I. Marigomez. Application of a battery of biomarkers in mussel digestive gland to assess long-term effects of the prestige oil spill in Galicia and bay of Biscay: tissue-level biomarkers and histopathology. *J. Environ. Monit.*, 13(4):915–932, 2011.

[28] W.S. Fisher, L.M. Oliver, J.T. Winstead and E.R. Long. A survey of oysters crassostrea virginica from Tampa bay, Florida: associations of internal defense measurements with contaminant burdens. *Aquat. Toxicol.*, 51(1):115–138, 000.

[29] J.A. Couch. *Chemically induced histopathology in aquatic invertebrates. In: Pathology of marine and estuarine organisms.* 1992.

[30] I. Marigomez M.P. Cajaraville A. Orbea and L. Garmendia. Effects of the prestige oil spill on cellular biomarkers in intertidal mussels-results of first year of studies. *Mar. Ecol. Prog. Ser.*, 306:177–189, 2006.

[31] U. Izagirre, L. Garmendia, M. Soto, N. Etxebarria and I. Marigomez. Health status assessment through an integrative biomarker approach in mussels of different ages with a different history of exposure to the prestige oil spill. *Sci. Total Environ.*, 493:65–78, 2014.

[32] O. Posada-Ureta, M. Olivares, L. Zatón, A. Delgado, A. Prieto, A. Vallejo, A. Paschke and N. Etxebarria. Uptake calibration of polymer-based passive samplers for monitoring priority and emerging organic

non-polar pollutants in WWTP effluents. *Anal. Bioanal. Chem.*, 408(12):3165–3175, 2016.

[33] I. Clausen and H.U. Riisgard. Growth, filtration and respiration in the mussel Mytilus edulis: no evidence for physiological regulation of the filter-pump to nutritional needs. *Mar. Ecol. Prog. Ser.*, 141:37–45, 1996.

[34] H. Wu, A.D. Southam, A. Hines, and M.R. Viant. High-throughput tissue extraction protocol for NMR- and MS-based metabolomics. *Anal. Biochem.*, 372(2):204 – 212, 2008.

[35] Mark R Viant. Revealing the metabolome of animal tissues using 1H nuclear magnetic resonance spectroscopy. *Methods Mol. Biol.*, 358:229–246, 2007.

[36] Madison-Qingdao Metabolomics Consortium Database. http://mmcd.nmrfam.wisc.edu (last visit: may 2016).

[37] Biological Magnetic Resonance Data Bank. http://www.bmrb.wisc.edu (last visit: 2016 may).

[38] The Human metabolome database. http://www.hmdb.ca (last visit: 2016 may).

[39] R.P. Ellis, J.I. Spicer, J.J. Byrne, U. Sommer, M.R. Viant, D.A. White and S. Widdicombe. 1H NMR metabolomics reveals contrasting response by male and female mussels exposed to reduced seawater pH, increased temperature, and a pathogen. *Environ. Sci. Technol.*, *48(12):7044–7052, 2014.*

[40] Mark R. Viant, Eric S. Rosenblum and Ronald S. Tjeerdema. NMR-based metabolomics: A powerful approach for characterizing the effects of environmental stressors on organism health. Environmental Science & Technology, 37(21):4982–4989, 2003.

[41] L.M Samuelsson, L. Forlin, G. Karlsson, M. Adolfsson-Erici and D.G. Joakim Larsson. Using NMR metabolomics to identify responses of an environmental estrogen in blood plasma of fish. Aquat. Toxicol., 78(4):341–349, 2006.

[42] W. Tuffnail, G.A. Mills, P. Cary and R. Greenwood. An environmental 1H NMR metabolomic study of the exposure of the marine mussel Mytilus edulis to atrazine, lindane, hypoxia and starvation. Metabolomics, 5(1):33–43, 2009.

[43] A. Hines, G.S. Oladiran, J.P Bignell, G.D Stentiford and Mark R Viant. Direct sampling of organisms from the field and knowledge of their phenotype: key recommendations for environmental metabolomics. Environ. Sci. Technol., 41(9):3375–3381, 2007.

[44] A. Delgado, A. Prieto, A. Vallejo, M. Irazola, A. Paschke, O. Posada-Ureta, M. Olivares and N. Etxebarria. Applicability of polydimethylsiloxane (PDMS) and polyethersulfone (PES) as passive samplers of more hydrophobic organic compounds in intertidal estuarine environments. Sci. Total Environ. (submitted), 2016.

[45] D. Mackay, W.Y. Shiu, K.-Ching Ma and Editors. Illustrated Handbook of Physical-Chemical properties and Environmental Fate for Organic Chemicals, Volume V: Pesticides. CRC, 1997.

Magnetic hyperthermia therapy project: colorectal liver metastasis

Chapter 3

Magnetic hyperthermia therapy project

3.1 Introduction

Cancer is the name for diseases in which abnormal cells divide without control and can spread through bloodstream or lymphatic system to other tissues of the body. It was once consider a fatal disease, but nowadays survival rate has increased owing to the early-stage detection. However, cancer remains the second deadliest disease after circulatory system diseases in the European Union [1]. According to GLOBOCAN 2012 [2] (a project to estimate the incidence of mortality and prevalence from major types of cancer worldwide), an estimated 14.1 million new cancer cases and 8.2 million cancer-related deaths occurred in 2012. The most commonly diagnosed cancers worldwide were those of the lung (13.0% of the total), breast (11.9%) and colorectum (9.7%). Among all the cancer types, the most common causes of cancer death were cancers of the lung (19.4% of the total), liver (9.1%), and stomach (8.8%) [2].

Colorectal cancer (CRC) is a disease in which the cells that line the colon or rectum of the gastrointestinal tract become abnormal and grow out of control. In the stage IV, the colon cancer spread specially to the liver, but it can also reach up other places such as the lungs, peritoneum or to lymph nodes. More than 50% of the patients with CRC develop metastasis, most frequently in the liver. In fact, colorectal liver metastasis (CLM) is the main cause of cancer-related morbidity and mortality in colorectal cancer [3, 4]. Currently, the clinical treatment options are surgical resection (partial hepatectomy), liver transplantation, local ablation with radiofrecuency or precutaneous ethanol injection, chemoembolization, transcatheter therapy and systemic therapies (such as sorafenib) [5]. Surgical resection remains as the first-line treatment option for patients with liver tumors, but only 15% to 20% of the patients are suitable for surgical resection. Unfortunately, the cancer recurrence after curative resection is common for the 50% to 75% of the patients within two years [4,6–8]

One of the features of cancers is the chaotic vascularisation due to the unregulated and fast growth of cells, which gives rise to a defective blood perfusion. As a result, the tumours and the surrounding tissues present a lower pH and a lower oxygen pressure than the healthy tissue. These conditions make less effective the radiotherapy and the chemotherapy due to the impossibility to reach the aimed therapeutic dose to the affected regions. In contrast, this fact is favourable in the hyperthermia therapies (temperature increments in the range of $42\,°C$-$46\,°C$) since the poor vascularisation in tumours causes a higher thermal sensitivity. It is well known the fact that sustained temperature above $42\,°C$ causes necrosis of living cells. Actually, hyperthermia causes the alteration of

structural and enzymatic proteins that can induce apoptosis (programmed cell death) [9].

Heat has been known and used as a cancer treatment since very ancient times. The oldest reference is dated around 3000 BC and it was found in the Edwin Smith Egyptian papyrus [10]. Fortunately, improvements in methodology and technology have allowed a substantial progress in the field of the hyperthermia therapies in the last two decades. For example, the integration of nanotechnology has been the key to obtain a better localization of tumours and to have access to unattainable tumours so far. In addition, many researches have showed that the combination of hyperthermia with different therapies, such as radiotherapy or chemotherapy, enhances their own effectiveness [9].

Depending on the temperature increment, the effects of the hyperthermia therapies are different. In the case of an increment above $46\,^\circ$C and under $56\,^\circ$C of a cancerous tissue, the therapy is called thermal ablation, and the cell death is directly produced mainly by coagulative necrosis [11]. This treatment is really effective, but the release of necrotic materials can cause critical systemic side effects and an important inflammatory response [9]. In the case of mild hyperthermia, the treatment is performed between $41\,^\circ$C to $46\,^\circ$C, inducing apoptosis.

Among all the hyperthermia modalities, we want to highlight the use of magnetic nanoparticles (MNPs) as mediators for localized magnetic mild hyperthermia. The MNPs act as inductive mediators and, in the presence of an electromagnetic field, can deliver heat in an alternating current (AC) magnetic field. The use of inductive mediators seems to be the best choice since the tissues do not have intrinsic magnetic materials that can be heated. However, it is impossible to avoid the resistance heating by eddy

currents since the electromagnetic field is never equal to zero [12]. Eddy currents are not exclusive of magnetic materials and also occur in tissues, even if the specific electrical conductivity is about eight orders of magnitude smaller than in metals [13].

Technically speaking, the application of the radiofrequency has to make compatible the amplitude and frequency of the AC magnetic field with the comfort threshold of the patients within the limits of minimum penetration and neuromuscular stimulation [14].

In addition to the physical constraints, the use MNPs in hyperthermia has to overcome two more constraints. On the one hand, the MNPs must be compatible with the guest cells and, on the other hand, the MNPs should show defined magnetic features.

Regarding the biocompatibility, the MNPs introduced in the systemic circulation have to interact with a diversity of immunologically active cell types and pass over a large macrophague population in the liver, termed Kupffer cells [15]. Therefore, in order to avoid the recognition by these cells and to target the MNPs to tumour cells, so called active targeting, MNPs are functionalised by ligands such as cyclic arginine – glycine – aspartic acid (RGD). The use of cyclic RGD peptides as ligands in MNPs allows to target integrin-expressing tumour cells and let have a longer half-life in the blood. The targeting or the localisation of MNPs in the cancerous tissues is crucial to avoid the damage in healthy tissues.

Regarding the magnetic features, the intrinsic magnetization of iron oxides (Fe_xO_y) and their natural presence in the body (e.g. ferritin, hemosiderin, transferrin, hemoglobin) make them the best candidates for magnetic hyperthermia therapies [16]. In addition, the lethal dose of iron oxide nanoparticles is in the range of 300 and 600 mg of iron per kilogram

(body mass) [12,17,18]. Therefore, maghemite and magnetite nanoparticles are widely investigated for magnetic hyperthermia therapies.

Finally, biomedical application of MNPs requires a proper dispersion in a phosphate-buffered saline (PBS) aquatic medium. Thus, the colloids have to be stabilized against agglomeration in aquatic medium by using a protecting shell for each NP, such as a polymeric shell or hydrophilic molecules. The use of small NPs, with smaller diameters than 20 nm, is recommended to obtain a stable dispersion.

The use of MNPs is not limited to hyperthermia, since they are currently used as contrast agents in magnetic resonance imaging [17] and as targeted drug delivery systems [19], which offers a wider range of applications.

3.1.1 Overview of the magnetic hyperthermia experiments

Over the last six years, a multidisciplinary group from the University of the Basque Country (UPV/EHU) has worked together in the development of a magnetic hyperthermia treatment for the CLM. Our multidisciplinary work is constituted by the Department of Surgery, Radiology and Physical Medicine, the Department of Radiology from the Hospital Galdakao-Usansolo, the MIMASPEC research group (Department of Electricity and Electronics), the Department of Organic Chemistry I (Donostia), the Department of Inorganic Chemistry and the IBeA research group (Ikerketa eta Berrikuntza Analitikoa from the Department of Analytical Chemistry).

The experiments carried out in this study are focused on the magnetic hyperthermia treatment for the CLM. Along these years, *in vitro*, *ex vivo* and *in vivo* experiments have been carried out to study and to develop the surgical procedures for the nanoparticle infusion, the synthesis of magnetic nanoparticles and their functionalisation, the design of the electromagnetic

applicator prototypes and the diagnosis techniques. Many research works and conference communications are part of the outcome of this project [20–30].

The main outcomes of the developed research are reflected in the last *in vivo* experiments. The main objective of these *in vivo* experiments was to achieve a temperature increment in tumour tissues. For this purpose WAG/RiJHsd rats (male *Rattus norvegicus* laboratory rats) were inoculated in the left hepatic lobe with CC-531 colon adenocarcinoma cells. Once the tumor induction was confirmed by ultrasonographic examinations (around $0.8\,cm^3$ after 31 days from the inoculation) [31], the rats were injected with $1\,mL$ of iron oxide magnetic nanoparticles functionalized with RGD (MNPs-RGD). The animals were maintained under isoflurane inhalation anaesthesia during the procedure. The magnetic fluid infusion, that takes $3\,min$, was carried out using a surgical microscope (Leica M651) for the required laparatomy to infuse it using a microcannula into the splenic artery through the hepatic artery.

The main steps in the prepation of MNPs-RGD were three [30]. First, the MNPs were synthesised by thermal decomposition of iron(0) pentacarbonyl with oleic acid and oleylamine. Then, in order to transfer the NPs to physiological medium, the NPs were capped with poly(maleic anhydride-alt-1-octadecene) (PMAO) and polyethylene glycol (PEG). The last step was to functionalise them with RGD using a click reaction [32]. This step is critical to increase the affinity of the MNPs to cancerous cells via integrins. The cyclic RGD peptides act as $\alpha V\beta 3$ integrins antagonist on angiogenesis. The mean nanoparticle size was determined on $19\pm3\,nm$ using transmission electron microscopy (TEM). The magnetization of the MNPs was measured dispersed in water. They showed a significant specific

absorption rate (SAR, describes the energy amount converted into heat per time and mass) above $10\,\text{kAm}^{-1}$, which makes them suitable for in vivo experiments. The infused magnetic fluid was prepared in $10\,\text{mM}$ PBS to achieve concentrations of $1\,\text{mg/mL}$ of iron. The affinity of the MNPs-RGD to the integrins was checked using a iodinated contrast (two iodine atoms linked to the MNPs-RGD) and observed by magnetic resonance imaging (MRI).

Four independent optic fibre thermometers were placed inside the tumour, healthy liver, rectum and the air surrounding to monitor the evolution of temperatures during hyperthermia experiments. During the procedure, the rats were anaesthetized and analgesized with valium, ketamine and medetomidine. The rats were introduced one by one in the Prototype EM04 for the treatment. The field frequency was $606\,\text{kHz}$ whereas the intensity was kept at $14\,\text{kAm}^{-1}$ until the temperature control sensor (placed in the healthy liver) reach $43\,°\text{C}$. After this point, the intensity was varied in the range of $6\,\text{kAm}^{-1}$-$14\,\text{kAm}^{-1}$ until fulfil the $21\,\text{min}$ treatment. The averaged maximum temperature values measured in healthy liver and tumor were $3.2\,°\text{C}$ and $2.7\,°\text{C}$ respectively larger in the case of rats with MNPs than in rats without MNPs.

The livers were extracted $12\,\text{h}$ and $10\,\text{days}$ after the hyperthermia treatment in order to perform histological analysis, iron determination, Raman and FTIR imaging and NMR metabolomic analysis. In addition, several enzymathic activities were measured in plasma. For the histological analysis hematoxylin and eosin stain (H&E stain) as well as Perl's Prussian blue were used.

The iron concentration in tumours and healthy tissues was quantified by inductively coupled plasma mass spectrometer (ICP-MS) after an acid

digestion. The iron concentration results showed that a considerable fraction of MNPs had been deposited on healthy hepatic tissues while in tumours the difference among animals with MNPs and control animals was very small. This last fact is attributed to the poor vascularization of the tumour.

The histological analysis with Perl's Prussian blue revealed MNP localisation in the peritumoral area (periphery of the tumours) but also revealed a large amount of iron in Kupffer cells on the healthy liver tissues.

According to histological analysis and ICP-MS measurements, a large amount of MNPs was deposited in the healthy livers. Therefore, targeting strategy was not accomplished as expected. This was the reason why tumour and healthy tissue temperatures experimented a similar increment during hyperthermia treatments. However, if we have a look to H&E stain samples, a significative necrosis was induced in liver tumours (40% of necrosis), with a minimum necrosis in healthy tissues.

Taking into account all the results, we can conclude that the temperature increment can be the result of the electrical currents induced by the main inductor (eddy current), the presence of MNPs, and the poor vascularisation inside the tumours that can make the cancer cells more sensitive to hyperthermia.

3.1.2 The need of diagnosis techniques

Biomedical research has shown a growing interest in early and high throughput diagnosis techniques to overcome the risk of classical approaches (i.e. biopsies [5]) and to gain information about the specific features of the tissues.

In 2001, it was reported for the first time a non-invasive diagnosis based on a combination of imaging and laboratory findings [33]. Nowadays, ultrasonography, computed tomography (CT), MRI, angiography and positron emission tomography (PET) are the most known imaging techniques for cancer diagnosis. Several studies have demonstrated that dynamic contrast-enhanced MRI and 4-phase multidetector CT are the most effective imaging techniques for detecting tumours smaller than 2 cm. However, the studies showed an underestimation of 25–30% [34, 35]. Due to a 10% of false positive diagnosis on this type of lesions, the non-invasive diagnosis still remains a challenging issue.

The cancer staging and classification define outcome prediction and treatment assignment. Technologies such as genome-wide DNA microarray, real-time reverse transcription-Polymerase Chain Reaction (qRT-PCR), proteomic and inmunostaining studies have been used to identify biomarkers for early-diagnosis. Thereby, many markers identified in genomic studies are prospectively assessed by a low cost technique such as immunohistochemistry. Though molecular classification based on gene signatures or molecular abnormalities is not ready for clinical application, huge advances have been done in the last years [5].

Therefore, in the framework of the hyperthermia research mainstream we took the chance to introduce two new research lines to complement the aims of the main project and to support a better understanding of the processes involved in the proliferation of cancer cells and the hyperthermia treatment. The two research lines that were tackled were:

- The metabolomic profiling of liver tissues under the different preclinical treatments to assure the fitness of the treatment and to complete the biochemical understanding to support improved clinical

treatments. The description and discussion of this work is included in section 3.2.

- The hyperspectral imaging of liver tissues with FTIR and Raman spectroscopies to differentiate healthy and tumour tissues and to help in the assessment of the hyperthermia benefit. This work is thoroughly described in section 3.3.

3.2 Metabolomics in magnetic hyperthermia therapy

3.2.1 Introduction to liver metabolism

Healthy liver

The rat liver is a soft and dark red glandular organ located in the upper side of the abdominal cavity. The rat liver is divided into four lobes; median and left lateral lobes (70% of the liver) and right lateral and caudate lobes (30% of the liver). The mean weight of rat liver is around $3\,g$ for $100\,g$ of body weight.

The liver receives its blood supply from the portal vein and from the hepatic artery. The main percentage of the blood comes from the portal vein, which drains from the spleen and intestines whereas the remaining, the oxygenated blood, is delivered by the hepatic artery. These blood vessels subdivide into small capillaries known as liver sinusoids, which then lead to a lobe. Each lobule is made up of millions of hepatic cells (hepatocytes), which are the basic metabolic cells.

The liver is the key in the metabolic control of the body. The main functions of the healthy liver are [36–38]:

(i) *Macronutrient metabolism.* Glucose is stored in the liver and muscle as glycogen. Glucose is absorbed from the intestine and passes into liver cells through portal vein to hepatocites. Once the glucose is in the hepatocite, it is rapidily phosphorilated by gluco-(hexo)-kinase to glucose 6-phosphate (G6P) and this is metabolized to pyruvate (glycolythic pathway) or converted into glycogen. Afterwards, on the one hand, pyruvate is channelled into the mitochondria and it

is oxidized to generate ATP through the tricarboxylic acid cycle (TCA) and oxidative phosphorilation. On the other hand, pyruvate is used to synthesize fatty acids through lipogenesis. Most of the liver's energy requirements come from amino acid and fatty acid oxidation, therefore, most of the glucose is converted into glycogen. The liver acts as glucose buffer: it stores the glucose when its concentration in blood is high and releases it from the glycogen when its concentration in blood falls. The liver is the main organ in which the gluconeogenesis takes place. The major precursors are lactate, glycerol and amino acids, principally alanine. Regarding the G6P, it is also used to generate nicotinamide adenine dinucleotide phosphate (NADPH via the pentose phosphate pathway) that is required in lipogenesis and in the biosynthesis of other bioactive molecules.

(ii) *Fatty acid (FA) metabolism.* Liver gets energy from fats. When there is a good supply of FA, they are degraded to Acetyl-CoA by β-oxidation in the mitochondria. Alternatively, they can form ketone bodies, acetoacetate and β-hydroxybutarate that are released to general circulation. In addition, fatty acids may also be esterified with glicerol to form triglicerides that are stored in the hepatocyte for future energy needs of the liver and for hepatic secretion of lipoproteins. The fatty acids are also necessary in the esterification of hepatic cholesterol and phospholipid synthesis. The hepatic cholesterol is incorporated to the hepatic membrane structure, to the biliar salt catabolism, and stored once it is esterified.

(iii) *Bile formation.* It is an alkaline electrolyte solution (97% water) that contain bile salts (sodium and potasium salts of bile acids

conjugated to glycine and taurine) and bile pigments (products of haemoglobin breakdown, bilirubin). The bile salts together with phospholipids form micelles around lipids to transport them to the intestine. Therefore, they are essential in the digestion and absorption of lipids.

(iv) *Protein metabolism.* The proteins are hydrolysed to amino acids and dipeptides for absoption since they cannot be stored by the body. One of the functions of the liver is the synthesis of non-essential amino acids from other amino acids, glucose and fatty acids. The amino acids are the essential *bricks* to build the cells. Amino acids can be deaminated to the corresponding keto acids (such as pyruvate and α-ketoglutarate), which are oxidized to obtain energy in the citric acid cycle. The released amine group is metabolized to urea in the urea cycle. Actually, this process only happens in the liver. Additionally, most of the plasma proteins such as albumin, globulin and fibrinogen are synthesized in the liver with the exception of inmunoglobulins.

(v) *Detoxification and the regulation of hormones and cholesterol.* All the chemical toxic compounds and pharmacological drugs are metabolized in the liver. The process is based on the inactivation of the substance creating a more ionized molecule to excrete it via bile or urine. Steroid hormones and cholesterol are also conjugated to glucuronide or sulphate (less active molecules) to excrete them in the bile in order to regulate the balance.

(vi) *Immune system.* Kupffers cells play an important role in the normal physiology and homeostasis of the liver as well as participating in the responses to toxic compounds. Activation of Kupffer cells by toxic

agents results in the release of an array of inflammatory mediators, growth factors and reactive oxygen species. Therefore, Kupffer cells are able to clean a large volume of blood from bacteria, fungi, parasites, worn-out blood cells, etc.

The main functions of the mammalian liver have been already summarized but it is important to point out that the rat liver has some differences. One of the differences for instance is that rats have no gall bladder and the biliar acid that they synthesize in the liver (a mixture of cholic acid, chenodeoxycholic acid, alpha-muricholic acid and beta-muricholic acid) is excreted to the intestine directly. Another difference is the capacity to synthesize Vitamin C (ascorbic acid) in the liver. Actually, it plays important roles neutralizing free radicals, preventing from cancer and scurvy.

The metabolic processes in liver are tightly regulated by neuronal and hormonal systems (such as insuline). They are altered under stress factors such as starving, exercise, trauma or sepsis. When cancer appears, the normal metabolic pathways are also altered. The biological processes involved in the transformation of normal cells into malignant cancer cells has been the subject of a large research effort for many decades [39].

Cancer metabolic biomarkers

Metabolomics of cancer tissue samples have shown that altered cellular metabolism is a characteristic of almost all cancer types [40]. The metabolic reprogramming in cancer is promoted by the activation of oncogenes and the loss of tumor suppressors, resulting in enhanced nutrient uptake to supply energetic and biosynthetic pathways [41]. This happens regardless of the location of the tumour [42]. In metabolomic studies of cancer,

samples such as tissue, serum [43], plasma [44], saliva [45], urine [46] and breath [47] have been used to discover its biomarkers, i.e. the compounds that are enhanced or lessened significantly from the normal conditions and early before any major manifestation of the disease is observed by other means. Both NMR-based and MS-based metabolomics approaches have been widely used in cancer research. The ideal biomarkers for cancer have applications in determining predisposition, early detection, assessment of prognosis and treatment response [48].

The main altered metabolic pathways associated with cancer are described below and summarized in Figure 3.1 [52]. Reprogrammed gene expressions lead into enhanced glycolysis, enhanced mitochondrial biogenesis and enhanced glutamine catabolism, giving rise to biomass assimilation [41].

The enhanced glycolysis observed during the proliferation period is described as the *Warburg* effect [49, 50]. This effect is featured by the high rate of glycolysis through the fermentation pathway regardless the presence of oxygen. As a consequence, the concentration of lactic acid is higher and the pH of the surrounding of the cell is lower, making the environment toxic for normal cells and promoting the tumour proliferation. Besides the overproduction of lactate, the enhanced glycolysis modifies the metabolism of amino acids, nucleotides and lipids [51], all necessaries for the proliferation of tumour cells [42].

In the mitochondria, the acetyl CoA (formed from the pyruvate) and amino acids are used as substrates for anabolic reactions involved in generating fatty acids, ketone bodies, steroids and protein acetylation [53]. The NADPH, which is required for fatty acid synthesis, is produced by increased glutaminolysis. Glutamine is an abundant amino acid and
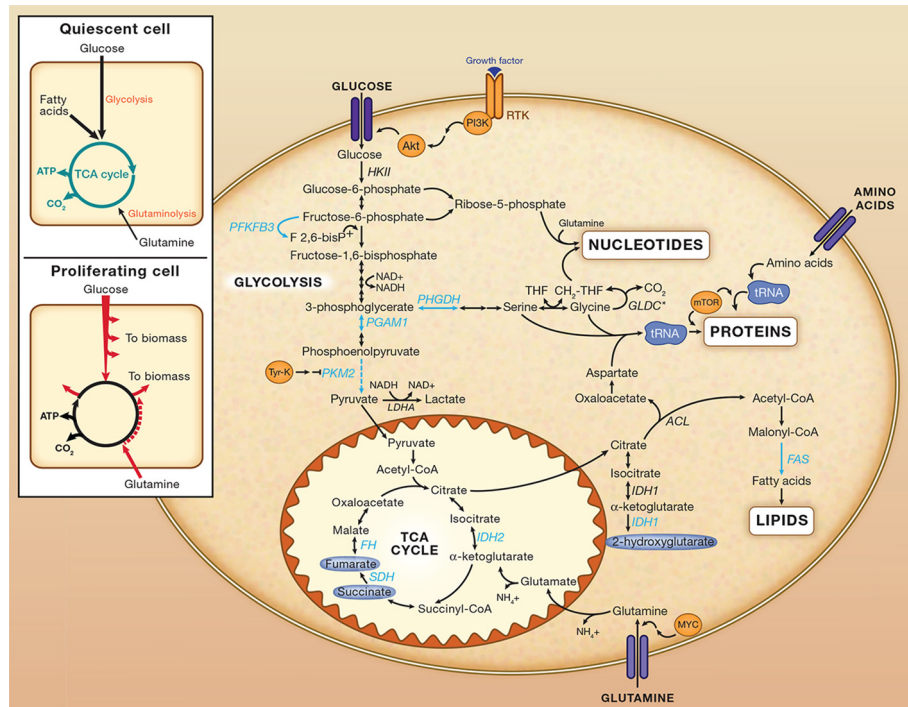
Figure 3.1: The overall pathways involved in the glycolysis and TCA cycle as well as some anabolic pathways are shown. Additionally, the differences observed in normal and tumour tissues are shown.

glutaminolysis provides energy to tumour cells when glycolysis energy production is not sufficient. In addition, glutamine degradation products are used for anabolic processes. The glutamine provides two nitrogen atoms to synthesize hexosamines, nucleotides and amino acids [41]. Furthermore, glutamine is necessary in the synthesis of gluthathione, an abundant antioxidant in cancer cells that takes part in the redox homeostasis and cancer cell survival in response to oxidative stress [54].

Besides, the glucose and the glutamine, pyruvate, hydroxybutyrate, acetoacetate, acetate and free fatty acids are all substrates for the

bioenergetic pahtways that support tumour growth. The ketone bodies, hydroxybutyrate and acetoacetate, and the acetate are produced in cells undergoing autophagy and are catabolic substrates specially in hypoxia and nutrient stress situations [54].

Amino acids are the building blocks of proteins, and together with the increased synthesis of nucleotides and lipids, are needed in cell construction for tumour proliferation. For instance, L-asparagine is required for protein synthesis and is a key initiator of pyrimidine synthesis and nitrogen donor for purine synthesis [54].

The modification of nucleosides is produced by methylation and oxidative damage to the DNA, and both of these processes are known to be related to the cancer development. These modified nucleosides are not reused by cells and ultimately are excreted in the urine [42].

Fatty acid synthesis is also increased in tumours. Lipids are involved in many tumour processes including cell invasion, migration, and proliferation. Choline, phosphocholine, phosphatidylcholine (PC) and glycerophosphocholine are needed for cell wall synthesis. Lysophosphatidylcholines (lysoPCs) are lipid intermediates that can be used to form PCs. Phosphatidylinositols have been reported to be involved in signaling for cancer cell growth motility and proliferation. Sphingolipids have also been reported as tissue biomarkers of cancer for their role in cancer growth and proliferation. As we can see, the study of lipids is really helpful to understand the cancer processes and one of the reason to exist a specialised area of metabolomics that evaluates the lipid profiles, lipidomics [42].

Metabolomics in cancer therapy and biomedicine

The study of the metabolic alteration has given rise to an increase interest in therapeutic strategies based on drugs targeting tumour metabolic processes [54]. Nevertheless, the metabolic pathways of a tumour are able to adapt quickly making difficult to find the definitive tumour metabolic inhibitor [54].

Metabolomic studies are a kind of end-of-pipe omic science that integrates the effects of genes, gene expression and protein as well as the environment. Since the metabolic profile, i.e. the distribution of the metabolome is highly sensitive to many of the changes, this profile is highly informative about the general status of the tissue, biofluid or organism. For this reason, metabolomics is increasingly popular to diagnose disease and to understand the fundamental causes of disease or the disease mechanisms to identify novel drug targets or customize drug treatments and monitor therapeutic outcomes [55]. However, the number of samples needed to observe a significant difference and the requirements for a proper design of the experiments increase the complexity of the experiments.

The growing accessibility of metabolomic studies is also leading into the personalized and precision medicine to create individually designed medical treatments according to specific metabolomic profiles as well as to help in the diagnosis and monitorization of the patient [55]. In cancer studies the tumours are not only classified by their origin tissue, but their molecular characteristics to find the best therapy strategy for each case. However, *one-size-fits-all* approach, where a standard treatment is given and then adjusted based on trial and error therapy strategy, is still the most common form of cancer treatment [56]. Metabolomics is helping in the advance from the *one-size-fits-all* approach to the precision medicine. In this way,

it would be possible to identify subgroups of patients that would benefit from a specific drug, as well as to identify patients that would be likely to suffer toxicity or develop resistance.

Recent emerging trend in metabolomics has given rise to advances in quantification and automation for clinical applications [55]. Nowadays, NMR analyses can be completed in less than a few minutes per sample and these developments have clearly helped in the renewal of NMR metabolomics [57]. Liquid chromatography coupled to mass spectrometry (LC-MS) is also becoming increasingly automated and quantitative through the use of commercial kits and *blackbox* systems [55]. We have to highlight also the exciting technological advances in *in vivo* and *in vitro* metabolite imaging NMR, magnetic resonance spectroscopy (MRS), positron emission tomography (PET), matrix assisted laser desorption-ionization (MALDI)-MS, secondary ion MS (SIMS) or desorption electrospray ionization MS (DESIMS) techniques [58].

Nowadays, a tumour now can be understood as individual specialized cell types within a tumour-microenvironment built in a multistep tumorigenesis [59]. One of the features is that tumours show similar features of complex ecosystems where nutrients are cycled very efficiently. For instance, the lactate shuttle can be understood in the same way that the nitrogen cycle works. Actually, the metabolic organization of cells within tumours is similar to that of colonies of heterotrophic organisms, forming a multicompartmental tumour metabolism. Evidences indicate that aerobic cells proliferate best when they are clustered and some glycolytic cells are present. This new perspective changes completely the way to understand the tumour microenvironment since the old reductionist point of view described it as tumour cells that showed an homogeneous behaviour [54].

Actually, the scientists found interesting the fact to study the metabolic differences within tumour tissues to get a deeper understanding of all processes.

From this new point of view, researchers have described eight hallmarks that constitute the organizing principle for rationalizing the complexities of neoplastic disease; sustaining proliferative signaling, evading growth suppressors, resisting cell death, enabling replicative immortality, inducing angiogenesis, activating invasion and metastasis, reprogramming of energy metabolism and evading immune destruction. Based on these hallmarks, researchers are developing metabolic therapies to target each of the hallmarks mentioned above as we can see in the Figure 3.2 [59].
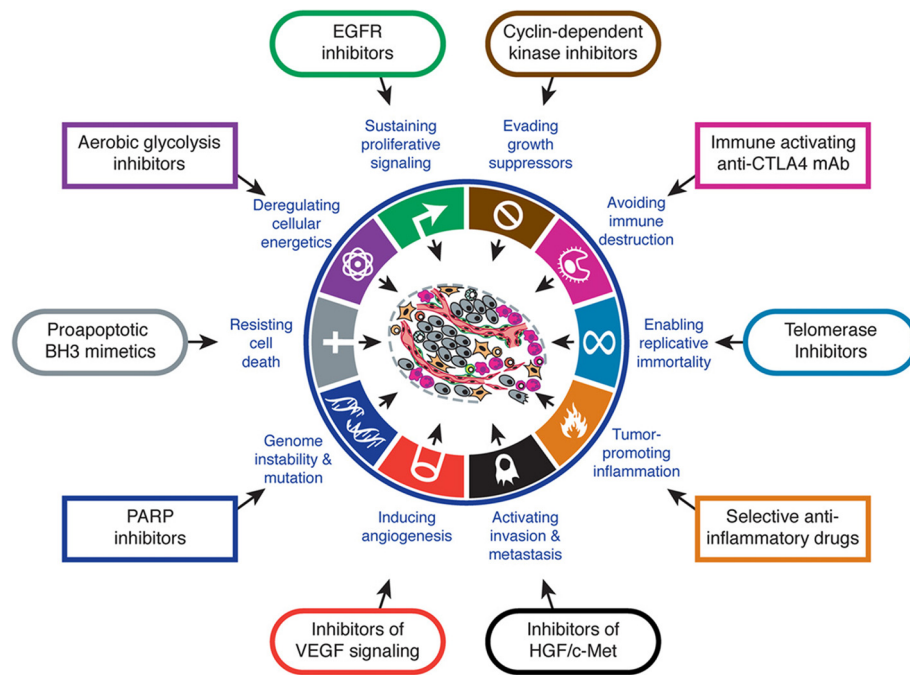
Figure 3.2: Cancer hallmarks and therapy strategies.

Hyperthermia therapy: metabolic changes

During the development of this project, an issue was questioned over and over again: Does our magnetic hyperthermia procedure cause any chronic damage?.

A wide range of hyperthermia therapies have been used since 1960 and have been improved until nowadays. Since the beginning, the researchers studied and evaluated the mechanisms of tissue injury caused by these treatments in order to asses their effectiveness in the tumour destruction and their undesirable effects in healthy tissues [60].

Two types of damages are described in the bibliography. On the one hand, we find the primary damage caused during the hyperthermia therapy (HT) and, on the other hand, the secondary damage related with the indirect effects that produce progressive tissue damage [60].

In the previous research works metabolic changes were observed in all cell compartments during and after exposure to elevated temperatures [61]. HT makes increase rates of metabolic reactions during the heat treatment followed by disregulation of metabolism after HT. More energy is needed by heated cells, in order to maintain ion gradients through membranes, structural characteristics in the various cell compartments and so on [61]. Therefore, a strong decrease of glycogen can be expected. Besides, an important degradation of lipids occurs, in particular the free fatty acids and esterified fatty acids, surely as a consequence of the depletion of glucose. Under these conditions, the acidic metabolites, β-hydroxybutyrate and acetoacetate are formed by ketogenesis, and their concentrations are increased. Apparently, the liver metabolism is changed to acidosis metabolic conditions, as observed in lactate maximum level at 1-6 h [62]. This pattern is often attributed to a decrease in the blood flow

and oxygenation, but it can be also a consequence of the enhanced flow of lactate from peripheral organs and tissues [61]. In some HT cases, mitochondrial dysfunction appears to be more relevant and irreversible heat-induced injury, due to changes in its ultrastructure [60].

The primary damage caused by the HT can induce an inhibition of DNA, RNA and protein synthesis as well as disturbances in membrane function and cytoskeleton. Desnaturalization of membrane proteins is apparently important in these processes, which can induce cell death. As a consequence of changes of membrane functions, the concentrations of ions such as Ca^{2+} and other factors of the cytosol are apparently altered in cells and their compartments [61]. Gluthathione in its reduced and oxidized form is also coupled to the intracellular redox equilibria. Therefore, after HT the reduced gluthathione increases due to the produced oxidative stress.

3.2.2 Objectives

In the framework of the hyperthermia project it was considered interesting to asses a global analysis of the treatment under different preclinical cases. The underlying hypothesis was that the recovery from the magnetic hyperthermia therapy was accomplished some hours after the treatment. However, it was necessary to confirm this hypothesis with evidences. NMR metabolomic study was considered as the main strategy. By means of the NMR metabolic study we hoped to increase the knowledge about the metabolic pathways that the CLM shows, to create a model to distinguish among healthy and metastatic tissue, to identify the metabolic effects caused by the hyperthermia therapy and to ensure that our methodology to apply magnetic hyperthermia therapy does not cause damage.

3.2.3 Materials and methods

Animals and preparation

The animal protocol was carried out in agreement with the Ethical Committee of Animal Welfare (CEBA) at the University of the Basque Country, Leioa, Spain (CEBA/140/P02-01/2010/AlonsoVarona). WAG/RiJHsd rats (male *Rattus norvegicus* laboratory rats, around 300 g) were inoculated in the left hepatic lobe with CC-531 colon adenocarcinoma cells (CC-531 cell line). Once the tumour induction was confirmed by ultrasonographic examinations, around $0.8 \, \text{cm}^{-3}$ after 31 days from the inoculation, five groups rats were used in this work for the study of each case:

(i) C: Control sample, hepatic healthy tissue from a healthy rat without any treatment.

(ii) HRTC: hepatic healthy tissue from a rat that developed a tumour.

(iii) HHT12h: hepatic healthy tissue from a healthy rat 12 h after the hyperthermia protocol without NPs.

(iv) HRTHT12h: hepatic healthy tissue from a rat that developed a tumour and 12 h after the hyperthermia protocol without NPs.

(v) HRTHTSI12h: hepatic healthy tissue from a rat that developed a tumour and 12 h after the saline infusion that emulates the surgical protocol for the NP infusion and the hyperthermia protocol.

(vi) HSI12h: hepatic healthy tissue from a healthy rat 12 h after the saline infusion that emulates the surgical protocol for NP infusion.

(vii) HHT10d: hepatic healthy tissue from a healthy rat 10 days after the hyperthermia protocol without NPs.

(viii) HRTHT10d: hepatic healthy tissue from a rat that developed a tumour and 10 days after the hyperthermia protocol without NPs
.

In the same way, we used the same pattern to identify the tumour samples: TC (tumour control), THT12h (12 h after HT), THT10d (10 days after HT) and THTSI12h (sham surgery and 12 h after HT).

A quality control sample batch (5 new samples) was created using a mixture of tumour and healthy tissues obtained from the above mentioned groups. This quality control sample batch was used to ensure the efficacy and quality of the chemometrical data treatment.

The surgical procedure and the hyperthermia procedure have been previously explained in the introduction (see section 3.1.1 on page 117).

After 12 h or 10 d, blood was retrieved to measure some enzyme activities and the liver was removed for NMR based metabolomic analysis separating the tumour from the healthy tissue. All the samples were snap-frozen in liquid N_2 and afterwards they were kept at $-80\,°C$. This procedure was done under isoflurane inhalation anaesthesia and the rats were killed by cervical dislocation.

NMR metabolomics

The methodology applied in liver and tumour tissues, the sample preparation and the measurement conditions, was the same that we have described in the previous chapter and follows the combined methodology described by Professor Mark Viant and coworkers [63, 64]. In this case,

we used $\sim$100 mg of sample in all the cases and though we obtained and measured both the aqueous and non-aqueous phases, only the results of the former ones are discussed. In this chapter we only show the ^{1}H NMR acquired data from the hydrophilic extracts of the samples.

The acquired ^{1}H NMR spectra were imported to MATLAB using the *RBNMR* function and processed using the PLS Toolbox. Then, the data were preprocessed, using COW alignment, variable selection (water and TMSPA signal as well as spectral areas without peaks were removed), logarithm (log10) transformation, normalization (taking into account all variables area), mean center and orthogonal signal correction (OSC). Finally, PCA analysis was performed in order to get a general idea of how the samples were distributed and to check if any outlier should be removed. If PCA analysis showed a clustering of the samples, then PLS-DA and/or OPLS-DA (PLS-DA with OSC) analysis was performed. By means of these supervised chemometric tools, we wanted to enhance the differences among the groups trying to identify the key variables of the clustering on PLS projections (VIP). In order to ensure the data treatment and analysis procedure (to get meaningful results) a quality control sample batch was used [42]. In all cases, the quality control sample batch showed a perfect clustering (in PCA and (O)PLS-DA analysis) and it was clearly distinguished from the rest of the data. Finally, VIP data were studied to obtain the metabolome profile for each sample group. VIP peaks were exported from MATLAB to EXCEL to obtain the heatmaps and graphical representations of the identified metabolites in order to obtain a fast and clear idea of the most meaningful differences among the sample groups. The identification was done based on the literature [65–69] and free data bases available in the internet [70–72]

Enzyme activity assays

Enzymatic activity was measured in the serum samples collected from the rats. The analysis was carried out at University Hospital of Basurto using kits for humans that are valid for rats. The measured enzymes (in enzyme units per litre) were:

(i) *Alanine aminotransferase (ALT) or glutamate-pyruvate transaminase (GPT)* is an enzyme that catalyzes the transfer of amino groups to form the hepatic metabolite oxaloacetate. ALT is abundant in the cytosol of the hepatocytes and its activity in the liver is about 3000 times higher than serum activity. When the hepatocellular tissue is injured or death, ALT is released from damaged liver cells and this causes rise in ALT levels of serum [73].

(ii) *Aspartate aminotransferase (AST)* is also called *serum glutamic oxaloacetic transaminase* (GOT). AST catalyzes the interconversion of aspartate and α-ketoglutarate to oxaloacetate and glutamate. ALT is found predominantly in the liver while AST is found also in the heart, skeletal muscle, kidneys, brain and erythrocytes. Thus, ALT is a more specific indicator of liver inflammation than AST. However, elevated AST values (at least 10 times above the normal range) are an evidence of the destruction of hepatocytes [74].

(iii) *Creatine kinase* (CK) is an enzyme that catalyses the reversible phosphorilation of creatine using adenosine triphosphate (ATP) to create phosphocreatine and adenosine diphosphate (ADP). The enzyme is abundantly expressed in both the mitochondria and the cytosol. Elevate levels of CK can indicate damage in cells from skeletal muscle, heart and brain. When tissue destruction happens

due to necrosis or inflammation, the CK levels rise indicating tissue damage related with surgery [75].

(iv) *Lactate dehydrogenase* (LDH) is an enzyme that catalyzes the interconversion of pyruvate to lactate and NADH to NAD^+. LDH is found throughout the body in low concentrations, and also in the liver. Elevated levels of LDH may also indicate tissue destruction due to surgery procedures [75].

3.2.4 Results and discussion

The metabolomic results were divided in three main sections where the colorectal liver metastasis metabolome profile was studied and the effects of the magnetic hyperthermia therapy were assessed on hepatocellular tissues and on tumour tissues. Finally, enzyme activity assays were performed in serum to assure the effects of the magnetic hyperthermia in the cases of study.

CLM metabolic profiling

The first step was to characterise the samples and to establish the basal level of the tissues without any surgery or HT treatment. In this case, healthy rats (C) and rats that suffer CLM (HTRT and TC) were considered. This task gave us the chance to study closer the CLM and to obtain the metabolome profiles of the hepatocelullar tissues of rats that suffered CLM and their corresponding tumour tissues.

In Figures 3.3, 3.4 and 3.5 we show the scores and the laodings obtained from the PLS-DA analysis of a data set and in the Table 3.1 we show the errors of the calibration (RMSEC) and the cross validation (RMSECV). Three principal components (PC) or latent variables (LV) are enough to

Table 3.1: RMSEC and RMSECV values of the created PLS-DA model.

	C	H-RT-C	T
RMSEC	0.09	0.08	0.09
RMSECV	0.22	0.29	0.13

explain the 81.81% of the variance of the x matrix (variables) and the 96.58% of the variance of the y matrix (classes). The first PC, that explains the 68.18% of the model variance, differentiates clearly the tumour tissue from the hepatocellular tissue.
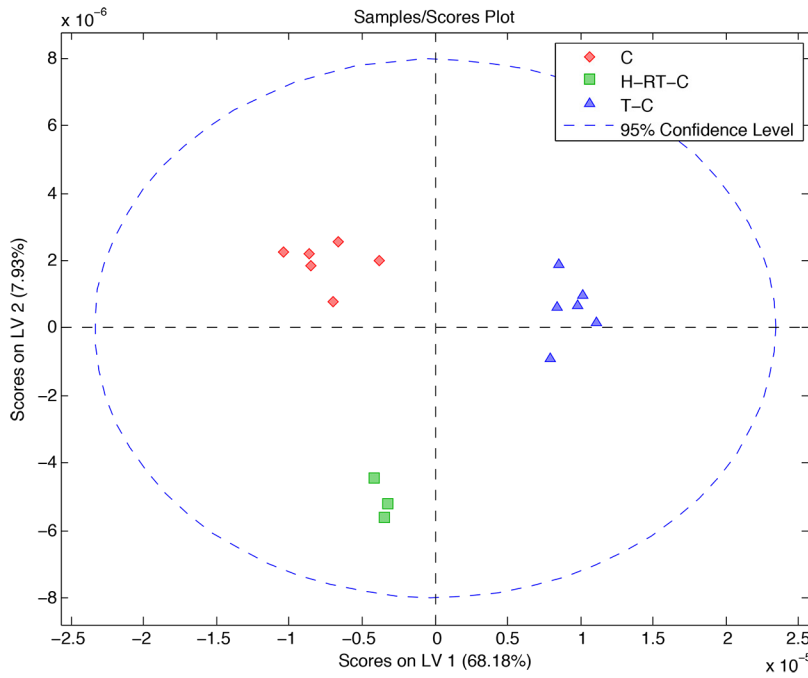
Figure 3.3: PLS-DA scores from a data set that combines healthy rats (C) and rats that suffered CLM (HRTC and TC). *Key information to understand the abbreviations: control (C), hepatocellular tissue (H), rat with CLM (RT) and tumour (T).* LV (Latent Variable) is the same as PC (Principal Component)
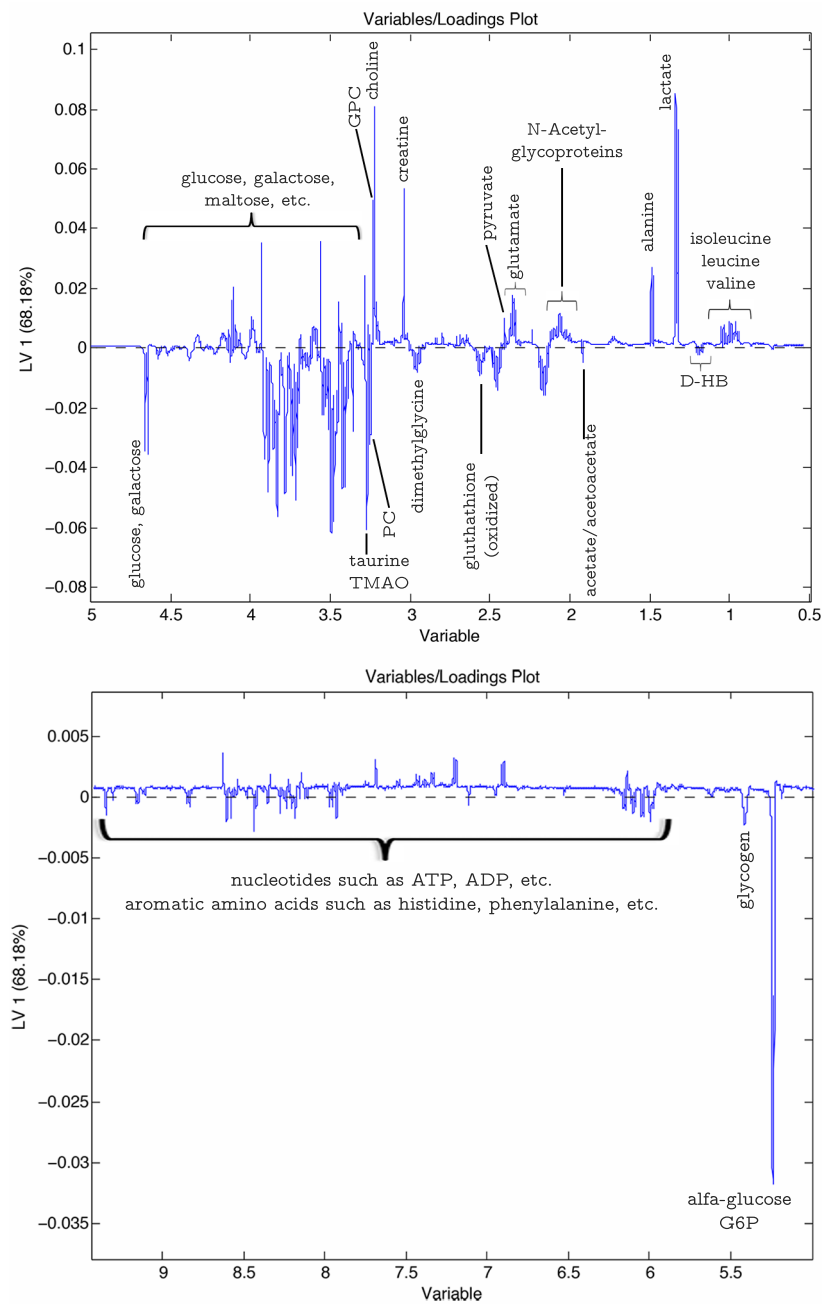
Figure 3.4: Loadings of first PC (68.28% of the variance explained) of the PLS-DA analysis obtained from a data set that combines healthy rats (C) and rats that suffer CLM (HRTC and TC).
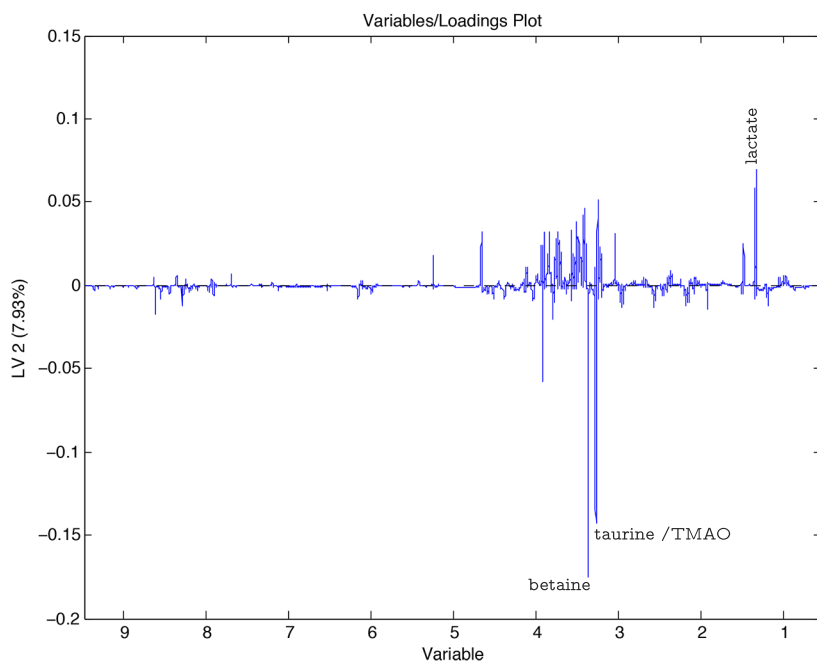
Figure 3.5: Loadings of the second PC (7.93% of the variance explained) of the PLS-DA analysis obtained from a data set that combines healthy rats (C) and rats that suffer CLM (HRTC and TC).

As we can observed in the Figure 3.4, the tumour is characterised by a higher concentration of lactate, leucine, alanine, glutamate, pyruvate, choline and creatine among others. Meanwhile, the hepatocellular tissue is characterised by a higher concentration of acetoacetate, D-hydroxybutyrate, dimethylglycine, glucose, galactose and glycogen among others.

The second PC, that explains the 7.93% of the model variance, differentiates the hepatocellular tissue of healthy rats from rats that suffered CLM. The main differences between these tissues is shown in the Figure 3.5. The metabolites that have a higher weight in this differentiation are the lactate, which characterised the healthy rats (with a higher concentration), and the betaine and taurine or trimethylamine-N-oxide (TMAO), which characterised the rats that suffered CLM. However, for a deeper analysis we recommend the use of VIP instead of the loadings since they show the positive projections of each class giving us the chance to compare the metabolite signals among the classes.

In Table 3.2 we have collected the normalized VIP values taking the control samples as reference ones. From the relative values we have modelled colors to show the level of the variations. For instance, the signal of the D-hydroxybutyrate increases twice in the case of the hepatocellular tissue from a rat that suffered CLM while the signal in the tumour is much lower.

Table 3.2: The signal increment of the most meaningful metabolites obtained from the VIP showed in a heatmap refered to the healthy tissue (C). *Key information to understand the abbreviations: control (C), hepatocelluler tissue (H), rat with CLM (RT) and tumour (T).*

metabolite	ppm	C	H_RT_C	T
leucine/isoleucine	0,966	1,00	0,57	1,26
valine	0,984	1,00	0,12	1,53
D-Hydroxybutyrate	1,187	1,00	2,23	0,30
lactate	1,325	1,00	0,85	1,29
alanine	1,492	1,00	0,99	1,09
lysine	1,719	1,00	0,46	1,34
acetate, acetoacetate	1,921	1,00	2,36	0,22
N-acetyl functions of glycoprotein	2,053	1,00	0,31	1,43
glutamine	2,152	1,00	0,73	1,15
glutamate	2,359	1,00	0,37	1,40
pyruvate	2,408	1,00	0,24	1,39
gluthathione (oxidized)	2,559	1,00	1,46	0,77
aspartate	2,805	1,00	0,46	1,34
creatine	3,040	1,00	0,43	1,34
choline	3,225	1,00	0,17	1,52
GPC (sn-glycerol-3-phosphocholine)	3,233	1,00	0,52	1,39
PC (phosphatidylcholine)	3,250	1,00	1,38	0,77
taurine, trimethylamine-N-oxide	3,271	1,00	2,04	0,40
betaine	3,359	1,00	2,51	0,13
α-glucose	3,424	1,00	1,18	1,34
glycine	3,553	1,00	0,59	1,43
citrate	3,562	1,00	0,20	1,43
threonine	3,609	1,00	0,22	1,46
free glycerol	3,651	1,00	0,17	1,49
ascorbic acid	4,504	1,00	2,42	0,20

Based on the collected data, we are able to understand the metabolic processes that a CLM cancer tissue exhibits. We observe an enhancement of the glycolysis since an increment of pyruvate (mostly formed from the glucose) and lactic acid occurs. Together with this enhancement, the tumour tissues show an increment of the levels of most of the amino acids (leucine, valine, aspartate, etc.) [51] since they are needed for the proliferation of tumour cells [42]. In the mitochondria, the NADPH that is required for biosynthesis is produced by increasing the glutaminolysis. Indeed, we observe a higher signal of glutamine in tumours. The glutamine is also important in the acetylation of proteins. For instance, N-acetylglycoproteins and N-acetylglucosamine are important for their role in cell recognition. The tumour cells that are proliferating need to generate these molecules and this is the reason for the increment in N-acetyl functions of glycoproteins. A product of the glutamine metabolism is the glutamate, which also appears increased in tumour tissues. Glutamate is a cell-signaling molecule in many tissues and, additionally, its secretion is associated with peripheral tissue injury and inflammation, probably due to the propagation process of tumour cells to adjacent hepatocellular tissues [76].

In tumour tissues we see an important increment in choline and, according to the literature [77], the choline metabolism plays an important role in the proliferation of tumour cells (membrane structure). Choline is important as a precursor of acetylcholine and phosphatidylcholine, as a methyl donor in various metabolic processes, and in lipid metabolism.

The high correlation between glycine and the proliferation proliferation across cancer cells [78] is also obserced in the results showed in Table 3.2.

The rapidly growing cells appeared to need glycine for synthesis of purine nucleotides required for continuing the synthesis of DNA.

The relationship among choline, betaine and TMAO in serum has been studied in the literature as colorectal biomarkers [79]. In our model we observe that the betaine in the hepatocelullar tissue of the rat with CLM is higher than in healthy rats and tumour tissues while the choline concentration is much lower. This fact is curious since the betaine comes from either the diet or by the oxidation of choline. Taking into account that all rats had the same diet, the difference should be found in the choline metabolism. Therefore, the choline metabolism is also affected in the hepatocellular tissue of the rats with CLM. Betaine works as a methyl donor to obtain methionine from homocysteine and produces also N,N-dimethylglycine. Furthermore, the donation of methyl groups is important to proper liver function, cellular replication and detoxification reactions [80]. Betaine also works as an osmolyte and protects cells from hyperosmotic stress that can lead to chronic inflammation, a risk factor for colorectal cancer [79]. In addition, important changes in ascorbic acid were observed. The tumour tissue does not produce ascorbic acid, while the H-RT-C tissues show an increment in its concentration to work as antioxidant against the tumour.

Choline can also undergo catabolism by the intestinal bacteria to form trimethylamine (TMA), which is further converted to trimethylamine N-oxide (TMAO) by the liver [79]. Indeed, we also found increased the TMAO in the hepatocelluler tissue of rats with CLM, supporting the hypothesis that the choline metabolism is altered in this tissue.

The VIPs show an increment of gluthathione (oxidized) in the hepatocellular tissue of rats with CLM, showing a clear signal of oxidative

stress. This stressed situation of HRT tissues is also evident due to a higher concentration of D-hydroxybutyrate. The ketogenesis is activated in three main cases. The first one is when we have an excess of Acetyl CoA comparing to oxalacetate in the TCA cycle, in the case that esterified fatty acids are β-oxidized when we have a depletion of glucose, or when we have an excess of fatty acids. In this case, and taking into account the stress evidences, this fact can be an indicative of problems in the TCA cycle.

Hyperthermia effects of healthy tissues

.

In Figure 3.6, we observe the scores plot of the OPLS-DA model built with the data set that contains hepatocellular tissue of healthy rats and rats with CLM that have suffered the different treatment procedures. The model was built using three PC and the three PC explain the 54.07% of the variance of the x matrix (variables) and the 33.64% of the variance of the y matrix (classes). The samples that suffered HT after 12 h are located at the left side of the scores plot. In contrast, the samples that suffered only the sham operation and saline infusion are located clearly at the right and up side of the scores plot. This clear differentiation suggest that the metabolic answer of each type of stress is different. In addition to this, the samples that suffered both treatments are located at the left edge of the data distribution, being the most distant samples from the control samples. This class clustering suggests that the metabolome profile is a good mediator of the stressing effects. Finally, we observe that the control samples and the samples that suffered HT after 10 days are clustered together. This clear differentiation suggests that the metabolic answer to each type of stress is different. This data clustering shows that the rats fully recovered the basal

metabolic state after 10 days. In the Table 3.3 we show the RMSEC and RMSECV values of the OPLS-DA model.
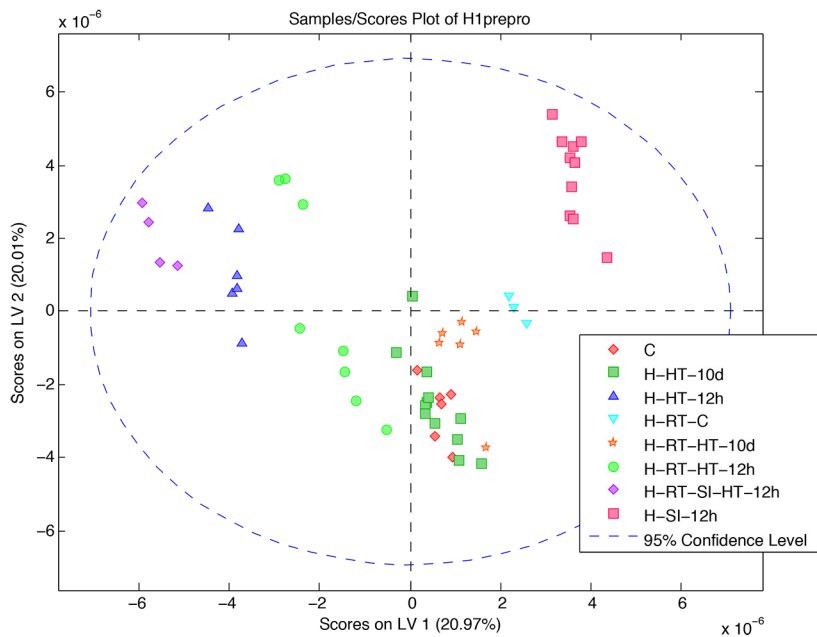
Figure 3.6: OPLS-DA scores from a data set that combines healthy rats (C, HHT12h, HSI12h and HHT10d) and rats that suffered CLM (HRTC, HRTHT12h, HRTSIHT12h and HRTHT10d) under different procedures. *Key information to understand the abbreviations: control (C), hepatocelluler tissue (H), rat with CLM (RT), hyperthermia therapy procedure (HT), sham surgery using saline infusion (SI) and period of time elapsed since the procedure (12 hours or 10 days).*
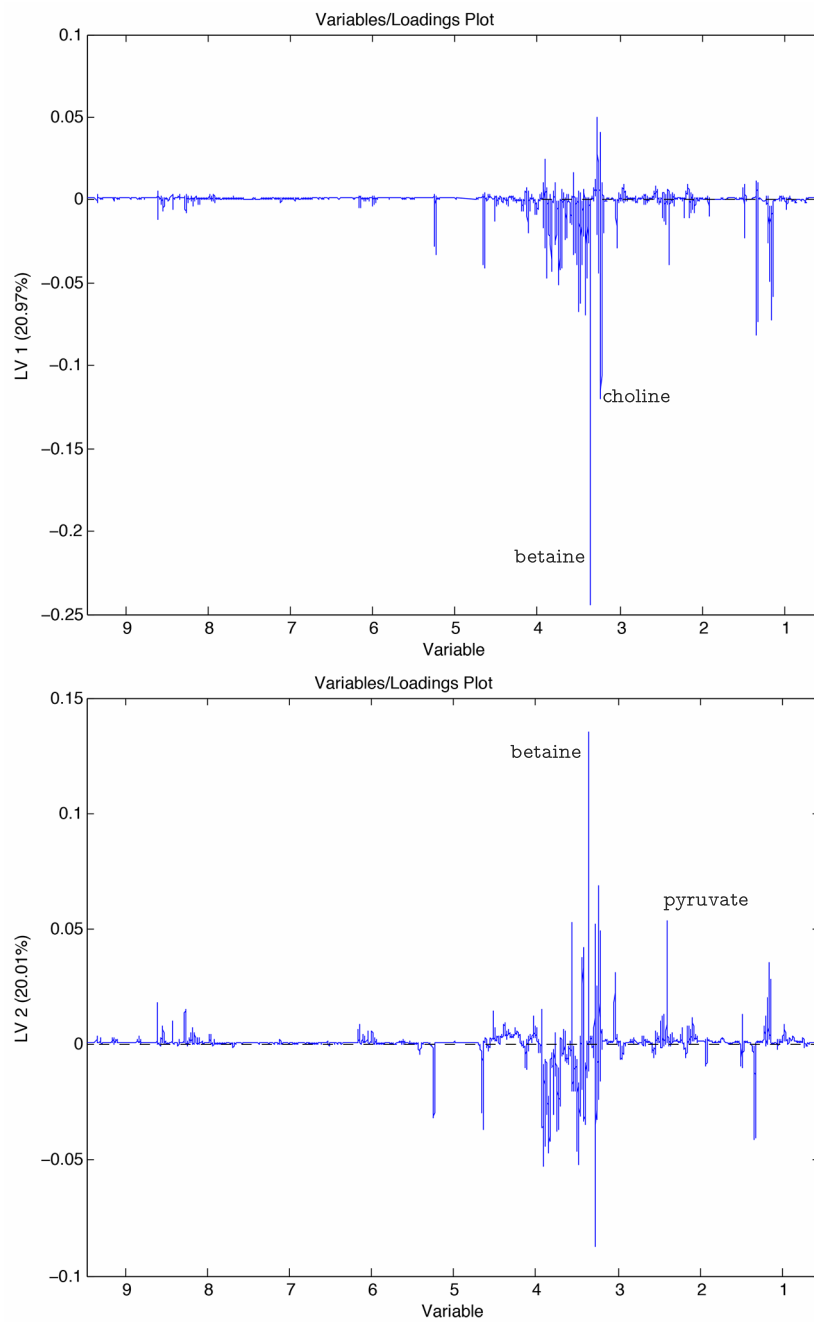
Figure 3.7: Loadings of the first and second PC of the OPLS-DA analysis obtained from a data set that combines healthy rats and rats that suffereded CLM under different procedures.

The most meaningful metabolites identified in the VIPs have been summarized in the Table 3.4 as we proceed in the previous case. Additionally, to provide further insight into possible interactions, some of the metabolites showed in the Table 3.4 have been plotted in the Figures 3.8 and 3.9. At first glance, metabolites such as glucose, lactate, fumarate, D-hydroxybutarate, glutathione (oxidized), betaine and L-asparagine show the same pattern (see Figures 3.8 and 3.9). We observe an important metabolic increment in the treated rats after 12 h with higher levels of the mentioned metabolites. For sure, this metabolic increment is the answer to the stress that the cells suffered under HT and surgery. Thus, the liver need to increase their metabolism in order to survive and keep the integrity and, therefore, a higher assumption of glycogen is observed as an increase demand of glucose.

The ratio of the lactate-pyruvate signal with the lactate is plotted in Figure 3.10. In the rats that suffered HT therapy, the pyruvate forms lactate instead of Acetyl CoA, which suggests a malfunctioning of TCA cycle while the glycolysis works fine. One clear evidence of this, it is the increment of lactate proportion (it is the double). Therefore, we can conclude that there is a reduced mitochondrial activity under HT. In the case of the sham operation (HSI12h) we observe an increment of lactate as a consequence of the injury caused during the surgery and the saline infusion that could damage the endothelium. However, the proportion between

Table 3.3: RMSEC and RMSECV values of the created PLSDA model.

	C	HHT10d	HHT12h	HRTC	HRTHT10d	HRTHT12h	HRTSIHT12h	HSI12h
RMSEC	0.28	0.35	0.27	0.18	0.29	0.32	0.21	0.11
RMSECV	0.29	0.37	0.31	0.21	0.32	0.35	0.25	0.21

Table 3.4: The signal increment of the most meaningful metabolites obtained from the VIP showed in a heatmap refered to the healthy tissue (C). Key information to understand the abbreviations: control (C), hepatocelluler tissue (H), rat with CLM (RT), hyperthermia therapy procedure (HT), sham surgery using saline infusion (SI) and period of time elapsed since the procedure (12 hours or 10 days).

metabolite	ppm	C	H_RT_C	H_HT_12h	H_RT_HT_12h	H_RT_SI_HT_12h	H_SI_12h	H_HT_10d	H_RT_HT_10d
leucine/isoleucine	0,966	1,00	0,30	0,46	0,34	0,50	0,81	1,18	0,47
valine	0,984	1,00	0,19	0,23	0,17	0,28	0,72	1,20	0,38
D-Hydroxybutyrate	1,187	1,00	2,24	11,39	6,54	10,84	5,39	0,95	2,62
lactate	1,325	1,00	0,81	3,24	1,94	3,12	1,86	1,23	0,98
alanine	1,492	1,00	1,60	1,39	1,36	1,36	1,15	0,92	1,26
lysine	1,719	1,00	0,20	0,21	0,17	0,27	0,71	1,20	0,39
acetate, acetoacetate	1,921	1,00	1,47	0,22	0,87	0,24	0,59	0,84	1,27
glutamate	2,133	1,00	0,41	1,22	0,68	1,23	1,14	1,21	0,52
pyruvate	2,408	1,00	0,26	0,49	0,33	0,53	0,83	1,19	0,44
glutamine	2,480	1,00	0,21	1,43	0,74	1,42	1,23	1,23	0,48
gluthathione (oxidized)	2,565	1,00	0,91	3,91	2,06	3,77	2,24	1,17	1,04
asparagine	2,960	1,00	0,46	2,86	1,53	2,78	1,84	1,21	0,75
creatine	3,040	1,00	0,43	0,87	0,60	0,89	0,98	1,16	0,59
choline	3,225	1,00	2,75	9,24	5,83	8,78	4,43	0,84	2,82
GPC (sn-glycerol-3-phosphocholine)	3,233	1,00	0,37	0,55	0,42	0,59	0,85	1,17	0,52
PC (phosphatidylcholine)	3,250	1,00	1,14	3,53	1,85	1,63	2,02	3,41	2,10
betaine	3,359	1,00	2,25	4,65	3,41	4,44	2,49	0,76	2,12
α-glucose	3,424	1,00	3,07	4,07	2,84	3,87	1,93	0,43	2,45
glycine	3,553	1,00	1,35	6,01	3,26	5,75	3,04	1,07	1,22
citrate	3,562	1,00	0,53	0,25	0,31	0,30	0,73	1,22	0,53
threonine	3,609	1,00	1,01	0,57	0,81	0,59	0,81	1,00	0,98
free glycerol	3,651	1,00	1,77	13,50	7,19	12,83	6,07	1,12	2,29
glucose-1-Phophate-(Glycogen)	4,504	1,00	0,00	0,22	0,07	0,28	0,73	1,25	0,26
ascorbic acid	4,515	1,00	0,26	0,92	0,48	0,94	1,02	1,23	0,41
glycogen	5,416	1,00	0,01	0,15	0,03	0,22	0,70	1,25	0,25
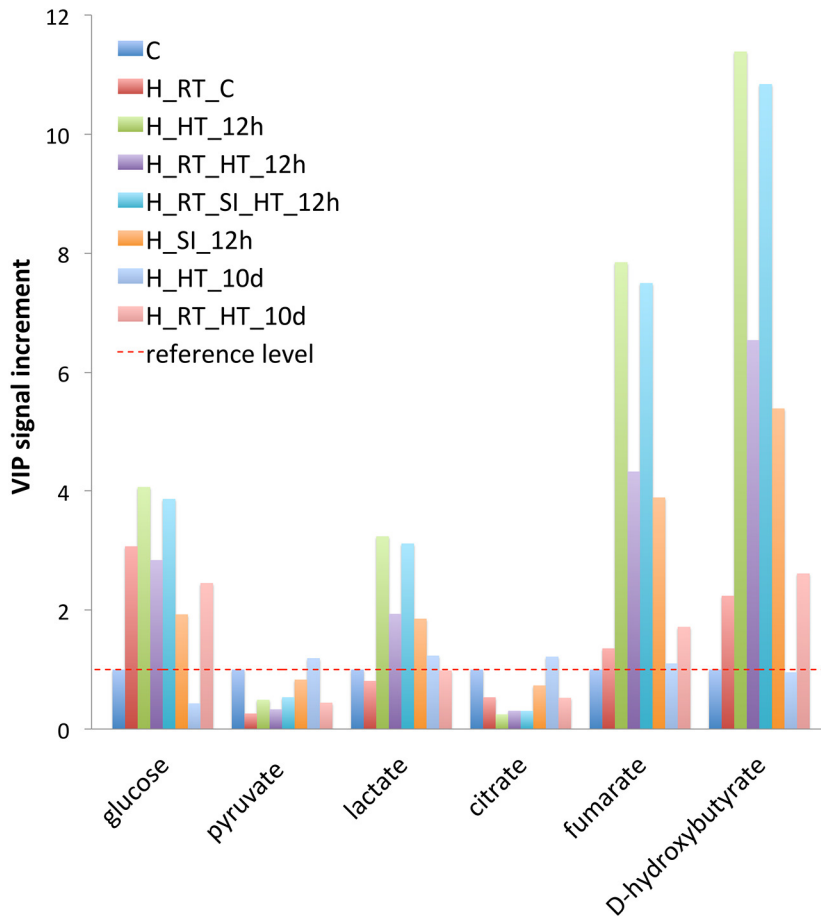
Figure 3.8: The signal increment of the most meaningful metabolites obtained from the VIP showed graphically and refered to the healthy tissue (C). *Key information to understand the abbreviations: control (C), hepatocelluler tissue (H), rat with CLM (RT), hyperthermia therapy procedure (HT), sham surgery using saline infusion (SI) and period of time elapsed since the procedure (12 hours or 10 days).*

pyruvate-lactate is still normal. Thus, in this case, the mitochondria is working without any problem.
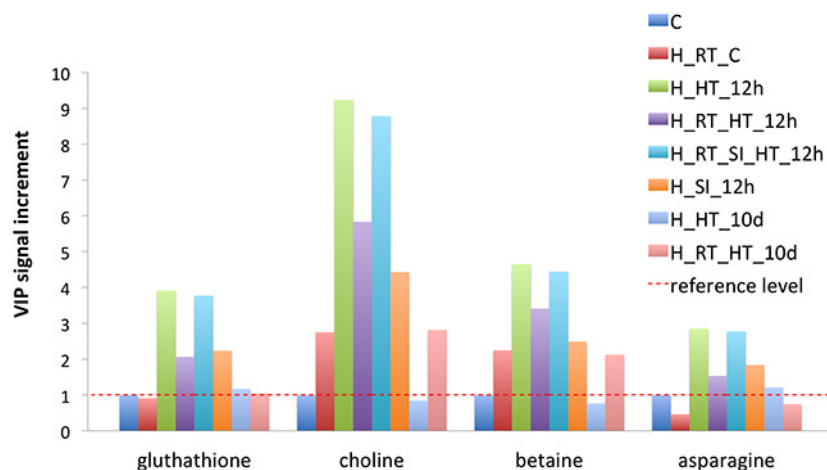
Figure 3.9: The signal increment of the most meaningful metabolites obtained from the VIP showed graphically and refered to the healthy tissue (C). *Key information to understand the abbreviations: control (C), hepatocelluler tissue (H), rat with CLM (RT), hyperthermia therapy procedure (HT), sham surgery using saline infusion (SI) and period of time elapsed since the procedure (12 hours or 10 days).*

In the TCA cycle there is needed a continuous supply of oxalacetate as well as glutamine to produce the α-ketoglutarate. Indeed, we observe an increment of glutamine levels in the livers that are under stress. We also observe an increment of L-asparagine and aspartate that are precursors of the oxalacetate. The fumarate is also incremented while the citrate shows a depletion.

We have to highlight the increment of the ketogenesis, which can be noticed by means of an increment of D-hydroxybutarate as well as the increment of the gluthathione (oxidized), indicating oxidative stress.

Last but not least, it is really important the role that betaine and choline plays in the OPLS-DA model as we can see in the first PC (see Figure 3.7). The choline and betaine are both higher in the liver with CLM but it is higher in the cases that suffered hyperthermia. This is not a surprising fact since the betaine works as osmolite in the system and choline takes part in the formation of betaine.

In general, we can conclude that the metabolic differences observed in the cases after 12 h from having suffered some treatment, are recovered for the 10th day. The measured biomarkers show that almost all the values are in agreement with the basal or reference level. Therefore, our methodology for hyperthermia treatment seems to be harmless for the hepatocellular tissue since it is able to recover the health status in ten days.
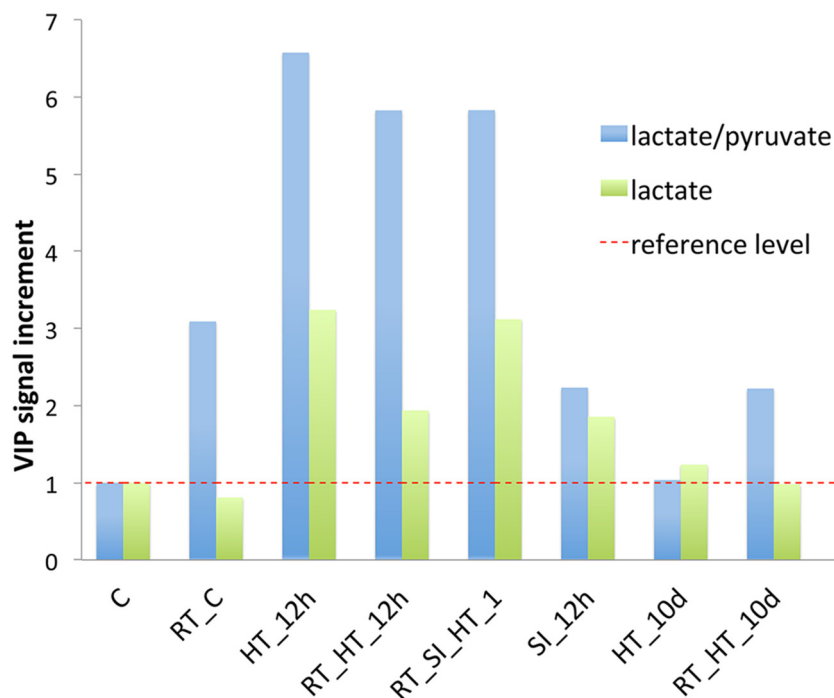
Figure 3.10: The signal increment of the most meaningful metabolites obtained from the VIP showed graphically and refered to the healthy tissue (C). *Key information to understand the abbreviations: control (C), hepatocelluler tissue (H), rat with CLM (RT), hyperthermia therapy procedure (HT), sham surgery using saline infusion (SI) and period of time elapsed since the procedure (12 hours or 10 days).*

Hyperthermia effects of tumour tissues
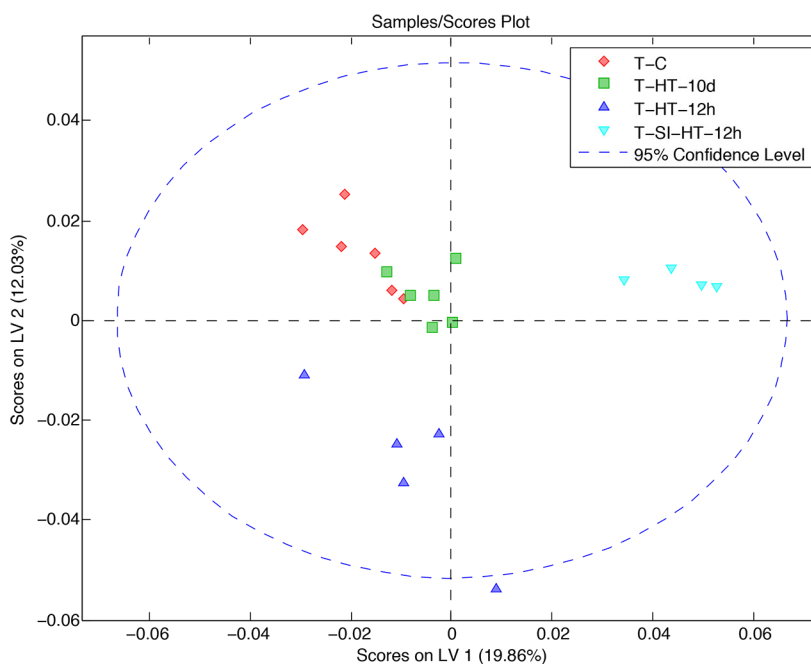
Figure 3.11: OPLS-DA scores from a data set that combines tumour tissues from rats that suffered CLM (TC, THT10d, THT12h and TSIHT12h) under different procedures. *Key information to understand the abbreviations: control (C), tumour (T), hyperthermia therapy procedure (HT), sham surgery using saline infusion (SI) and period of time elapsed since the procedure (12 hours or 10 days).*

In the same way that we have studied the last two issues, we built a new OPLS-DA model to observe the clustering of tumour samples after the different treatments. Three PC are needed to build the model and to explain the 41.23% of the variance of the x matrix (variables) and the 78.05% of the variance of the y matrix (classes). We show the RMSEC and RMSECV of the models in Table 3.5. In Figure 3.11, we find three main

Table 3.5: RMSEC and RMSECV values of the created PLSDA model.

	T-C	T-HT-10d	T-HT-12h	T-SI-HT-12h
RMSEC	0.25	0.25	0.18	0.11
RMSECV	0.48	0.44	0.54	0.34

groups in the score plot: the tumour tissue 12 h since HT at the low part of the plot, the tumour tissue 12 h since the sham operation and HT at the right-up side and the last group where tumour control tissue appears together with the tumour tissues after 10 days since HT.

Regarding to the loadings of the model (see Figure 3.12), in the first PC four signals are increased (glucose, betaine, lactate and butyrate) that characterise the positive-right side of the scores plot. In the second PC, which helps us to distinguish the tumour tissues that suffered HT, we have the betaine, choline, creatine, alanine, lactate and butyrate signals increased. As we have done in the previous cases, we focused on the VIPs to study the profiles of each class. In Table 3.6 and Figure 3.13, one signal that stand out is the α-glucose in the case of tumours that suffered both treatments. The tumour tissue shows a completely different behaviour if we compare it with the hepatocellular tissue.
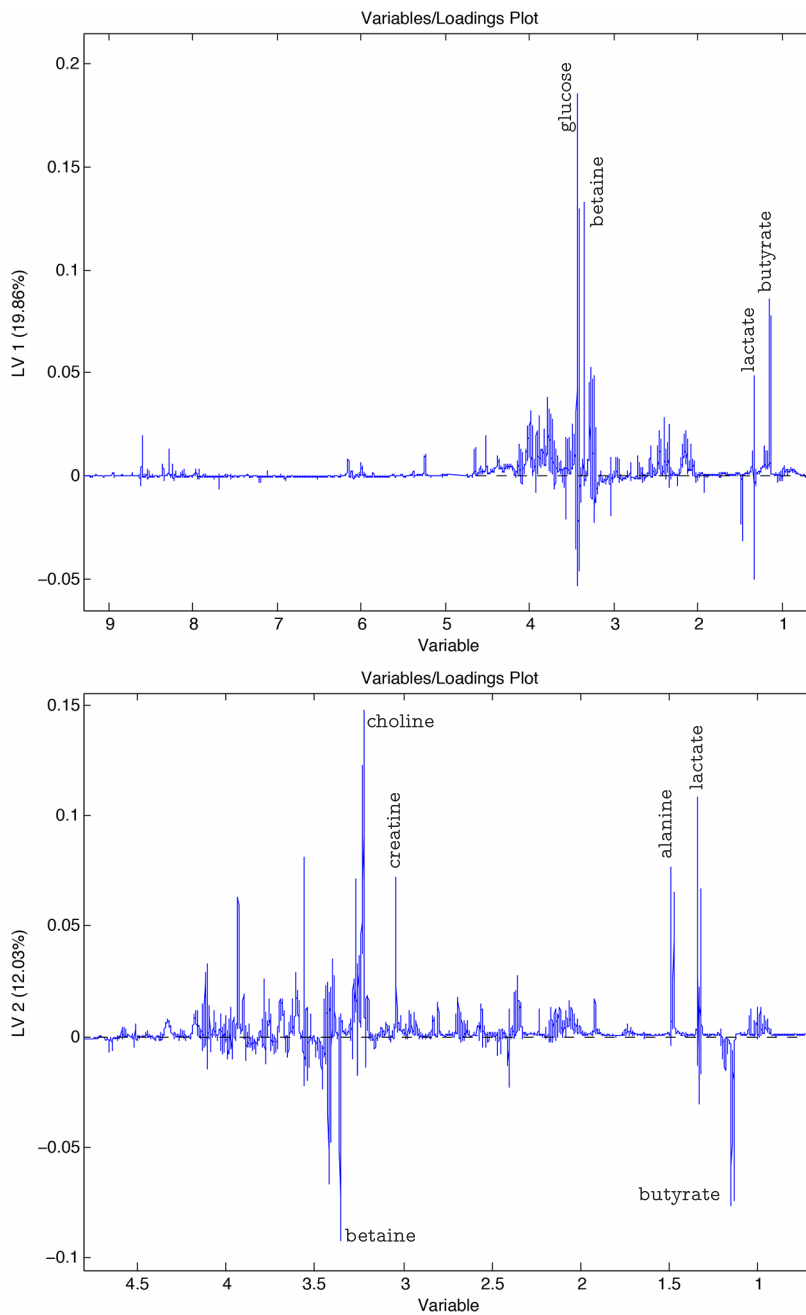
Figure 3.12: Loadings of the first and second PC of the OPLS-DA analysis obtained from a data set that combines tumour tissues from rats that suffer CLM under different procedures.

One of the most important metabolic differences that we can observe in Table 3.6 is the reduction of the lactate in two cases, THT12h and TSIHT12h. Though the enhancement of lactate is often linked with the *Warburg effect*, in this case we observe a significant alteration of this pathway. However, we observe an important increment of glycine in both cases. Besides, the tumour tissues that belong to the rats after HT and SI are especially characterised by an increment of valine, pyruvate, gluthathione (oxidized), anserine, glycine and α-glucose. Taking into account the fact that this class shows the highest values of gluthathione (oxidized), it can suggest that this class suffered the highest stress. In ten days, the tumour cells that suffered hyperthermia treatment still showed important differences in the metabolic profile. Most of the metabolites levels are decreased while a few metabolites are enhanced, such as D-hydroxybutyrate, lactate, creatine and betaine.

Table 3.6: The signal increment of the most meaningful metabolites obtained from the VIP showed in a heatmap refered to the tumour control tissue (TC). *Key information to understand the abbreviations: control (C), tumour (T), hyperthermia therapy procedure (HT), sham surgery using saline infusion (SI) and period of time elapsed since the procedure (12 hours or 10 days).*

| metabolite	ppm	T_C	T_HT_10d	T_HT_12h	T_SI_HT_12h
leucine/isoleucine	0,966	1,00	0,28	2,76	0,21
valine	0,984	1,00	0,28	0,15	2,57
D-Hydroxybutyrate	1,187	1,00	2,39	0,43	0,17
lactate	1,325	1,00	2,04	0,75	0,32
alanine	1,492	1,00	0,43	3,45	0,31
lysine	1,719	1,00	0,52	2,14	0,23
acetate, acetoacetate	1,921	1,00	0,46	2,41	0,51
N-acetyl functions of glycoprotein	2,053	1,00	0,20	2,14	0,85
pyruvate	2,408	1,00	0,18	1,22	2,51
gluthathione (oxidized)	2,559	1,00	0,27	1,11	1,83
aspartate	2,692	1,00	0,22	2,24	0,77
dimethylglycine	2,941	1,00	0,61	1,38	1,15
anserine	2,962	1,00	0,67	0,89	1,43
creatine	3,042	1,00	1,58	1,66	0,24
choline	3,225	1,00	1,04	1,94	0,14
GPC (sn-glycerol-3-phosphocholine)	3,233	1,00	0,12	2,40	0,62
taurine, trimethylamine-N-oxide	3,271	1,00	0,23	2,55	0,99
glycine	3,555	1,00	0,65	1,71	1,61
betaine	3,359	1,00	1,90	0,16	0,19
α-glucose	3,424	1,00	0,32	0,48	8,09
citrate	3,562	1,00	0,92	1,95	0,31
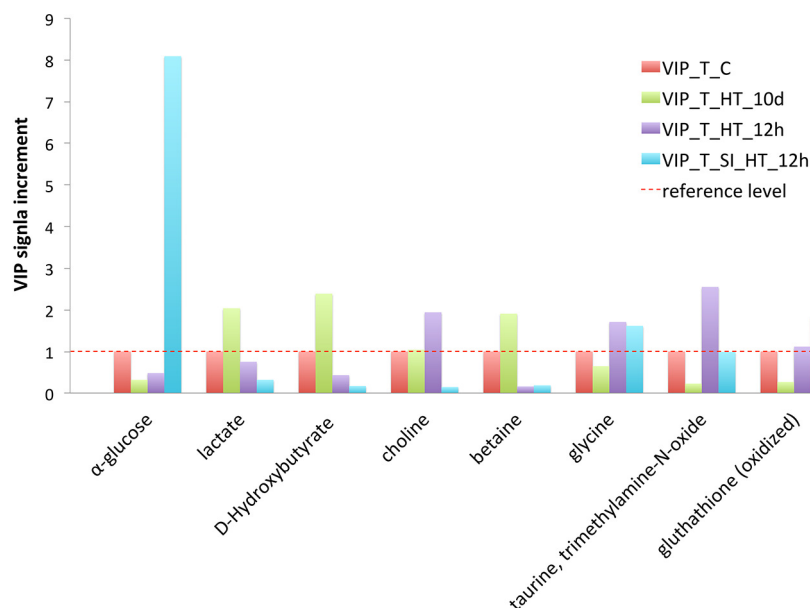
Figure 3.13: The signal increment of the most meaningful metabolites obtained from the VIP showed graphically and refered to the tumour control tissue (TC). *Key information to understand the abbreviations: control (C), tumour (T), hyperthermia therapy procedure (HT), sham surgery using saline infusion (SI) and period of time elapsed since the procedure (12 hours or 10 days).*

Biochemical blood analysis

The measurement of enzymatic activity is a reliable test used in common medical practices in hospitals. The alanine aminotransferase (GPT-ALT) and the aspartate aminotransferase (GOT-AST) levels show a significative increase in the rats that suffered HT and surgery in less than 12 hours (see Figure 3.14). These enzymes provide information about the state of the liver. Thus, we can observe that in 10 days after any treatment the rats recovered their basal levels. Together with these enzymes, we also measured

the enzymatic activity of creatine kinase (CK) and lactate deshidrogenase (LDH) as we can see in the Figure 3.14. CK show a significant increment only in the serum of rats that have suffered saline infusion and HT. In the case of LDH, the rats that have suffered saline infusion show a significant increment. The CK and LDH results suggest that inflammation processes happen when the rats get the saline infusion protocol. This is an expected result due to the surgery process and the cannula inserted in the artery that can cause tissue damage such as the endothelial injury. Nonetheless, in ten days the rats showed the basal enzymatic activity levels.

These NMR results are in agreement with the overall picture observed in the distribution of several biomarkers in serum. The increment of ALT and AST matched with the increments observed in the NMR spectra of lactate, glutamate and aspartate.
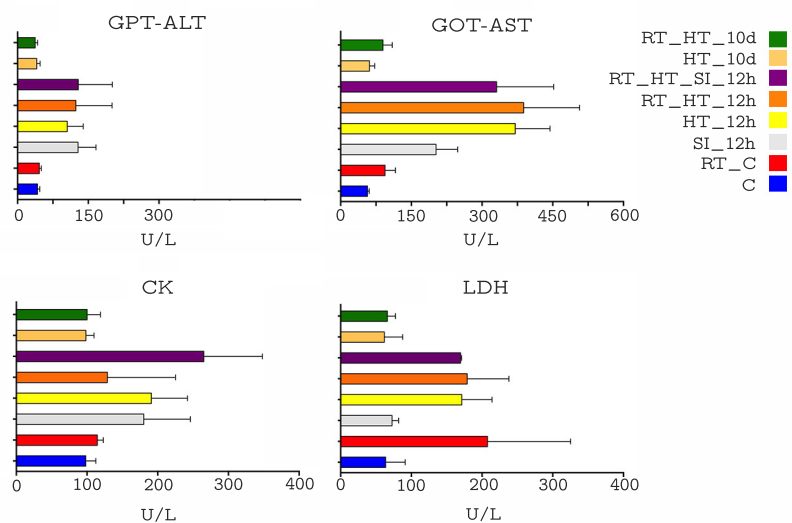
Figure 3.14: Alanine aminotransferase (GPT-ALT), aspartate aminotransferase (GOT-AST), creatine kinase (CK) and lactate dehydrogenase (LDH) enzyme activities (units per litre) measured in serum to check hepatic or sytemic damage in the rats that have undergone different treatments. *Key information to understand the abbreviations: control (C), hepatocelluler tissue (H), rat with CLM (RT), hyperthermia therapy procedure (HT), sham surgery using saline infusion (SI) and period of time elapsed since the procedure (12 hours or 10 days).*

3.2.5 Conclusion

According to the results discussed before we can conclude that the hyperthermic treatment does not cause any irreversible damage to the liver since significant traits of liver recovery were measured under all experimental conditions.

In addition to these findings we would like to emphasize the usefulness of this analysis to understand the main mechanisms of actions involved during the whole HT treatment. On the one side, most of the observed effects are effectively explained by the proliferation of tumour cells and by the overall inflammation induced by the HT and the surgery. Based on these findings and the preclinical studies have gained an additional information that may be useful to test and support further treatments based on the administration of drugs either to improve the efficiency of the HT in the elimination of tumour cells or to compensate the side effects on the healthy tissues and to promote a shorter restoration of the liver functionality.

Though the development of metabolomic analysis was satisfactory, we would like to show the ways in which this work could be followed in the near future:

- The analysis of the non-polar fraction is still waiting to be run and though the information that can be achieved is significantly shorter in terms of the number of metabolites that can be annotated, it should be accomplished in the short term.

- In addition to the 1H-NMR spectra 2D JRES spectra were also collected and it was treated but not in depth. These spectra is simpler than the 1D since the proton-proton coupling is only plotted in the second dimension and, therefore the annotation of the main peaks of the JRES projection can be proceeded more easily.

- The annotation of the metabolites has been carried out based on the literature data and there are still quality assurance/quality control issues that should be considered. For instance, though the instrumental analysis is able to provide a very high resolution in the

measured displacement (δ, ppm) most of the data found provides a lower resolution (2 digits) which limits the unambiguous assignment.

- The use of a program such as MVAPACK (freeware) [81] or Chenomx (http://www.chenomx.com) to validate the whole procedure (from data treatment to peak annotation) is also a take home message. Additionally, the use of software applications to allocate the metabolites in the pathways would allow a better understanding of these results.

3.3 Hyperspectral image analysis of rat liver with CLM

3.3.1 Introduction

Molecular vibrational spectroscopy allows to characterise the structure of biomolecules such as proteins, lipids, nucleic acids and carbohydrates [82–86]. The spectroscopic analysis of biological samples provides a characteristic spectrum, a kind of *biochemical fingerprint* based on its overall biochemical composition [87]. Thus, the obtained spectrum is the result of the superposition of all the constituents in the measured sample, which may contain useful information for diagnosis purposes [88,89]. When the samples are complex so are the resulting spectra. Therefore, the use of multivariate analysis together with a proper spectra pretreatment allow to get chemical information, especially when subtle biochemical differences are expected among samples. In this way, it is possible to differentiate among cells and tissues in different stages of their life cycle and to observe changes caused by diseases [87, 90, 91].

Nowadays, histopatological analysis of tissues is one of the most common clinical diagnosis tools, which relies largely on changes in tissue structure to classify disease processes. In contrast, molecular vibrational spectroscopies are minimally invasive, non-destructive, rapid, easy to automate and reproducible, which is an important progress because it facilitates the interpretation of pathologist using automated classification systems. Moreover, the latest advances in clinical applications of spectroscopic techniques allow *in vivo* measurements and diagnosis in real-time as well as the analysis of tissues obtained in biopsies and even aspirated cells [88].

Significant advances in cancer diagnosis and prognosis using spectroscopic techniques have lead into clinical implementation. Examples such as *Raman4Clinics* (http://www.raman4clinics.eu/) and *Clinical Infrared and Raman Spectroscopy for Medical Diagnosis* (http://clirspec.org/) are proof of this progress [84]. In fact, FTIR, Raman spectroscopy and its derivatives coupled with multivariate analysis have been widely used in research to classify neoplasia in tissues such as brain [92], breast [93], bladder [94, 95], colorectal [96–98], esophageal [99] and prostate [100] using both, point by point spectroscopy and imaging approaches.

Raman and FTIR Spectroscopy

It is almost a century since Adolf Smekal predicted the inelastic scattering of light. However, it was in 1928 when Professor Chandrasejara Venkata Raman demonstrated the Raman effect. Raman spectroscopy uses monochromatic light (NIR, visible or UV range lasers) to interact with the sample and to obtain the inelastic scattering or Raman effect. The Raman effect is the excitation of photons to virtual energy states and the consequent loss (Stokes) or gain (anti-Stokes) of energy that occurs due to the interaction of light with vibrational modes associated with chemical bonds within the sample. This shift in energy corresponds to vibrational modes of polarizable molecules [84].

When Raman spectra are going to be acquired one should consider the wavelength of the exciting laser because the excitation energy is different. Depending on the energy the scattering efficiency change and therefore, different integration times should be used. Additionally, what is more disappointing, is the fact that many biological and organic samples when are

analysed with a green lasers such as 532 nm, may promote its fluorescence, and may overlap any underlying Raman signal. In contrast, the use of a red laser such as 785 nm that has a lower photon energy, may not promote the electronic transition avoiding the fluorescence and hence the Raman signal is easier to detect.

Nowadays, the most used Raman spectroscopies are spontaneous Raman spectroscopy, resonance Raman spectroscopy (RRS), surface enhanced Raman spectroscopy (SERS), tip-enhanced Raman spectroscopy (TERS), coherent anti-stokes Raman scattering (CARS), stimulated Raman spectroscopy (SRS) and spatially offset Raman spectroscopy (SORS) [101].

Fourier transform infrared spectroscopy (FTIR) is a vibrational spectroscopy that relies on the absorbance, transmittance or reflectance of infrared light. In FTIR, light is absorbed in different proportions and at distinct frequencies that correspond to the vibrational frequencies of the biological molecules within the sample. The most widely used infrared spectroscopies are FTIR transmitance, attenuated total reflectance FTIR (ATR-FTIR) and near-infrared spectroscopy (NIR) [102].

Additionally, FTIR and Raman spectroscopies, both can be used coupled to a microscope, which offers an additional value in image analysis.

Raman and FTIR measurements can provide complementary information about the sample [103]:

(i) FTIR spectroscopy depends on a change in dipole moment of a molecule, whereas Raman depends on a change in polarizability.

(ii) FTIR spectroscopy measures absolute frequencies at which a molecule absorbs radiation, while Raman measures relative frequencies at which a sample scatters radiation.

(iii) FTIR spectroscopy is sensitive to heteronuclear functional group vibrations and polar bonds, especially -OH stretching in water. Meanwhile, Raman is sensitive to homonuclear molecular bonds and enable the distinction among C−C, C=C and C≡C. Therefore, Raman spectroscopy is the best option to measure in water media.

(iv) Fluorescence interferes in Raman spectroscopy but not in FTIR spectroscopy.

Sample preparation for Raman and FTIR imaging

Sample preparation is a crucial step to get the full potential of Raman and FTIR spectroscopy. The most used methods are [104]:

(i) *Formalin fixation and paraffin embedding* is the most used methodology by pathologist for histological examination of tissue sections. However, the presence of paraffin in the measurements complicates the extraction of biological information since its presence hides many peaks of interest. Even though, there are some approaches that, using chemometric tools, are able to remove the paraffin signal [105], dewaxing is the typical procedure. These dewaxing protocols involve the use of solvents such as xylene, alcohols or hexane, which may also produce alterations in tissues.

The formalin-fixed tissues show a reduction in the amide I peak attributed to the formation of tertiary amides. In addition, formalin or ethanol induces coagulation of the globular proteins present in the cytoplasm that can lead into damages on structural integrity of organelles. Another disadvantage of using ethanol in the embedding protocol is that precipitates lipid molecules that are not preserved

through the primary fixation step. Finally, in case that the paraffin embedded samples is dewaxed it has to take into account important lipid loses as well as the reduction of glycogen signal, as we observed experimentally in our laboratory.

(ii) *Snap-freezing* of fresh tissue is preferred for molecular-based studies since this method avoids the use of organic solvents that causes degradation or loss of some molecular components. However, it has to take into account that the thawing and dehydration process that suffers the frozen sample at room temperature can result in changes in the relative intensities of the amide I and methyl bending modes, probably due to protein depolymerization.

3.3.2 Aims of this work

The aim of this work is to develop the methodology to run hyperspectral image analysis by means of Raman and FTIR spectroscopy on rats livers that suffer CLM to complete hystopathological analysis. During this project, sample preparation, data importation to MATLAB and chemometric analysis were optimized and implemented in order to characterise and distinguish the tumour and healthy tissues of rats with CLM.

3.3.3 Materials and methods

Sample preparation

Liver tissues were obtained from WAG/RiJHsd rats (male *Rattus norvegicus* laboratory rats). Some of those rats were inoculated in the left hepatic lobe with CC-531 colon adenocarcinoma cells while rats without

inoculation were used as control samples. The rats were sacrificed in order to remove surgically the liver as described above. The livers were directly snap-frozen in liquid nitrogen (77 K). Two consecutive cryosections of 10 μm (the maximum thickness for transmitance FTIR measurements) were cut in a cryotome (Leica CM-3050) in the snap-frozen samples. One section was mounted in a metallic sample holder for Raman analysis and the other one was mounted in a ZnSe sample holder for infrared analysis (see Figure 3.15).

Infrared imaging

Infrared images were obtained using a Jasco 4200 spectrophotometer coupled to IMV-4000 infrared multichannel viewer (JASCO corporation, Tokyo, Japan). The microscope is equipped with a mobile platform and a 16 channel linear array MCT detector cooled by liquid nitrogen. The spectral range is limited by zinc selenide optics from 4000 to $750\,\mathrm{cm}^{-1}$.The spectral resolution was $4\,\mathrm{cm}^{-1}$ and the spatial resolution using a 16x cassegrain objective was $12.5\,\mu\mathrm{m}$. The transmittance images were acquired using 64 scans. Before any measurement the instrument was autoaligned and the focus was manually optimized using the backgrounds obtained from each channel of the detector (see Figure 3.15).

Raman imaging

Raman analyses were carried out by means of inVia Renishaw confocal microRaman spectrometer (Renishaw, Gloucestershire, UK) coupled to a DMLM Leica microscope provided with s 50x lens using 785 nm excitation laser. Data acquisition was carried out using WiRE 3.2 software package (Renishaw). Spectra were acquired in different ranges between 150 and

$3200\,\mathrm{cm}^{-1}$ ($1\,\mathrm{cm}^{-1}$ spectral resolution). Point-by-point mapping and StreamLine (line scan acquisition mode) technology were employed to acquire Raman chemical images. The acquisition time was set at $20\,\mathrm{s}$ to point-by-point analysis and $60\,\mathrm{s}$ to streamline analysis. The quality of the measurements was assured by means of an internal calibration and a diary calibration with a silicon chip. Additionally, in order to ensure the optimum image acquisition conditions the laser spot and the detector alignment were tested regularly and corrected in the cases that it was necessary (see Figure 3.15).
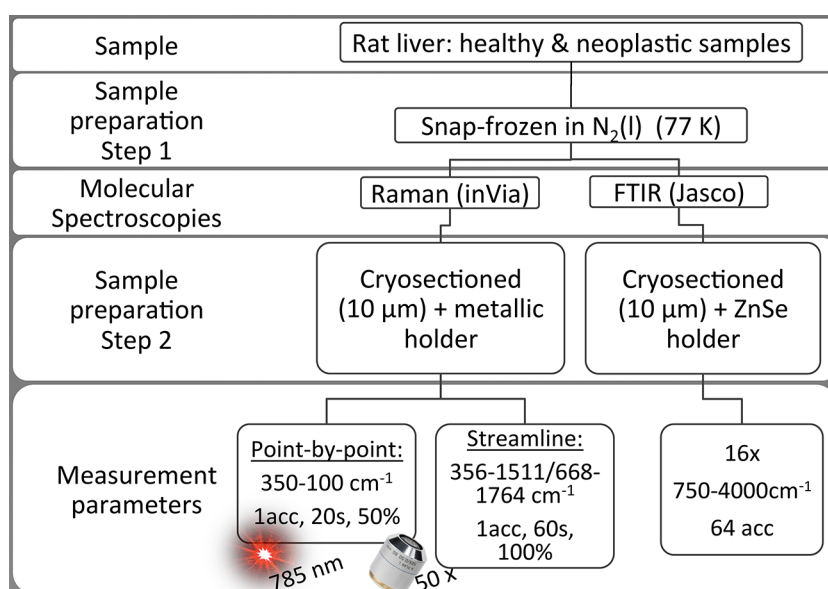
Figure 3.15: The main preparation and measurement steps followed to acquire spectroscopic images from healthy and tumour tissues.
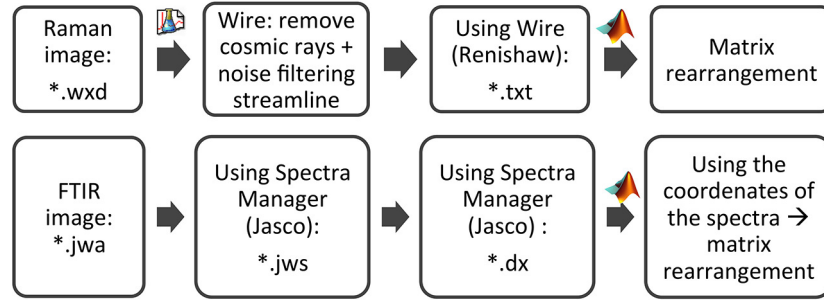
Figure 3.16: The main steps followed to import the data to MATLAB.

Data processing

The data obtained were imported to MATLAB following the steps that are shown in Figure 3.16. The last step, to obtain the mat file, for both data types, was carried out using a script wrote in MATLAB by ourself and with the assistance of Frans W J van den Berg and José Manuel Amigo (University of Copenhagen, Denmark).

In Figures 3.17 and 3.18 we show the steps that we followed to import the Raman map acquired using point-by-point configuration in the Renishaw InVia microscope into Matlab. In addition, in Figures 3.19 and 3.20 we show the steps that we followed to import the Raman image acquired using streamline configuration in the Renishaw InVia microscope into Matlab (for the snake streamline configuration we should modify the script to rebuild the acquired data matrix).

The infrared images were acquired using a Jasco microscope. The original image file needs to be exported at once using individual spectrum in which file-name appears its xy position (from *.jwa to *.jws). Then, using the Jasco software we exported the *.jws files in batches to JCAM-

dx files. Therefore, we built a script to read and form the image matrix again in Matlab (see Figure 3.21).

```matlab
function [X,wn] = readRamanImage(filename)
% function [X,wn] = readRamanImage(filename)
% FvdB 120518
%
% Read Raman image from text-file

if (nargin==0)
    filename = [];
end
if isempty(filename)
    filename = uigetfile('*.txt');
    if ~filename
        disp('No file selected');
        return;
    end
end

clc;
disp(['Reading file ' filename]);
% Determine total N (number of lines in file) from loop
disp('Determining number of entries - takes a short while');
N = numel(textread(filename,'%1c%*[^\n]'));
disp([' - ' num2str(N) ' entries found']);
maxN = 1e6; % Memory/matrix size to read file at once
if (N<=maxN)
    disp('Small file, read at once');
    X = dlmread(filename,'',[0 0 N-1 3]);
    wn = unique(X(:,3));
    Nw = length(wn);
    Nx = length(unique(X(:,2)));
    Ny = length(unique(X(:,1)));
    disp([' - ' num2str(Nw) ' wavenumber channels found']);
    disp([' - ' num2str(Nx) ' rows found']);
    disp([' - ' num2str(Ny) ' columns found']);
    if (N~=Nw*Nx*Ny)
        error('ERROR: N is not equal to N-wn x N-x x N-y ???');
    else
        disp('Check N = N-wn x N-x x N-y !');
    end
    X = reshape(X(:,4),Nw,Nx,Ny);
    X = permute(X,[2 3 1]);
```

Figure 3.17: Script I to import the Raman map acquired using the point-by-point configuration in the Renishaw InVia microscope and the Renishaw Wire 3.2 software.

```matlab
else
    disp('Big file, read in steps');
    % Determine N-wavenumber and N-x from first maxN points
    X = dlmread(filename,'',[0 0 maxN 2]);
    wn = unique(X(:,3));
    Nw = length(wn);
    Nx1 = length(unique(X(:,1)));
    Nx2 = length(unique(X(:,2)));
    Nx = max([Nx1 Nx2]);
    clear X;
    disp([' - ' num2str(Nw) ' wavenumber channels found']);
    disp([' - ' num2str(Nx) ' rows found']);
    Ny = N/Nw/Nx;
    disp([' - ' num2str(Ny) ' columns found']);
    if (N~=Nw*Nx*Ny)
        error('ERROR: N is not equal to N-wn x N-x x N-y ???');
    else
        disp('Check N = N-wn x N-x x N-y !');
    end
    % Read the actual data, and reshape into cube of size Nx x Ny x Nw
  %  disp('Reading data - takes a while');
    %X = dlmread(filename,'',[0 3 N-1 3]);
    %X = reshape(X,Nw,Nx,Ny);
    %X = permute(X,[2 3 1]);
end
disp('Finished');
```

Figure 3.18: Script II to import the Raman map acquired using the point-by-point configuration in the Renishaw InVia microscope and the Renishaw Wire 3.2 software.

```matlab
function [X,wn] = readRamanImagestream(filename)
% function [X,wn] = readRamanImage(filename)
% FvdB 120518
%
% Read Raman image from text-file

if (nargin==0)
    filename = [];
end
if isempty(filename)
    filename = uigetfile('*.txt');
    if ~filename
        disp('No file selected');
        return;
    end
end

clc;
disp(['Reading file ' filename]);
% Determine total N (number of lines in file) from loop
disp('Determining number of entries - takes a short while');
N = numel(textread(filename,'%1c%*[^\n]'));
disp([' - ' num2str(N) ' entries found']);
maxN = 1e6; % Memory/matrix size to read file at once
if (N<=maxN)
    disp('Small file, read at once');
    X = dlmread(filename,'',[0 0 N-1 3]);
    wn = unique(X(:,3));
    Nw = length(wn);
    Nx = length(unique(X(:,2)));
    Ny = length(unique(X(:,1)));
    disp([' - ' num2str(Nw) ' wavenumber channels found']);
    disp([' - ' num2str(Nx) ' rows found']);
    disp([' - ' num2str(Ny) ' columns found']);
    if (N~=Nw*Nx*Ny)
        error('ERROR: N is not equal to N-wn x N-x x N-y ???');
    else
        disp('Check N = N-wn x N-x x N-y !');
    end
    X = reshape(X(:,4),Nw,Nx,Ny);
    X = permute(X,[2 3 1]);
```

Figure 3.19: **Script I** to import the Raman image acquired using the streamline configuration in the Renishaw InVia microscope and the Renishaw Wire 3.2 software.

```matlab
else
    disp('Big file, read in steps');
    % Determine N-wavenumber and N-x from first maxN points
    X = dlmread(filename,'',[0 0 maxN 2]);
    wn = unique(X(:,3));
    Nw = length(wn);
    Nx1 = length(unique(X(:,1)));
    Nx2 = length(unique(X(:,2)));
    Nx = max([Nx1 Nx2]);
    clear X;
    disp([' - ' num2str(Nw) ' wavenumber channels found']);
    disp([' - ' num2str(Nx) ' rows found']);
    Ny = N/Nw/Nx;
    disp([' - ' num2str(Ny) ' columns found']);
    if (N~=Nw*Nx*Ny)
        error('ERROR: N is not equal to N-wn x N-x x N-y ???');
    else
        disp('Check N = N-wn x N-x x N-y !');
    end
    % Read the actual data, and reshape into cube of size Nx x Ny x Nw
    disp('Reading data - takes a while');
    X = dlmread(filename,'',[0 3 N-1 3]);
    X = reshape(X,Nw,Nx,Ny);
    X = permute(X,[2 3 1]);
end
disp('Finished');
```

Figure 3.20: **Script II** to import the Raman image acquired using the streamline configuration in the Renishaw InVia microscope and the Renishaw Wire 3.2 software.

```matlab
function [x1, y1, fileList, IR, wn]=irakdx()
files = dir('*.dx');
dirIndex = [files.isdir];
fileList = {files(~dirIndex).name}';
r=length(files);
    for a=1:r
    data(a)=jcampread(files(a).name);
    wn= data(a).Blocks.XData;
    IR(a,:)= data(a).Blocks.YData;
    end

    for i=1 : r;
    [~,y]=strtok(fileList(i,:),'X');
    [x,y]=strtok(y,'_Y');
    [a]=strtok(x,'X');
    [b]=strtok(y,'_Y');
    [c,d]=strtok(b,'.dx');
    x1(i)=str2double(a);
    y1(i)=str2double(c);
    end


end
================================================

[x1, y1, fileList, IR, wn]=irakdx();
x1=x1';
y1=y1';
wn=wn';
X=[x1,y1,IR];
Nx1=length(unique(X(:,1)));
Ny1=length(unique(X(:,2)));
Nwn=length(unique(wn));
X=sortrows(X,-2);
X=sortrows(X,1);
data = reshape(IR,Ny1,Nx1,Nwn);
```

Figure 3.21: Script used to import the infrared image acquired in the Jasco microscope to Matlab.

Principal component analysis (PCA) and multivariate curve resolution (MCR) chemometric methods were chosen in order to extract information from liver tissue spectroscopic analyses. In chemometric applications, spectral signal preprocessing is a crucial step to obtain good results since it is necessary to reduce noise as well as to remove instrumental undesirable responses. This first step includes spectral and spatial algorithms such as spectral filters (cosmic ray removal in case of Raman spectra), normalization, mean centring, derivative transformation (Savitsky-Golay), standard normal variate (SNV) and smoothing.

In multivariate curve resolution alternating least squares (MCR-ALS) analysis, once the number of different components were estimated using singular value decomposition (SVD), ALS optimization was performed applying some constraints, such as non-negativity, and unimodality or closure. All data treatment was performed using MATLAB (version 7.0, MathWorks, Natick, MA, USA), PLS toolbox (version 7.0) and MIA toolbox (version 2.8).

3.3.4 Results and Discussion

Infrared results

The microscopical observations of the samples helped us to choose the area that is shown in Figure 3.22 to perform the transmittance FTIR image analysis. In order to distinguish between tumour and healthy tissues PCA and MCR-ALS analysis were performed. However, prior to the PCA analysis, smoothing, SNV and mean centring transformations were applied to original data.

Once the principal components (PCs) were calculated in the spectral range of 750 to $1800\,cm^{-1}$, the score maps and loadings were generated.
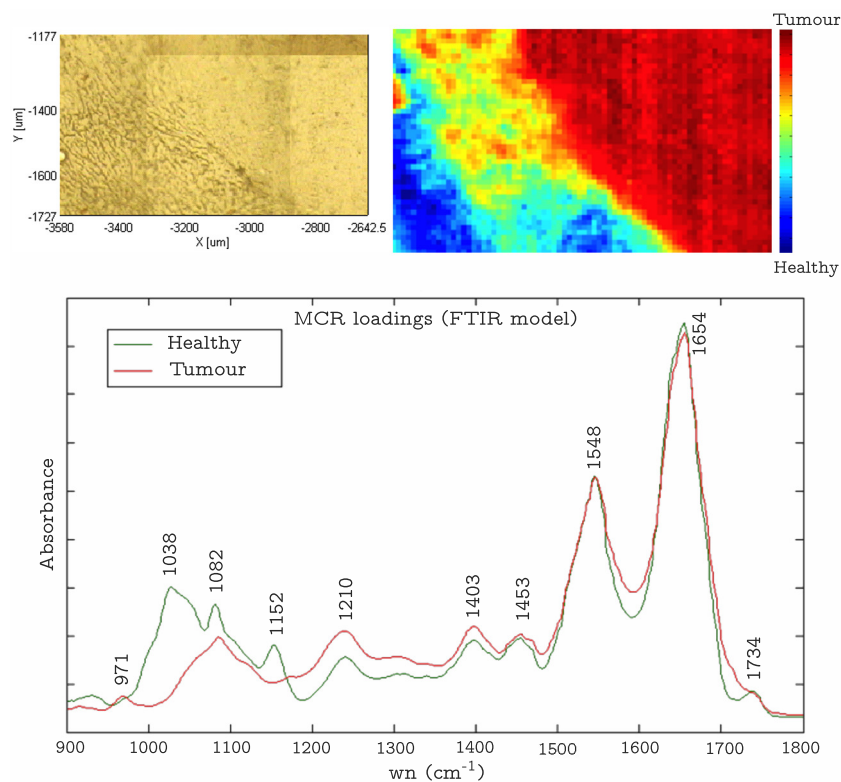
Figure 3.22: FTIR results obtained from a rat liver with CLM. In the image we observe the microscopic image, the pseudocolor score image obtained in the PCA analysis and the two main components obtained in the MCR-ALS analysis.

The first two principal components were enough to explain the 99 % of the total variance. In Figure 3.22 the pseudocolour score image of the first PC can be observed. In the image, the two main areas are well differentiated, healthy area (blue colour) and the tumour area (red color). The pixels of the infrared image were coloured based on the position of each pixel in the PC score plot, and those, in turn, are distributed taking into account the corresponding PC loadings. The study of the loadings is

necessary towards a deeper understanding of the changes observed in the tissue. However, the results obtained in the MCR-ALS analysis gave us in return the profiles of the main two spectra present in the matrix data (see Figure 3.22). Together with the assignment of the signals (see Table 3.7), we can compare the two main profiles. The healthy tissue is mainly characterized by higher concentrations of glycogen or/and polysaccharides $(1038\,\mathrm{cm}^{-1})$ and carbohydrates $(1153\,\mathrm{cm}^{-1})$. In contrast, the neoplastic tissue is characterised by the amide II $(1548\,\mathrm{cm}^{-1})$ and amide I $(1654\,\mathrm{cm}^{-1})$ bands that in general terms correspond to proteins.

Even though the PCA analysis and MCR-ALS analysis are able to explain two main groups or components, we can observe a yellowish area which is a kind of interphase where none of the two components are the main ones. In fact, this area shows a mixture of both spectra features.

Table 3.7: Assignation of the main Raman peaks of the components obtained by MCR-ALS analysis and showed in Figure 3.23.

Raman shift	Assignment
971 cm^{-1}	DNA
1038 cm^{-1}	glycogen, ν_s(C-O) polysaccharides
1082 cm^{-1}	ν_s(PO$_2$ $^-$) nucleic acids
1152 cm^{-1}	carbohydrates
1210 cm^{-1}	ν_{as}(PO$_2$ $^-$) nucleic acids
1403 cm^{-1}	ν(COO$^-$) fatty acids, amino acids chain
1453 cm^{-1}	ν(CH$_2$) fatty acids
1548 cm^{-1}	amide II, δ(N-H) and ν_s(C-N) proteins
1654 cm^{-1}	amide I, ν_s(C=O) protein
1734 cm^{-1}	lipids, ν_s(C=O) ester group

3.3.5   Raman results

Regarding the Raman results, PCA and MCR-ALS analysis are shown in Figure 3.23 and Table 3.8.

In this case, similarly to the FTIR analysis, both areas (the healthy in blue and the neoplastic in red) are easily distinguished in the Figure 3.23. In addition to these features, what it is more appealing from this plot is the transition area (in yellow) that can be observed between the healthy and neoplastic areas. It shows transitional spectra that did not belong to none of two main classes but it did not have an unique profile.

As it can be observed in Figure 3.23, the glycogen ($478\,\mathrm{cm}^{-1}$) is one of the most relevant signals that determines the differences between the healthy and tumour tissues. In addition to this, and in a similar way as observed in the FTIR analysis, (S-S) protein signal is more intense in neoplasic tissue. Moreover, in the Raman results, higher signal values of nucleotides and DNA were observed in the neoplastic tissue compared to the healthy one.

Cancer cells need to produce higher amount of amino acids to build the new cells and this is the reason to observe amide I signal increments. In contrast, the presence of a more intense Amide III signal in the healthy tissue spectra could be related with the more organized structure of the proteins of the healthy tissue, since the Amide III signal is typical of proteins in their secondary structure, and due to the impaired metabolism in the neoplastic cells, proteins could be more instable. The proliferation of cancer cells without control usually leads in the aneuploidy of the cells. In other words, the presence of cells with higher amount of chromosomes than the normal is typical of the tumours. Therefore, it is not surprising that under these experimental situations, neoplastic tissue presented higher

amounts of nucleic acids (especially DNA). Finally, regarding glycogen, in the present work higher intensity of the glycogen signal is observed in the healthy tissue.
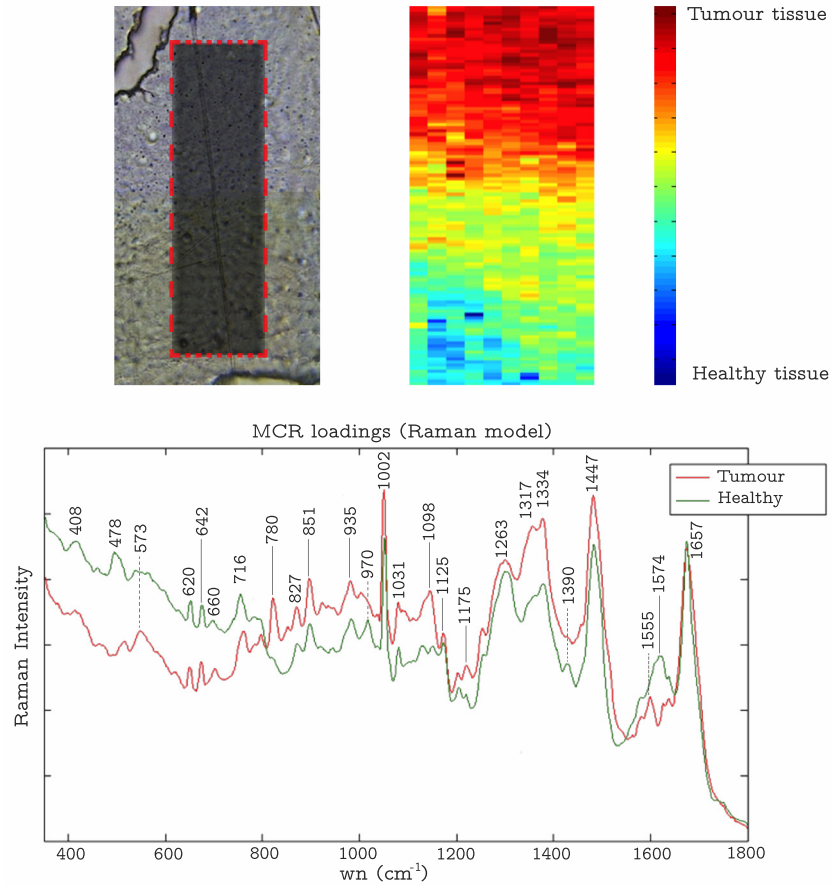
Figure 3.23: Raman results obtained from a rat liver with CLM. In the image we observe the microscopic image and the selected area in red, the pseudocolor score image obtained in the PCA analysis and the two main components obtained in the MCR-ALS analysis.

Table 3.8: Assignation of the main Raman peaks of the components obtained by MCR-ALS analysis and showed in Figure 3.23.

Raman shift	Assignment
479 cm^{-1}	glycogen
573 cm^{-1}	tryptophan, cytosine, guanine, disulphide, glycogen
620 cm^{-1}	phenylalanine
642 cm^{-1}	guanine, tyrosine, thymine, amide IV, v(C-S)
660 cm^{-1}	thymine, guanine
716 cm^{-1}	phosphatidylcholine
780 cm^{-1}	thymine, cytosine, nucleotides, uracil ring
827 cm^{-1}	O-P-O stretching (DNA, nucleic acids), tyrosine, proline, hydroxyproline
851 cm^{-1}	amino acids, tyrosine, proline, glycogen, valine, polysaccharides
935 cm^{-1}	collagen, glycogen, proline, valine, protein backbone (α-helix conformation)
970 cm^{-1}	phosphate monoester groups of phosphorilated
1002 cm^{-1}	phenylalanine, v(C-C) aromatic ring
1031 cm^{-1}	collagen, proline, phenylalanine, v(C-C) keratin
1099 cm^{-1}	v(C-N) lipid
1125 cm^{-1}	C-N (proteins), C-O carbohydrates, lipids
1175 cm^{-1}	v(C-C)
1263 cm^{-1}	amide III, v(C-N), deformation (N-H), =C-H in plane deformation
1317 cm^{-1}	amide III, C-H bending, phospholipids, lipids, triglycerides, adenine, CH3CH2 twisting, CH2 deformation
1334 cm^{-1}	nucleic acids, purine bases, glycogen, amino acids
1390 cm^{-1}	nucleic acids, purine bases, glycogen, amino acids
1447 cm^{-1}	CH3CH2 bending modes, CH2 deformation, deoxyribose, glucose
1555 cm^{-1}	amide II, tryptophan
1574 cm^{-1}	purine bases, nucleic acids
1657 cm^{-1}	amide I (proteins), vs (C=O), lipids

3.3.6 Conclusions

One of the main contribution of this work was the development of a suitable procedure to measure hyperspectral images of liver tissues by both FTIR and Raman spectroscopies. Though the description was limited to the final procedure, we succeed to fine tune all the step, from snap-freezing and cryosection to final measurements. Addtionally, we were able to define the measuring procedures in both techniques to get the best available images.

In this sense, the quality of the Invia images were not obtained in the best conditions since the streamline accumulates the spectra quite slowly and the sensitivity of the detector was not at the required conditions. In fact, recently we were able to measure some samples in a new equipment and the results were much more promising though the laser was the red one.

The developed methodology is feasible and allowed us to characterised the colorectal liver metastasis profile by means of Raman and FTIR analysis. The increment of amino acids (amide I signal increment), glycogen and nucleic acids concentration in tumour tissue comes into agreement with the results obtained in the NMR metabolomics section, since when cancer cells are in proliferation show an important enhancement of the metabolism.

Finally, it is important to emphasize the quality of the multivariate image models that allow a net mapping of the tissues and the identification of biomolecules in healthy and tumour tissues. The fact that better images are technically available in the near future allows us to think that more information could be achieved.

3.4 Conclusion of the magnetic hyperthermia project

From the scientific point of view the Hyperthermia project allowed us to tackle two complementary aims that were not accomplished before. Both analysis offered us the chance to develop the required methodologies and once we succeed with the hard work, the way is open to new challenges.

First of all, the importance of bioanalytical procedures has been proven and finally the fit-for-purpose of the NMR and hyperspectral imaging has been satisfactorily shown.

As it has been pointed out in the previous sections, both approaches have shown some strengths and opportunities. Regarding the later ones, we would like to point some new challenges that could be included in future works:

- MALDI imaging techniques are among the best approaches in tissue analysis. Though some trials were performed we did not succeed in the analysis of the functionalised nanoparticles in liver tissues.

- SERS imaging is also a promising approach to couple SERS active NPs and Raman imaging and to find out the way the functionalised NPs are attached to the tumour cells. Part of the training needed to develop the SERS experiments was carried out in a short stage at the University of Strathclyde, as it is reported in the next chapter.

  We would like to highlight the efforts made for all participants of this project. Everyone that has worked in such a big multidisciplinary team, knows how difficult is to coordinate all together. Moreover, when biological issues are involve the time periods increase exponentially and experiments are much more

complicate. Even though this is not the only cause to do only two experiments per year, actually the synthesis of a magnetic nanoparticle batch also takes one month. We can say that we all have made efforts to make progress this project from chaos to heaven. In return, we can say proudly that the interaction between all these areas of knowledge allows us to evolve and improve ourself as scientist.

References

[1] Eurostat Statistics Explained (European Union). Statistics on causes of death in the European Union (EU). retrived from http://ec.europa.eu/eurostat/statistics-explained/index.php, 2015 (Last visit, May 2016).

[2] International Agency for Research on Cancer (Wold Health Organization). Globocan 2012: Latest world cancer statistics. retrieved from https://www.iarc.fr., 2013 (Last visit, May 2016).

[3] A. Stein and H.J. Schmoll. Systemic treatment of liver metastases from colorectal cancer. *Ther. Adv. Med. Oncol.*, 5(3):193–203, 2013.

[4] B. Lintoiu-Ursut, A. Tulin and S. Constantinoiu. Recurrence after hepatic resection in colorectal cancer liver metastasis -review article-. *J. Med. Life*, 8(Spec Issue):12–14, 2015.

[5] European Association for the Study of the Liver, European Organisation for Research, and Treatment of Cancer. EASL–EORTC clinical practice guidelines: Management of hepatocellular carcinoma. *J. Hepatol.*, 56(4):908–943, 2012.

[6] M.S. Park, N.J. Yi, S.Y. Son, T. You, S.W. Suh, Y.R. Choi, H. Kim, G. Hong, K.B. Lee, K.W. Lee, S.Y. Jeong, K.J. Park, K.S. Suh and J.G. Park. Histopathologic factors affecting tumor recurrence after hepatic resection in colorectal liver metastases. *Ann. Surg. Treat. Res.*, 87(1):14–21, 2014.

[7] K.M. Chan, T.H. Wu, C.H. Cheng, W.C. Lee, J.M. Chiang, J.S. Chen, and J.Y. Wang. Prognostic significance of the number of tumors and aggressive surgical approach in colorectal cancer hepatic metastasis. *World J. Surg. Onc.*, 12(1):1–8, 2014.

[8] K.R. Sheth and B.M. Clary. Management of hepatic metastases from colorectal cancer. *Clin. Colon Rectal Surg.*, 18(3):215–23, 2005.

[9] P. Moroz, S.K. Jones and B.N. Gray. Status of hyperthermia in the treatment of advanced liver cancer. *J. Surg. Oncol.*, 77(4):259–269, 2001.

[10] J. van der Zee. Heating the patient: a promising approach? *Ann. Oncol.*, 13(8):1173–1184, 2002.

[11] S.A. Curley. Radiofrequency ablation of malignant liver tumors. *Ann. Surg. Oncol.*, 10(4):338–347, 2003.

[12] S. Mornet, S. Vasseur, F. Grasset and E. Duguet. Magnetic nanoparticle design for medical diagnosis and therapy. *J. Mater. Chem.*, 14(14):2161–2175, 2004.

[13] D. Ortega and Q.A. Pankhurst. Magnetic hyperthermia. *Nanoscience (Cambridge, U. K.)*, 60–88, 2013.

[14] D.A. Hill. Further studies of human whole-body radiofrequency absorption rates. *Bioelectromagnetics*, 6(1):33–40, 1985.

[15] I.N. Crispe. The liver as a lymphoid organ. *Annu. Rev. Immunol.*, 27(1):147–163, 2009.

[16] F. Fiévet R. Brayner and T. Coradin, editors. *Nanomaterials: A Danger or a Promise?* Springer, 2013.

[17] K.J. Landmark. Dendrimer-coated iron-oxide nanoparticles as targeted MRI contrast agents. *PhD thesis, University of Michigan*, 2008.

[18] S. Wada, L. Yue, K. Tazawa, I. Furuta, H. Nagae, S. Takemori and T. Minamimura. New local hyperthermia using dextran magnetite complex (DM) for oral cavity: experimental study in normal hamster tongue. *Oral Dis.*, 7(3):192–195, 2001.

[19] H. Oliveira, J. Thevenot, O. Sandre and S. Lecommandoux. Magnetic field triggered drug release from polymersomes for cancer therapeutics. American Chemical Society, 2015.

[20] B. Herrero, H. Marin, M. Insausti, F. Plazaola, E. Garaio, L. Hernandez, C. Del Campo, J.J. Echevarria-Uraga, I. García-Alonso and A. Saiz-Lopez. Liver hyperthermia induced by different iron magnetic nanoparticles "ex- vivo" and correlation to pathological damage in the tissue. *Br. J. Surg.*, 100(1):12, 2013.

[21] J. Alonso, H. Khurshid, V. Sankar, Z. Nemati, M. H. Phan, E. Garayo, J. A. Garcia and H. Srikanth. Feco nanowires with enhanced heating powers and controllable dimensions for magnetic hyperthermia. *J. Appl. Phys.*, 117(17):17D113/1–17D113/4, 2015.

[22] E. Garaio, O. Sandre, J.M. Collantes, J.A. Garcia, S. Mornet and F. Plazaola. Specific absorption rate dependence on temperature in magnetic field hyperthermia measured by dynamic hysteresis losses (AC magnetometry). *Nanotechnology*, 26(1):015704/1–015704/18, 18 pp., 2015.

[23] E. Garaio, J.M. Collantes, F. Plazaola, J.A. Garcia and I. Castellanos-Rubio. A multifrequency electromagnetic applicator with an integrated AC magnetometer for magnetic hyperthermia experiments. *Meas. Sci. Technol.*, 25(11):115702/1–115702/10, 2014.

[24] E. Garaio, J. M. Collantes, J.A. Garcia, F. Plazaola, S. Mornet, F. Couillaud and O. Sandre. A wide-frequency range AC magnetometer to measure the specific absorption rate in nanoparticles for magnetic hyperthermia. *J. Magn. Magn. Mater.*, 368:432–437, 2014.

[25] I. Castellanos-Rubio, M. Insausti, E. Garaio, I. Gil de Muro, F. Plazaola, T. Rojo and L. Lezama. Fe3O4 nanoparticles prepared by the seeded-growth route for hyperthermia. electron magnetic resonance as a key tool to evaluate size distribution in magnetic nanoparticles. *Nanoscale*, 6(13):7542–7552, 2014.

[26] F. Plazaola, E. Garaio, J.M. Collantes, I. Castellanos, M. Insausti, I. Gil de Muro and J.A. Garcia. Specific absorption rate of magnetite nanoparticle powders with and without surrounding organic ligands. *J. Nanosci. Nanotechnol.*, 12(9):7451–7455, 2012.

[27] M. Insausti, J. Salado, I. Castellanos, L. Lezama, I. Gil de Muro, J.M. de la Fuente, E. Garaio, F. Plazaola and T. Rojo.

Tailoring biocompatible Fe3O4 nanoparticles for applications to magnetic hyperthermia. *Proc. SPIE*, 8232(Colloidal Nanocrystals for Biomedical Applications VII):823210/1–823210/8, 2012.

[28] J.J. Echevarria-Uraga, I. García-Alonso Montoya, J.L. Miguélez Vidales, F. Sanz Sánchez, F. Plazaola Muguruza, M. Insausti Peña, N. Etxebarria Loizate and B. Fernández-Ruanova. Administración intrarterial de un magnetofluido termoterapéutico en un modelo experimental de metástasis hepáticas. Estudio de distribución con resonancia magnética y espectrometría. *Radiología*, 54(3):251–259, 2012.

[29] J.J. Echevarria-Uraga, I. Garcia-Alonso, F. Plazaola, M. Insausti, N. Etxebarria, A. Saiz-Lopez and B. Fernandez-Ruanova. Study of the intra-arterial distribution of Fe3O4 nanoparticles in a model of colorectal neoplasm induced in rat liver by MRI and spectrometry. *Int. J. Nanomed.*, 7:2399–2410, 2012.

[30] *Funcionalización y estudio de nanopartículas de magnetita para su aplicación en terapias de hipertermia magnética (thesis)*. University of the Basque Country, 2015.

[31] I. Díaz Sanz, B. Herrero de la Parte, J.L. Miguélez Vidales, I. Zabalza Estévez, J.J. Echevarria Uraga, I. García-Alonso Montoya and B. Fernández-Ruanova. Ultrasonographic characterisation of an experimental model of liver metastases from colon carcinoma in rats. *Radiología*, 52(1):37–44, 2010.

[32] J.M. Aizpurua, I. Azcune, R.M. Fratila, E. Balentova, M. Sagartzazu-Aizpurua and J.I. Miranda. "Click"synthesis

of nonsymmetrical bis(1,2,3-triazoles). *Org. Lett.*, 12(7):1584–1587, 2010.

[33] J. Bruix, M. Sherman, J.M. Llovet, M. Beaugrand, R. Lencioni, A.K. Burroughs, E. Christensen, L. Pagliaro, M. Colombo and J. Rodés. Clinical management of hepatocellular carcinoma. conclusions of the barcelona-2000 EASL conference. *J. Hepatol.*, 35(3):421–430, 2016.

[34] A. Colli, M. Fraquelli, G. Casazza, S. Massironi, A. Colucci, D. Conte and P. Duca. Accuracy of ultrasonography, spiral CT, magnetic resonance, and alpha-fetoprotein in diagnosing hepatocellular carcinoma: a systematic review. *Am. J. Gastroenterol.*, 101(3):513–523, 2006.

[35] M. Burrel, J.M. Llovet, C. Ayuso, C. Iglesias, M. Sala, R. Miquel, T. Caralt, J.R. Ayuso, M. Sole, M. Sanchez, C. Bru and J. Bruix. MRI angiography is superior to helical CT for detection of HCC prior to liver transplantation: an explant correlation. *Hepatology*, 38(4):1034–1042, 2003.

[36] I. Campbell. Liver: metabolic functions. *Anaesth. Int. Care Med.*, 7(2):51–54, 2 2006.

[37] *Shackelford Cirugía del aparato digestivo Tomo III, 3a edición.* G.D. Zuidema, 1991.

[38] *Bockus. Gastroenterología. 4a edición. Tomo IV Hígado.* J.E. Berk and col., 1987.

[39] T.N. Seyfried and L.M. Shelton. Cancer as a metabolic disease. *Nutr. Metabolism*, 7(1):1–22, 2010.

[40] M.G. Vander Heiden, L.C. Cantley and C.B. Thompson. Understanding the Warburg effect: the metabolic requirements of cell proliferation. *Science*, 324(5930):1029–1033, 2009.

[41] L.K. Boroughs and R.J. DeBerardinis. Metabolic pathways promoting cancer cell survival and growth. *Nat. Cell Biol.*, 17(4):351–359, 2015.

[42] R.D. Beger. A review of applications of metabolomics in cancer. *Metabolites*, 3(3):552, 2013.

[43] T. Kobayashi, S. Nishiumi, A. Ikeda, T. Yoshie, A. Sakai, A. Matsubara, Y. Izumi, H. Tsumura, M. Tsuda, H. Nishisaki, N. Hayashi, S. Kawano, Y. Fujiwara, H. Minami, T. Takenawa, T. Azuma and M. Yoshida. A novel serum metabolomics-based diagnostic approach to pancreatic cancer. *Cancer Epidemiol. Biomarkers Prev.*, 22(4):571–579, 2013.

[44] J.F. Xiao, R.S. Varghese, B. Zhou, M.R. Nezami Ranjbar, Y. Zhao, T.H. Tsai, C. Di Poto, J. Wang, D. Goerlitz, Y. Luo, A.K. Cheema, N. Sarhan, H. Soliman, M.G. Tadesse, D. Hazem Ziada and H.W. Ressom. LC–MS based serum metabolomics for identification of hepatocellular carcinoma biomarkers in egyptian cohort. *J. Proteome Res.*, 11(12):5914–5923, 2012.

[45] S.K. Yan, B.J. Wei, Z.Y. Lin, Y. Yang, Z.T. Zhou and W.D. Zhang. A metabonomic approach to the diagnosis of oral squamous cell carcinoma, oral lichen planus and oral leukoplakia. *Oral Oncol.*, 44(5):477–483, 2008.

[46] S. Ganti and R.H. Weiss. Urine metabolomics for kidney cancer detection and biomarker discovery. *Urol. Oncol.*, 29(5):551–557, 2011.

[47] A. Peralbo-Molina, M. Calderon-Santiago, F. Priego-Capote, B. Jurado-Gamez and M.D. Luque de Castro. Metabolomics analysis of exhaled breath condensate for discrimination between lung cancer patients and risk factor individuals. *J. Breath Res.*, 10(1), 2016.

[48] M. Muc-Wierzgoń, E. Nowakowska-Zajdel, S. Dziegielewska-Gesiak, T. Kokot, K. Klakla, E. Fatyga, E. Grochowska-Niedworok, D. Waniczek and J. Wierzgoń. Specific metabolic biomarkers as risk and prognostic factors in colorectal cancer. *World J. Gastroenterol.*, 20(29):9759–9774, 2014.

[49] O. Warburg, K. Posener and E. Negelein. Metabolism of carcinoma cells. *Biochem. Z.*, 152:309–344, 1924.

[50] O. Warburg. On the origin of cancer cells. *Science*, 123:309–314, 1956.

[51] R.A. Gatenby and R.J. Gillies. Why do cancers have high aerobic glycolysis? *Nat. Rev. Cancer*, 4(11):891–899, 2004.

[52] L.W.S. Finley, J. Zhang, J. Ye, P.S. Ward and C.B. Thompson. Snapshot: cancer metabolism pathways. *Cell Metab.*, 17(3):466–466, 2013.

[53] F. Pietrocola, L. Galluzzi, J.M. Bravo-San Pedro, F. Madeo and G. Kroemer. Acetyl coenzyme a: a central metabolite and second messenger. *Cell Metab.*, 21(6):805–821, 2015.

[54] U.E. Martinez-Outschoorn, M. Peiris-Pages, R.G. Pestell, F. Sotgia and M.P. Lisanti. Cancer metabolism: a therapeutic perspective. *Nat. Rev. Clin. Oncol.*, 2016.

[55] D.S. Wishart. Emerging applications of metabolomics in drug discovery and precision medicine. *Nat. Rev. Drug Discov.*, 2016.

[56] M.S.A. Palmnas and H.J. Vogel. The future of NMR metabolomics in cancer therapy: Towards personalizing treatment and developing targeted drugs? *Metabolites*, 3(2):373, 2013.

[57] S. Ravanbakhsh, P. Liu, T.C. Bjordahl, R. Mandal, J.R. Grant, M. Wilson, R. Eisner, I. Sinelnikov, X. Hu, C. Luchinat, R. Greiner and D.S. Wishart. Accurate, fully-automated NMR spectral profiling for metabolomics. *PLoS ONE*, 10(5), 2015.

[58] E.M. Weaver and A.B. Hummon. Imaging mass spectrometry: From tissue sections to cell cultures. *Adv. Drug Deliv. Rev.*, 65(8):1039–1055, 2013.

[59] D. Hanahan and R.A. Weinberg. Hallmarks of cancer: The next generation. *Cell*, 144(5):646–674, 2016.

[60] M. Nikfarjam, V. Muralidharan and C. Christophi. Mechanisms of focal heat destruction of liver tumors. *J. Surg. Res.*, 127(2):208–223, 2005.

[61] C. Streffer. Metabolic changes during and after hyperthermia. *Int. J. Hyperthermia*, 1(4):305–19, 1985.

[62] E.V. Inzhevatkin, A.A. Savchenko, A.B. Egorova, A.I. Al'brant and V.P. Nefedov. Metabolism in perfused rat lived at different terms

after short-term hyperthermia. *Bull. Exp. Biol. Med.*, 129(4):350–351, 2000.

[63] H. Wu, A.D. Southam, A. Hines and M.R. Viant. High-throughput tissue extraction protocol for NMR- and MS-based metabolomics. *Anal. Biochem.*, 372(2):204 – 212, 2008.

[64] M.R. Viant. Revealing the metabolome of animal tissues using 1H nuclear magnetic resonance spectroscopy. *Methods Mol. Biol.*, 358:229–246, 2007.

[65] M. Vinaixa, M.A. Rodriguez, A. Rull, R. Beltran, C. Blade, J. Brezmes, N. Canellas, J. Joven and X. Correig. Metabolomic assessment of the effect of dietary cholesterol in the progressive development of fatty liver disease. *J. Proteome Res.*, 9(5):2527–2538, 2010.

[66] Z. Miao, M. Jin, X. Liu, W. Guo, X. Jin, H. Liu and Y. Wang. The application of HPLC and microprobe NMR spectroscopy in the identification of metabolites in complex biological matrices. *Anal. Bioanal. Chem.*, 407(12):3405–3416, 2015.

[67] R. Amathieu, P. Nahon, M. Triba, N. Bouchemal, J.C. Trinchet, M. Beaugrand, G. Dhonneur and L.L. Moyec. Metabolomic approach by 1H NMR spectroscopy of serum for the assessment of chronic liver failure in patients with cirrhosis. *J. Proteome Res.*, 10(7):3239–3245, 2011.

[68] M.E. Bollard, N.R. Contel, T.M.D. Ebbels, L. Smith, O. Beckonert, G.H. Cantor, L. Lehman-McKeeman, E.C. Holmes, J.C. Lindon, J.K. Nicholson and H.C. Keun. NMR-based metabolic profiling identifies

biomarkers of liver regeneration following partial hepatectomy in the rat. *J. Proteome Res.*, 9(1):59–69, 2010.

[69] S. Ghosh, A. Sengupta, S.Sharma, and H.M. Sonawat. Metabolic fingerprints of serum, brain, and liver are distinct for mice with cerebral and noncerebral malaria: a (1)H NMR spectroscopy-based metabonomic study. *J. Proteome Res.*, 11(10):4992–5004, 2012.

[70] The Human metabolome database. http://www.hmdb.ca (last visit: 2016 may).

[71] Madison-Qingdao Metabolomics Consortium Database. http://mmcd.nmrfam.wisc.edu (last visit: may 2016).

[72] Biological Magnetic Resonance Data Bank. http://www.bmrb.wisc.edu (last visit: 2016 may).

[73] A.M. Di Bisceglie, H.C. Bodenheimer Jr., W. Ray Kim and S. L. Flamm. Serum activity of alanine aminotransferase (ALT) as an indicator of health and disease. *Hepatology*, 47(4):1363–1370, 2008.

[74] X.J. Huang, Y.K. Choi, H.S. Im, O. Yarimaga, E. Yoon, and H.S. Kim. Aspartate aminotransferase (AST/GOT) and alanine aminotransferase (ALT/GPT) detection techniques. *Sensors*, 6(7):756–782, 2006.

[75] G.M. Graeber, G.P. Clagett, R.E. Wolf, P.J. Cafferty, J.W. Harmon and N.M. Rich. Alterations in serum creatine kinase and lactate dehydrogenase: Association with abdominal aortic surgery, myocardial infarction and bowel necrosis. *Chest*, 97(3):521–527, 1990.

[76] J. Fazzari, H. Lin, C. Murphy, R. Ungard and G. Singh. Inhibitors of glutamate release from breast cancer cells; new targets for cancer-induced bone-pain. *Sci. Rep.*, 5:8380, 2015.

[77] K. Glunde, Z.M. Bhujwalla and S.M. Ronen. Choline metabolism in malignant transformation. *Nat. Rev. Cancer*, 11(12):835–848, 2011.

[78] M. Jain, R. Nilsson, S. Sharma, N. Madhusudhan, T. Kitami, A.L. Souza, R. Kafri, M.W. Kirschner, C.B. Clish and V.K. Mootha. Metabolite profiling identifies a key role for glycine in rapid cancer cell proliferation. *Science*, 336(6084):1040–1044, 2012.

[79] S. Bae, C.M. Ulrich, M.L. Neuhouser, O. Malysheva, L.B. Bailey, L. Xiao, E.C. Brown, K.L. Cushing-Haugen, Y. Zheng, T.Y.D. Cheng, J.W. Miller, R. Green, D.S. Lane, S.A.A. Beresford and M.A. Caudill. Plasma choline metabolites and colorectal cancer risk in the women's health initiative observational study. *Cancer Res.*, 74(24):7442–7452, 2014.

[80] *MARTINDALE: 'Martindale — the Extra Pharmacopoeia'.* A.G. Lipman, 1993.

[81] B. Worley and R. Powers. Mvapack: A complete data handling package for NMR metabolomics. *ACS Chem. Biol.*, 9(5):1138–1144, 2014.

[82] C. Kendall, M. Isabelle, F. Bazant-Hegemark, J. Hutchings, L. Orr, J. Babrah, R. Baker and N. Stone. Vibrational spectroscopy: a clinical tool for cancer diagnostics. *Analyst*, 134(6):1029–1045, 2009.

[83] Luca Quaroni and Theodora Zlateva. Infrared spectromicroscopy of biochemistry in functional single cells. *Analyst*, 136(16):3219–32, 2011.

[84] H.J. Butler, L. Ashton, B. Bird, G. Cinque, K. Curtis, J. Dorney, K. Esmonde-White, N.J. Fullwood, B. Gardner, P.L. Martin-Hirsch, M.J. Walsh, M.R. McAinsh, N. Stone and F.L. Martin. Using Raman spectroscopy to characterize biological materials. *Nat. Protocols*, 11(4):664–687, 2016.

[85] M.J. Baker, J. Trevisan, P. Bassan, R. Bhargava, H.J. Butler, K.M. Dorling, P.R. Fielden, S.W. Fogarty, N.J. Fullwood, K.A. Heys, C. Hughes, P. Lasch, P.L. Martin-Hirsch, B. Obinaju, G.D. Sockalingum, J. Sule-Suso, R.J. Strong, M.J. Walsh, B.R. Wood, P. Gardner and F.L. Martin. Using Fourier transform IR spectroscopy to analyze biological materials. *Nat. Protoc.*, 9(8):1771–1791, 2014.

[86] A.C. Sekhar Talari, Z. Movasaghi, S. Rehman and I. Rehman. Raman spectroscopy of biological tissues. *Appl. Spectrosc. Rev.*, 50(1):46–111, 2015.

[87] D.I. Ellis and R. Goodacre. Metabolic fingerprinting in disease diagnosis: biomedical applications of infrared and raman spectroscopy. *Analyst*, 131:875–885, 2006.

[88] O.J. Old, L.M. Fullwood, R. Scott, G.R. Lloyd, L.M. Almond, N.A. Shepherd, N. Stone, H. Barr and C. Kendall. Vibrational spectroscopy for cancer diagnostics. *Anal. Methods*, 6:3901–3917, 2014.

[89] C. Krafft, B. Dietzek and J. Popp. Raman and CARS microspectroscopy of cells and tissues. *Analyst*, 134:1046–1057, 2009.

[90] C. Krafft, G. Steiner, C. Beleites and R. Salzer. Disease recognition by infrared and Raman spectroscopy. *J. Biophotonics*, 2(1-2):13–28, 2009.

[91] K. Chen, C. Yuen, Y. Aniweh, P. Preiser and Q. Liu. Towards ultrasensitive malaria diagnosis using surface enhanced Raman spectroscopy. *Sci. Rep.*, 6:20177, 2016.

[92] K. Gajjar, L.D. Heppenstall, W. Pang, K.M. Ashton, J. Trevisan, I.I. Patel, V. Llabjani, H.F. Stringfellow, P.L. Martin-Hirsch, T. Dawson and F.L. Martin. Diagnostic segregation of human brain tumours using Fourier-transform infrared and/or Raman spectroscopy coupled with discriminant analysis. *Anal. Methods*, 5:89–102, 2012.

[93] J. Surmacki, J. Musial, R. Kordek and H. Abramczyk. Raman imaging at biological interfaces: applications in breast cancer diagnosis. *Mol. Cancer*, 12:48–48, 2013.

[94] S. Li, L. Li, Q. Zeng, Y. Zhang, Z. Guo, Z. Liu, M. Jin, C. Su, L. Lin, J. Xu and S. Liu. Characterization and noninvasive diagnosis of bladder cancer with serum surface enhanced Raman spectroscopy and genetic algorithms. *Sci. Rep.*, 5:9582, 2015.

[95] E.G. Ahmed, N.A. Al-Muslet, M.M. Ahmed, M.A. Moharam and W. Musaad. The use of Fourier infrared spectroscopy and laser - Raman spectroscopy in bladder malignancy diagnosis, a comparative study. *Appl. Phys. Res.*, 2(1):108–117, 2010.

[96] D. Lin, S. Feng, J. Pan, Y. Chen, J. Lin, G. Chen, S. Xie, H. Zeng and R. Chen. Colorectal cancer detection by gold nanoparticle based surface-enhanced Raman spectroscopy of blood serum and statistical analysis. *Opt. Express*, 19(14):13565–13577, 2011.

[97] L. Mavarani, D. Petersen, S.F. El-Mashtoly, A. Mosig, A. Tannapfel, C. Kotting and K. Gerwert. Spectral histopathology of colon cancer tissue sections by Raman imaging with 532 nm excitation provides label free annotation of lymphocytes, erythrocytes and proliferating nuclei of cancer cells. *Analyst*, 138(14):4035–4039, 2013.

[98] S. Li, G. Chen, Y. Zhang, Z. Guo, Z. Liu, J. Xu, X. Li and L. Lin. Identification and characterization of colorectal cancer using Raman spectroscopy and feature selection techniques. *Opt. Express*, 22(21):25895–25908, 2014.

[99] M.S. Bergholt, W. Zheng, K. Lin, K.Y. Ho, M. Teh, K.G. Yeoh, J.B. So and Z. Huang. In vivo diagnosis of esophageal cancer using image-guided Raman endoscopy and biomolecular modeling. *Technol. Cancer Res. Treat.*, 10(2):103–112, 2011.

[100] I.I. Patel, J. Trevisan, P.B. Singh, C.M. Nicholson, R.K. Gopala Krishnan, S.S. Matanhelia and F.L. Martin. Segregation of human prostate tissues classified high-risk (UK) versus low-risk (India) for adenocarcinoma using Fourier-transform infrared or Raman microspectroscopy coupled with discriminant analysis. *Anal. Bioanal. Chem.*, 401(3):969–982, 2011.

[101] A. Rae, R. Stosch, P. Klapetek, A.R. Hight Walker and D. Roy. State of the art Raman techniques for biological applications. *Methods*,

68(2):338–347, 2014.

[102] B.C. Smith and Editor. *Fundamentals of Fourier Transform Infrared Spectroscopy, 2nd Edition.* CRC Press, 2010.

[103] Saleh and Gupta. *Nanomaterial and polymer membranes: synthesis, characterization and applications.* Elsevier, 2016.

[104] E. Gazi, F. Lyng and P. Gardner. *Biomedical applications of synchrotron infrared microscopy: a practical approach.* RSC Publishing, 2011.

[105] E. Ly, O. Piot, R. Wolthuis, A. Durlach, P. Bernard and M. Manfait. Combination of FTIR spectral imaging and chemometrics for tumour detection from paraffin-embedded biopsies. *Analyst*, 133:197–205, 2008.

SERS for bioimaging and biosensing

Chapter 4

SERS for bioimaging and biosensing

4.1 Introduction

Nowadays, it is clear that the nanoparticles (NPs) and everything around them are trending topic. Just taking a look at the amount of publications of the last ten years is enough to get an approximate idea. However, we have to go centuries back to find the first application of the NPs. The Lycurgus Cup is one of the most famous examples of colloids and dates back to roughly around the 5th century B.C. However, the science behind colloids was not investigated until 1857, when Michael Faraday reported the first method of synthesising red solution of colloidal gold and investigate its optical properties [1].

Noble metals in medicine have been known and used since very ancient times. The Egyptians added gold to certain foods for spiritual, mental and bodily purification over 5,000 years ago. It is worth mentioning the use of gold colloid for the syphilis since the Middle Ages until the 20th

century [1]. Today, the gold NPs (AuNPs) have become an important biomedical resource. Among all the interesting properties of AuNPs, we will stand out those three that makes AuNPs one of the best choices for biomedical applications:

(i) *The ease of modifying the surface of the AuNPs.*

(ii) *The ability to be used as biosensor.* AuNPs show surface plasmon resonance bands in the visible region that make them easy to characterise. The special optical and electronic features make them appropriate to be used as biosensors.

(iii) *Their biocompatibility.* It has been proven that AuNPs are biocompatible and non-toxic.

AuNPs present special characteristics that make them very useful in the field of spectroscopy. In fact, the gold and silver NPs (AgNPs) are the most used substrates for surface-enhance Raman spectroscopy (SERS). The colloidal NPs prepared by wet chemistry are simple to prepare, to scale-up the synthesis and to characterize. Moreover, it is easy to achieve a high morphological uniformity while providing flexibility to tune different shapes, sizes, dispersion in different solvents and great possibilities in surface chemistry and besides, are inexpensive.

4.1.1 Surface-enhanced Raman spectroscopy (SERS)

SERS is a technique that enhances Raman scattering of molecules adsorbed onto a metal surface that has a nanoscale roughness. Typically observed enhancement factors are on the order of $10^4 - 10^6$ but can be as high as $10^7 - 10^{12}$ for some systems, allowing even single molecule detection [2–6].

The field of SERS is lately undergoing a large development. The high amount of publications in art and archaeology [7], forensic sciences [8], analytical, life science and biophysical applications [9], among others, reflects the multidisciplinary nature of SERS. Since its discovery (in 1974 by Fleischman [10]), many theories have been proposed regarding the SERS mechanism, but only two are still in use today: the electromagnetic (EM) effect and chemical effect. On the one hand, the EM enhancement theory is based on the interaction of the transitional moment of an adsorbed analyte with the electric field of surface plasmons induced by the incoming light on the nanoscale metal. On the other hand, the chemical transfer theory describes the analyte as being chemically bonded to the surface of the nanoscale metal, and the excitation occurs through charge-transfer resonance from the metal to the analyte and back to the metal again. Though, it is widely accepted that both theories describe the overall SERS effect, the dominant process is thought to be the EM enhancement [9].

EM interaction of light with NPs can generate collective electron charge oscillations, so called *localized surface plasmon resonances* (LSPRs). Plasmonic resonance in NPs such as gold and silver occurs at visible-near infrared region, corresponding to typical electronic excitations in matter. Thus, the coupling between the LSPRs of the nanostructures and the EM fields emitted by molecules located in close proximity to the NP surface leads to the modification of the molecular radiative properties [11], such as the enhancement of the Raman scattering (see Figure 4.1). The SERS intensity depends on the excitation wavelength and the strength of the plasmons propagating on the surface of the NP. Hence, it is important the science and the engineering that involves the design of NPs to maximize the surface plasmon resonance [11,12]. Several wet chemistry methods have
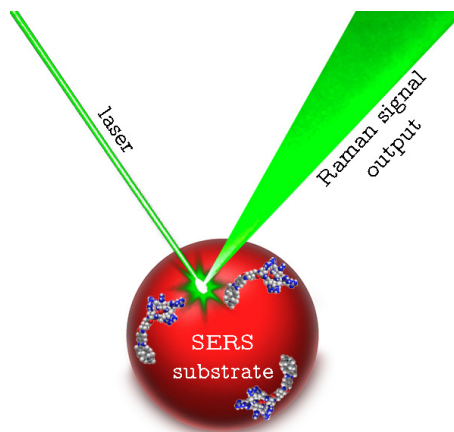
Figure 4.1: SERS effect using a labelled nanoparticle.

been developed for the synthesis of colloidal metal nanoparticles, such as chemical reduction, laser ablation and photoreduction. The complexity of plasmon resonances regarding to shape, size and interactions is enough to justify the entire field of plasmonics, a burgeoning branch of photonics [9].

The SERS active substrates must be considerably smaller than the wavelength of the exciting radiation, usually in the 10-80 nm range. In fact, when the NP size is too large, the intensity of the plasmonic resonance decrease due to the lost of energy happened through the surface scattering of the conduction electrons. However, when the size is too small, the NPs are barely able to support the plasmon resonances giving rise to low SERS enhancements. In the size range of interest, the isolated spherical AgNPs in dispersion showed a plasmon resonances in the spectral range of $\sim 380 - 420$ nm while the AuNPs showed at $\sim 515 - 550$ nm. It is worth mentioning that the AgNPs can provide larger SERS enhancements than AuNPs. However, the red-shift induced by object interaction and/or shape-and-size effects can push the resonance of AuNP beyond 600 nm. In this

way the AuNPs become one of the best choices for biological, biomedical and forensic application, since many of these applications with SERS are based on NIR lasers. It is therefore not surprising the choice of Au for these type of applications, especially if we also take into account the higher performance of AuNPs in terms of stability against oxidation, a greater reproducibility in the preparation and a much lower toxicity. Regarding the last property, in the case of AgNPs is well known the antimicrobial application [13] due to its higher toxicity. In fact, it is important to use a proper coating agent to avoid the oxidation and the resulting release of silver ions that cause the rise on the toxicity [14].

The LSPR frequencies depend on the size, the geometry (shape), the composition, as well as the dielectric environment around the NPs, the inter-particle distances and the polarization of the incident light [15]. All those features play an important role in the success of SERS sensing.

Regarding the shape, it can affect in a factor of 10^2 in the EM enhancement ability. Comparing NPs of similar edge length, the LSPR position may significantly differ affected by different geometries. There are many SERS-active nanostructures reported in the literature (cubes, rings, nanoshells, nanoflowers, etc.), it is interesting to highlight the gold nanostars structures [16]. The Au nanostar example is interesting since we can generate additional high local EM enhancements in the tips, obtaining high SERS enhancements. Therefore, tuning the anisotropic shape we can improve in the control of the increment of LSPR [17].

In the case of the stability, NPs require a stabilising ligand on their surface to remain dispersed in solution and to avoid the aggregation. For instance, the most common citrate reduction method for AuNPs generates a cover layer of negatively charged citrate ligands on the surface of each

NP. In this way, the aggregation of NPs is electrostatically prevented. The colloidal suspension is a metastable system. Its stability is determined by the long-range Van der Waals interactions, the short-range electrostatic repulsions, the steric effects and hydrodynamic forces [12].

Even though NPs already show strong SERS enhancement, if we want to obtain stronger SERS signals, it is necessary the interaction of NPs among them to generate the plasmon coupling. Successful researches in the last decades have allowed an increase on the controlled assembly strategies for colloidal NPs [18]. In fact, the plasmon coupling between adjacent NPs, occurring for pairs (dimers), larger clusters, or even aggregate films of NPs can give rise to 10^3-10^4 times the SERS enhancement observed on an isolated NP. The interjunction regions created when we aggregate the NPs are so called *hot spots* [19].

The easiest strategy to induce NP aggregation is based on the addition of electrolytes such as NaCl and KBr that causes a modification of the NP surface chemistry via strong halide–metal interactions. In this way, we decrease Coulombic repulsions that ensure the NP stability. Another strategy is to introduce charged molecules or polymers to build electrostatic bridges between the NPs. For instance, in the case of citrate-coated AgNPs (negatively charged surface), we can add an aqueous solution of spermine hydrochloride (the spermine allows us to build positively charged bridges).

Regardless of the mentioned strategies to increase SERS phenomenon, the aggregation occurs randomly and in an uncontrolled way. In order to control the assembly issues we have two main options. The first one is the control of the aggregation kinetics and the second one is the use of self-assembly molecular NP crosslinkers. Up to now, the second choice has

turned out to be the most efficient option. Molecular linkers are classified into two categories [12]:

(i) *Bifunctional molecules = Non-biological linkers.* These type of linkers contain functional groups to bind to the NP surface using covalent bounds or electrostatic interations. Functional groups such as dithiol- or diamine- usually are placed at opposite ends of the molecular structure. A good example is the ultrasensitive detection of polycyclic aromatic hydrocarbons (PAH) by means of SERS using molecular linkers that act as hosts for PAHs. Linkers such as pyrene and calixarene generate dimers that concentrate the PAHs in the hot spots allowing the detection of 10^{-7}-10^{-8} M of non-SERS-active PAHs [20].

(ii) *Molecules with selective recognition ability = Biological linkers.* Biomolecules, such as antibodies and antigens, proteins and DNA, have been employed to promote the assembly of NPs in response to external stimuli such as the presence of target analyte, changes in pH or UV irradiation. Actually, the DNA fits perfectly for this type of applications due to its capacity for molecular recognition, structural plasticity and post-assembly reconfiguration of the nanostructure under a molecular stimuli. In this area, Graham and co-workers [21] were pioneers in the study of reversible aggregation of oligonucleotide-functionalized NPs containing a Raman reporter by ssDNA hybridization to manipulate SERS signals. For instance, this strategy allowed to spread the use of SERS to ultra-sensitive DNA detections and to study mutations in DNA sequences.

If we go back to the easiest example of plasmon coupling, i.e. the dimer, it is important to emphasize the effect that the polarization direction

(taking into account the dimer axis) of the incident light has on the SERS enhancement as well as the effect of the wavelength of the incident laser and the orientation of SERS active molecules. Different excitation lines could be used depending on the NP. The choice of the laser wavelength is a critical step in the characterisation of NPs and therefore, to optimise the protocol to real applications. Among all the possible applications, we are interested in biomedical applications and more specifically, in bioimaging an biosensing applications.

4.1.2 Biomedical Applications

The nanotechnology applications suits to biomedicine. Diagnostic techniques (sensors), drugs delivery vehicles, therapies and tissue engineering (prostheses and implants) are the most remarkable successes or research lines [22–24]. Within all the biomedical applications that we can find for the AuNPs and AgNPs, we are going to focus on the role that they can play as bioimaging agents and biosensors. Bioimaging is used to develop body images, tissues and anatomical area down to the molecular level. Thereby, plasmonic nanoprobes can be used for disease diagnosis and also for physiology and anatomy studies [25, 26].

The bioimaging nowadays is still a hot topic in the scientific community. This is due to the continuous development, improvement and implementation of new technological advances as well as to high throughput bioinformatic tools. Among all the interesting branches of bioimaging, probing live cells is an important field in cell biology to detect intracellular biomolecules or to investigate cellular processes by means of optical techniques [27–31]. Spectroscopic methods can be used to collect directly information from cellular signatures such as lipids,

nucleotides and proteins. Furthermore, these spectroscopic techniques can also be used combined with NPs as labels used intracellularly to collect biological information indirectly so as to work as probes for bioimaging and biosensing.

Fluorescent imaging is the most widely used technique for bioimaging. The specific fluorophores such as fluorescent proteins, probes and dyes enable the study of gene expression, protein interactions and many cellular processes. However, as the old saying goes, *not all that glitters is gold*, undesirable effects such as photobleaching are observed with many fluorophores. This irreversible photodegradation affects seriously to the sensitivity of fluorescence detection. Besides, we can find autofluorescence and other background effects that can hinder the measurements. Depending on the research objective, sometimes different fluorophores are needed, which require different binding chemistries and different environmental conditions. However, the multiplex imaging, the possibility to measure multiple fluorophores, is limited since the spectral bands are very broad and overlapping can occur.

By contrast, SERS active functionalised NPs (nanotags) cannot be photobleached and it allows the use of higher laser powers and longer data acquisition times to reach sensitive measurements. Furthermore, they can be easily resolved from the background thanks to its Raman *fingerprint*. Lately Raman spectroscopy is achieving a wider acceptance in biomedical researches since it is a non-destructive, non-invasive method, which requires minimal sample preparation and it can even offer label-free analyses. The narrow spectral peaks, the possibility to combine a large number of labels to enable multiplexed assays, the minimal interference from aqueous media and the possibility to be excited in the near-IR

make SERS an ideal bioanalytical technique for the analysis of complex biochemical environments.

Live-cell studies based on Raman and SERS provide information about native chemical compositions and dynamic processes of cellular constituents *in vivo* [15, 30]. In fact, part of the interest of the research community is focused on the development of *in vivo* and in real time imaging systems in order to study dynamic processes like cell migration and also morphological and physiological changes on cells, organs or even in living specimens. SERS reported molecules have already been proved to be useful for multiplexed imaging [32] and it has also been used for *in vivo* tumor targeting [33]. Both studies were developed using living mice.

4.2 Aims of this work

All this introduction is aimed to provide the context for the work that I carried out in the Centre for Molecular Nanometrology under the supervision of Professor Duncan Graham at the University of Strathclyde (Glasgow, Scotland). Taking into account the use of Raman and SERS imaging in live-cell studies we tackled the use of Osmium (II) polypyridyl polyarginine conjugate and its Ruthenium (II) analogue combined with SERS active NPs to use them as live-cell imaging probes.

Before I start explaining the work I did, it is interesting revisit the work carried out until that moment with these compounds in the same field.

Osmium (II) polypyridyl polyarginine conjugate $[\mathbf{Os(bpy)_2(pic-arg_8)}]^{10+}$ and its Ruthenium (II) analogue were synthesised and are being studied by Tia E. Keyes and her research group from the National Centre for Sensor Reseach (Dublin, Ireland). In fact, they submitted these compounds to the Professor Graham's

laboratory to evaluate the suitability for SERS bioimaging in live-cells studies. As a result of a previous study developed by the group of Prof. Keyes, we can mention the work published in Dalton Transactions where they explain thoroughly the observations done using those compounds as probes for cell imaging [34]. Actually, it was the first time that the capacity of this Os compound was examined with this purpose. In the mentioned study, photophysics, cell uptake and cytotoxicity of this Os-complex were performed and compared with its Ru analogue. The Os complex exhibits emission maxima at 726 nm, in the near-IR region, whereas the Ru complex at 610 nm. These wavelengths match with the biological optical window, being suitable for bioimaging since we can study simultaneously the biological composition of the cells or tissues, and the Os complex and its analogue. The Os compound shows a shorter luminiscent lifetime ($\sim$33 ns) comparing to the Ru compound (between 478 ns and 775 ns). Besides, its stability is higher regardless the dissolve oxygen concentration in solution and it shows a weak temperature dependency. In fact, no photobleaching was observed for the Os complex. In both cases the cell uptake and distribution were similar. Only slight differences were pointed out for the nuclear uptake since it was observed that the uptake is photo or thermally activated. They both showed a rapid transmembrane transport throughout the cytoplasm and organelles, and both exhibited low citotoxicity at levels lower than 100 µM.

4.3   Materials and Methods

4.3.1   Nanoparticle preparation

Based on the previous experience of the group [35] with Ag and Au nanoparticles, two well-known preparation methodologies were selected for this work. All reagents needed for the preparation of nanoparticles used within this chapter, including silver nitrate and sodium tetrachloroaurate (high purity), were obtained from Sigma Aldrich, UK.

Silver nanoparticles

The most common SERS active AgNPs are prepared through Ag^+ reduction by citrate [36] or hydroxylamine [37]. In fact, among these two colloidal systems, the AgNPs prepared with hydroxylamine exhibit a higher enhancement factor, a larger surface available for the adsorption of molecules and lack of interference peaks in the spectra [38]. Therefore, we used the hydroxylamine approach described by Leopold and Lendl in 2003 [37]. The preparation consist of four steps:

(i) Clean the labware including an Erlenmeyer flask. This step is very important in the colloid preparation. We soaked the glassware in aqua regia for at least 4 h. Then, we rinsed the glassware with distilled water and collected that water into a beaker neutralising it with sodium carbonate before disposal of chemical waste. Finally, we washed the material down sink with excess distilled water.

(ii) Place 90 mL of distilled water (dH$_2$O) and put it into a conical flask (250 mL). Then add 0.0119 g of NaOH (3.33×10^{-3} M) and 0.0104 g of hydroxylamine hydrochloride (1.67×10^{-3} M) into the above flask while stirring.

(iii) Separately, dissolve $0.0169\,$g of silver nitrate in $10\,$mL of dH$_2$O ($10^{-2}\,$M) and add it dropwise into above flask while stirring.

(iv) Continue stirring for another $15\,$min.

Following the mentioned steps we can obtain colloids with a λ_{max} of $408\,$nm and an average spherical particle diameter between 23 and $67\,$nm (see Figure 4.2).
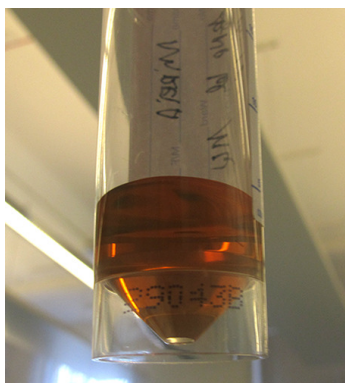

Figure 4.2: AgNP prepared using hydroxylamine.

Gold nanoparticles

The preparation method for citrate-capped gold colloid is also based on methods refereed in the literature [36, 39, 40]. We obtained gold colloid of a diameter around $20\,$nm and λ_{max} of $520\,$nm (see Figure 4.3).The preparation of citrate reduced gold is described in the following steps:

(i) Clean the glassware including a $1\,$L 3 necked round bottom flask and a glass link stirrer with aqua regia as described above.

(ii) Add 500 mL of dH$_2$O to the round bottomed flask with 50 mg of sodium tetrachloroaurate (NaAuCl$_4$) and heat using a Bunsen burner until boiling. Stir continuously.

(iii) Then, add in once to the previous mixture 7.5 mL of sodium citrate (0.075 g in dH$_2$O).

(iv) Boil for 15 min.

(v) Finally, allow to cool stirring for 25 min.
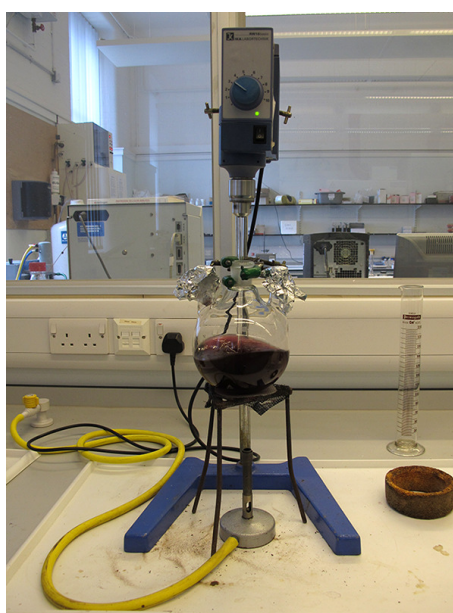

Figure 4.3: Preparation of citrate reduced gold colloid.

4.3.2 Characterisation of NPs

The obtained colloids were studied using classical characterisation methodologies such as UV-Vis spectroscopy, zetasizer (size and zeta

potential) and SERS. We did not find the need to observed them by SEM or TEM since we followed established methodologies and we wanted to reassure whether the colloids were suited for SERS measurements. Three replicate measurements were performed for each analysis.

UV-Vis spectroscopy

AgNPs and AuNPs are both visually and spectroscopically detectable at lower concentration and colorimetric changes are related to particle size, composition, extinction efficiency, concentration and aggregation. The listed properties are directly related to the SERS capacity. However, the plasmon resonance condition also depends on the distance- and wavelength-dependent dielectric function of the NP and its medium. Actually, we used UV-Vis spectroscopy to quantify the light that was absorbed and scattered by our colloids. For the case of spherical particles, it is possible to calculate the contribution of each effect using the *Mie theory* [41]. This is the analytical solution of Maxwell's equations for the scattering of light by spherical particles.

Scattering of a sample is very sensitive to the aggregation state of the colloid, and its contribution increases as the particles aggregate. UV-Vis spectroscopy is useful for monitoring the stability of colloids since the original extinction peak decreases in intensity due to the reduction of stable NPs. The formation of aggregates will broaden the peak or a secondary peak will form at longer wavelengths.

The UV-Vis spectroscopy was used to estimate the concentration of the NPs using the Beer-Lambert law (see Equation 4.1). Beer's Law states that molar absorptivities are constant for each wavelength, those commonly called molar extinction coefficients. The extinction is the loss of transmitted

light due to absorption and scattering of the colloid. In the literature, generalized table of extinction coefficient data can be found for AgNPs and AuNPs from a range of NP sizes [42, 43].

$$A = \varepsilon.l.C \qquad (4.1)$$

UV-Vis absorption spectra were recorded on a Varian Cary 300 Bio UV-Vis spectrophotometer using 1 cm path length cell, 400 µL of sample volume, measured at room temperature and obtaining the spectra within 200 nm and 800 nm wavelengths. A distilled water blank was run prior to any sample analysis to establish a baseline. The NPs that we needed were those that present narrow peaks at 410 nm for AgNPs and at 520 nm for AuNPs. All the measurements were done using the same spectrometer and quartz cuvette or cell. The cuvette was always cleaned with a big amount of water first, and then, we cleaned with Hellmanex detergent (Hellma Analytics).

Zetasizer

The Malvern Nano ZS instrument (Worcestershire, England), known as zetasizer, was used in order to ensure NPs stability and determine their size. The Malvern Nano ZS instrument allows to observe a particle diameter from 0.3 nm to 10 µm using the Dynamic Light Scattering (DLS) measurement principle and the patented NIBS (Non-Invasive Back Scatter) technology. The light source employed for these measurements was a He-Ne laser (633 nm and 4 mW). This technique measures the diffusion of particles moving under Brownian motion, and converts this into size distribution using the Stokes-Einstein equation. In order to ensure the precision and repeatability we used NIST traceable latex standards (20 nm and 40 nm silica bits, nanospheres) before each measurement. The measurements were

performed using a sample volume of 800 µL. Together with the size, we also measured the Polidispersity index (PDI).

The Malvern Nano ZS instrument allowed us also to measure the zeta (ζ) potential using patented M3-PALS (Phase analysis Light Scattering) technology. Laser Doppler Micro-electrophoresis was used to measure zeta potential. An electric field was applied to our colloids, which then moved with a velocity related to their zeta potential. The measured velocity enabled the calculation of electrophoretic mobility, and from this we obtained the zeta potential distribution. The accuracy was ensured using a NIST reference material for aqueous systems ($-42\,\text{mV} \pm 2\,\text{mV}$). The measurements used to be programmed with a Standard Operating Procedure (SOP) to carry out the size and zeta potential measurements.

4.3.3 Nanoparticle functionalisation: SERS and the stability study

The Osmium(II) and Ruthenium (II) (bis-2,2-bipyridyl)-2(4-carboxylphenyl) imidazol [4,5f][1,10] phenanthroline were prepared and conjugated to octaarginine, a cell penetrating peptide, by the research group of Tia Keyes [34, 44–46]. The obtained two compounds showed in the Figure 4.4 had been used as fluorescent bioimaging agents before but we wanted to study their bioimaging ability as SERS nanotags.

The study of the stability of SERS nanotags was essential to understand the results that we obtained. A simple approach to SERS labelling is based on self-assembled of Raman labels adsorbed onto the surface of NPs. In the functionalisation process, two types of interactions are described due to the nature of the labels [47, 48]:
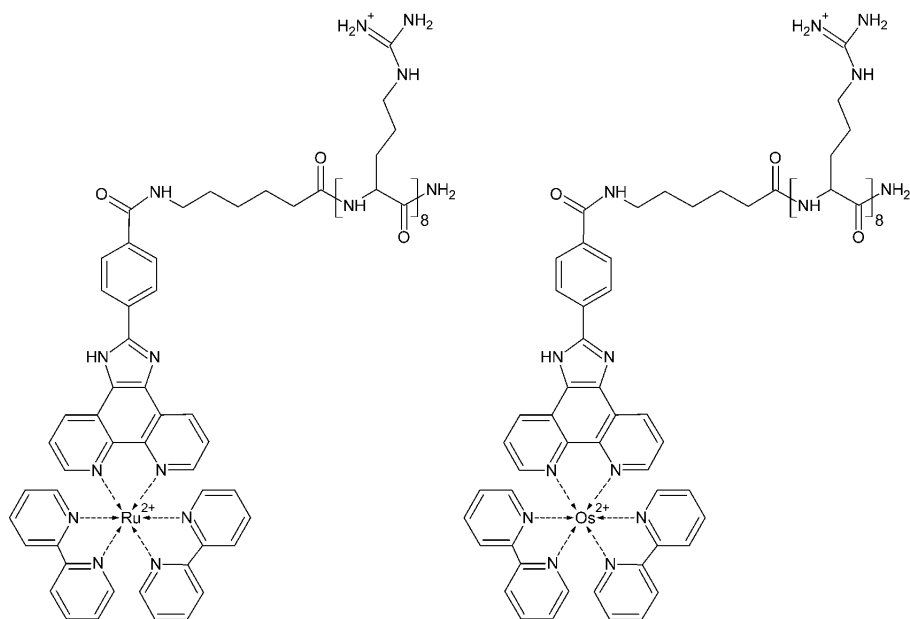
Figure 4.4: Structure of $[\text{Ru}(\text{bpy})_2(\text{pic}-\text{arg}_8)]^{10+}$ and $[\text{Os}(\text{bpy})_2(\text{pic}-\text{arg}_8)]^{10+}$.

Physical assembly involves weak physical forces such as electrostatic interactions between the Raman label and the NP surface. This type of labels is commonly used as SERS label since it exhibits strong SERS signals.

Chemical assembly involves the formation of a stable chemical bond between the Raman label and the NP surface. Even if this type of labels generates strong SERS signals, they are not as strong as those that are present in the physical assembly.

Assessment of the stability of these nanotags in cell culture media and culture conditions was carried out over 48 h. In addition to the stability study in culture media, the functionalised colloids kept at room

temperature were also measured in parallel. Once the stability study was concluded, the results were tested *in-vitro* (this experimental subsection is described below). Based on the literature, the stability study in culture media was developed following these steps [47]:

(i) Centrifuge the NPs using 3000 rpm for 20 min to ensure the homogeneity of the colloid, using only the supernatant.

(ii) Functionalise the NPs mixing 1000 μL of colloid and 30 μL of organometallic complex (both from 4.7×10^{-4} M solutions) for 30 min.

(iii) Add the functionalised NPs into 5 mL of culture media and mix them.

(iv) Keep the mixture in the incubator at culture conditions (in an incubator at 37 °C and 5% CO_2) until use.

(v) 1000 μL of the mixture was pipetted at 0, 1, 2, 4, 24 and 48 hours and collected in Eppendorf vials.

(vi) Centrifuge immediately at 8000 rpm for 5 min and discard the supernatant solution, obtaining the precipitated phase (pellet).

(vii) Re-suspend the pellet in 100 μL of culture media in order to preconcentrate and measure into a well of a microplate (96-Well Black Microplates, F-bottom, fluorotrac 600 from Greiner Bio-One, Germany). It is important to ensure that the microplate does not give interferences.

(viii) Measure the mixture using a Raman microscope as explained below. The measurement conditions were chosen taking into account the nature of the colloid.

Ag colloid mixtures were measured on a WITec confocal Raman microscope alpha300 R (WITec GmbH, Ulm Germany) fitted with a piezo-driven XYZ scan stage (see Figure 4.5). All samples were measured using a 532 nm diode laser, with a 600 g/mm grating and coupled to a Peltier cooled charge-coupled device (CCD) detector. A 100 x objective (Olympus MPlan, NA = 0.9) was employed. The parameters were; an integration time of 5 s and 5 accumulations.

Au colloid mixtures were measured in the same conditions described above but using a 632.89 nm excitation laser and a 600 g/mm grating.
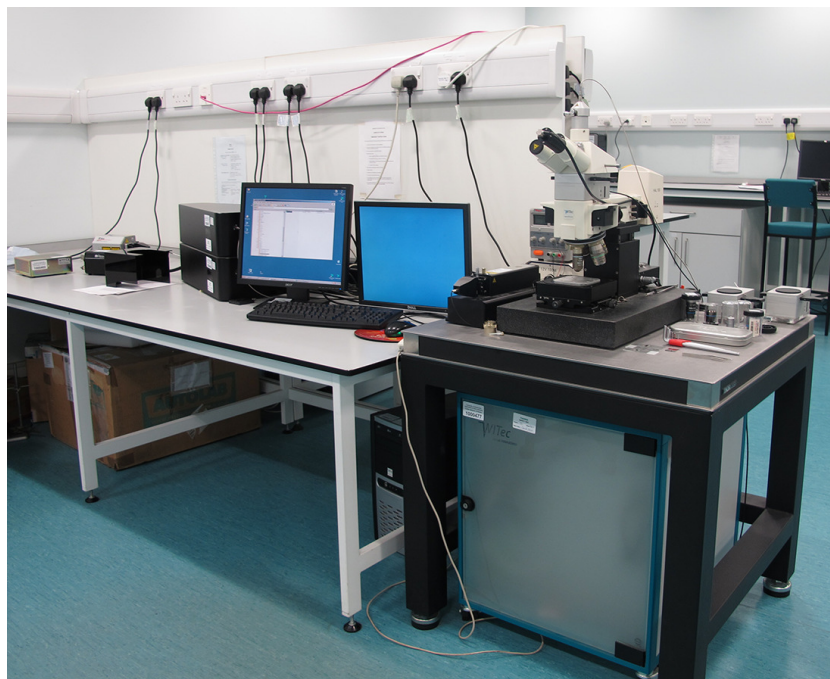

Figure 4.5: WITec confocal Raman microscope alpha300 R.

4.3.4 Cell culture

Cell line

Chinese Hamster Ovary (CHO) cells are a laboratory-cultured cell line derived from cells of the ovaries of Chinese hamsters. There are two main reasons to choose this cell line for this work. On the one hand, this mammalian cell line is commonly used in biological, medical and pharmaceutical research due to the small size of Chinese hamsters and low chromosome number. On the other hand, it is well-known the resistance of these cells.

Culture medium

CHO cells were grown in Ham's F12 nutrient media (Gibco) supplemented with fetal bovine serum (10 %), penicillin (1 % v/v, 10,000 I.U./mL) and streptomycin ($10 \, \mathrm{mg \, mL^{-1}}$). The culture medium was stored at $4 \, °\mathrm{C}$.

Growing cells from frozen samples

CHO cells were stored in liquid nitrogen until use. The vials were unfrozen by agitation in a $37 \, °\mathrm{C}$ water bath and removed immediately upon thawing. The cells were transferred from the vials to the T25 flask containing previously warmed growth media (in an incubator at $37 \, °\mathrm{C}$ and 5% CO_2 for $1 \, \mathrm{h}$) and grown in the incubator.

Subculturing

Cell cultures have to be passaged before they reach confluence. Below, we detailed the steps that we followed for each passage.

(i) Pre-warm all reagents in the incubator at 37 °C; the culture media, the phosphate-buffered saline (PBS) and the trypsin (frozen in the freezer until use).

(ii) Clean the biological safety cabinet with Virkon cleaner first, and then with 70 % ethanol.

(iii) Spray reagent bottles down with ethanol before introduce them inside the hood. Proceed in the same way with all the material necessary for the passage, such as flasks, falcon tubes, test tubes and pipettes.

(iv) Observe the cells flask under the microscope and evaluate if the culture is confluent, that is, if they cover almost all the base (to ensure that the cells are actively dividing). In the case that the culture is confluent, proceed to the passage.

(v) Shake softly the culture flask inside the hood to release from death cells.

(vi) Decant medium from T25 culture flask and wash the cell layer with 3 ml (5 mL for a T75 culture flask) of PBS. Decant PBS.

(vii) Add 1 mL of trypsin and keep it in the incubator for 2 min approximately.

(viii) During this period prepare two T25 flasks (5 mL) and one of T75 (10 mL) with culture media and keep them inside the incubator until the passage.

(ix) Swirl briefly the flask with trypsin to ensure that all cells have been detached. Check it under the microscope.

(x) Add 1 mL of culture media to neutralize the trypsin.

(xi) Count the cells using a hemacytometer. Determine the cell viability using trypan blue exclusion method (1:1 mixture of 0.1 % trypan blue and 100 µL cell sample). This staining method uses a diazo dye that selectively penetrates cell membranes of dead cells, colouring them in blue whereas live cells are excluded from staining. Use the Equation 4.2 to calculate the number of viable cells.

$$Viable\ cells/mL = \frac{total\ cell\ counted}{No.\ of\ squares} \times dilution\ factor \times 10^4 \quad (4.2)$$

(xii) Taking into account the average concentration of cells (if the estimation is around 1×10^6 cells/mL), add 500 µL to T25 flasks of the cell suspension and 1000 µL to the T75 flask.

(xiii) Use standard conditions for incubation: 37 °C and 5 % CO_2 in an incubator.

(xiv) Check daily the cultures to ensure their viability and the confluence to proceed to the passage every time that is necessary.

4.3.5   Cell uptake experiment

Before starting with the real experiments we tested all the process using 4-mercaptobenzoic acid (4-MBA). After some experiments, we established the most adequate culture protocol for the uptake and live-cell SERS imaging. The cell uptake experiments were performed with CHO cells from passage 8 to 18 and these are the steps that we followed:

(i) One day before add 3 mL of culture media to the μ-Dish and insert it into a Petri-dish to ensure the cleanliness in the incubator.

(ii) Take 5×10^5 cell/mL and put in a μ-Dish 35 mm high Glass Bottom (Ibidi, Martinsried, Germany) with 3 mL of culture media.

(iii) Add the functionalised NPs in the μ-Dish and mixed it softly. In this way we had $1000\,\mu$L of AuNP, $60\,\mu$L of organometallic complex $(1.2 \times 10^{-6}\,\mathrm{M})$ and $3\,\mathrm{mL}$ of culture media. Keep the μ-Dish inside the Petri-dish in the incubator.

(iv) Clean with PBS 4 times to ensure removal of the NPs located in the surface of cells (previously tested in the research group).

(v) Add $3\,\mathrm{mL}$ of PBS and it is ready to SERS imaging.

4.3.6 Live-cell SERS bioimaging and biosensing

The choice of the instrument for this experimental step was based on the features offered by each instrument for cell imaging. We used a Renishaw InVia Raman microscope for non-invasive *in-vitro* imaging since the microscope offered the possibility to use a bottom light source to observe the cells (see Figure 4.6).

Figure 4.6: Renishaw inVia Raman microscope.

SERS mapping was performed using Renishaw inVia Raman spectrometers equipped with a 633 nm laser and an Olympus 60 x (NA = 1) water immersion objective. A grating of 1800 lines/mm was used with a RenCam CCD. The Renishaw spectrometer grating was centred to acquire the spectra between 1245.4 cm^{-1} and 1609.2 cm^{-1} and 10 s of acquisition was used. Line mapping was performed using the StreamLine Raman mapping system (Renishaw plc, UK). SERS maps were coloured by integrating the area under the characteristic peak between 1472 cm^{-1} and 1492 cm^{-1} taking into account the baseline. The confocal configuration allows to acquire 3D images. The main objective of this type of volume imaging was to ensure the uptake of the labelled NPs. The mapped volume was configured to acquire spectra with a step size of 1 µm in the z direction. The zeta range was defined in ± 1 µm, and the selected depth (2 µm) matched more or less with the thickness of a common CHO cell.

4.4 Results and Discussion

4.4.1 Characterisation of the colloids

In Table 4.1 we have summarized the results of a number of characterisation methods, including UV-Vis spectroscopy, nanosizer (size and ζ potential) and SERS measurements.

In the case of hydroxylamine reduced SERS active AgNPs, dynamic light scattering (DLS) measurements revealed an average particle diameter of $\sim$49 nm and the UV-Vis absorption spectrum showed an intense absorption peak at 408 nm (see Figure 4.7). Together with the size, it is important to check and to obtain polydispersity index (PDI) values lower than 0.7 to ensure that we do not have a polydisperse system [49].

According to the size and the λ_{max} obtained, the adequate extinction coefficient was found in the literature [42] to estimate the concentration of colloid based on the absorption of the UV measurements that is originated from the surface plasmons' absorption of the AgNPs. The colloid concentration was determined to be 0.194 nM according to Beer's Law using an extinction coefficient of $2.87 \times 10^{10}\,\mathrm{M^{-1}\,cm^{-1}}$.

Regarding the zeta (ζ) potential and according to Saade et al. [50], the colloid stability was confirmed with values lower than $-30\,\mathrm{mV}$ ($\zeta \leq -30\,\mathrm{mV}$).
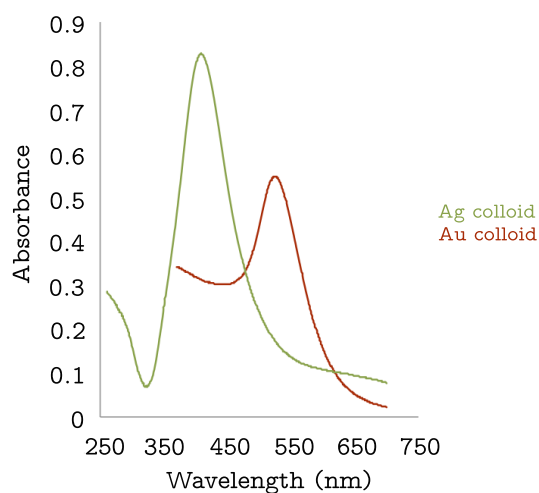

Figure 4.7: UV-Vis spectra of silver and gold colloids (diluted).

Table 4.1: Characterisation data of colloids used in experimentation.

NP	Size (nm)	PDI (nm)	ζ Potential (mV)	λ_{max} (nm)	C (nM)
Ag	49.1 ± 0.2	0.29	-35 ± 1	408	0.194
Au	20.0 ± 0.2	0.38	-39 ± 1	520	1.277

In the case of citrate reduced SERS active AuNPs, DLS measurements revealed an average particle diameter of ∼20 nm with a PDI value of 0.38, a ζ potential of -39 mV and the UV-Vis absorption spectrum showed an intense absorption peak at 520 nm (see Figure 4.7). The colloid concentration was estimated to be 1.277 nM using an extinction coefficient of $8.78 \times 10^8 \, \mathrm{M}^{-1} \, \mathrm{cm}^{-1}$ [42,43].

4.4.2 Nanoparticle functionalisation: SERS and the stability study

The stability study of the functionalised NPs was carried out over 48 h in cell culture media and in the functionalised colloid itself, in culture conditions and at room temperature, respectively. The stability of both Ru and Os complexes, as labels, were studied with silver and gold colloids.

In the first case of study, AgNPs functionalised with Ru complex, both in media and in the functionalised mixture, showed an unstable behaviour. A clear change in SERS signal was observed in the Figures 4.8 and 4.9. Even visually was noticeable since the colloid colour changed to greyish. Undoubtedly, the analyte itself is acting as an aggregating agent. The Raman signal obtained from the functionalised mixture diminished rapidly when the chemically labelled colloids were added to the culture media. The main signals obtained with this functionalised mixture were 441.8, 528.5, 802.1, 917.3, 1175.4, 1295.8, 1370.1 and 1618.3 cm^{-1}.

In the second case of study, AgNPs functionalised with Os complex, we noticed a different behaviour comparing to the Ru analogue. In this case, the functionalised mixture was stable at room temperature as we can see in Figure 4.10. In contrast, in culture media and in culture conditions it was
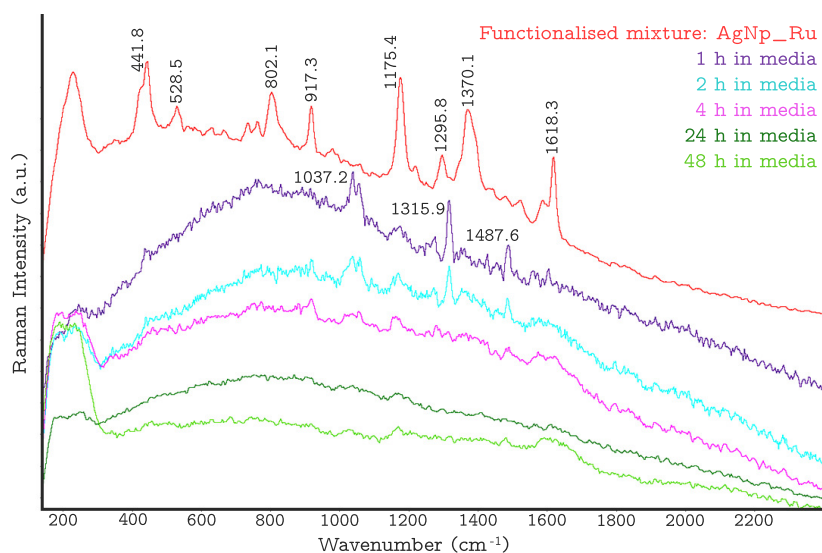
Figure 4.8: Stability study of AgNPs functionalised with Ru complex in culture media.
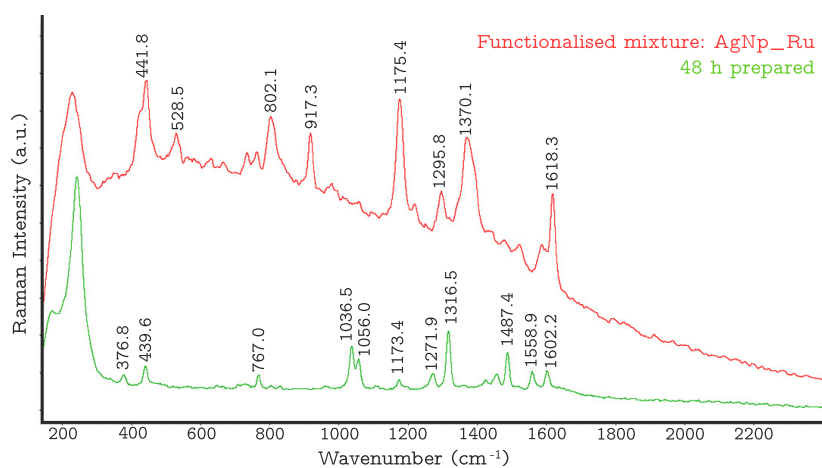

Figure 4.9: Stability study of AgNPs functionalised with Ru complex in distilled water.

unstable as we can observe in Figure 4.11. The main signals obtained in this case were 443.3, 669.3, 1026.8, 1172.8, 1267.2, 1320.4, 1485.0, 1553.6 and 1604.8 cm^{-1}.
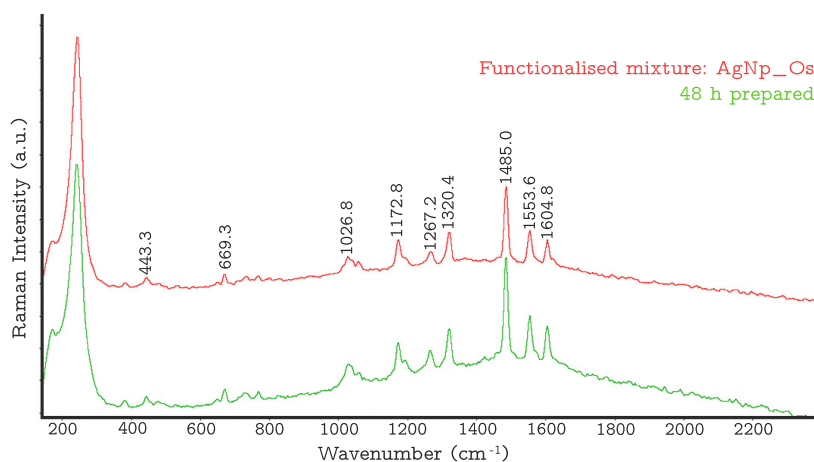

Figure 4.10: Stability study of AgNPs functionalised with Os complex in distilled water.

In the third case of study, AuNPs functionalised with Ru complex, the functionalised mixture was stable at room temperature as we can see in Figure 4.12, but in culture media and in culture conditions it was unstable as we can observe in Figure 4.13. The main signals obtained with this functionalised mixture were 441.2, 1035.3, 1173.8, 1273.5, 1317.2, 1604.8 and 1621.8 cm^{-1}.

Last but not least, the AuNPs labelled with Os complex was the only combination that worked properly and showed stable responses in both conditions as it can be seen in the Figures 4.14 and 4.15. In contrast to the physically absorbed labels, in this case, the Raman signals showed similar intensities after 24 h of incubation in the cell culture media and no appreciable signal degradation was noticed. The characteristics peaks for
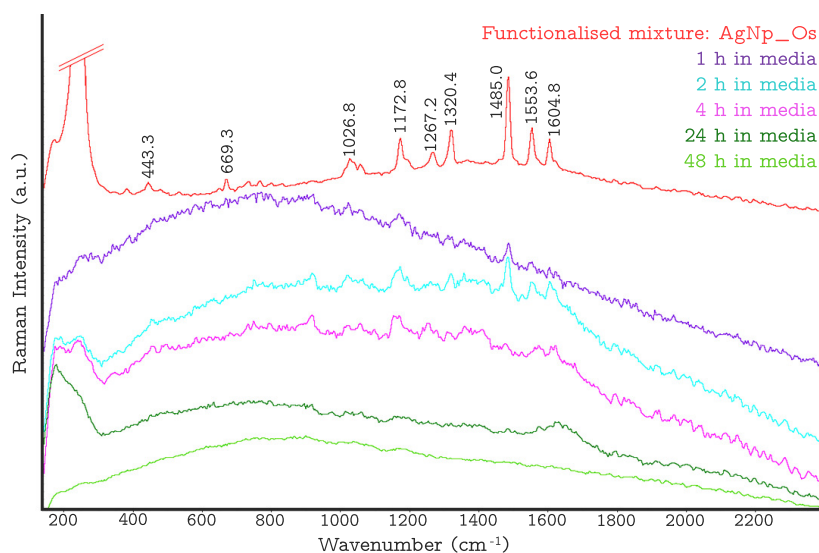
Figure 4.11: Stability study of AgNPs functionalised with Os complex in culture media.

the gold colloid functionalised with Os complex were 668.4, 1026.7, 1173.0, 1266.4, 1321.1, 1485.4, 1553.9 and 1604.8 cm^{-1}.

Once the four cases have been described, it is time to point out the reasons that can be affecting to the stability of the first three functionalised mixtures comparing to the last one.

The only positive result obtained in the stability study was obtained using the Os complex as label. As we have mentioned in the introduction section, the Os compound shows a higher thermal stability than the Ru compound. Moreover, the Os complex, comparing to the Ru complex, also shows a higher photo stability and it is independent from the dissolved oxygen concentration [34]. Therefore, in cell culture conditions the Ru complex is not stable enough as shown before.

The composition of the colloids and the characteristics of each coating agent could be the reason of the lack of stability for the cases based on silver colloids. If we compare the preparation of AuNPs with AgNPs' preparation, the use of citrate ions shows a more alkaline media solution nature. It is a known fact that the existence of nitrogen oxides (as a consequences of the reduction process of silver nitrate) on the Ag colloid prepared using the hydroxylamine which have acidic properties, directly affects on the pH of the colloids with time. The citrate ions provide higher repulsion forces between NPs and therefore, leads to a more stable colloid [38]. This fact may affect to the stability in culture media conditions.
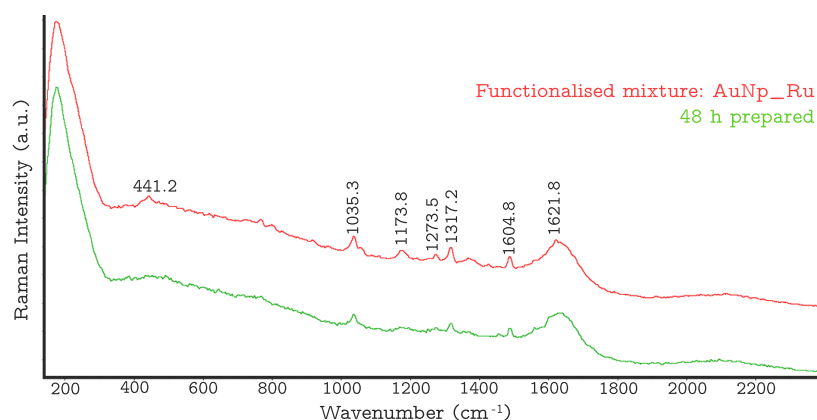

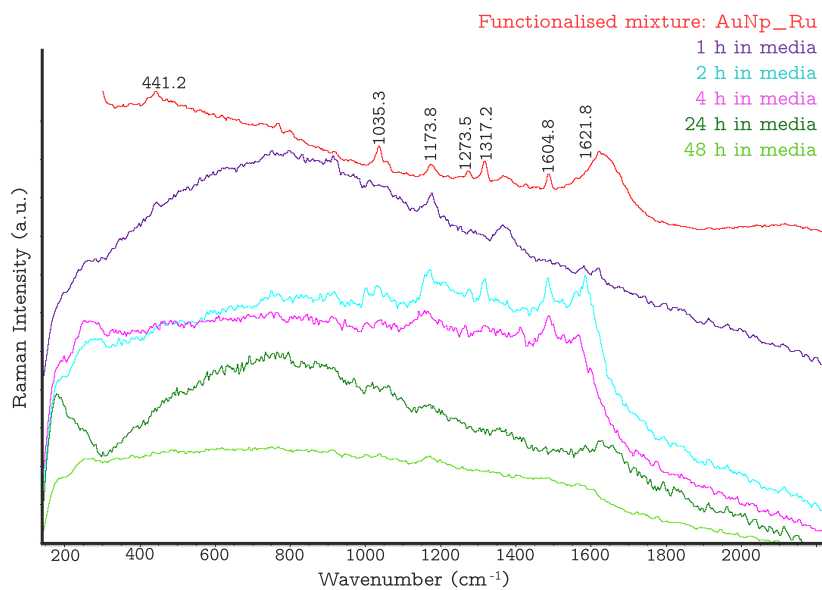**Figure 4.12:** Stability study of AuNPs functionalised with Ru complex in distilled water.

Figure 4.13: Stability study of AuNPs functionalised with Ru complex in culture media.
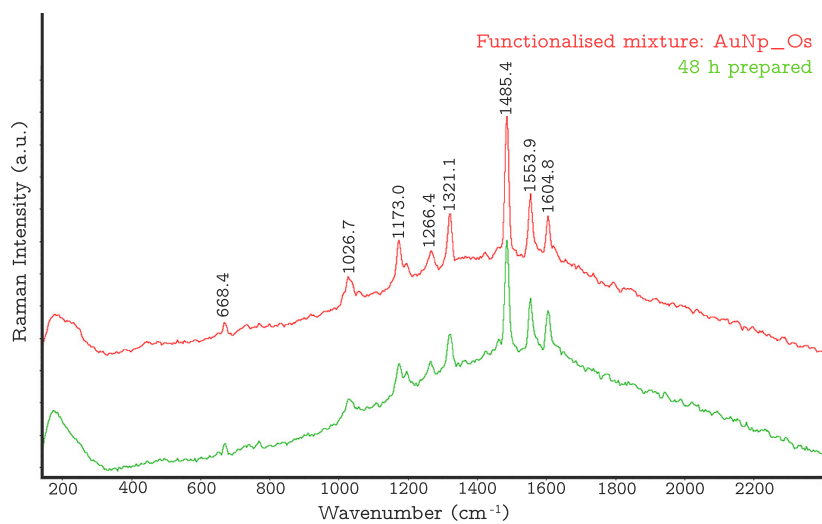

Figure 4.15: Stability study of AuNPs functionalised with Os complex in distilled water.
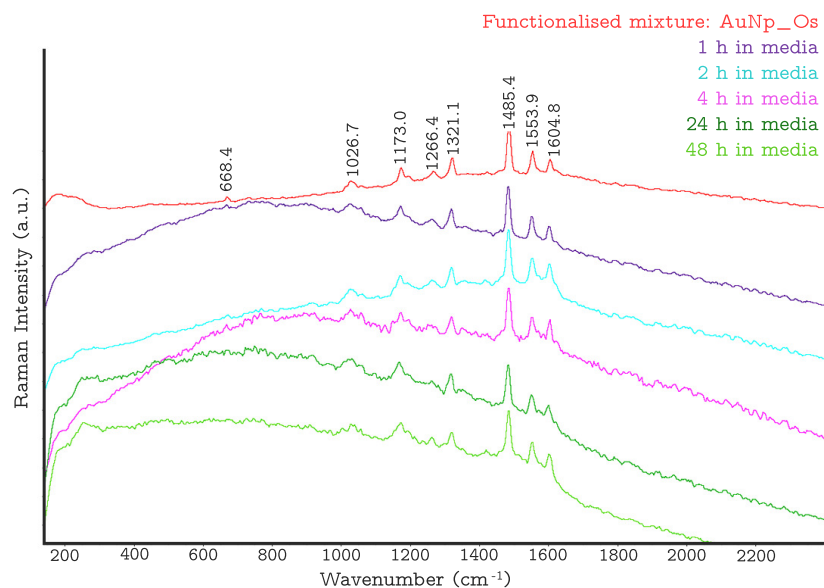
Figure 4.14: Stability study of AuNPs functionalised with Os complex in culture media.

4.4.3 Uptake experiment

First of all, a study of the background signals was performed to verify the absence of interferences in the spectral region where the main SERS signals of the Osmium (II) polypyridyl polyarginine conjugate appear. In Figure 4.16 we can see that the main peaks at 1266.4, 1321.1, 1485.4, 1553.9 and 1604.8 cm^{-1} have no significant interferences. Besides, the identification of all peaks in the Raman spectra guarantee the presence of the Os complex without any doubt.

The uptake experiments were performed in different periods of time (4 h and 24 h) to check the progression of the uptake, using a concentration of AuNPs of 1.6×10^{-10} M and a concentration of Os complex of 1.8×10^{-8} M in the culture media. In Figure 4.17 we can see the chemical images built

using signal to baseline area from $1472\,\mathrm{cm}^{-1}$ to $1492\,\mathrm{cm}^{-1}$ overlapped with white light images. These concentrations are the minimum that we tested. In case to want a higher uniformity and uptake of the labelled NPs, the concentrations can be increased with positive results.
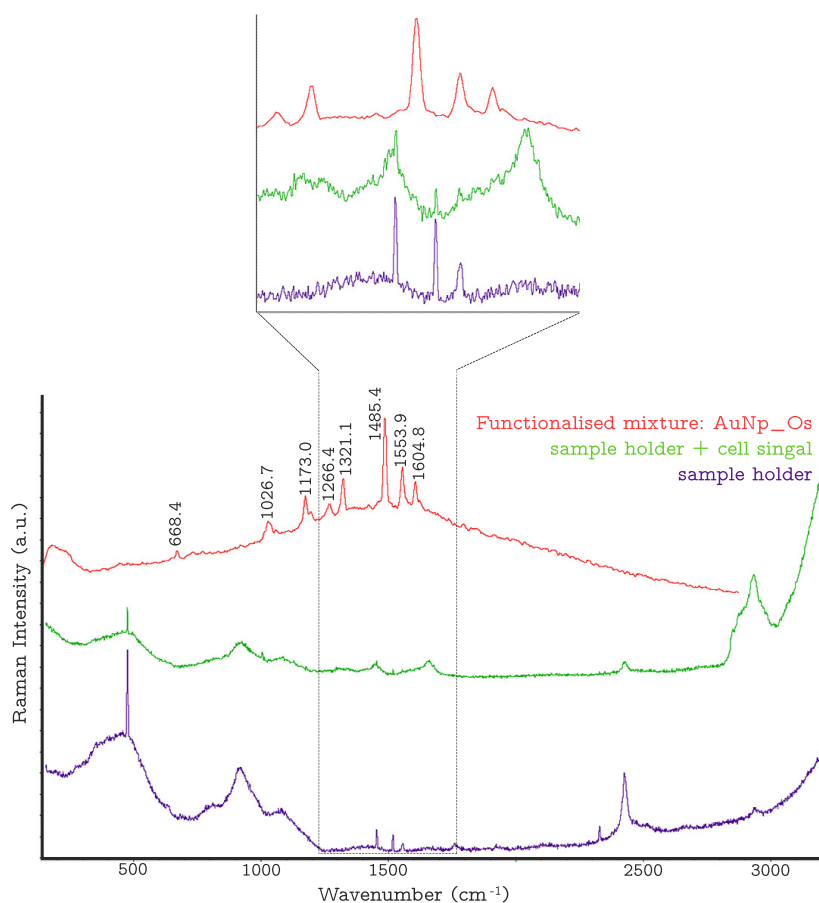

Figure 4.16: Study of the background signals of the culture sample holder and the cells using the $532\,\mathrm{nm}$ laser.

In order to verify the uptake of the labelled NPs happened in $4\,\mathrm{h}$, the CHO cells were analysed using volume mapping as we can see in the

Figure 4.18. The 3D chemical image was built using signal to baseline area between $1472\,\mathrm{cm}^{-1}$ and $1492\,\mathrm{cm}^{-1}$ overlapped with the white light image. Together with this image, the x, y and z planes are represented to make easier the visual confirmation of the uptake of the functionalised NPs.
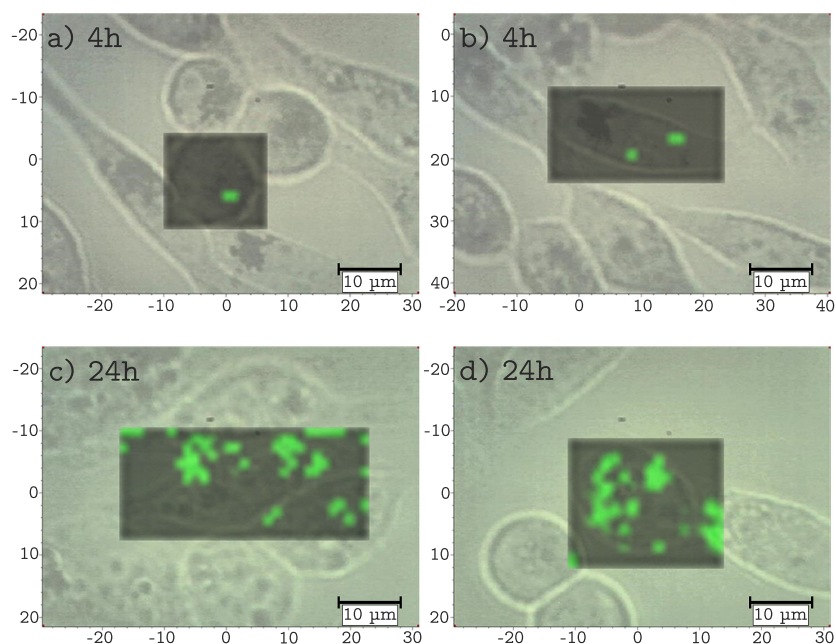

Figure 4.17: Uptake experiment of AuNPs functionalised with Os complex using CHO cells cultured for 4 (a and b images) and 24 hours (c and d images). Chemical images built using signal to baseline area from $1472\,\mathrm{cm}^{-1}$ to $1492\,\mathrm{cm}^{-1}$ and overlapped with white light images of CHO cells.
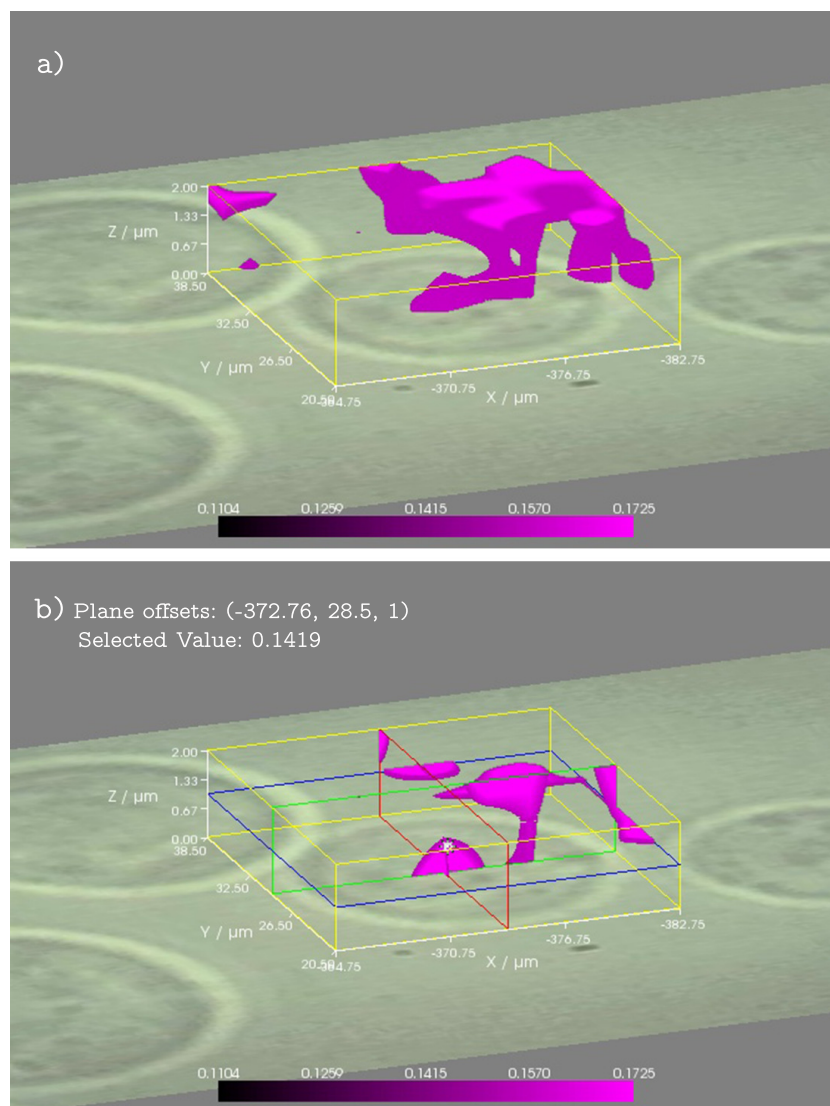
Figure 4.18: Uptake experiment of AuNPs functionalised with Os complex using CHO cells cultured for 4 hours. a) 3D chemical image built using signal to baseline area from $1472\,\mathrm{cm}^{-1}$ to $1492\,\mathrm{cm}^{-1}$ and overlapped with white light image of CHO cells. b) the same 3D SERS image (a) sectioned in x, y and z planes.

4.5　Conclusion

In conclusion, Osmium (II) polypyridyl polyarginine conjugate, used as SERS label with citrate capped gold colloidal nanoparticles, has been proven to be useful in live cell imaging for long-term dynamic experiments due to the stability of the probe.

The suitability of the Osmium complex instead of the Ruthenium analogue can be explained in terms of the higher thermal and photoreactive stability of the Os complexes, as it has been pointed in the literature [34]. Actually, the stability showed in aerated solutions, the weak temperature dependency and the resistance to photobleaching allowed us to achieved bioimages.

The AuNPs functionalised with this complex show interesting features regarding the spectroscopic properties to allow the acquisition of live-cells SERS bioimages. In this sense it was interesting to test that AuNPs were much more efficient and stable than the AgNPs in culture media and in culture conditions regardless the indicative of high stability features of both NPs. The NPs used for the experiments showed a uniform size distribution and had a negative and relative high zeta potential, indicating stability. Two well-known preparation methods were used for the citrate-capped gold colloids and for the hydroxylamine-reduced silver colloids. Between the two options, the citrate-capped gold colloid resulted to be the adequate one for our purpose. Besides, the gold nanoparticles have been proven to be much more biocompatibles due to their superior stability and lower toxicity.

The differences among the two NP types are huge; the composition, the preparation process, the coating layer, the charge, etc. Many are the factors that can be affected by the culture conditions. However, being practical, we wanted to find the best possible combination for SERS bioimaging

in living cells and we found it; the AuNPs prepared with citrate and labelled with the Osmium (II) polypyridyl polyarginine conjugate. By means of this work, we have proven the efficiency of this combination. The reasons to consider as an efficient combination is the fact that we have been working with 1.6×10^{-4} µM of Os complex, while for Raman Resonance Spectroscopy and Fluorescense is needed to use 70 µM in the cell cultures [34]. In this work we have also observed the fast distribution of the functionlised AuNPs in the cell cytoplasms through an active membrane transport mechanisms coupled with the octa-arginine conjugation. This feature is in good agreement with the findings pointed by Keyes and co-workers in the seminal works.

References

[1] M. Daniel and D. Astruc. Gold nanoparticles: Assembly, supramolecular chemistry, quantum-size-related properties, and applications toward biology, catalysis, and nanotechnology. *Chem. Rev.*, 104(1):293–346, 2004.

[2] E.C. Le Ru, E. Blackie, M. Meyer and P.G. Etchegoin. Surface enhanced Raman scattering enhancement factors: A comprehensive study. *J. Phys. Chem. C*, 111(37):13794–13803, 2007.

[3] S. Nie and S.R. Emory. Probing single molecules and single nanoparticles by surface-enhanced Raman scattering. *Science*, 275(5303):1102–1106, 1997.

[4] K. Kneipp, Y. Wang, H. Kneipp, L.T. Perelman, I. Itzkan, R.R. Dasari and M.S. Feld. Single molecule detection using surface-enhanced Raman scattering (SERS). *Phys. Rev. Lett.*, 78(9):1667–1670, 1997.

[5] P.G. Etchegoin and E.C. Le Ru. Resolving single molecules in surface-enhanced Raman scattering within the inhomogeneous broadening of Raman peaks. *Anal. Chem.*, 82(7):2888–2892, 2010.

[6] A.B. Zrimsek, A. Henry and R.P. Van Duyne. Single molecule surface-enhanced Raman spectroscopy without nanogaps. *J. Phys. Chem. Lett.*, 4(19):3206–3210, 2013.

[7] F. Pozzi and M. Leona. Surface-enhanced Raman spectroscopy in art and archaeology. *J. Raman Spectrosc.*, 47(1):67–77, 2016.

[8] C. Muehlethaler, M. Leona and J. R. Lombardi. Review of surface enhanced Raman scattering applications in forensic science. *Anal. Chem.*, 88(1):152–69, 2016.

[9] S. Schluecker. *Surface Enhanced Raman Spectroscopy: Analytical, Biophysical And Life Science Applications.* Wiley-VCH Verlag GmbH & Co. KGaA, Weinheim, 2011.

[10] M. Fleischmann, P.J. Hendra and A.J. McQuillan. Raman spectra of pyridine adsorbed at a silver electrode. *Chem. Phys. Lett.*, 26(2):163–6, 1974.

[11] V. Giannini, A.I. Fernandez-Dominguez, Y. Sonnefraud, T. Roschuk, R. Fernandez-Garcia and S.A. Maier. Controlling light localization and light-matter interactions with nanoplasmonics. *Small*, 6(22):2498–2507, 2010.

[12] L. Guerrini and D. Graham. Molecularly-mediated assemblies of plasmonic nanoparticles for surface-enhanced Raman spectroscopy applications. *Chem. Soc. Rev.*, 41(21):7085–7107, 2012.

[13] G.A. Sotiriou and S.E. Pratsinis. Engineering nanosilver as an antibacterial, biosensor and bioimaging material. *Curr. Opin. Chem. Eng.*, 1(1):3–10, 2011.

[14] S. Kittler, C. Greulich, J. Diendorf, M. Koeller and M. Epple. Toxicity of silver nanoparticles increases during storage because of slow dissolution under release of silver ions. *Chem. Mater.*, 22(16):4548–4554, 2010.

[15] J. Langer, S.M. Novikov and L.M. Liz-Marzan. Sensing using plasmonic nanostructures and nanoparticles. *Nanotechnology*, 26(32):1–28, 2015.

[16] L. Rodriguez-Lorenzo, R.A. Alvarez-Puebla, I. Pastoriza-Santos, S. Mazzucco, O. Stephan, M. Kociak, L.M. Liz-Marzan and F.J. Garcia de Abajo. Zeptomol detection through controlled ultrasensitive surface-enhanced Raman scattering. *J. Am. Chem. Soc.*, 131(13):4616–4618, 2009.

[17] M. Grzelczak, J. Perez-Juste, P. Mulvaney and L.M. Liz-Marzan. Shape control in gold nanoparticle synthesis. *Chem. Soc. Rev.*, 37(9):1783–1791, 2008.

[18] J.M. Romo-Herrera, R.A. Alvarez-Puebla and L.M. Liz-Marzan. Controlled assembly of plasmonic colloidal nanoparticle clusters. *Nanoscale*, 3(4):1304–1315, 2011.

[19] N. J. Halas, S. Lal, W. Chang, S. Link and P. Nordlander. Plasmons in strongly coupled metallic nanostructures. *Chem. Rev.*, 111(6):3913–3961, 2011.

[20] L. Guerrini, J.V. Garcia-Ramos, C. Domingo and S. Sanchez-Cortes. Sensing polycyclic aromatic hydrocarbons with dithiocarbamate-functionalized Ag nanoparticles by surface-enhanced Raman scattering. *Anal. Chem.*, 81(3):953–960, 2009.

[21] D. Graham, D. G. Thompson, W. Ewen Smith and K. Faulds. Control of enhanced Raman scattering using a DNA-based assembly process of dye-coded nanoparticles. *Nat. Nanotechnol.*, 3(9):548–551, 2008.

[22] X. Yang, M. Yang, B. Pang, M. Vara and Y. Xia. Gold nanomaterials at work in biomedicine. *Chem. Rev.*, 115(19):10410–10488, 2015.

[23] S. Pina, J. M. Oliveira and R.L. Reis. Natural-based nanocomposites for bone tissue engineering and regenerative medicine. *Adv. Mater.*, 27(7):1143–1169, 2015.

[24] P. Newman, Z. Lu, S. I. Roohani-Esfahani, T.L. Church, M. Biro, B. Davies, A. King, K. Mackenzie, A. I. Minett and H. Zreiqat. Porous and strong three-dimensional carbon nanotube coated ceramic scaffolds for tissue engineering. *J. Mater. Chem. B*, 3:8337–8347, 2015.

[25] T. Vo-Dinh, H. Wang and J. Scaffidi. Plasmonic nanoprobes for SERS biosensing and bioimaging. *J. Biophotonics*, 3:89–102, 2010.

[26] Z. Luo, K. Zheng and J. Xie. Engineering ultrasmall water-soluble gold and silver nanoclusters for biomedical applications. *Chem. Commun.*, 50:5143–5155, 2014.

[27] K.A. Antonio and Z.D. Schultz. Advances in biomedical Raman microscopy. *Anal. Chem.*, 86(1):30–46, 2014.

[28] T. Ozawa, H. Yoshimura and S.B. Kim. Advances in fluorescence and bioluminescence imaging. *Anal. Chem.*, 85(2):590–609, 2013.

[29] N. Siraj, B. El-Zahab, S. Hamdan, T.E. Karam, L.H. Haber, M. Li, S. O. Fakayode, S. Das, B. Valle, R. M. Strongin, G. Patonay, H. O. Sintim, G. A. Baker, A. Powe, M. Lowry, J.O. Karolin,

C.D. Geddes and I.M. Warner. Fluorescence, phosphorescence, and chemiluminescence. *Anal. Chem.* , 88(1):170–202, 2015.

[30] J. Kneipp, H. Kneipp, B. Wittig and K. Kneipp. Novel optical nanosensors for probing and imaging live cells. *Nanomedicine*, 6(2):214–226, 2010.

[31] F. Pinaud, S. Clarke, A. Sittner and M. Dahan. Probing cellular events, one quantum dot at a time. *Nat. Methods*, 7(4):275–285, 2010.

[32] C.L. Zavaleta, B.R. Smith, I. Walton, W. Doering, G. Davis, B. Shojael, M.J. Natan and S.S. Gambhir. Multiplexed imaging of surface enhanced Raman scattering nanotags in living mice using noninvasive Raman spectroscopy. *Proc. Natl. Acad. Sci. U. S. A.*, 106(32):13511–13516, 2009.

[33] X. Qian, X. Peng, D.O. Ansari, Q. Yin-Goen, G.Z. Chen, D.M. Shin, L. Yang, A.N. Young, M.D. Wang and S. Nie. In vivo tumor targeting and spectroscopic detection with surface-enhanced Raman nanoparticle tags. *Nat. Biotechnol.*, 26(1):83–90, 2008.

[34] Aisling Byrne, Ciaran Dolan, Roisin D. Moriarty, Aaron Martin, Ute Neugebauer, R.J. Forster, A. Davies, Y.Volkov and T.E. Keyes. Osmium(II) polypyridyl polyarginine conjugate as a probe for live cell imaging; a comparison of uptake, localization and cytotoxicity with its ruthenium(II) analogue. *Dalton Trans.*, 44(32):14323–14332, 2015.

[35] J. Wrzesien and D. Graham. Synthesis of SERS active nanoparticles for detection of biomolecules. *Tetrahedron*, 68(4):1230–1240, 2012.

[36] P. C. Lee and D. Meisel. Adsorption and surface-enhanced Raman of dyes on silver and gold sols. *J. Phys. Chem.*, 86(17):3391–5, 1982.

[37] N. Leopold and B. Lendl. A new method for fast preparation of highly surface-enhanced Raman scattering (SERS) active silver colloids at room temperature by reduction of silver nitrate with hydroxylamine hydrochloride. *J. Phys. Chem. B*, 107(24):5723–5727, 2003.

[38] M.V. Canamares, J.V. Garcia-Ramos, S. Sanchez-Cortes, M. Castillejo and M. Oujja. Comparative SERS effectiveness of silver nanoparticles prepared by different methods: A study of the enhancement factor and the interfacial properties. *J. Colloid Interface Sci.*, 326(1):103–109, 2008.

[39] J. Turkevich, P. Cooper Stevenson and J. Hillier. A study of the nucleation and growth processes in the synthesis of colloidal gold. *Disc. Faraday Soc.*, 11:55–75, 1951.

[40] G. Frens. Controlled nucleation for the regulation of the particle size in monodisperse gold suspensions. *Nature*, 241(105):20–2, 1973.

[41] E.C. Le Ru and P. G. Etchegoin. *Principles of Surface-Enhanced Raman Spectroscopy.* Elsevier, Amsterdam, 2009.

[42] J. Yguerabide and E.E. Yguerabide. Light-scattering submicroscopic particles as highly fluorescent analogs and their use as tracer labels in clinical and biological applications: I. theory. *Anal. Biochem.*, 262(2):137–156, 1998.

[43] X. Liu, M. Atwater, J. Wang and Q. Huo. Extinction coefficient of gold nanoparticles with different sizes and different capping ligands. *Colloids Surf. B*, 58(1):3–7, 2007.

[44] L. Cosgrave, M. Devocelle, R.J. Forster and T.E. Keyes. Multimodal cell imaging by ruthenium polypyridyl labelled cell penetrating peptides. *Chem. Commun.*, 46(1):103–105, 2010.

[45] U. Neugebauer, Y. Pellegrin, M. Devocelle, R.J. Forster, W. Signac, N. Moran and T.E. Keyes. Ruthenium polypyridyl peptide conjugates: membrane permeable probes for cellular imaging. *Chem. Commun.*, (42):5307–5309, 2008.

[46] U. Neugebauer, L. Cosgrave, Y. Pellegrin, M. Devocelle, R.J. Forster and T.E. Keyes. Membrane permeable luminescent metal complexes for cellular imaging. *Proc. SPIE*, 8427(Biophotonics: Photonic Solutions for Better Health Care III):13, 2012.

[47] N.M.S. Sirimuthu, C.D. Syme and J.M. Cooper. Investigation of the stability of labelled nanoparticles for SE(R)RS measurements in cells. *Chem. Commun.*, 47(14):4099–4101, 2011.

[48] E.C. Le Ru and P.G. Etchegoin. *Metallic colloids and other SERS substrates*. Elsevier, Amsterdam, 2009.

[49] Malvern Instruments. Dynamic light scattering, common terms defined. *Application note*, 2011.

[50] J. Saade and C.B. de Araújo. Synthesis of silver nanoprisms: A photochemical approach using light emission diodes. *Mater. Chem. Phys.*, 148(3):1184–1193, 2014.

Ondorioak eta etorkizuneko lanak

Chapter 5

Ondorioak eta etorkizuneko lanak

Lan honetan gure lantalderako berriak ziren hainbat erronka aurrera atera ditugu. Izan ere, kimika analitikoa sailean aitzindariak izan gara hainbat esparrutan, NMR metabolomikan oinarritutako ingurumen toxikologia azterketetan baita azterketa medikoetan, eta era berean, irudi hiperespektralen analisi kimiometrikoan baita SERSean oinarritutako irudi analisian.

Garatutako lanari esker, ate berriak zabaldu ditugu gure ikerkuntza taldean. Metabolomikari dagokionez, laster batean, LC-HRMS ekipoa izango dugu eta orain arte ikasitakoak (batez ere datuen analisian) teknika honekin lortutako datuak osagarriak izanik, metabolomika arloan are haratago joateko aukera emango digu.

Arlo asko jorratu ditugu lan honetan eta aurrerantzean ere, gai hauetan sakontzeko uste sendoa dugu. Ingurumen metabolomikan lortutako emaitzak esanguratsuak izan dira eta garrantzitsua iruditzen zaigu interpretazio fisiologiko eta metaboliko sakonago bat ematea etorkizunean.

Hau bide egokira eramateko, ezinbestekoa da hainbat arloko adituen elkarlana, hots, biologoen, kimikarien, estatistikoen edota medikuen elkarlana sustatzea. Lan hau izan daiteke horren adibide gertua.

Hipertermia proiektuari dagokionez, oraindik hazten ari den proiektua da, eta etorkizun hurbil batean froga gehiago egiteko asmoa dugu, berriz ere, NMR metabolomika, Raman eta FTIR irudi hiperespektralak baliabide bezala erabiliz. Esan beharra dago, NMR metabolomikako neurketetan ere gehiago sakontzea nahi dugula. Izan ere, JRES neurketez baliatuz, espektroak sinplifikatu eta datu argiagoak lortzeko esperantza dugu.

Esan bezala, gure ikerkuntza taldean ate berriak zabaldu dira eta ilusio gehien egiten didana zera da, orain arte eskuratutako esperientziak nire lankideei laguntza eskaintzeko balio izatea.

Esaldi sinple batek laburbiltzen du eskuizkribu honen eta orokorrean, nire doktoretza tesiaren ondorio nagusia: asko ikasten ari naiz, eta asko dut ikasteko. Nik ere Socratesen paradoxa konpartitzen dut : badakit ez dakidala ezer (*I know that I know nothing*). Jakintza, zorionez, infinitua da eta gu, zientzialariok, kuriositateak bultzaturik eta borondate onenarekin, infinitua esploratzen eta ulertzen saiatzen jarraituko dugu, ikasteko eta zientzia ulertzeko grina da horretarako bidailagun erabakiorra.